UNIVERSITAT DE BARCELONA

Exploring the impact of the PD-1/PD-L1 axis on CAR-T cell function

Irene Andreu Saumell

Universitat de Barcelona
Facultat de Medicina i Ciències de la Salut
Programa de Doctorat en Biomedicina

Exploring the impact of the PD-1/PD-L1 axis on CAR-T cell function

Memòria presentada per

Irene Andreu Saumell

per optar al títol de

Doctor/a per la Universitat de Barcelona

Doctoranda
Irene Andreu Saumell

Directora
Sònia Guedan Carrió

Tutor
Pablo Engel Rocamora

Barcelona, 2024

Fundació de Recerca Clínic Barcelona – Institut d'Investigacions Biomèdiques Agustí Pi i Sunyer

Table of contents

Abbreviations

ºC: Celsius Grade

%: Percentage

α: Alfa

β: Beta

βME: β-MercaptoEthanol

γ: Gamma

µg: microgram

µL: microliter

π: Pi

A

ACK: Ammonium-Chloride-Potassium

ACT: Adoptive Cell Therapies

adj: Adjusted

AEs: Adverse Events

AF: Alexa Fluor

AICD: Activation-Induced Cell Death

ALL: Acute Lymphoblastic Leukemia

Allo-HSCT: allogeneic hematopoietic stem cell transplant

AML: Acute Myeloid Leukemia

ANOVA: Analysis Of Variance

ATCC: American Type Culture Collection

ATP: Adenosine TriPhosphate

APC: Antigen-Presenting Cell or AlloPhycoCyanin

Axi-cel: axicabtagene ciloleucel

B

B-ALL: B-cell Acute Lymphoblastic Leukemia

bp: base pairs

brex-cel: brexucabtagene autoleucel

BSA: Bovine Serum Albumin

BTC: Biliary Tract Cancer

BV: Brillant Violet

C

CAF: Cancer-Associated Fibroblast

CAIX: Carbonic Anhydrase IX

CAR: Chimeric Antigen Receptor

Cas9: CRISPR associated protein 9

CCL: Chemokine (C-C motif) ligand 1

CCR: Chimeric Cytokine Receptor

cDNA: complementary DNA

CD: Cluster of Differentiation

CD45: Cluster of Differentiation 45

CEA: CarcinoEmbryonic Antigen

CEAA: Committee for Animal Experimentation

cilta-cel: ciltacabtagene autoleucel

CLDN6: CLauDiN6

CLDN-18.2: CLauDiN-18.2

CLL: Chronic Lymphocyte Leukemia

cm: centimeters

CO_2: Carbon dioxide

CR: Complete Response

CRC: ColoRectal Carcinoma

CRi: Complete Response with incomplete hematologic recovery

CRISPR: Clustered Regularly Interspaced Short Palindromic Repeats

CRS: Cytokine Release Syndrome

CSF2: Colony-Stimulating Factor 2

CSV: Comma-Separated Value

CTL: Cytotoxic T Lymphocyte

CTLA-4: Cytotoxic T Lymphocyte-Associated Protein 4

Cy7: Cyanine-7

Cy5.5: Cyanine-5.5

D

DMEM: Dulbecco's modified Eagle Medium

DMG: Diffuse Midline Glioma

DMSO: DiMethyl SulfOxide

DNA: DeoxyriboNucleic Acid

dDNTP: DeoxyNucleotide TriPhosphate

dsDNA: double strand DNA

DSBs: DNA double-Strand Breaks

E

EC: Esophageal Carcinoma

ECM: ExtraCellular Matrix

E.Coli: *Escherichia coli*

EDTA: EthyleneDiamineTetraacetic Acid

EFS: Event-Free Survival

EF1α: Elongation Factor 1 α

EGFR: epidermal growth factor receptor

ELISA: Enzyme-Linked ImmunoSorbent Assay

EMA: European Medicines Agency

E:T: Effector:Target

F

FACS: Fluorescence Activated Cell Sorting

FasL: Fas Ligand

FBS: Fetal Bovine Serum

FAP: Fibroblast Associated Protein

FC: Fold Change

FcR: Fc receptor

FcγR: Fc gamma receptor

FDA: Food and Drug Administration

FL: Follicular Lymphoma

FOXP3: Forkhead bOX P3

FRβ: Folate Receptor Beta

G

g: Acceleration of gravity

g: gram

GBM: GlioBlastoMa

GC: Gastric Cancer

GD2: disialoganglioside

GEA: Gene Enrichment Analysis

GEJ: GastroEsophageal Junction cancer

GM-CSF: Granulocyte Macrophage Colony Stimulating Factor

GO: Gene Ontology

GPC3: GlyPCan 3

Grβ: Granzyme Beta

GVHD: Graft Versus Host Disease

H

h: hours

HA: High Affinity

HCC: HepatoCellular Carcinoma

HER2: Human Epidermal Growth Factor Receptor 2

HEPES: 4-(2-hydroxyethyl)-1-piperazineethanesulfonic acid

HL: Hodgkin Lymphoma

HLA: Human Leukocyte Antigens

HRP: HorseRadish Peroxidase

I

ICAM-1: InterCellular Adhesion Molecule-1

ICD: Immunogenic Cell Death

ICSD: IntraCellular Signalling Domain

ICE: Inference of CRISPR Edits

ICI: Immune Checkpoint Inhibitors

ICOS: Inducible T-cell COStimulator

ICS: IntraCellular Staining

ICV: Intracerebroventricular

ID: Identification name

ide-cel: idecabtagene vicleucel

IDIBAPS: Institut D'Investigacions Biomèdiques August Pi i Sunyer

IFN: Interferon

Ig: Immunolobulin

IHC: ImmunoHistoChemistry

IL: InterLeukin

IL-13Rα: InterLeukin-13 Receptor α

INDEL: INsertions and DELetions

IP: IntraPeritoneally

IQR: InterQuartile Range

irAEs: immune-related Adverse Events

IS: Immunological Synapse

ITIM: Immunoreceptor Tyrosine-based Inhibitory Motif

ITSIM; Immunoreceptor Tyrosine-based Switch Motif

IU: International Units

IV: Intravenous

K

kb: kilobase

Kd: Dissociation constant

KIR2DS2: Killer cell Immunoglobulin-like Receptor 2DS2

KO: Knock Out

L

L: Litre

LA: Low Affinity

LAG-3: Lymphocyte Activation Gene-3

LB: Luria Broth

LD: LymphoDepletion

L/D: Live and Dead

LFA-1: Lymphocyte Function-associated Antigen-1

liso-cel: lisocabtagene maraleucel

log_2: logarithm to the base 2

LV: Lentiviral Vector

M

M: Molar

mA: milliampere

MCL: Mantle Cell Lymphoma

MCRPC: metastatic castration-resistant prostate cancer

MDSC: Myeloid Derived Suppressor Cell

MFI: Mean Fluorescence Intensity

mg: milligram

MHC: Major Histocompatibility Complex

min: minutes

MIP: Macrophage Inflammatory Protein

mL: milliliter

mm: millimeter

mm^2: square millimeter

mm^3: cubic millimeter

mM: millimolar or metastatic Melanoma

MM: Multiple Myeloma

MOI: Multiplicity Of Infection

MPD: Malignant Pleural Disease

MPM: Malignant Pleural Mesothelioma

mTNBC: metastatic Triple Negative Breast Cancer

MSC: Mesenchymal Stem Cell

MUC1: Mucin-1

MW: Molecular Weight

N

NA: Not Applicable

NaOH: Sodium hydroxide

NB: NeuroBlastoma

NCI: National Cancer Institute

NEB: New England Biolab

NFW: Nuclease-Free Water

ng: nanogram

NHEJ: Non-Homologous End Joining

NHL: Non-Hodgkin Lymphoma

NK: Natural Killer

nm: nanometer

NEAA: Non-Essential AminoAcids

NSCLC: Non-Small Cell Lung Cancer

NSG: NOD SCID Gamma mice

O

ORR: Overall Response Rate

OS: Overall survival

OV: Oncolytic Virus

OVN: Overnight

P

PAM: Protospacer Adjacent Motif

PBMCs: Peripheral Blood Mononuclear Cells

PBS: Phosphate Buffer Saline

PCR: Polymerase Chain Reaction

PEBL: Protein Expression Blocker

PFS: Progression-Free Survival

Pgk: Phosphoglycerate kinase 1

PD-1: Programmed cell Death-1

PD-L1: Programmed cell Death Ligand-1

PD-L2: Programmed cell Death Ligand-2

PE: PhycoErythrin

PerCP: Peridinin Chlorophyll Protein

PFA: ParaFormAldehyde

PMA: Phorbol Myristate Acetate

P/S: Penicillin/Streptomycin

PSA: Prostate-Specific Antigen

PSI: Polyfunctional Strength Index

PSMA: Prostate-Specific Membrane Antigen

Q

Q: Quartile

R

RFS: Relapse-Free Survival

RNA: RiboNucleic Acid

RNP: RiboNucleoProtein

ROI: Region Of Interest

r/r: relapsed or refractory

rpm: revolutions per minute

RPMI: Roswell Park Memorial Institute

RT: Room Temperature

RT-qPCR: Real Time quantitative PCR

S

SA: StreptAvidin

SC: SubCutaneous

sCR: stringent Complete Response

scFv: Single-chain variable fragment

SEM: Standard Error of the Mean

SD: Standard Deviation

sgRNA: single guide RNA

SHP-2: Src Homology region 2 domain-containing Phosphatase-2

SLBs: Supported Lipid Bilayers

SN: SuperNatant

S.O.C.: Super Optimal broth + Catabolic repressor

spCas9: *streptococcus pyogenes*Cas9

ssRNA: single-strand RNA

T

TAA: Tumour Associated Antigen

TAE: Tris-Acetate EDTA

TALEN: Transcription Activator-Like Effector Nucleases

T-ALL: T-cell acute lymphoblastic leukemia

Taq: *Thermophilus aquaticus*

TBS: Tris-Buffered Saline

TCR: T-Cell Receptor

TE: Tris-EDTA

TGF-β: Transforming Growth Factor-β

TIL: Tumour Infiltrating Lymphocyte

TIM-3: T cell Immunoglobulin and Mucin-domain containing-3

tis-cel: tisagenlecleucel

TLBL: T-cell LymphoBlastic Lymphoma

TNBC: Triple Negative Breast Cancer

TNF: Tumour Necrosis Factor

TMD: TransMembrane Domain

TME: Tumor MicroEnvironment

TRAC: T-cell Receptor Alpha Constant

tracrRNA: transactivating crRNA

TRAF: TNF Receptor-Associated Factor

TRUK: T-cell Redirected for Universal cytokine-mediated Killing

T_{Reg}: Regulatory T-cell

TSA: Tumor Specific Antigen

t-SNE: t-distributed Stochastic Neighbor Embedding

U

U: Units

UTD: Untransduced T-cells

V

V: Voltage

V_H: Variable heavy chain

V_L: Variable light chain

VSV: Vesicular Stomatitis Virus

W

W: Wat

WT: Wild-Type

WPRE: Woodchuck hepatitis virus Post-transcriptional Regulatory Element

Z

ZFNs: Zinc Finger Nucleases

Nucleotides

A adenine**; T** thymine**; G** guanine**; C** cytosine**; U** uracil

Presentation

Adoptive T cell transfer (ACT) therapy designed to express chimeric antigen receptors (CARs) has produced impressive clinical responses in certain cancer patients. Together with immune checkpoint blockade therapy, CAR-T cells are revolutionizing the field of cancer therapies. CARs are genetically engineered hybrid receptors that combine an antibody-derived extracellular domain with intracellular signalling domains derived from endogenous T cell receptors and costimulatory signals, which can induce T cell activation. The introduction of a CAR into a T cell successfully redirects the T cell with a new antigen specificity. Clinical outcomes achieved until date with CAR-T cell therapy for the treatment of solid tumours are yet far from the unprecedented success witnessed in hematologic malignancies. Despite this, recent works provide for the first-time clear evidence of objective antitumour responses in patients with hard-to-treat solid tumours. These results are highly encouraging and provide proof of the potential of CAR-T cells in this setting. Nevertheless, several obstacles remain to be addressed, including the trafficking of CAR-T cells to the solid mass, the tumour heterogeneity and loss of antigen expression, and the nutrient-restricted and immunosuppressive tumour microenvironment (TME), among others. One of the most prominent and well-studied T cell inhibitory axis is the programmed cell death protein-1 (PD-1)/ programmed death cell ligand-1 (PD-L1) checkpoint pathway. T cell activation following antigen recognition results in PD-1 upregulation, along with an intracellular signalling cascade that leads to the release of Th1 cytokines. These cytokines, in turn, induce the upregulation of inhibitory ligands such as PD-L1 on tumour cells but also on other cell populations within the TME. The interaction between PD-1 on T cells and PD-L1 on tumours ultimately leads to T cell suppression. As these activated T cells are potentially tumour specific infiltrating T cells (either endogenous or adoptively transferred T cells modified to express CARs), preventing the binding between PD-1 and PD-L1 might rescue antitumor T cell cytotoxicity and result in increased efficacy of cell-based

immunotherapies. In the context of CAR-T cell therapy, outcomes of disrupting PD-1 expression may vary depending on the specific CAR used, the type of tumour to be targeted or the different preclinical models employed (such as tumour cells engineered to express constitutively high levels of PD-L1, wild type tumour cell lines or patient derived cancer cells). The principal aim of this thesis was to examinate how different CAR configurations influence CAR-T cell sensitivity to PD-1/PD-L1 inhibition. Moreover, we sought to elucidate the impact of variations in target antigen density on CAR-T cell susceptibility to this inhibition.

To address the challenge of model variability and deepen our comprehension of how different CAR constructs might be influenced by this pathway, we developed preclinical models expressing varying PD-L1 densities that better predict the efficacy of CAR-T cells. Our approach involved engineering tumour cell lines to express PD-L1 at absent, low, or high levels, enabling systematic investigation of diverse CAR configurations both *in vitro* and *in vivo*. Additionally, we established a synthetic model utilizing glass-supported lipid bilayers (SLBs) to precisely control the presence of target antigens and PD-L1 molecules, without additional inhibitors of CAR-T cell function. Through the utilization of these preclinical models, we delved into the impact of PD-1/PD-L1 axis inhibition on CAR-T cells designed to target specific antigens, with either low (LA) or high affinity (HA), and incorporating different co-stimulatory domains (i.e., CD28, ICOS or 4-1BB). Our findings revealed that LA CAR-T cells exhibit heightened sensitivity to PD-1/PD-L1 axis-mediated inhibition in comparison to HA CARs. Consequently, disruption of PD-1 enhanced the functional capabilities of LA CAR-T cells, while providing no discernible advantage to HA CAR-T cells. This trend was consistent across CARs featuring CD28 and ICOS co-stimulatory domains. Interestingly, CAR-T cells comprising 4-1BB co-stimulatory domain displayed intrinsic resistance to PD-L1-mediated inhibition. Furthermore, our observations suggest that low levels of the targeted antigen increased the susceptibility of HA CAR-T cells to inhibition via this axis.

Introduction

1 | Introduction

1. Introduction

1.1. Cancer Immunology

Cancer remains a significant global concern, standing as one of the leading causes of death worldwide, with around 12.7 million reported cases globally. Projections indicate that this number will rise to 21 million by 2030, underscoring the urgent need to delve into the complexities of cancer biology and advance treatment approaches[1]. In 2000, Hanahan and Weinberg introduced a pivotal concept in cancer research by identifying six fundamental hallmarks shared by all cancer cells, regardless of the specific type. These include sustaining proliferative signalling, evading growth suppression, enabling replicative immortality, activating invasion and metastasis, inducing angiogenesis, and resisting cell death[2]. Subsequently, in 2011, they expanded this framework to encompass ten hallmarks, incorporating additional aspects such as reprogramming cellular metabolism, genomic instability, tumour-promoting inflammation, and avoiding immune destruction[3].

1.1.1. Tumour-promoting inflammation

Initially observed by Rudolf Virchow in the 19th century, the presence of leukocytes within tumours marked the inception of a potential link between inflammation and cancer. However, in the past decade, substantial evidence has emerged, affirming the pivotal role of inflammation across various stages of tumour progression. Within the complex milieu of the tumour microenvironment, immune cells engage in intricate and dynamic interactions with cancer cells[4]. Notably, these inflammatory cells exhibit dualistic behaviour, with both tumour-suppressing and tumour-promoting properties, present in varying proportions within neoplastic lesions[3]. Unlike their transient involvement in normal wound healing and infection responses, immune inflammatory cells persist within sites of chronic inflammation, thereby influencing responses to therapeutic interventions. Among the spectrum of tumour-promoting inflammatory cells, macrophage subtypes, mast cells, neutrophils, as well as T and B lymphocytes,

1 | Introduction

play significant roles. Conversely, certain subclasses of B and T lymphocytes, along with innate immune cell types, exhibit discernible tumour-suppressive responses. The equilibrium between conflicting inflammatory responses within tumours is poised to serve as a critical determinant in prognosis and potentially inform therapeutic strategies aimed at redirecting these cells towards effective tumour eradication [5].

1.1.2. Mechanisms to evade the immune system

An unresolved challenge in tumour formation lies in the intricate interplay between the immune system and tumour development and progression. The long-standing concept of immune surveillance postulates that cells and tissues are under constant scrutiny by a vigilant immune system, tasked with recognizing and eliminating the majority of incipient cancer cells and nascent tumours[5]. Although this immune-mediated surveillance operates through both innate and adaptive mechanisms, the antitumor responses can be hindered by the microenvironment through a process known as immunosuppression[6]. This process typically occurs progressively throughout tumour development, and once a tumour becomes established, a repertoire of strategies is employed to evade immune surveillance (Fig. 1.1). These include antigen loss, down-regulation of major histocompatibility molecules, and modulation of endogenous antigen presentation pathways. Additionally, tumours secrete immunosuppressive factors such as transforming growth factor-beta (TGF-β), impeding the infiltration of cytotoxic T-lymphocytes (CTLs) and natural killer (NK) cells. Concurrently, cancer cells recruit immunosuppressive inflammatory cells, including regulatory T cells (T_{Reg}) and myeloid-derived suppressor cells (MDSCs), further suppressing immune responses. Moreover, they exploit immune checkpoint control mechanisms to evade immune detection [5–8].

1 | Introduction

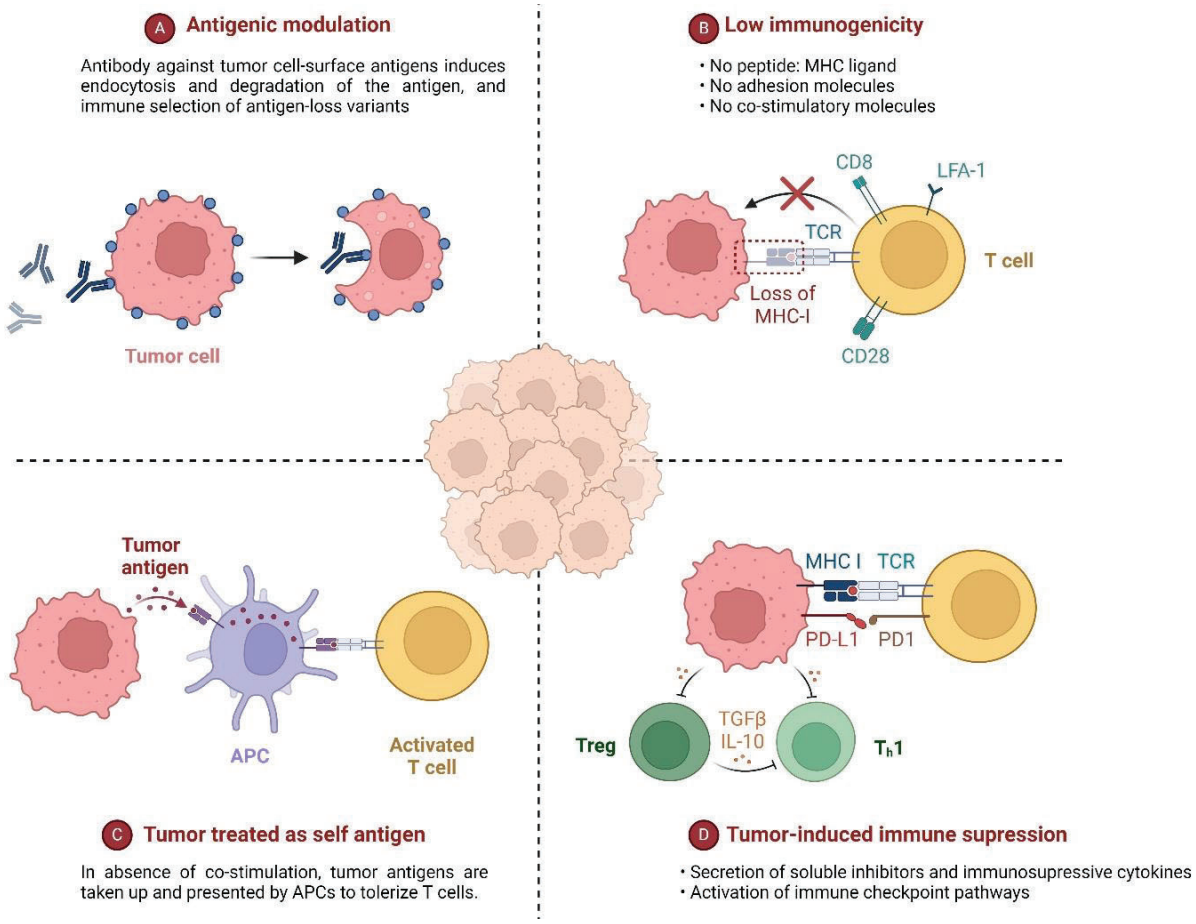

Figure 1.1 | Overview of tumour immune evasion mechanisms. a The loss-antigen variant of tumour cells leads to lack of tumour recognition by T cells. **b** MHC class I molecules can be downregulated on tumour cells and CD8+ T cells are not able to recognize tumour cells. **c** In the absence of co-stimulation, APCs uptake tumour antigens and present them to T cells, inducing tolerance. **d** T cell responses are inhibited by the involvement of immunosuppressive cells, such as Tregs and by inhibitory receptors and their corresponding ligands. APC, Antigen Presenting Cell; MHC, major histocompatibility complex; Treg, Regulatory T cell and Th1, Lymphocyte T helper 1. Created with Biorender.com.

T-cells, as the primary effector immune cells, express multiple autoinhibitory cell surface receptors, including lymphocyte-activation gene 3 (LAG-3), programmed cell death protein 1 (PD-1), and cytotoxic T-lymphocyte-associated protein 4 (CTLA-4), which regulate their response. To enhance tumour tolerance and evade immune eradication, tumour cells can upregulate ligands to these receptors within the tumour microenvironment (TME). A significant paradigm of tumour immune evasion through autoinhibitory pathways is exemplified by the modulation of the PD-1/PD-L1 axis, explained in section 1.2.1.2. Understanding the mechanisms by which cancer cells can

1 | Introduction

evade the immune system is crucial to design new cancer treatment modalities that aim at orchestrating an effective antitumour immune reaction [5,6,9].

1.2. Cancer Immunotherapy

The concept of utilizing the immune system as a therapeutic tool against neoplastic diseases traces back to the 19th century. Wilhelm Busch and Friedrich Fehleisen were among the earliest to document an epidemiological link between immune function and cancer. However, it was in the 20th century that the concept of cancer immunotherapy gained renewed attention and traction. In 1909, Paul Ehrlich proposed the concept that the human body continually generates neoplastic cells, which are promptly eliminated by the immune system. Independently, Thomas and Burnet pioneered the 'cancer immunosurveillance' hypothesis, positing that the immune system detects and eliminates tumour-associated neoantigens comparable to its response against transplanted tissue, thereby impeding carcinogenesis[10]. This notion laid the foundation for manipulating the immune system to combat cancer, giving birth to immunotherapy. Over the past two decades, the progress of cancer immunotherapy has marked a significant milestone in the annals of cancer treatment. This innovative approach has not only elicited unparalleled clinical responses in patients with otherwise treatment-resistant tumours but has also facilitated enduring clinical remission in individuals previously considered incurable [9,10].

For an effective anticancer immune response, a sequence of steps, known as the cancer-immunity cycle (Fig.1.2), must be activated and followed [11]. Initially, neoantigens produced by cancerous cell growth are released and captured by dendritic cells (DCs) on major histocompatibility complex (MHC)I and MHCII molecules for processing. This step (step 1) must be accompanied by immune-boosting signals to prevent tolerance to tumour antigens, such as proinflammatory cytokines and factors released from dying tumour cells or the gut microbiota. Following antigen capture, DCs present these antigens to T-cells (step 2), priming them for action against cancer-specific targets (step 3). The balance between effector T-cells and T_{Regs} at this stage is crucial for determining the nature of the immune response. Finally, activated effector T-cells migrate and

infiltrate the tumour site (steps 4 and 5), where they recognize and bind to cancer cells through specific interactions between T-cell receptors (TCRs) and their cognate antigens (step 6), ultimately leading to cancer cell destruction (step 7). The process is cyclic, as the killing of cancer cells releases more antigens, initiating the cycle again and broadening the immune response. However, in cancer patients, this cycle often falters. The aim of cancer immunotherapy is to restart the cancer-immunity cycle, fostering a self-sustained immune response against tumours while avoiding excessive autoimmune reactions [10,11].

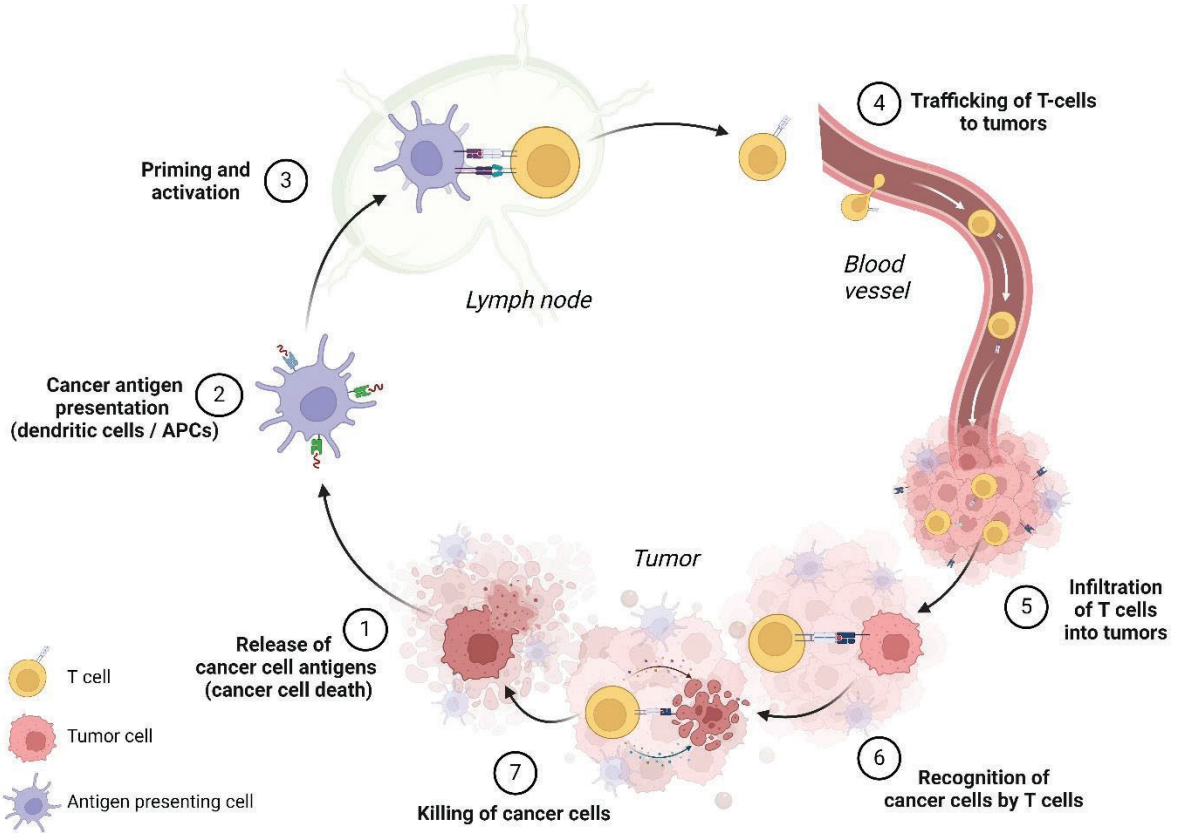

Figure 1.2 | The cancer-immunity cycle. Cancer immunity is orchestrated through a cyclic process, characterized by self-propagation. This cycle accumulates immune-stimulatory factors, potentially bolstering and diversifying T-cell responses. Conversely, inhibitory factors also influence these processes, giving rise to immune regulatory feedback mechanisms that may hamper or restrict immunity progression. Breaking down this process into seven key stages, it starts with the liberation of antigens from cancer cells and ends with the complete elimination of cancerous cells. Adapted from [11]. Created with BioRender.com

1 | Introduction

1.2.1. Immune-checkpoint inhibitors (ICI)

Several evolutionarily conserved negative regulators of T-cell activation function as pivotal 'checkpoint molecules', intricately modulating the immune response to prevent hyperactivation[12]. As many of these immune checkpoints operate through ligand-receptor interactions, they are susceptible to inhibition by antibodies or modulation through recombinant forms of ligands or receptors. This has sparked a surge in research and deployment of pharmacological modulators designed to target these interactions, collectively known as immune checkpoint therapies [13–16]. These advances mark the start of an exciting new phase in cancer treatment. Over just 7 years, the Food and Drug Administration (FDA) greenlit seven immune checkpoint inhibitors (ICIs) for use in more than eighty-five oncology indications [17]. The two immune-checkpoint receptors that have received significant attention in clinical cancer immunotherapy, CTLA-4 and PD-1, exert their biological effects at specific anatomical sites and temporal stages during the T cell lifespan: CTLA-4 acts during T-cell priming and activation, while the PD-1/PD-L1 axis operates mainly during the effector phase (Fig. 1.3)[13], although additional roles during T-cell priming in secondary lymphoid organs have been recently reported [18]. Consequently, they synergistically complement each other, ensuring the maintenance of T-cell responses that balance self-tolerance with robust protection against pathogens and neoplastic growth. The successful targeting of CTLA-4 and PD-1 with monoclonal antibodies by numerous pioneering research groups has led to their emergence as treatments for a diverse array of refractory cancers. This research culminated in the landmark approval by the FDA of the first immunotherapeutic agents within this class: anti-CTLA-4 (Ipilimumab, Yervoy) in 2011, anti-PD-1 (Pembrolizumab, Keytruda and Nivolumab, Opdivo) in 2014 and anti-PD-L1 (Atezolizumab) in 2016, followed by the awarding of the 2018 Nobel Prize in Physiology or Medicine to James P. Allison and Tasuku Honjo [10,15].

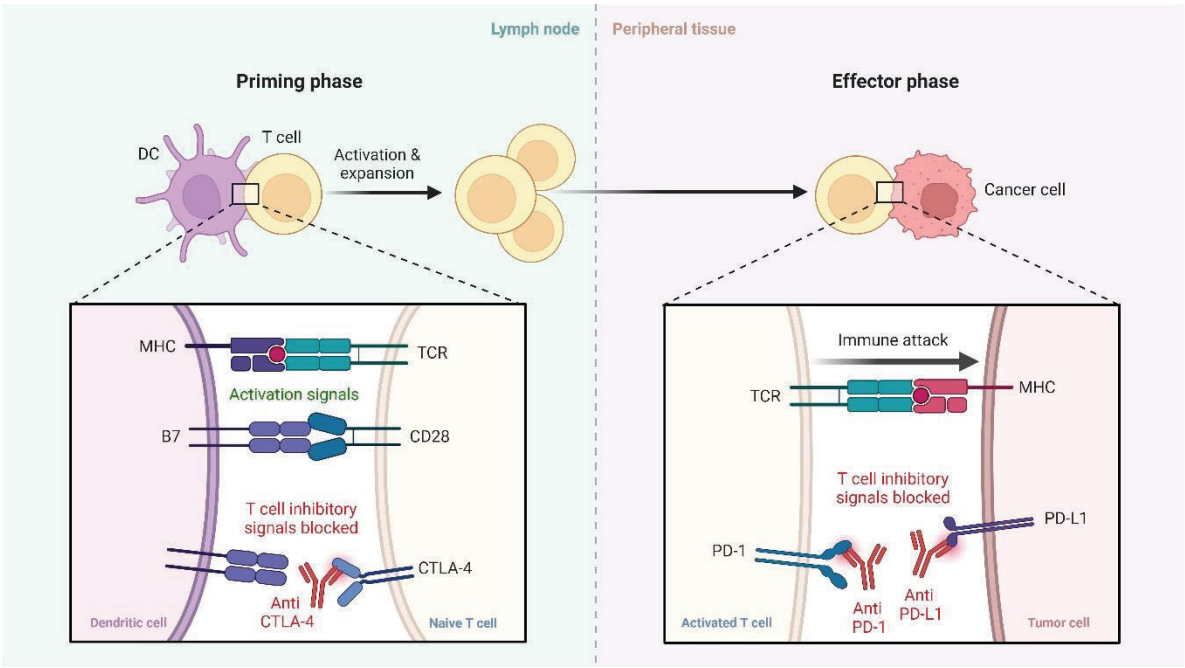

Figure 1.3 | Blockade of CTLA-4 or PD-1 signalling in tumour immunotherapy. CTLA-4 is swiftly up-regulated following T-cell activation, initiating negative regulation signalling by binding with B7 costimulatory molecules on APCs. While CD28-B7 binding triggers activation signals, CTLA-4-B7 binding delivers inhibitory signals, primarily occurring during the priming phase of T-cell responses within lymph nodes. PD-1 inhibitory receptor expression arises in T-cells upon prolonged antigen exposure, leading to negative regulation upon ligation with PD-L1 and PD-L2 ligands, primarily found in inflamed tissues and TME. PD-1 interaction predominates in the effector phase of T-cell responses within peripheral tissues. Blockade of PD-1 or PD-L1 with antibodies preferentially reinvigorates activated T-cells. CTLA-4, Cytotoxic T-lymphocyte–associated antigen-4; CD28, Cluster of differentiation 28; TME, tumour microenvironment; PD-1, programmed cell death-1; PD-L1, Programmed cell death ligand 1; PD-L2, Programmed cell death ligand 2. Adapted from[19] . Created with BioRender.com.

1.2.1.1. Cytotoxic T-Lymphocyte Antigen 4 (CTLA-4)

CTLA-4 is exclusively expressed on T-cells, where it plays a critical role in regulating the early stages of T cell activation. CTLA-4 functions primarily by counteracting the activity of the T cell co-stimulatory receptor CD28, which amplifies T cell signalling upon antigen recognition. Specifically, the affinity of CD80 for CD28 is approximately 4 μM, while for CTLA-4 it is about 0.2 μM. Similarly, the affinity of CD86 for CD28 is around 20 μM, compared to about 2 μM for CTLA-4[20]. Due to this higher affinity, CTLA-4 effectively competes with CD28 for binding to CD80 and CD86, resulting in the inhibition of T-cell activation. Additionally, CTLA-4 can deliver inhibitory signals to T-cells, further

1 | Introduction

modulating their activation. Studies suggest that CTLA-4 also confers signalling-independent T-cell inhibition by sequestering CD80 and CD86 from CD28 engagement and actively removing them from APCs. Knockout mouse models lacking CTLA-4 demonstrate the critical role of CTLA-4 in maintaining immune tolerance, with *Ctla4* knockout mice exhibiting lethal systemic immune hyperactivation[13,14,21]. In cancer immunotherapy, CTLA-4 blockade has shown promising results, particularly in metastatic melanoma, leading to significant improvements in overall survival in certain patients[22]. Additionally, several other anti-CTLA-4 monoclonal antibodies besides ipilimumab have been approved, including tremelimumab, while others such as quavonlimab are currently under development [23]. However, challenges remain in understanding the precise mechanisms of CTLA-4 blockade and optimizing its therapeutic efficacy, particularly regarding T_{Reg} depletion and identification of predictive biomarkers. Ongoing research efforts aim to enhance the efficacy of anti-CTLA-4 antibodies through engineered Fc domains to achieve T_{reg} depletion and improve clinical outcomes [15].

1.2.1.2. Programmed cell death-1 (PD-1)

The discovery of PD-1 (CD279) by T. Honjo and colleagues in 1992 [24] marked a significant milestone in understanding immune regulation, particularly regarding its role as a crucial negative regulator of T cell-mediated immune responses. PD-1 is a 288 amino acid protein that primarily functions as an inhibitory receptor on T-cells, engaging with its ligands PD-L1 (CD274 or B7-HI) and PD-L2 (CD273 or B7-DC) [19,25]. While PD-L2 expression is predominantly confined to professional APCs, PD-L1 exhibits a considerably broader distribution across various tissues, both healthy and cancerous. Upon ligand binding, the immunoreceptor tyrosine-based inhibitory (ITIM) and immunoreceptor tyrosine-based switch motifs (ITSM) present in the cytoplasmic tail of PD-1 are phosphorylated and recruit tyrosine phosphatases such as Src homology region 2 domain-containing phosphatase-2 (SHP-2). SHP-2 can then dephosphorylate signalling components downstream of TCR and CD28 pathways, including CD3ζ, ZAP70 and PKCθ, as detailed in Figure 1.4 [25,26]. Despite the pivotal role of SHP-2 in mediating the inhibitory effect of PD-1, recent evidence suggests that it can also happen in a motif-

independent manner through the regulation of actin cytoskeleton dynamics at the immunological synapse (IS) [27].

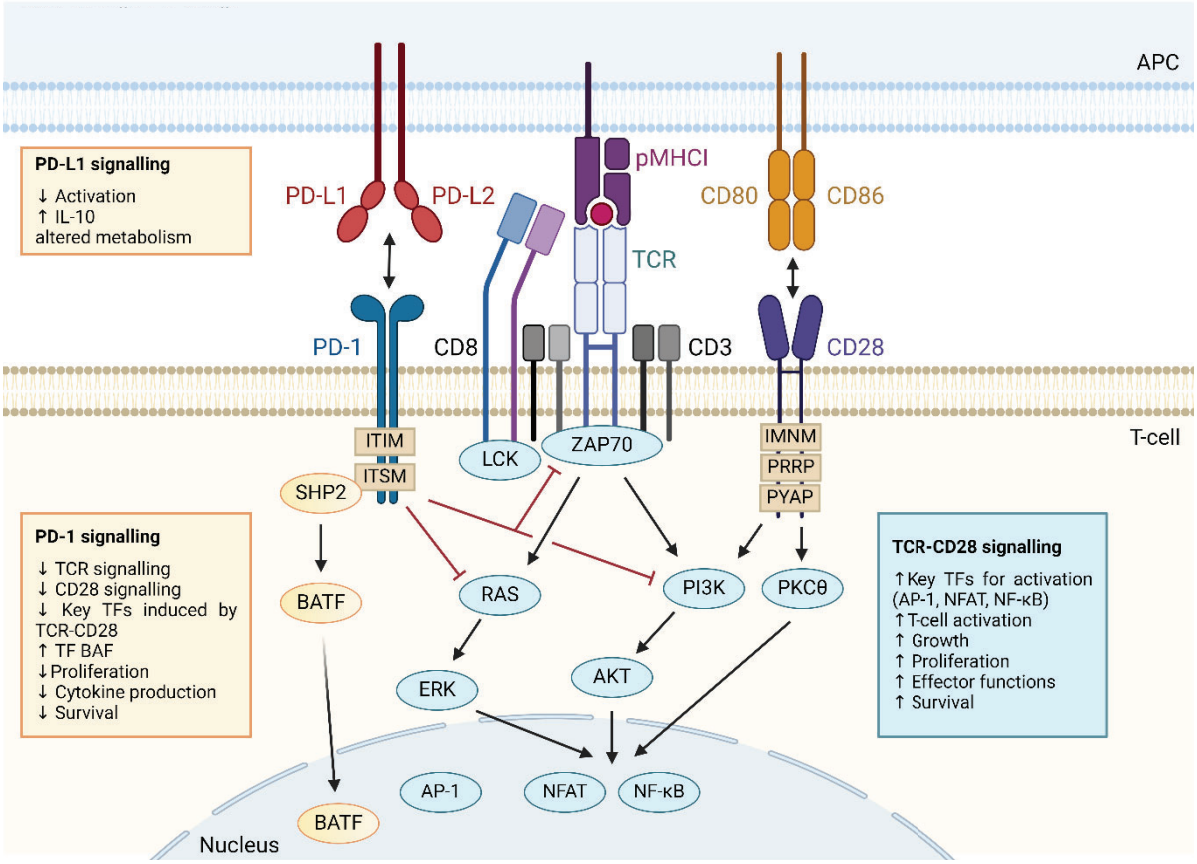

Figure 1.4 | Mechanisms of PD-1 signalling in T-cells. In T-cells, the inhibitory signal mediated by PD-1 requires presentation of pMHCI molecules by the same cell expressing PD-L1 and PD-L2. PD-1 achieves its inhibitory function by recruiting phosphatases, such as SHP2, to the ITSM within its tail. These phosphatases act to counterbalance the positive signalling events initiated by the TCR, which interacts with pMHCI, and CD28, which interacts with CD80 and/or CD86. Specifically, they inhibit downstream molecules like ZAP70 and disrupt signalling pathways including PI3K–AKT and RAS. Consequently, there is a collective decrease in the activation of TFs crucial for T cell activation, such as AP-1, NFAT, and NF-κB, thereby affecting processes like proliferation, effector functions, and survival. Moreover, PD-1 can further inhibit T cell functions by upregulating the expression of TFs like BATF, which in turn dampens effector transcriptional programs. While there is evidence suggesting that PD-1 ligands may induce signalling upon engagement with PD-1, the exact motifs and mechanisms underlying this process remain unknown. Signalling motifs are depicted in yellow boxes, while circles represent key proteins within signalling pathways and pivotal TFs. AP-1, Activator Protein-1; BATF, basic leucine zipper transcriptional factor ATF-like; ITIM, Immunoreceptor Tyrosine-based Inhibitory Motif; ITSM, Immunoreceptor Tyrosine-based Switch Motif; NFAT, nuclear factor of activated T-cells; NF-κB, nuclear factor-κB; PI3K, Phosphoinositide 3-kinase; pMHCI, peptide–MHC class I complex; PD-1, Programmed Death Cell-1; PD-L1, Programmed cell Death Ligand 1; PD-L2, Programmed cell

Death Ligand 2; SHP2, Src homology region 2 domain-containing phosphatase-2; TCR, T-Cell Receptor; TF, Transcription Factor. Adapted from [28]. Created with Biorender.com.

The PD-1 pathway is a central regulator of the host physiology, acting as a brake to prevent excessive T-cell activation, regulating the humoral immunity through regulating $CD4^+$ T follicular helper (T_{FH}) and T follicular regulatory (T_{FR}) cell responses and mediating central and peripheral T-cell tolerance, thus protecting tissues from immune-mediated damage [25,29,30]. During acute infections, PD-1 expression is induced on the T-cell membrane immediately after antigen recognition by the TCR, declining as the immune response resolves. In this setting, PD-1 has also been shown to play a regulatory role during the transition of naive-to-effector CD8 T cell differentiation [31]. In contrast, it's expression remains elevated over time when persistent antigen exposure occurs (e.g, during chronic infections or cancer), contributing to T-cell exhaustion (T_{ex}) and leading to sustained immune suppression. T_{ex} T-cells are characterized by a progressive decline in effector functions, sustained high expression of inhibitory receptors (such as PD-1, CTLA-4, LAG-3 and TIM-3), metabolic dysregulation, impaired memory recall and self-renewal, and distinct transcriptional and epigenetic profiles. While PD-1 signalling is not required for the induction of $CD8^+$ T-cell exhaustion, this pathway plays a critical role in maintaining the exhausted state [32–34].

In the context of a tumour, PD-1 signalling can impede T-cell antitumour immunity through various mechanisms, which may exhibit variability across tumour types due to the TME heterogeneity and tissue-specific tolerance mechanisms [25]. For instance, PD-1 can hinder T cell trafficking to tumours and their effector functions, particularly in T-cells activated by tumour-antigen-bearing APCs. Moreover, tumour-infiltrating T cells may still face PD-1-mediated regulation and exhaustion in the tumour milieu, exacerbated by the pro-inflammatory cytokines they produce, notably IFN-γ, which can further drive PD-L1 expression on cancer cells or other TME constituents and promote adaptive resistance and immunosuppression [35,36].

The therapeutic potential of blocking the PD-1 pathway in cancer treatment has been demonstrated in preclinical studies and clinical trials, leading to the FDA approval of anti-PD-1 antibodies such as pembrolizumab and nivolumab, as well as anti-PD-L1

antibodies including durvalumab and atezolizumab, among others, for treating over 20 types of cancer. The efficacy of these antibodies has been notably demonstrated by evincing response rates spanning from 20 to 50%. Moreover, they have engendered durable clinical responses in a subset of patients [37–39]. Nonetheless, response rates are still limited for most of them, and immune-related adverse events are also observed in human patients and mice receiving anti-PD-1 therapy. Significantly, recent research underscores the pivotal role of predictive biomarkers in optimizing the efficacy of PD-1 blockade therapies, with the frequency of PD-1$^+$CD8$^+$ T cells relative to PD-1$^+$ T_{reg} cells in the TME emerging as a superior predictor of clinical efficacy [40] compared to traditional markers like PD-L1 expression or tumour mutational burden [41]. All these insights highlight the multifaceted role of PD-1 in immune regulation and its potential as a therapeutic target in cancer immunotherapy, emphasizing the need for continued research efforts to decipher its complex signalling pathways and exploit them for therapeutic benefit.

1.2.2. Adoptive cell transfer (ACT)

A key challenge with ICIs stems from the limited availability of endogenous tumour-specific effector T cells [42]. Adoptive cell transfer (ACT) presents a promising solution to surmount this obstacle. ACT stands as a highly personalized and pioneering cancer therapy. It involves the extraction of a patient's own T-cells, which are then expanded and activated outside the body before being reintroduced back into the patient's system to target and eradicate cancer cells. The origins of this approach date back over six decades, when it was shown that lymphocytes were the orchestrators of allograft rejection in experimental animals[43]. The ability to use ACT was facilitated by the characterization of T-cell growth factor interleukin-2 (IL-2) in 1976, which offered a method to cultivate T lymphocytes *ex vivo* while preserving their potent effector functions. Since then, the landscape of ACT has evolved substantially, particularly with the ground-breaking work of the Rosenberg group at the National Cancer Institute (NCI) in the early 1980s [44,45]. ACT-based therapies bypass the need for active immunization and therefore have potential efficacy in immunologically compromised patients with cancer. Moreover, they offer numerous advantages over conventional treatments. They

1 | Introduction

allow for the manipulation of the host (i.e., pre-conditioned with chemotherapy) before cell transfer, creating a favourable microenvironment that bolsters antitumour immunity. Additionally, ACT enables the recovery of antitumour lymphocytes capable of discerning between cancerous and healthy cells, while establishing sustained surveillance. While ACT primarily encompasses three T-cell approaches —TILs, TCR-engineered T-cells, and CAR-engineered T-cells— other strategies have been developed, including lymphokine-activated killer (LAK) cells, cytokine-induced killer (CIK) cells, γδ T cells, and NK cells. Furthermore, ACT can synergize with existing therapies such as checkpoint inhibitors and oncolytic viruses, augmenting their efficacy and broadening treatment options for patients (Fig. 1.5) [46,47]. ACT has shown promising results in certain cancers, and ongoing research aims to expand its use to a broader range of cancer types. For cancers with high mutational burden, options such as checkpoint inhibitors and TILs are effective. In cases of low mutational burden, strategies involving redirected high-affinity TCR-T cells can be considered, alongside CAR-T cells if suitable surface markers are identified [47].

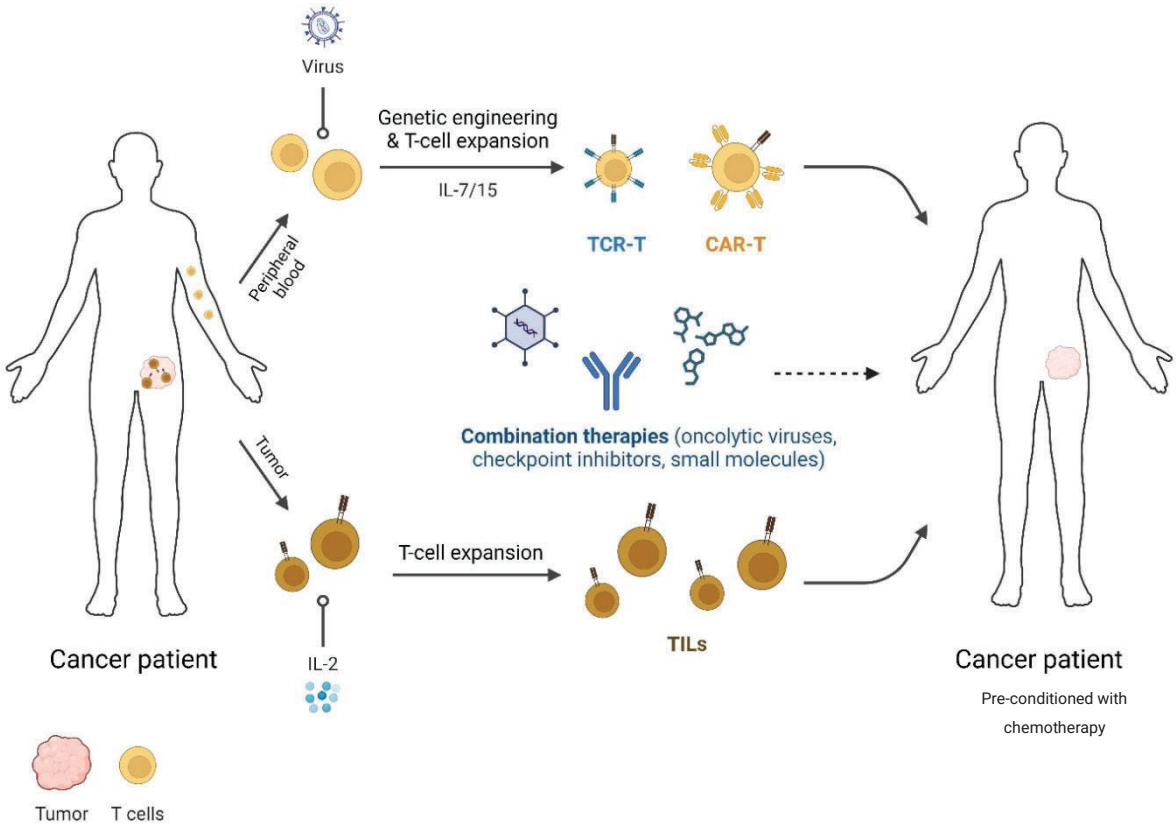

Figure 5 | Adoptive T cell transfer therapies. Tumour-specific T cells can either be harvested from tumours or engineered from peripheral T cells. To combat cancer effectively, these therapeutic T cells must infiltrate the tumour, multiply, and survive the immunosuppressive

tumour microenvironment. CAR, chimeric antigen receptor; IL, interleukin; TCR, T cell receptor; TIL, tumour-infiltrating lymphocyte. Adapted from [47]. Created with BioRender.com.

1.2.2.1. Tumour-Infiltrating Lymphocytes (TILs)

ACT utilizing autologous TILs represents a potent strategy for inducing complete and lasting regressions, primarily in metastatic melanoma patients, but also in various other cancer types[48]. The rationale behind this success lies in the fact that, despite the presence of tumour-specific T cells within tumours, they frequently demonstrate a state of unresponsiveness [47]. TILs, defined as lymphocytes found within and around cancer cells, are generally sourced from resected tumour specimens, cultured in high IL-2 doses to generate pure lymphocyte culture and expanded rapidly with irradiated feeder lymphocytes, anti-CD3 antibodies, and IL-2. Within approximately five to six weeks, up to 10^{11} lymphocytes can be obtained for infusion back into patients [45,46].

Recent studies indicate that the efficacy of TIL therapy is primarily driven by T-cells targeting tumour-specific antigens, known as neoantigens. Given the heterogeneous nature of TIL populations, strategies to enrich the final TIL product in neoantigen-reactive T-cells, such as identifying PD-1 and 4-1BB as markers for tumour reactivity, have been explored [49,50]. Notably, PD-1 expression in the peripheral blood of melanoma patients has emerged as a potential indicator of neoantigen reactivity, offering a non-invasive avenue for tailoring personalized T-cell therapies [51]. Further efforts to augment TIL efficacy include refining recovery protocols and combining TIL therapy with other immunotherapy agents like anti-PD1 and anti-CTLA-4 antibodies [52]. Notably, in February 2024, the FDA approved Amtagvi (lifileucel) for treating metastatic melanoma [53]. This approval is a significant milestone as it becomes the first FDA endorsement for a TIL therapy and the first immune cell therapy for treating solid tumours.

1.2.2.2. Transgenic T-cell receptors (TCRs)

An alternative to the process of isolating TILs and to overcome limited availability and accessibility of these cells is to genetically modify T-cells obtained from peripheral blood to express transgenic TCRs able to recognize tumour antigens and induce cancer

1 | Introduction

cell killing. TCR gene transfer offers some advantages over TIL therapies, effectively addressing numerous practical challenges encountered in immunotherapy. These benefits include a minimally invasive leukapheresis procedure for acquiring autologous T cells, rapid development of potent cell products, meticulous pre-selection of TCRs for optimal potency, introduction of TCRs into minimally differentiated cell populations and the possibility to make concurrent genetic modifications to enhance T-cell function by bolstering survival, resistance to inhibitory ligands, and antigen-driven signalling through the TCR complex [42,54].

The foundation of TCR gene therapy began with significant discoveries in the 1980s, such as the isolation of genes encoding both mouse and human TCRs in 1984. Two years later, Michael Steinmetz conducted innovative research by transferring TCR genes from one T-cell to another, giving the second T-cell the same antigen specificity[55]. This pioneering experiment laid the groundwork for modern TCR gene therapy. By the turn of the millennium, advances in cloning techniques and viral delivery systems also improved the effectiveness of TCR-based therapies. Particularly, in 2000, Kranz's group demonstrated the ability to enhance TCR-antigen affinity through mutagenesis, addressing challenges associated with weak antigen binding [56,57]. In 2004, Rosenberg's team conducted the first TCR gene therapy trial, focusing on the MART-1 antigen in melanoma patients, achieving significant success, with some patients experiencing complete tumour regression [58]. The advent of the first TCR clinical trial in non-melanoma solid tumours in 2008, particularly synovial cell sarcoma, highlighted the potential of TCR-based approaches, yielding promising clinical responses[59]. However, challenges arose, including fatal toxicities[60,61], which dampened initial enthusiasm. Despite safety concerns, recent trials have shown acceptable toxicity, culminating in the FDA approval of the first TCR-based therapy for metastatic uveal melanoma in January 2022 [62,63].

1.2.2.3. Chimeric Antigen Receptors (CARs)

Two of the main limitations of transgenic TCR and TIL therapies are their dependency on external co-stimulation and on presentation of the targeted neoepitope via the MHC-I complex, which is often downregulated in cancer cells [64]. An alternative approach that

may address these challenges is to genetically modify T cells to express CARs that recognize their antigen in an MHC-independent manner. CARs are synthetic modular proteins designed to confer a specific recognition ability onto immune effector cells — primarily T cells, although various other cell types such as NK cells [65,66], macrophages [67] and dendritic cells[68] have been used— redirecting them towards cells expressing the corresponding target ligand, facilitating their elimination [69]. In contrast with natural TCRs, which create a highly organized immune synapse upon encountering antigens allowing for the recognition of even very low antigen densities, CAR-T cells exhibit a sensitivity to antigens roughly 1,000 times lower[70]. Consequently, CAR designs must prioritize the formation of a functional immune synapse to ensure efficient elimination of tumour cells [71].

CAR T-cell therapy was first engineered by Eshhar and colleagues from the Weizmann Institute of Science in the late 1980s[72]. This pioneering work was followed by significant contributions from Carl June and his team at the University of Pennsylvania as well as Michael Sadelain et al. at Memorial Sloan Kettering Cancer Center[73]. Together with other researchers, they have been instrumental in the development and refinement of this therapy. CARs aim to capitalize on the expansion, cytotoxicity, and persistence of natural T-cells for broader therapeutic utility. Each CAR-T cell has the capacity to eliminate numerous tumour cells and may contribute to immune surveillance, thereby preventing tumour recurrence through antigen release and supporting TILs to attack tumours, in a process known as cross priming[74].

A prototype CAR exhibit a modular architecture comprising five primary components: (I) a peptide leader, (II) an antigen-binding domain, (III) a hinge region, (IV) a transmembrane domain (TMD), and (V) an intracellular signalling domain. Each element serves a specific function, and achieving the optimal molecular design of the CAR involves exploring diverse variations of these constituent protein domains (Fig. 1.6) [73,75].

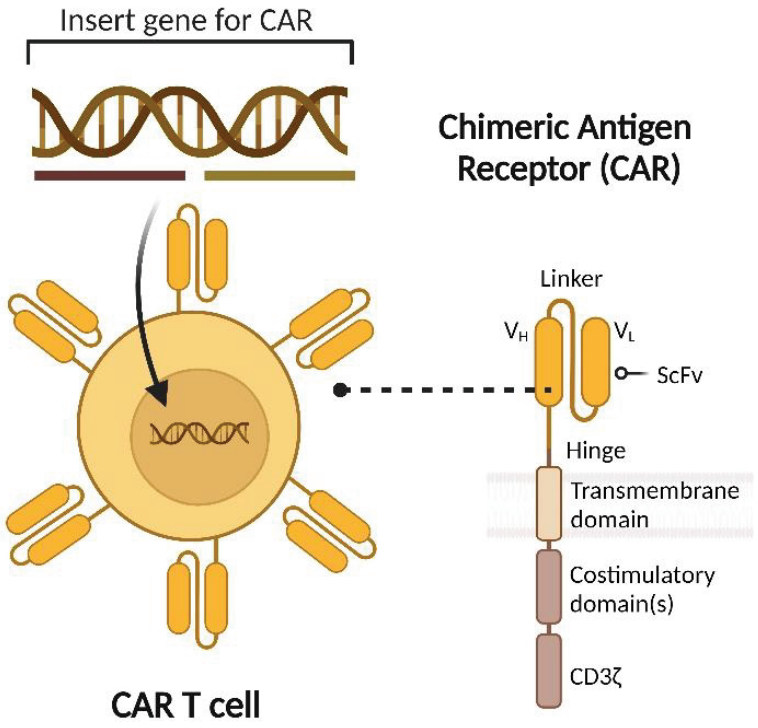

Figure 1.6 | Representative structure of a prototype CAR. CARs are engineered proteins combining an extracellular section, usually derived from the scFv of a monoclonal antibody, a hinge that provides conformational flexibility, a transmembrane domain that anchors the receptor in the cell surface together with intracellular signalling modules sourced from T cell signalling proteins. scFv, single chain Fragment variable; V_H, variable heavy chain; V_l, variable light chain. Created with BioRender.com

The coding sequence of CARs starts with a peptide leader to ensure its proper localization on the cell surface. This leader, often derived from human CD8α, IL-2, GM-CSF receptor α chain or murine Ig-kappa (IgK), guides CAR trafficking to the plasma membrane. Following the peptide leader, we found the antigen-binding domain. This domain constitutes the extracellular segment of the CAR responsible for identifying the target antigen and directing the specificity of a CAR-expressing cell accordingly. Typically, antigen-binding domains in CARs have been constructed from the variable heavy (V_H) and variable light (V_L) chains of murine or human monoclonal antibodies, linked together by a flexible linker to create a single chain variable fragment (scFv) [76]. The $(Gly_4Ser)_3$ peptide serves as the most prevalent linker, leveraging glycine residues for flexibility and serine residues for solubility, resulting in a properly folded scFv capable of recognizing and binding antigens [77,78]. While conventional CARs typically employ scFvs targeting extracellular antigens of cell-surface proteins expressed by cancer cells, thus facilitating major MHC-independent T cell activation, a novel class of CARs known as MHC-dependent, T cell receptor TCR-mimic CARs have also emerged, enabling recognition of intracellular tumour associated antigens (TAAs)[79]. Additionally, CARs have been designed to incorporate smaller, naturally occurring single-domain antibodies known as nanobodies, which consist of

the V_H domain of camelid heavy-chain antibodies. This type of CARs has been utilized in clinical trials, the approval in 2021 by the FDA of idecabtagene vicleucel (Abema) for relapsed or refractory multiple myeloma (MM)[80].

Several characteristics of the scFv extend beyond mere recognition and binding of the target antigen. For instance, the mode of interaction between the V_H and V_L chains, and consequently the relative position of the complementarity-determining regions, can influence the specificity and affinity of the CAR toward its target antigen. Crucially, the affinity of the scFv for the target antigen serves as a fundamental determinant of CAR function, requiring sufficient strength to effectively identify tumour cells, induce CAR signalling, and activate T-cells. Nonetheless, excessively high affinity may trigger activation-induced cell death (AICD) in the CAR-expressing cell, potentially resulting in toxicities. Moreover, the utilization of different scFvs with similar affinities for the same target protein can produce dissimilar effects on CAR-T cell function, further complicating CAR design. Another essential consideration when selecting the optimal scFv for CAR engineering is the target antigen density. For instance, utilizing a lower affinity scFv for the tumour antigen can redirect CAR-T cells to areas with increased antigen density, such as tumour cells. This strategy is particularly effective when the antigen is expressed at low levels on healthy cells [81]. Also, certain scFvs are associated with ligand-independent tonic signalling [82,83], demonstrated to diminish the efficacy of CAR-T cell therapy in preclinical models by inducing terminal effector T-cell differentiation, exhaustion, and/or AICD [83–86]. In addition to scFvs, alternative antigen-binding domains have been explored for CARs. For instance, T-cells expressing CARs with peptide domains developed de novo for binding to specific antigens [87], zetakine CARs incorporating cytokines fused to intracellular signalling domains, exemplified by those targeting the IL-13 receptor α2 (IL-13Rα2) [88] and CARs utilizing receptors such as CD27 or PD-1 to target CD70 or PD-L1 positive cells, respectively[89,90], among other innovative approaches.

The hinge and transmembrane domains (TMD) of CARs serve to link the extracellular antigen-binding domain to the intracellular signalling domain[73,76,91]. The hinge plays a crucial role by offering enough flexibility to navigate steric hindrance and providing adequate length to ensure accessibility to the target antigen. Importantly, variations in

1 | Introduction

the length and composition of the hinge can influence both antigen binding and signalling through the CAR. Long spacers provide the CAR with extra flexibility, enhancing its ability to access membrane-proximal epitopes or complex glycosylated antigens. On the other hand, CARs equipped with short hinges demonstrate greater effectiveness in binding membrane-distal epitopes [77]. Various amino acid sequences from proteins such as CD8, CD28, IgG1, or IgG4 have been employed in CAR hinge domains. However, some IgG-derived peptides may interact with Fcγ receptors (FcγRs) via their CH2 domain, resulting in off-target activation by myeloid and lymphoid cells expressing FcγRs. This interaction can lead to CAR T cell depletion and reduced persistence *in vivo* [76–78].

As a type I membrane protein, the CAR molecule requires anchoring to the plasma membrane to carry out its function efficiently [92]. The TMD, comprised of a hydrophobic α helix, serves to anchor the CAR within the T cell membrane and is typically sourced from type I proteins like CD3ζ, CD28, CD4, or CD8α. Despite being perhaps the least explored region of the CAR, emerging evidence indicates that the choice of transmembrane domain can impact the stability and functionality of the CAR [71,76,77]. CARs incorporating the CD28 TMD tend to exhibit greater stability compared to those utilizing the CD3ζ transmembrane region. However, the CD3ζ TMD facilitates CAR dimerization and integration into endogenous TCRs, potentially enhancing CAR-mediated T-cell activation. Notably, CAR-T cells equipped with CD8α hinge and TMD demonstrate reduced release of IFN-γ and TNF and are less susceptible to AICD compared to those with CD28-derived domains [78].

The intracellular signalling domain typically includes an activation domain and one or more co-stimulatory domains (Fig. 1.7). This element delineates the evolution of CAR-T cells into three generations. In the first-generation, CAR-T cell activation mainly starts with immunoreceptor tyrosine-based activation motifs (ITAMs) from CD3ζ [76], but signalling solely via these motifs was inadequate for eliciting productive T-cell responses [93]. In this line, the provision of a co-stimulatory signal has proven essential for promoting optimal T cell function, metabolism, and long-term persistence. T-cells transduced with CARs incorporating co-stimulatory domains alongside activation domains (second-generation), demonstrate the ability to produce IL-2 and undergo

proliferation upon repeated exposure to antigen[94,95]. Among the most extensively investigated co-stimulatory domains are those derived from CD28 or 4-1BB (CD137), and all CAR-T cell products approved by the FDA to date incorporate either one of these domains. While CD28-domain CAR-T cells and 4-1BB-domain CAR-T cells exhibit high response rates in patients, they display distinct functional and metabolic profiles [85,94–97]. T-cells expressing CARs with CD28 domains signal through the phosphatidylinositol 3-kinase (PI3K)-Akt pathway, resulting in elevated IL-2 production, differentiation into effector memory T-cells, and a preference for aerobic glycolysis. In contrast, CAR-T cells containing 4-1BB domains signal through the recruitment of TNF receptor-associated factor (TRAF) proteins, differentiate into central memory T-cells, and demonstrate increased mitochondrial biogenesis and reliance on oxidative metabolism [98–100]. T-cells engineered with CARs featuring alternative co-stimulatory domains have shown promise in preclinical models but await clinical testing. These domains include MYD88, CD40, OX40, ICOS, CD27 and KIR2DS2, and they share similarities with CD28 and 4-1BB costimulatory domains — ICOS belongs to the same family as CD28, and OX40 and CD27 belong to the same TNF receptor family as 4-1BB —. Notably, CD27 signalling enhances CAR T cell survival compared to CD28 [101], while incorporating ICOS promotes a Th1/Th17 phenotype in CD4+ T cells, enhancing helper functions and improving *in vivo* T-cell persistence [102]. Combining the advantageous properties of various intracellular domains within a single T cell is achievable through the development of third-generation CARs. These constructs often integrate one intracellular domain from the CD28 family with another from the TNFR family, facilitating simultaneous activation of diverse signalling pathways. While third-generation CARs typically exhibit lower expression levels compared to their second-generation counterparts, they often demonstrate enhanced effector functions [96,102]. Nonetheless, their clinical advantages remain unclear [76]. It is noteworthy that most studies comparing costimulatory domains have focused on CD4+ helper and CD8+ cytotoxic T cells, and the functionality of costimulatory domains varies depending on the subtype of T-cell [103,104].

Fourth-generation CARs, also known as T-cells redirected for universal cytokine-mediated killing (TRUCKs) or “armoured CARs” are designed to not only express the CAR but also to secrete specific cytokines either continuously or upon CAR engagement (Fig.

1 | Introduction

1.7)[105]. CAR-TRUCKS contribute to creating a proinflammatory milieu within solid tumours. They achieve this by releasing various cytokines, such as IL-7, IL-12, IL-15, IL-18, IL-23 or IL-36γ [106–110]. These cytokines can either act directly on the CAR-T cell itself or in a paracrine manner, drawing innate immune cells to the tumour site[111]. Alternatively, armoured CARs have the capability to secrete other proteins, such as checkpoint inhibitors or nanobodies, to bind to secondary targets[112,113]. Lastly, fifth-generation CARs (Fig. 1.7), much like their fourth-generation counterparts, are built upon the foundation of second-generation design. Yet, they innovate by incorporating truncated intracellular domains from cytokine receptors, which help boost JAK-STAT signalling. Consequently, fifth-generation CARs can deliver all three activation signals found in natural T cells: TCR engagement, co-stimulation, and cytokine engagement. This broader activation approach leads to better persistence *in vivo* and an improved antitumor response against both liquid and solid tumours compared to second-generation CARs [114].

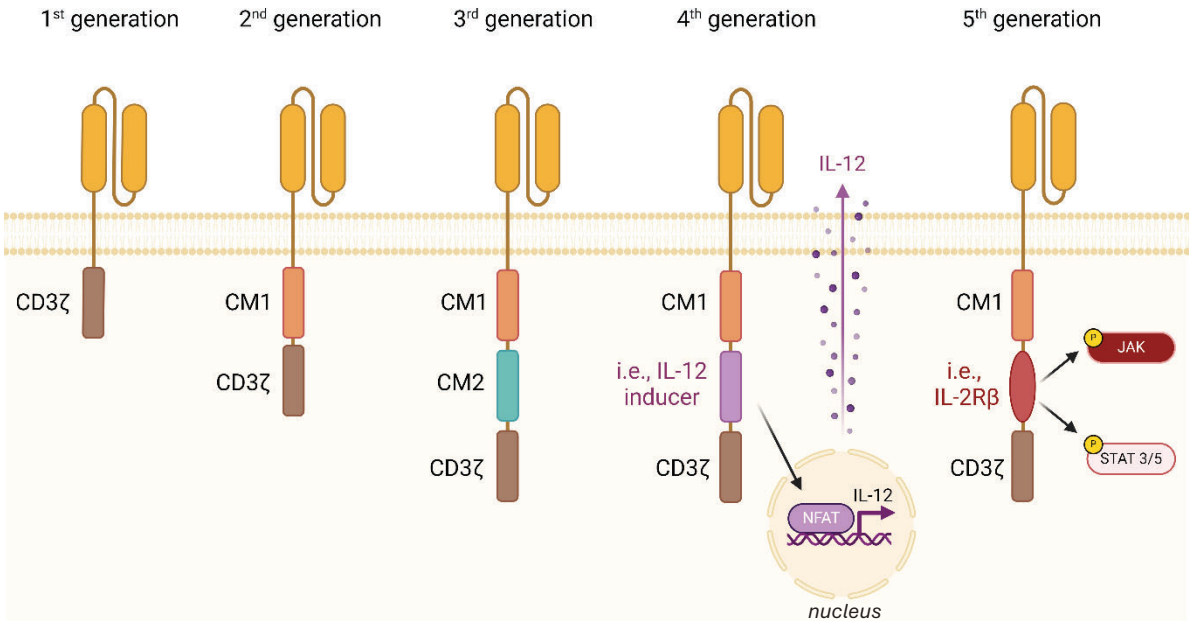

Figure 1.7 | Structural evolution of different generations of CAR constructs. First generation of CAR-T cells only incorporated ITAM motifs within the intracellular domain. The second generation introduced a single co-stimulatory molecule (CM1), while the third generation expanded upon this by integrating a second CM (CM2). The fourth generation of CARs was developed by building upon second-generation CARs, which contained 1–3 ITAMs, and pairing them with a chemokine (i.e., IL-12) expressed either constitutively or inducible. These engineered T-cells, also known as T-cells redirected for universal cytokine-mediated killing

(TRUCKs), aimed at bolstering antitumor efficacy. The fifth generation, also known as the 'next generation', retained the structural framework of second-generation CARs. However, it includes intracellular domains sourced from cytokine receptors (i.e., IL-2Rβ chain fragment). CM, co-stimulatory molecule; IL-12 activation of interleukin 12 transcription within the nucleus; IL-2Rβ truncated intracellular interleukin 2β chain receptor with a STAT3/5 or JAK phosphorylated. Adapted from [105]. Created with BioRender.com

1.3. CAR-T cells in haematological malignancies

The most significant clinical responses achieved with CAR-T cells thus far have been predominantly observed in patients diagnosed with specific haematological malignancies, particularly those expressing CD19 or B cell maturation antigen (BCMA)[70,115].

CD19 is a 95 kD type I transmembrane protein which extends across the plasma membrane. Its expression initiates during the pro-B cell stage, persisting until terminal plasma cell differentiation. CD19 is prevalent in most B-lineage lymphomas and leukaemia's, making it an ideal surface target antigen for CD19-targeted CAR-T cell therapy [116]. During the 2000s, the initial success of CD19 CAR-T cell therapy was demonstrated in xenograft mouse models, where first-generation CD19ζ CAR-T cells effectively eradicated CD19+ human leukaemia and lymphoma cells[117]. In 2010, the first clinical case report involved a second-generation CD19-28ζ CAR in a patient diagnosed with follicular lymphoma (FL) at the NCI. This was followed by successful treatments of patients with refractory chronic lymphocytic leukaemia (CLL) and relapsed B-cell acute lymphoblastic leukaemia (B-ALL) at Memorial Sloan Kettering Cancer Center[118]. A critical breakthrough came in 2011, when Dr. Carl June's team at the University of Pennsylvania reported that three adult patients with advanced CLL achieved complete or partial remission after receiving CD19-specific CAR-T cell therapy[119]. Consistent clinical success in the following years were also observed in B-ALL, with complete and durable responses reported in both adult and paediatric patients [120–122]. These achievements culminated in the FDA approval in 2017 of the first CD19-targeted CAR therapy — Tisagenlecleucel (Kymriah) — for relapsed or refractory (r/r) B-ALL in children and young adults [123] as well as refractory diffuse large B-cell lymphoma [124] marking it as the first FDA-approved cancer treatment modality based on genetic engineering of cells

1 | Introduction

(Table 1.1). Axicabtagene ciloleucel (Yescarta) was soon after approved for patients with r/r DLBCL [125]. In 2018, these therapies were approved in Canada and by the European Medical Agency (EMA) in the European Union and the United Kingdom. As of April 2024, long-term follow-up studies continue to underscore the enduring efficacy of CD19 CAR-T cell therapy[126,127], with notable cases like Emily Whitehead, the pioneering paediatric patient who remains cancer-free 12 years after treatment[128]. Furthermore, the FDA has approved additional CAR-T cell products targeting CD19, expanding treatment options for patients (Table 1.1). Among these, rexucabtagene autoleucel (Tecartus), approved for the treatment of mantle cell lymphoma (MCL) [129] and ALL[130], and lisocabtagene maraleucel (Breyanzi), approved for various types of r/r large B-cell lymphoma (LBCL)[131] (Table 1.1).

Other CAR T cell products that have received approval are those designed to target BCMA. BCMA, also known as TNFRSF17, is a member of the tumour necrosis factor receptor superfamily and plays a crucial role in the survival and proliferation of plasma cells. It is expressed preferentially by mature B lymphocytes, with minimal expression in hematopoietic stem cells or nonhematopoietic tissue. BCMA-directed CAR-T cell products, such as idecabtagene vicleucel (ide-cel) and ciltacabtagene autoleucel (cilta-cel), have demonstrated impressive efficacy in clinical trials, leading to their approval by regulatory authorities for treating patients with relapsed/refractory multiple myeloma (MM). Idecabtagene vicleucel (ide-cel) achieved an overall response rate (ORR) of 73%, with 33% of patients attaining a complete response (CR) and a median progression-free survival (PFS) of 8.8 months. Similarly, ciltacabtagene autoleucel (cilta-cel) exhibited an ORR of 97%, with 67% of patients achieving a stringent complete response (sCR) and a median duration of response (DOR) of 21.8 months[70,130].

Following the clinical success of CD19 and BCMA CAR-T cell, other B cell-specific surface markers were targeted to combat B cell malignancies. Anti-CD20 and anti-CD22 CAR T cell trials have demonstrated similar response rates in non-Hodgkin lymphoma (NHL) and B-ALL, respectively, compared to anti-CD19 CAR-T cell therapy (Table 1.1). CAR-T cell therapies targeting T-cell haematological diseases are also under clinical investigation, targeting molecules such as CD7 or CD30 (Table 1.1).

Target	Disease	Response rate*	Survival	Comments	Date of FDA approval	Refs.
CD19	B-ALL	CR or CRi: 81%	EFS: 50% OS: 76% at 12 months	Tis-cel approved for R/R B-ALL (≤25 yr of age)	2017 (August)	[123]
CD19	LBCL	CR: 58%	PFS: 44% at 12 months OS: 52% at 18 months	Axi-cel approved as 3rd line treatment for LBCL (>18 yr of age)	2017 (October)	[125]
CD19	LBCL	CR: 40%	RFS: 65% OS: 49% at 12 months	Tis-cel approved as 3rd line treatment for LBCL (>18 yr of age)	2018 (May)	[124]
CD19	MCL	CR: 67%	PFS: 61% OS: 83% at 12 months	Brex-cel approved for R/R MCL (>18 yr of age)	2020 (July)	[129]
CD19	FL	CR: 74%	PFS: 65% OS: 87% at 18 months	Axi-cel approved as 3rd line treatment for R/R FL (>18 yr of age)	2021 (March)	[132]
CD19	LBCL	CR: 53%	PFS: 44% OS: 58% at 12 months	Liso-cel approved for 3rd line LBCL (>18 yr of age)	2021 (February)	[131]
BCMA	MM	CR: 33%	Median PFS: 8.8 months OS: 78% at 12 months	Ide-cel approved for 5th line treatment for MM (>18 yr of age)	2021 (March)	[70]
CD19	B-ALL	CR: 56%	RFS: 58% at 6 months OS: 71% at 12 months	Brex-cel approved for R/R B-ALL (>18 yr of age)	2021 (October)	[130]
BCMA	MM	sCR: 67%	PFS: 77% OS: 89% at 12 months	Cilta-cel approved for 5th line MM (>18 yr of age)	2022 (February)	[133]
CD19	FL	CR: 69%	PFS: 67% at 12 months	Tis-cel approved for 3rd line treatment of FL (>18 yr of age)	2022 (May)	[134]
CD19	LBCL	(Axi-cel vs SOC) CR: 65 vs 39%	(Axi-cel vs SOC) EFS: 41% vs 16% OS: 61% vs 52% at 24 months	Axi-cel approved as 2nd line treatment for LBCL (>18 yr of age)	2022 (April)	[135]

1 | Introduction

CD19	LBCL	(Liso-cel vs SOC) CR: 66 vs 39%	(Liso-cel vs SOC) EFS: 45% vs 24% OS: 79% vs 64% at 12 months	Liso-cel approved as 2nd line treatment for LBCL (>18 yr of age)	2022 (June)	136
CD19	LBCL	CR: 78%	PFS: 75% OS: 91% at 12 months	Front line therapy for high-risk LBCL		137
CD22	B-ALL	CR: 70%	Median RFS: 6 months Median OS: 13.4 months	CD19-CAR T cell therapy had failed in 88% of these patients		138
CD22	LBCL	ORR: 86% CR: 67%	Median PFS: not reached	CD19-CAR T cell therapy had failed in 95% of these patients		139
CD30	HL	CR: 59%	PFS: 36% OS: 94% at 12 months	Greater CD30 CAR T persistence and higher PFS with fludarabine-based LD		140
CD7	T-ALL	CR: 90%	n.a.	Allogeneic donor-derived CD7-CAR T cells; GVHD grade 1–2 in 60% of patients		141
CD7	T-ALL or TLBL	CR: 7/8	n.a.	Autologous CD7-CAR T cells rendered fratricide-resistant using a CD7 PEBL		142
CD38	AML	CR or CRi: 4/6	50% relapse rate at 6 months	Allo-HSCT refractory patient population; no off-target effects on monocytes or lymphocytes		143
κ light chain	NHL, CLL, or MM	CR: 2/9	n.a.	Limited pre-treatment LD. One CR sustained for at least 3 yr		144
CD20	LBCL	CR: 54.5%	PFS 41.7% at 24 months	All patients had prior rituximab; longest CR at least 57 months		145

Table 1.1 | Targets of CAR T cell therapies for haematological malignancies with clinical evidence of efficacy. *If fewer than ten patients were treated, absolute response numbers are provided as a fraction; otherwise, they are provided as the percentage response rate. Allo-HSCT, allogeneic haematopoietic stem cell transplant; ALL, Acute lymphoblastic leukaemia, AML, acute myeloid leukaemia; CAR, chimeric antigen receptor; CD, cluster of differentiation; CLL, chronic lymphocyte leukaemia; CR, complete response; CRi, complete response with incomplete haematologic recovery; CRS, cytokine release syndrome; EFS, event-free survival;

FL, follicular lymphoma; GVHD, graft-versus-host disease; HL, Hodgkin lymphoma; IV, intravenous; LD, lymphodepletion; MCL, mantle cell lymphoma; MM, multiple myeloma; NHL, non-Hodgkin lymphoma; ORR, overall response rate; OS, overall survival; PEBL, protein expression blocker; PFS, progression-free survival; RFS, relapse-free survival; R/R, relapsed or refractory; sCR, stringent complete response; TLBL, T cell lymphoblastic lymphoma. Axi-cel, axicabtagene ciloleucel; brex-cel, brexucabtagene autoleucel; cilta-cel, ciltacabtagene autoleucel; ide-cel, idecabtagene vicleucel; liso-cel, lisocabtagene maraleucel; tis-cel, tisagenlecleucel. Adapted from [71].

1.3.1. Limitations of CAR-T cell therapy in haematological malignancies

Despite accumulating over 15 years of clinical experience, challenges continue to persist in the CD19 CAR therapy field. While response rates typically range from 50-80%, a subset of patients shows no response to autologous CAR-T cell therapy [146]. The primary mechanisms observed in haematological malignancies include CAR T-cell associated toxicities, antigen escape and insufficient T-cell persistence [78,91].

From a mechanistic standpoint, major toxicities associated with CAR T cell therapy can be broadly categorized into two distinct types. Firstly, general toxicities arise due to T cell activation, leading to the systemic release of heightened cytokine levels (referred to as systemic toxicities). Secondly, specific toxicities result from interactions between the CAR and its target antigen, expressed not only by malignant cells but also by non-malignant cells, termed as on-target, off-tumour effects [74,78,147].

Patients enrolled in numerous clinical trials, including all successful trials involving anti-CD19 CAR-T cells, have experienced severe and, in some cases, fatal increases in systemic cytokine levels [148]. These toxicities encompass cytokine-release syndrome (CRS), hemophagocytic lymphohistiocytosis (HLH), and/or macrophage activation syndrome (MAS), alongside a specific neurotoxicity termed immune effector cell-associated neurotoxicity syndrome (ICANS) [149].

CRS represents a systemic inflammatory reaction triggered by cytokine release from infused CAR-T cells potentially culminating in organ dysfunction. It stands as the most prevalent type of toxicity associated with CAR-T therapy. Typically, CRS can be clinically managed with tocilizumab (an anti-IL-6 receptor antibody), siltuximab (an anti-IL-6 antibody) or corticosteroids. CAR T-induced HLH/MAS is a rare, severe

1 | Introduction

hyperinflammatory syndrome diagnosed based on CRS symptoms and elevated serum ferritin and liver enzymes, hemophagocytosis, cytopenias, renal failure, pulmonary oedema, splenomegaly, and/or reduced NK cell activity. Treatment may involve chemotherapy if refractory to IL-6 pathway inhibition. ICANS is linked with blood-brain barrier disruption and increased cerebrospinal fluid cytokine levels. It may manifest as aphasia, altered mental state, tremors, headaches, and life-threatening cerebral oedema, often coinciding with or following CRS [150]. ICANS management may include corticosteroids and/or IL-6 pathway inhibitors if CRS symptoms are present along with adjunctive and supportive treatments for neurological symptoms [148].

Maintaining a balance between achieving effectiveness and reducing side effects is crucial in CAR-T cell therapy. This equilibrium is reached by ensuring that CAR-T cells are activated and release cytokines at an appropriate level, thereby avoiding excessive cytokine production. Various factors, including tumour size, antigen levels on cancer cells, CAR's ability to bind to the target antigen, and the presence of co-stimulatory elements within the CAR [151]. Therefore, the optimal activation threshold for CAR T cells varies between different CAR constructs. Nonetheless, to refine their activation, various components of the CAR can be modified, such as the choice of the costimulatory domain or engineering the CAR's components [152,153]. In addition to cytokine storms triggered by activated CAR-T cells, immune responses to CAR constructs by host immune cells can contribute to cytokine-related toxicities. Strategies to mitigate these toxicities include using human or humanized antibody fragments for CAR construction and modifying the extracellular hinge region and/or transmembrane domain to reduce immunogenicity [154]. Alternatively, CARs can be engineered to recognize bi-specific adapter molecules, linking CAR-T cells and cancer cells [155]. Another approach involves integrating 'off switches' or 'suicide genes' into CAR constructs to deactivate CAR-T cells. Recently, the use of synthetic biology has enabled the control of CAR-T cell activation through the application of logic-gating principles of electric circuits by combining regulatory elements like promoters, repressors, enhancers and regulated genes. These genetic circuits can then be integrated into T cells to address safety concerns through various approaches, such as killing switches, adapter switches, small-molecule drug switches[156]. Among them, the

use of iCas9 switches have shown high effectiveness and have been the subject of numerous clinical trials [157–159].

The on-target, off-tumour toxicity arises from the direct attack on normal tissues expressing the targeted antigen. In CD19 CAR-T cell therapies, this toxicity arises from the CAR T cell-mediated eradication of CD19+ B cell progenitors in the bone marrow, leading to B cell aplasia and subsequent hypogammaglobulinemia. However, this condition is generally non-life-threatening and can be managed effectively with periodic infusions of intravenous immunoglobulins. In addition, it has been reported that brain mural cells express CD19, suggesting a potential on-target mechanism for neurotoxicity in CD19-directed therapies[160]. Technologies aimed at reducing on-target, off-tumour toxicities could open avenues for developing more clinically effective CAR therapies, and several approaches are currently under development. Some of these strategies involve targeting antigens that are more specific to the tumour, optimizing the CARs interaction with cancer cells compared to non-malignant cells by introducing requirements for multiple antigens or the absence of a specific antigen and by limiting the spatial and temporal activity of CARs, as mentioned earlier [156].

Antigenic escape—defined as the complete or partial loss of target antigen expression by cancer cells—is observed in a significant proportion of patients treated with CAR-T cells [161]. To address this challenge, various combinatorial strategies targeting multiple antigens are being currently explored. One approach relies on the development of multi-target CAR-T cell therapies, which can be achieved by mixing different CAR-T cell products targeting single antigens before infusion or by transducing T-cells with multiple CAR constructs [162]. Alternatively, bi-specific CAR-T cells can be engineered, combining a single CAR molecule with two or more distinct binding domains. Clinical efficacy has been demonstrated with CD19/CD20 or CD19/CD22 bi-specific CAR-T cells in patients with B cell malignancies [163–165]. Another strategy involves modifying CAR-T cells to secrete bi-specific T-cell engagers (BiTEs). BiTEs typically consist of two scFvs, one specific to CD3 and the other to a TAA, connected by a flexible linker. These agents physically link a T cell to a cancer cell [166]. BiTE-secreting CAR-T cells effectively overcome antigen expression heterogeneity and prevent antigen escape [167], as

1 | Introduction

exemplified by the FDA-approved CD19-targeted BiTE, blinatumomab, for the treatment of ALL [168]. Furthermore, the use of 'armoured' CARs, which are engineered with immunomodulatory agents to engage and modulate other cells of the host's immune system is actively being investigated. For instance, incorporating the proinflammatory molecule CD40 ligand (CD40L) into CAR-T cells can activate professional APCs and augment the immunogenicity of tumour cells via CD40 engagement [169]. Clinical trials are currently underway to evaluate this approach [170].

Finally, a lack of persistence of therapeutic CAR-T cells has also been associated with treatment failure. To improve CAR-T cell persistence in patients, various strategies are currently being explored. One promising approach is the use of T-cell populations enriched with higher percentages of less differentiated T cell subsets, such as naive T cells, stem cell memory T (T_{SCM}) cells, and central memory T (T_{CM}) cells [76,78,171]. These subsets have demonstrated superior proliferative capacity compared to traditional CAR-T cell products [172,173] and are at present under evaluation in a clinical trial [174]. Moreover, administering CAR-T cells to patients at a defined 1:1 CD4+ to CD8+ T cell ratio has shown to result in dose-related increases in CAR-T cell expansion and reduced toxicities [175]. Several other methods are being refined to avoid T-cell differentiation in CAR-T cell therapy, as naive and memory T cells persist longer than effector T-cells[176]. One strategy focuses on optimizing conditions during the expansion phase of CAR-T cell production, either by multiple combinations of cytokines (like IL-7, IL-15, and IL-21 [177–179]), which significantly impacts their differentiation and effectiveness [180] or/and by manipulating key regulators of cell metabolism, such as glucose levels [181], with different drugs and molecules (i.e., PI3K-AKT-mTOR inhibitors, epigenetic drugs, and metformin) [182–184]. Another method employs genetically engineering of CAR-T cells to introduce positive immune factors such as interleukins and chemokine receptors [109,185,186], along with regulators of TCR signalling and downstream pathways [187–189]. All these approaches offer promising avenues for enhancing the therapeutic potential of CAR-T cell therapy.

1.4. CAR-T cells in solid tumours

The success of CAR-T cells in hematologic cancers underscores their potential in addressing the challenges posed by solid tumours, which account for over three-quarters of cancer-related deaths. However, achieving similar clinical responses in non-hematopoietic solid cancers presents a significant hurdle. Despite this, recent works provide clear evidence of objective antitumor responses in patients with hard-to-treat solid tumours [158,159,190] (Table 1.2). In fact, the most promising responses in solid tumours to date were observed in a clinical trial conducted by Del Bufalo and colleagues at Ospedale Pediatrico Bambino Gesù, using CAR-T cells targeting GD2 in neuroblastoma patients. Nine out of seventeen participants experienced a complete response, eight had a partial response and the three-year overall survival rate reached 60% [158]. Another promising clinical trial conducted by Changsong Qi and colleagues at Peking University Cancer Hospital has shown promising efficacy against gastric cancer using Claudin18.2-specific CAR T cells. Results from the phase I trial showed an overall response rate (ORR) of 48.6%, a disease control rate (DCR) of 73.0% and a six-month overall survival rate of 81.2%[190]. Unfortunately, in terms of clinical responses, antitumour activity has generally been limited (Table 1.2).

Target	Disease	Response rate*	Survival	Comments	Refs.
CD133	HCC, PDAC and CRC	3-month disease control rate was 65.2%	Median PFS: 5 months	Toxicities were self-recovered within 1 week	[191]
MUC1	NSCLC	11/20 stable disease and 9/20 progressive disease	n.a.	Anti-MUC1 CAR-T cells with PD-1 KO. No grade 3-5 AEs and CRS was observed.	[192]
MUC1	EC	6/9 stable disease and 3/9 progressive disease	2 patients with multiple CAR-T cycles OS: 24 months	Anti-MUC1 CAR-T cells with PD-1 KO. No grade 3-5 AEs and CRS was observed	[193]
GD2	NB	CR: 27% of patients with active disease	Median OS: 31 months	1st generation CAR expressed by EBV-reactive T-cells; one patient had sustained CR for at least 60 months	[194]

1 | Introduction

GD2	NB	OR: 63%	OS: 60% at 3 yrs	9/17 CR and 8/17 PR. 74% of CRS, 95% mild	[158]
GD2	DMG	9/10 patients with radiographic or clinical benefit	n.a.	Initial IV infusion followed by multiple ICV infusions; one patient had >95% reduction in tumour volume	[159]
GPC3	HCC	1/13 stable disease alive for 44.2 months and 2/13 partial responses	OS: 10.5% at 3yrs, 42% at 1yr and 50.3% at 6 months	Autologous CAR-GPC3 T-cell therapy following cyclophosphamide- and fludarabine-induced LD One patient experienced grade 5 CRS	[195]
HER2	Sarcomas	CR: 27%	n.a.	No on-target, off-tumour toxicity of HER2-CARs; patient with metastasis to bone marrow had a CR for >12 months	[196]
HER2	GBM	1/16 partial response for >9 months 7/16 stable disease and 8/16 progressed	Median OS: 11.1 months from 1st T-cell infusion	HER2-specific CAR–modified virus-specific T cells. No dose-limiting toxic effects	[197]
IL13Rα 2	GBM	Disease control rate: 50% (29/58)	Median OS: 7.7 months	2 PR, 1 CR and a second CR after additional CAR-T cycles off protocol.	[198]
EGFR	BTC	CR: 6%	Median PFS: 4 months	One out of 17 patients achieved a CR for at least 22 months. Manageable mucosal toxicities	[199]
EGFRv III	GBM	anti-EGFRvIII CAR-T cells did not demonstrate clinically meaningful impact	OS: 6.9 months Median PFS: 1.3 months	2/18 severe hypoxia, one fatal	[200]
Meso	MDP	OS: 83% at 1yr Median OS: 23.9 months	11% complete metabolic response by PET	Regionally delivered intrapleural CAR-T cell administration plus PD-1 blockade	[201]

Meso	MPM, OC, PDAC	OR: stable disease 11/15 patients	n.a.	Grade 4 sepsis in one patient	202
c-MET	mM and mTNBC	4/7 stable disease 3/7 disease progression	n.a.	cMet RNA CAR T cells	203
CEA	Liver metastasis	Median OS: 8 months 1 case of complete metabolic response by PET sustained for 13 months	n.a.	CAR-T cells were administered via hepatic artery infusion using pressure-enabled drug delivery + systemic IL-2. No grade 4 or 5 toxicities were observed	204,205
CLDN-18.2	GC or PC	OS: 81% at 6 months ORR: 48.6% Disease control rate: 73.0%	Median PFS: 3.7 months	83% of patients showed tumour regression; 11% showed reversible grade 3/4 gastro-intestinal toxicities	190
CLDN-6	relapsed/refractory CLDN-6^{+}	ORR: 31%, including 1 CR Disease control rate: 67%	n.a.	Anti CLDN-6-CAR-T cells + RNA vaccine Manageable toxicity	206
PSMA	MCRPC	5/13 patients had >30% reduction in PSA	Median PFS: 4.4 months Median OS: 15.9 months	PSMA CAR T cells expressing a dominant-negative TGFβRII. 5/13 patients with high-grade CRS, one fatal	170

Table 1.2 | Targets of CAR T cell therapies for solid tumours with clinical evidence of efficacy. *If fewer than ten patients were treated, absolute response numbers are provided as a fraction; otherwise, they are provided as the percentage response rate. AEs, adverse events; BTC, biliary tract cancer; CAR, chimeric antigen receptor; CEA, carcinoembryonic antigen; CD133, prominin I; CLDN6, claudin-6; CLDN18.2, claudin-18.2; CR, complete response; CRC, colorectal carcinoma; CRS, cytokine release syndrome; DMG, diffuse midline glioma; EC, oesophageal carcinoma; EGFR, epidermal growth factor receptor; GBM, glioblastoma; GC, gastric cancer; GD2, disialoganglioside; GPC3, glypican 3; HCC, hepatocellular carcinoma; HER2, human epidermal growth factor receptor 2; ICV, Intracerebroventricular; IL-2, interleukin 2; IV, intravenous; KO, knockout; LD, lymphodepletion; MCRPC, metastatic castration-resistant prostate cancer; Meso, mesothelin; mM, metastatic melanoma; MPD, malignant pleural disease; MPM, Malignant pleural mesothelioma mTNBC, metastatic triple-negative breast cancer; MUC, mucin; N.A., not applicable; NB, neuroblastoma; NSCLC, non-small cell lung cancer; PSMA, prostate-specific membrane antigen; OC, ovarian cancer; ORR, overall response rate; OS, overall survival; PC, pancreatic cancer; PD-1, programmed cell death ligand-1; PDAC,

1 | Introduction

pancreatic ductal adenocarcinoma; PET, positron emission tomography; PFS, progression-free survival; PSA, prostate-specific antigen; PSMA, prostate-specific membrane antigen; RNA, ribonucleic acid; TGFβRII, transcription growth factor beta receptor two; TNBC, triple-negative breast cancer. Adapted from [71].

In this work, our primary focus has been on the application of CAR-T cells in oncology, nevertheless, it's worth noting the recent promising outcomes in treating autoimmunity, chronic infections, cardiac fibrosis, senescence-associated diseases, and various other conditions [207–209].

1.4.1. Limitations of CAR-T cell therapy in solid tumours

In addition to the constraints outlined in section 1.3.1 regarding the limitations of CAR-T cell therapy in haematological malignancies, the application of CAR-T cells to target solid tumours encounters further obstacles that must be overcome to generate an effective anti-tumour response [210] (Fig. 1.8). First, the antigenic diversity inherent in solid tumours, which endows them with an effective mechanism to evade recognition by CAR-T cells. Conventional CAR-T cells are engineered to target a single antigen, rendering them incapable of identifying all cancerous cells within a tumour. Moreover, although initially effective in producing high response rates, a significant portion of patients treated with these single antigen-targeting CAR-T cells eventually experience either partial or complete loss of target antigen expression in malignant cells.

Secondly, the vasculature surrounding solid tumours is weakened and exhibits altered flow, hindering the trafficking of immune cells to the tumour site. Additionally, once immune cells reach the tumour, they often encounter physical barriers, such as cancer associated fibroblasts (CAFs) and collagen-rich stroma, which effectively prevent T-cell infiltration [211]. Finally, T-cells must also persist in a highly immunosuppressive and nutrient-restricted TMEs, characterized by cellular, molecular, and metabolic profiles that ultimately induce T-cell exhaustion and dysfunction [212]. Thus far, CAR-T cells have been insufficiently equipped to overcome these additional obstacles presented by solid tumours, prompting current research efforts to focus on surmounting these challenges [91,213,214].

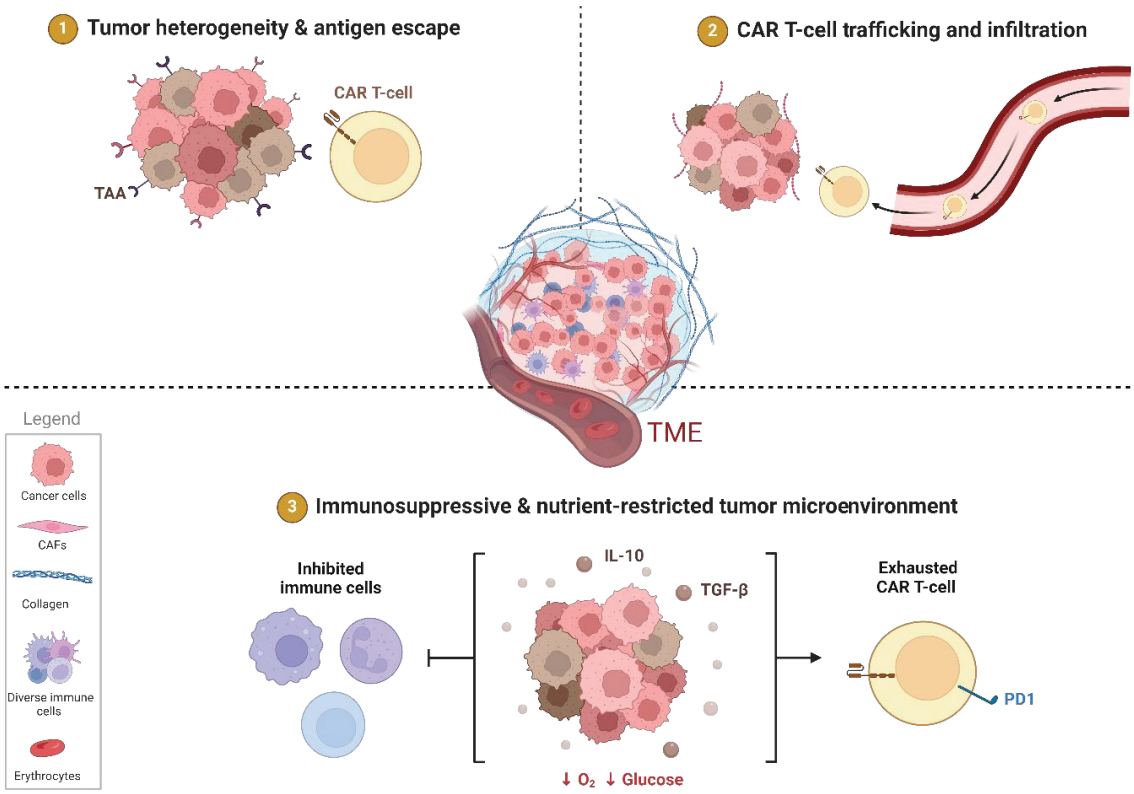

Figure 1.8 | Challenges for CAR T-cell immunotherapy in solid tumours. The limited success of CAR T-cell therapy in solid tumours can be accounted to many challenges, including: (1) the heterogeneous expression of TAA, leading to outgrowth of antigen-negative tumour variants; (2) inefficient trafficking of CAR T cells to tumour sites and (3) the metabolically hostile tumour microenvironment that includes the presence of immunosuppressive molecules (TGFβ, IL-10, PD-1, etc.) and cells (T-regs, MDSCs, etc.) and can lead to CAR T-cell exhaustion. CAF, Cancer associated fibroblast; CAR, Chimeric Antigen Receptor; IL-10, Interleukin-10; MDSCs, Myeloid derived suppressor cells; O_2, oxygen; PD1, Programmed cell death protein-1; TAA, Tumour associated antigen; TGFβ: Transforming growth factor beta; TME, tumour microenvironment; T_{regs}, Regulatory T-cells. Created with BioRender.com

An essential factor in overcoming antigenic diversity in solid tumours lies in the selection of target antigens, and this challenge is exacerbated by the lack of truly unique tumour-specific target antigens [215]. The optimal tumour antigen should exhibit high and uniform expression on tumour cells while being absent in healthy tissues. However, most tumour antigen targets identified thus far, for both haematological and solid malignancies, display shared expression in subsets of healthy cells, heightening the risk of on-target, off-tumour toxic effects [213,216]. For example, early trials at Erasmus University documented cholestasis in renal cell carcinoma patients receiving CAR-modified T cells targeting carbonic anhydrase IX (CAIX), expressed on bile duct epithelial cells[217]. Likewise, low ERBB2 expression on lung epithelia potentially

1 | Introduction

contributed to fatal lung toxicity observed in another reported case[218]. However, HER2-targeted CARs used in trials of patients with sarcoma have been better tolerated, with no reported CRS or ICANS[219]. To mitigate the risk associated with targeting antigens which are associated with, but not exclusive to, tumour cells, several engineering strategies have been devised to enhance the specificity of CAR-T cells or tune their affinity, as outlined in chapters 1.3.1 and 1.4.1.2, respectively. Furthermore, strategies aimed at overcoming antigen heterogeneity can be categorized into three primary approaches: targeting multiple tumour antigens, engineering CAR T cells to eliminate antigen-negative tumour cells and modulating the TME to facilitate activation of the endogenous immune system, thereby enabling epitope spreading [210,214,220]. Specific methods employed are detailed in Table 1.3.

Another critical aspect that can be improved is the CAR-T cell trafficking and infiltration into the solid mass. Unlike disseminated, circulating tumours, solid malignancies pose a physical barrier that excludes T-cells through a complex network of molecular and cellular mechanisms. This barrier is frequently reinforced by the downregulation of critical T cell recruiting chemokines or adhesion molecules essential for extravasation [213,221]. Additionally, a significant issue often overlooked is the potential redirection of CAR-T cells towards lymphoid tissues rather than solid tumours. Current CAR-T cell manufacturing is influenced by trials focused on CD19-targeted therapies for B cell leukaemia or lymphoma, stressing the importance of lymph node and/or bone marrow trafficking. T-cells with high levels of CCR7 and CD62L expression tend to migrate to lymph nodes or bone marrow. Hence, current protocols aim to produce CAR-T cells predominantly of a central memory cell phenotype, which may favour lymphoid tissue homing over tumour trafficking[214].

Briefly, the process of trafficking into tumours begins with circulating T-cells identifying chemokines secreted by endothelial cells and adhered to their surfaces. These chemokines serve as a pivotal molecular determinant governing the extent of cytotoxic T-cell infiltration within solid malignancies, predominantly localized in the tumour stroma rather than regions abundant in cancer cells. [213]. After this endothelial recognition, T-cells undergo rolling adhesion mediated by selectins, followed by adhesion facilitated by integrins. Guided by chemokines (notably CXCL9, CXCL10,

CXCL11, and CCL5) T-cells transmigrate into the tumour stroma, regulated by T-cell C-C chemokine receptors (CCRs) and C-X-C chemokine receptors (CXCRs) such as CXCR3 and CCR5. However, within the tumour stroma, physical barriers are encountered, including perivascular cells, extracellular matrix proteins, and mesenchymal stromal cells, primarily CAFs [213,214]. A subset of T-cells migrates through the stromal compartment, and a minority of these cells eventually penetrate, and infiltrate regions densely populated with cancer cells, guided by chemotactic signals secreted from the TME. Inside the solid mass, CAR-T cells undertake the critical function of recognising and eliminating cancer cells, a process reliant on the interaction with intercellular adhesion molecule 1 (ICAM-1) receptor on the tumour cell surface. However, this process is highly inefficient, with only a limited number of T cells effectively interacting with tumour cells. Several factors contribute to this inefficacy[76,213,214]: Firstly, there is often a disparity between the CCRs present on CAR-T cells and the chemokines generated by solid tumours. Activated CD8+ T cells typically express CXCR3, CXCR4, and CCR5. However, many tumours produce myeloid cell-attracting chemokines instead. This discrepancy may be addressed by modifying CAR-T cells to express myeloid cell-attracting CCRs or other CCRs not commonly found on activated T-cells, and by altering the TME to attract CXCR3-expressing CAR-T cells [222]. Another major constrain are the deficiencies in adhesion receptors, which may hinder CAR-T cell penetration into the solid mass. Tumour blood vessels are frequently leaky and dysfunctional, with aberrant characteristics that contribute to tumour hypoxia. Additionally, these blood vessels are often under-expressing selectins, such as VCAM and ICAM1, essential for T-cell rolling and subsequent migration into tumours [223]. In certain cancer types, these challenges can be circumvented through more direct delivery methods, rather than conventional intravenous infusions [224]. Finally, tumours often feature a dense network of fibroblasts that produce abundant extracellular matrix, creating a physical barrier preventing T-cell infiltration into regions with higher tumour cell densities. This matrix also influences T cell function through collagen receptors like LAIR1, which can inhibit T-cell activity and modulate cytokine expression, including TGF-β. TGF-β has garnered considerable attention owing to its multifaceted role. Not only does it exert direct effects on T-cells [225], but it also orchestrates signalling pathways in stromal cells, fostering a phenotype that confers protection upon tumours against

1 | Introduction

immune surveillance [226]. To address this challenge, one approach is to engineer CAR-T cells with enzymes like heparinase or hyaluronidase to degrade the matrix [227]. Another strategy involves depleting tumour-associated macrophages (TAMs) or CAFs using CARs targeting folate receptor β (FRβ)[228] or fibroblast activation protein (FAP)[229], respectively. Among the stromal cells within the TME, CAFs have attracted attention as a promising therapeutic target due to their extensively researched role in facilitating tumour progression and impeding immune cell infiltration [230]. Alternative strategies employed to enhance the trafficking, infiltration and persistence of CAR-T cells in solid malignancies are detailed in Table 1.3.

In addition to physical barriers hindering T-cell infiltration, the TME displays biological features that are thought to contribute to progressively reduce CAR-T cell cytotoxicity, including low pH, hypoxia, nutrient deprivation and high levels of reactive oxygen species (ROS) [214]. Moreover, it is populated with suppressive cell types such as T_{Reg} cells, MDSCs and TAMs, all of which foster immune tolerance and can directly engage with CAR-T cells through inhibitory ligands expressed on their surface (e.g., PD-L1/2, B7-H3/4). Their chemokine and cytokine expression profile (encompassing TGF-β, IL-4 and IL-10) acts not only by excluding cytotoxic T cells, but also recruiting additional immunosuppressive cells and polarizing those already infiltrating the tumour site towards an inhibitory phenotype. Another critical factor contributing to CAR-T cell exhaustion in the context of solid tumours is the sustained exposure to the target antigen, which can lead to prolonged activation of CAR-T cells, ultimately resulting in functional exhaustion and diminished anti-tumour efficacy [231–233]. On top of these extrinsic, tumour-associated factors, there are others inherent to CAR-T cell therapy that can lead to hypofunction, such as epigenetic changes [234] and CAR-specific issues including the degree of tonic signalling or the expression of immune checkpoints (such as PD-1, CTLA4, TIM3, TIGIT and LAG3) on their surface.

All the problems posed by solid tumours mentioned above are being currently addressed to reinvigorate CAR-T cells through specific approaches that are listed in Table 1.3.

1 | Introduction

Problem	Solutions
Heterogeneity	• CAR T cells targeting multiple antigens (bispecific and pooled CAR-T cells) • Switch on or off CAR-T cells • Secretion of bispecific T cell engagers to engage non-targeted tumour antigens with endogenous CD3+ T cells • Secretion of agonists that will enhance cross-presentation, such as FLT3L, IL-12, type 1 IFNs or STING agonists • Condition patients with cyclophosphamide to reduce Treg levels and activate DCs • Combination of CAR-Ts with oncolytic adenoviruses or with oncolytic viruses engineered to express the truncated form of the antigen
Trafficking	• Introduce chemokine or adhesion receptors • Engineer T-cells to express enzymes capable of digesting the TME • Engineer CAR-T cells against stromal cell-associated antigens • Reduce the numbers of fibroblasts or matrix • Alter T-cell adhesion properties during expansion • Local administration instead of systemic when possible • Embedding CAR-T cells in functionalized biopolymer scaffolds • Modify CARs design, e.g., Hinge, TMD and costimulatory signalling • Alternative non-LV or RV transduction and *in vivo* delivery of CARs • Co-deliver CAR-T cells with other immunotherapeutic agents such as ICIs and STING injections • Administer CAR-T cells secreting antibodies
Persistence	• Use of optimized cytoplasmatic domains • Introduce multiple co-stimulatory domains • Use mostly undifferentiated cells (expose cells to IL-7 and/or IL-15 as opposed to IL-2 during expansion) • CAR-T ligand vaccination • Multiple injections
	• Knockdown of intracellular inhibitors • Protect from agents promoting an immunosuppressive TME such as PGE_2, adenosine or TGF-β (by introducing dominant-negative TGF-βR2 alleles) • CAR-T cells targeting T_{Regs}, MDSCs and M2-like TAMs • Metabolic/ROS-mediated protection (catalase)

1 | Introduction

Hypofunction	• Augmenting HIF in CAR T-cells, which contributes to better adaptation of CAR T-cells in hypoxic TME - HiCAR • Engineering CAR T-cells to address hypoxia-adenosinergic immunosuppression – RIAD-CAR • Protecting CAR T-cells from oxidative stress – CAR-CAT • Combining CAR T-cells with lactate dehydrogenase (LDH) blockade • Activate the TME • Introduce changes in the microbiota • Engineering CAR T-cells to express dominant-negative receptors, switch receptors or blocking antibodies • Disrupt T cell inhibitory receptors by genome editing

Table 1.3 | Approaches to augment CAR T cell efficacy in patients with solid tumours. CAR, chimeric antigen receptor; CD, cluster of differentiation; CTLA-4, cytotoxic T-lymphocyte antigen-4; DCs, dendritic cells; ICIs, immune checkpoint inhibitors; IFNs, interferons; IL, Interleukin; LV, lentivirus; MDSCs, myeloid-derived suppressor cells; PD-1, programmed death cell protein-1; PGE_2, prostaglandin E_2; ROS, reactive oxygen species; RV, retrovirus; STING, stimulator of interferon genes; TAMs, tumour associated fibroblasts; TGF-β, transforming growth factor beta; TGFβR2, transforming growth factor beta receptor 2; TMD, transmembrane domain; TME, tumour microenvironment; Treg, CD4+ T regulatory cells. Adapted from [214].

1.4.1.1. PD-1/PD-L1 axis blockade in CAR-T cell therapy

Among the strategies proposed to foster CAR-T cell function in solid tumours, one of the most extensively explored is the blockade of the PD-1/PD-L1 axis, probably due to the clinical results derived from the use of monoclonal antibody therapies targeting these checkpoints alone [235]. This axis has garnered significant attention in the field due to the success of monoclonal antibody therapies targeting these checkpoints alone. As discussed earlier, PD-1 is considered to play an important role in regulating T-cell exhaustion, and this has also been reported for CAR-T cells [236]. Initially expressed on all T-cells during activation, PD-1 expression levels decrease when the antigen is cleared. However, in the case of solid tumours where the antigen persists, PD-1 expression remains high and sustained, leading to an impaired capacity to eliminate cancer cells. Moreover, recent clinical trials have revealed that PD-L1 is upregulated on tumour cells following CAR T-cell therapy [201,237], and this overexpression has been shown to inhibit CAR-T cell function, serving as a mechanism of adaptive immune evasion [236] (Fig. 1.9).

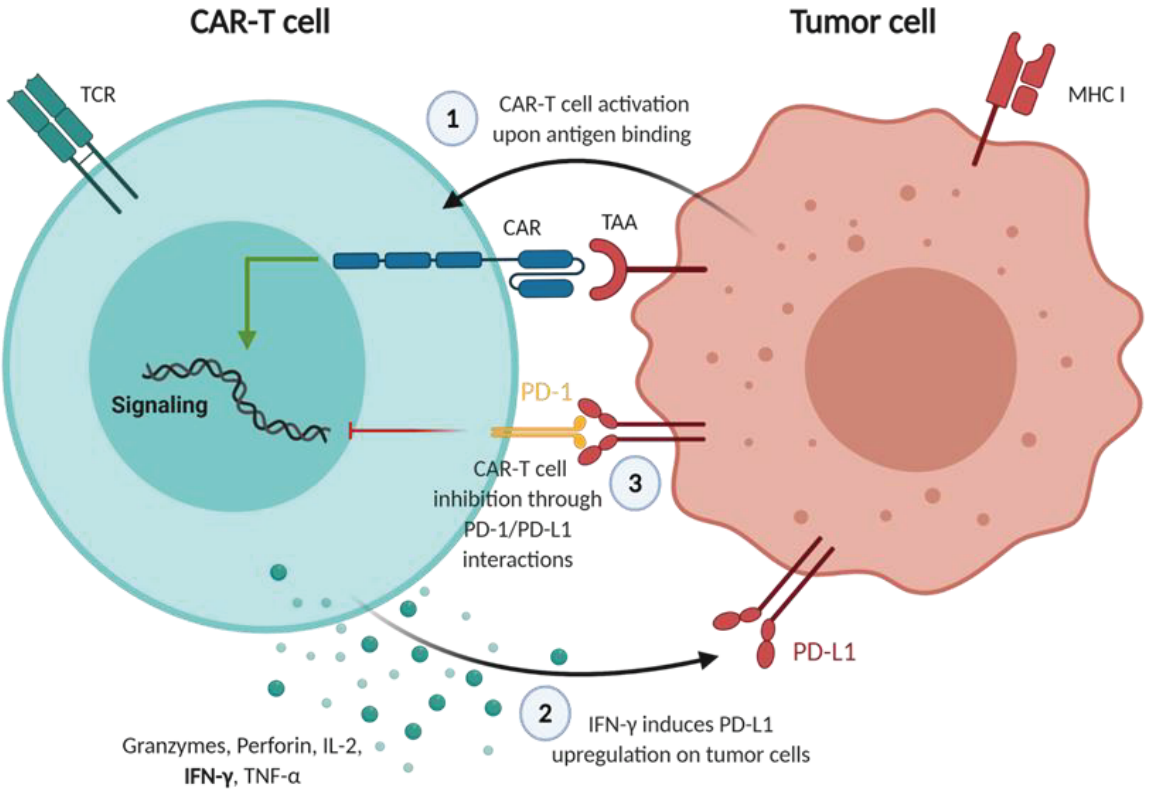

Figure 1.9 | PD-1/PD-L1 upregulation loop following CAR-T cell therapy. Upon recognition and binding of a TAA, CAR-T cells, undergo activation, triggering signalling pathways that lead to upregulation of PD-1 (1). Concurrently, CAR-T cells initiate secretion of molecules, including IFN-γ, which subsequently induces upregulation of PD-L1 expression in tumour and other immunosuppressive cells in the TME (2). Binding of CAR-T cells to PD-L1 expressed on tumour cells results in the inhibition of CAR-T cell function (3). CAR, chimeric antigen receptor; IFN-γ, interferon gamma; MHC-I, major histocompatibility complex-I PD-1, programmed cell death protein-1; PD-L1, programmed cell death ligand-1; TAA, tumour-associated antigen; TCR, T-cell receptor. Created with Biorender.com

The aforementioned success of therapies based on monoclonal antibodies that block PD-1/PD-L1 interaction would suggest that the inhibition or elimination of this molecule from CAR-T cells could prevent the acquisition of an exhausted phenotype. Consequently, several approaches have emerged to accomplish this objective, including blocking antibodies (in combination [201] or secreted by the CAR-T cells themselves [238]), downregulation of PD-1 (by shRNA-mediated knockdown [239] or by relocating PD-1 to Golgi/ endoplasmic reticulum using retention peptides [240]), genetic disruption (by TALEN [241] or CRISPR/Cas9 [242,243]) or expression of a dominant-negative receptor (DNR) [236]. Many of these approaches are currently undergoing evaluation in

1 | Introduction

clinical trials, most of them focusing on the combination of CAR-T cells with ICIs (Table 1.4).

NCT Number	Study	Conditions
NCT04581473	Efficacy, Safety and Pharmacokinetics of CT041 Autologous CAR T-cell Injection	GC, PC, GEJ
NCT04134325	PD-1 Inhibitors After CD30.CAR T Cell Therapy	r/r NHL
NCT05489991	TmPSMA-02 CAR-T cells	mCRPC
NCT04213469	PD-1-CD19-CAR-T cells	r/r BCL
NCT05812326	PD-1 KO Anti-MUC-1 CAR-T Cells	Advanced BC
NCT03179007	CTLA-4 and PD-1 Antibodies Expressing MUC1-CAR-T Cells	MUC1 + Advanced Solid Tumour
NCT04768608	PD-1 Integrated Anti-PSMA CAR-T cells	CRPC
NCT04337606	Chidamide in Combination with Decitabine in relapsed NHL After CAR therapy	NHL
NCT03287817	CD19/22 CAR T Cells (AUTO3)	DLBCL and r/r DLBCL
NCT04920617	DPX-Survivac and Pembrolizumab with and w/o Intermittent Low-dose cyclophosphamide	r/r DLBCL
NCT05631899	CAR-DC Vaccine and ICIs	Solid tumours, EphA2, KRAS G12V, G12C and G12D
NCT05631886	Combination of CAR-DC Vaccine and ICIs in Malignant Tumours	Solid Tumour, Lymphoma, EphA2 overexpression, TP53 R273H, TP53 R175H, TP53 R248Q and TP53 R249S
NCT04836507	Efficacy and Safety of CRC01	r/r LBCL, DLBCL, PMBCL, TFL
NCT06248697	MSLN-CAR T Cells Secreting PD-1/CTLA-4 nanoantibody	Advanced solid tumours
NCT03182816	CTLA-4 and PD-1 Antibodies Expressing EGFR-CAR-T Cells	EGFR + Advanced Solid Tumour
NCT03182803	CTLA-4 and PD-1 Antibodies Expressing Mesothelin-CAR-T Cells	MSLN + Advanced Solid Tumour
NCT05659628	CD19 CAR-T Expressing IL-7 and CCL19 combined with Anti-PD1	DLBCL

NCT03525782	Anti-MUC1 CAR T Cells and PD-1 Knockout Engineered T Cells	NSCLC
NCT04134325	PD-1 Inhibitors After CD30.CAR T Cell Therapy	r/r HL
NCT05732948	PD-1 Silent PSMA/PSCA Targeted CAR-T	Prostate cancer
NCT03198546	GPC3-CAR-T Cells	Cancer With GPC3 expression
NCT05155189	Armoured CAR-T Cell Injection C-CAR031	Advanced HCC
NCT04489862	αPD1-MSLN-CAR T Cells	MSLN+ Advanced Solid Tumours
NCT05979792	CD7 CAR-T Cell	r/r CD7-positive peripheral TCL
NCT02937844	Autologous Chimeric Switch Receptor Modified T Cells	Recurrent GBM multiforme
NCT04539444	CD19/22 CART Cells Combined With PD-1 Inhibitor	r/r BCL
NCT03706326	CAR T and PD-1 Knockout Engineered T Cells	EC
NCT05089266	αPD1-MSLN-CAR T	MSLN+ Advanced Solid Tumours
NCT04577326	Mesothelin-targeted CAR T-cell	Mesothelioma
NCT05812326	PD-1 KO anti-MUC1 CAR-T cells	Advanced BC
NCT03747965	PD-1 KO mesothelin-directed CAR-T cells with conditioning of PC	MSLN+ multiple Solid Tumours
NCT03356782	Safety and Efficacy Evaluation of 4th Generation Safety-engineered CAR T Cells	Sarcoma
NCT03540303	Cytoplasmic Activated PD-1 CAR T Cells	r/r BCL
NCT04995003	HER2 CAR-T cells in combination with checkpoint blockade	Advanced sarcoma
NCT03916679	MESO-CAR T Cells Therapy	r/r Epithelial OC
NCT02873390	PD-1 Antibody Expressing CAR-T Cells	EGFR Family Member + Advanced Solid Tumour
NCT04768608	PD1 Integrated Anti-PSMA CART	CRPC
NCT03932955	MC-19PD1 CAR-T	r/r BCL
NCT05694364	Dose Escalation/Dose Expansion Study of PRGN-3007 UltraCAR-T Cells	Advanced Haematologic and Solid Tumour Malignancies

1 | Introduction

NCT05779917	Mesothelin/GPC3/GUCY2C-CAR-T Cells	Solid tumours
NCT01822652	3rd Generation GD-2 Chimeric Antigen Receptor and iCaspase Suicide Safety Switch	Neuroblastoma
NCT04162119	BCMA-PD1-CART Cells	r/r MM
NCT03726515	CART-EGFRvIII + Pembrolizumab	GBM
NCT03545815	CRISPR-Cas9 Mediated PD-1 and TCR Gene-KO Mesothelin-directed CAR-T Cells	MSLN+ Multiple Solid Tumours
NCT05620342	Autologous CAR T-Cells Targeting the GD2 Antigen	Lung cancer
NCT03874897	Chimeric Antigen Receptor T Cells Targeting claudin18.2	Solid tumours
NCT02862028	PD-1 Antibody Expressing CAR-T Cells	EGFR Family Member Advanced Solid Tumour (Lung, Liver and Stomach)
NCT03298828	CD19 CAR and PD-1 Knockout Engineered T Cells	CD19 + malignant B-cell derived leaukaemia and lymphoma
NCT03208556	iPD1 CD19 eCAR T Cells	r/r BCL
NCT03980288	4th Generation Chimeric Antigen Receptor T Cells	GPC3 + tumours

Table 1.4 | Ongoing clinical trials investigating the efficacy of CAR-T cells in combination with PD-1 inhibition. Source for these data: **https://clinicaltrials.gov.** BC, breast cancer; BCL, B-cell lymphoma; CAR, chimeric antigen receptor; CCL, chemokine (C-C motif) ligand; CD, cluster of differentiation; CRC, colorectal cancer; CRPC, castrate-resistant prostate cancer; CTLA-4, cytotoxic T-lymphocyte antigen-4; DC, dendritic cell; DLBCL, diffuse large B-cell lymphoma; EC, oesophageal cancer; EGFR, epidermal growth factor receptor; GBM, glioblastoma; GC, gastric cancer; GEJ, Gastroesophageal junction; GPC3, glypican-3; HCC, hepatocellular carcinoma; ICIs, immune-checkpoint inhibitors; IL, interleukin; LBCL, large B-cell lymphoma; MM, multiple myeloma, MSLN, mesothelin; MUC-1, mucin-1; NHL, non-Hodgkin lymphoma; NSCLC, non-small cell lung cancer; r/r, relapsed or refractory; TFL, transformed follicular lymphoma; OC, ovarian cancer; PD-1, programmed cell death protein-1; PC, pancreatic cancer; PMBCL, primary mediastinal B-cell Lymphoma; PSMA, prostate-specific membrane antigen.

While data from current clinical trials remains limited, evidence from preclinical models highlights the potential of targeting the PD-1/PD-L1 axis to improve CAR-T cell therapy [236,238,242–247]. Nevertheless, it is worth noting that certain studies have raised concerns regarding the long-term disruption of PD-1, with some reports showing

induction of T cell exhaustion and impaired persistence [248–250], implying certain discrepancies in the field. The conflicting findings observed in these investigations can be attributed to several factors, including the diversity in PD-1 disruption methodologies, varying PD-L1 expression in the preclinical models used and CAR constructs employed (Table 1.5). Therefore, a deeper examination of these factors is crucial to refine our understanding and optimize therapeutic strategies targeting the PD-1/PD-L1 axis in CAR-T cells.

Effect of PD-1/PD-L1 disruption	PD-1 disruption methodology	Preclinical model	CAR construct	Refs.
Beneficial	• Antibody checkpoint blockade • shRNA-based gene knockdown • DNR	MSTO-211H human pleural mesothelioma cells	LV 2nd generation MSLN-28ζ	236
Beneficial	CRISPR/Cas9	CD19⁺ PDL1⁺ K562 human cell lines	LV 2nd generation CD19-BBζ	242
Beneficial	• Antibody checkpoint blockade • PD-1 – CD28 switch-receptor	EMMESO (derived from a patient's tumour) PC3-PSCA and PC3-PSCA-PDL1⁺ tumour cell lines	mRNAs encoding 2nd generation SS1- or PSCA-BBζ	246
Beneficial	blocking scFv	PDL1⁺ haematologic and solid tumours	RV 2nd generation CD19- or MUC16ecto-28ζ (mouse and human)	238
Beneficial	CRISPR/Cas9	GPC3⁺PLC/PRF/5 naturally expressing PDL1 human cell line	LV 2nd generation GPC3-28ζ	245
Beneficial	CRISPR/Cas9	Nalm6-PDL1 PC3-PDL1 human cell lines	LV 2nd generation universal CD19- or PSCA-BBζ	243
Beneficial	CRISPR/Cas9	BT549 human cell line	LV 2nd generation MSLN-BBζ	244

1 | Introduction

Beneficial (only in intracranial injection)	CRISPR/Cas9	U87vIII naturally expressing PDL1 human cell line	AAV6 2nd generation universal EGFRvIII-BBζ	247
Detrimental (only *in vitro* experiments)	Anti-PD1 Nanobody	Nalm6 and Nalm6-PDL1 human cell lines	LV 3rd generation CD19-28-BBζ	248
Detrimental (at long-term)	shRNA-based gene knockdown	A549–19luc human cell lines	LV 2nd generation CD19-BBζ	249
Neutral	CRISPR-Cas9	Nalm6	LV 2nd generation CD19-BBζ	250

Table 1.5 | Preclinical data on PD-1 disruption in CAR-T cell therapy. 2nd, second; 3rd, third; AAV6, adeno-associated virus 6; Cas9, CRISPR associated protein 9; CD, cluster of differentiation; CRISPR, clustered regularly interspaced short palindromic repeats; DNR, dominant negative receptor; EGFRVIII, epidermal growth factor VIII; GPC3, glypican 3; luc, luciferase; LV, lentivirus; mRNA, messenger ribonucleic acid; MSTO, mesothelioma; MSLN, mesothelin; MUC16, mucin-16; RV, retrovirus; PD1, programmed cell death protein 1; PDL1, programmed cell death ligand 1, PSCA, prostate stem cell antigen; Refs., references; shRNA, short hairpin ribonucleic acid.

1.4.1.2. Affinity-tuning in CAR-T cell therapy

Target-mediated toxicity is a significant challenge in the development CAR-T cells for ACT, particularly in the context of solid tumours. As previously mentioned, this is partly due to the presence of target antigens on healthy tissues and a heterogeneous expression pattern in tumours. Therefore, understanding the sensitivity of CAR-T cells to targets expressed at low densities and the therapeutic window of antigen density is crucial for optimizing their efficacy and safety.

Already in 2004, Chmielewski et al. demonstrated that CAR-T cells with high-affinity receptors do not necessarily result in a more potent activation compared to those with lower affinity. Instead, high-affinity receptors were less capable of discriminating between cells with varying antigen expression levels[251]. In line with this, Sara Ghorashian and colleagues showed increased proliferation and cytotoxicity *in vitro* and antitumour activity *in vivo* using a novel CD19 CAR (CAT) with a >40-fold lower affinity than FMC63[252], the high-affinity binder used in many clinical studies. Notably, in a phase I clinical trial (CARPALL study, NCT02443831), 12 out of 14 patients with r/r pediatric B-

ALL treated with CAT CAR-T cells achieved molecular remission, and 11 of 14 showed prolonged persistence, with enhanced CAR-T cell expansion compared with published clinical data using FMC63-based CAR-T cell products. Noteworthy, toxicity was low, with no severe CRS, while survival rates were comparable to those in published studies[121,123,175,253].

Recent studies have explored similar approaches to improve the safety profile of CAR-T cells in solid tumours through the optimization of CAR affinity. This can be particularly important for targets that have led to severe toxicities (e.g., ErbB2, CAIX). In a study by Liu et al., it was shown that CARs targeting ErbB2 or EGFR with reduced affinity could mitigate severe on-target toxicities while retaining *in vivo* efficacy[254]. By lowering the affinity of the scFv, they significantly improved CAR-T cell therapeutic index, demonstrating robust antitumor activity with reduced reactivity against normal tissues expressing physiological levels of the target antigen. This has also been recently confirmed using murine CAR constructs in immunocompetent mouse models[255]. Similarly, Wang et al. demonstrated that low-affinity fine-tuned CAR-T cells targeting CAIX had a wider therapeutic window compared to high-affinity counterparts that showed serious adverse events in the first anti-CAIX CAR-T clinical trial[256]. On top of this, low-affinity CAR-T cells against other target molecules (e.g., ICAM-1, GPC3) have also been proven to outperform high affinity CAR-T cells[257,258].

As evidenced by these reports, increasing CAR affinity beyond a certain threshold does not always enhance T-cell activation and can lead to adverse effects, such as on-target, off-tumour toxicity and reduced killing capability, underscoring the importance of affinity tuning in CAR-T cell therapy. This approach offers a promising strategy to expand the use of CAR-T cells against solid tumours by targeting TAAs more selectively, thus improving their safety profile.

Hypothesis and Objectives

2. Hypothesis and Objectives

In this study, we **hypothesize** that distinct CAR constructs may demonstrate varying sensitivities to PD-1/PD-L1 inhibition, with PD-L1 expression levels and target antigen density potentially influencing these sensitivities. To this end, the **main objective** of this work is to investigate the impact of different CAR constructs on the sensitivity of CAR-T cells to inhibition by the PD-1/PD-L1 axis. To achieve this, the study is divided into four specific objectives:

Specific objective 1. To develop preclinical models expressing varying PD-L1 densities that better predict the efficacy of CAR-T cells.

Specific objective 2. To assess the impact of the PD1/PDL1 axis on the functionality of CAR-T cells with diverse scFv affinities.

Specific objective 3. To explore the role of target antigen density in the sensitivity of CAR-T cells with different affinities to PD-1/PD-L1-mediated inhibition.

Specific objective 4. To analyze the influence of the PD-1/PD-L1 axis on CAR-T cells incorporating different co-stimulatory domains (CD28, ICOS, or 4-1BB).

By addressing these objectives, this study aims to provide comprehensive insights into the optimization of PD-1/PD-L1 targeting in combination with CAR-T cells.

Materials and Methods

3. Materials and Methods

3.1. DNA manipulation

3.1.1. Plasmid DNA isolation from prokaryotic cells

Bacteria serve as an effective vector for the amplification of exogenously inserted Deoxyribonucleic acid (DNA), typically in the form of plasmids. This process, known as transformation, enables the replication of the plasmid alongside bacterial DNA, resulting in the production of a large quantity of the vector. Through this mechanism, bacteria efficiently generate amplified copies of the DNA insert. For the transformation of bacteria, the One Shot® Stbl3 chemically competent *E. coli* strain (Thermo Fisher - #C737303) were used. Bacterial aliquots of 25 µL stored at -80ºC were thawed on ice, and a final volume of 2 µL of DNA ligation was added and gently mixed. Subsequently, the mixture was placed on ice for 30 minutes and heat-shocked for 30-45 seconds in a 42ºC water bath. Following this, the bacteria were incubated on ice for 2 minutes, immediately resuspended in 200 µL of pre-warmed (37ºC) Super Optimal Broth + Catabolic repressor (S.O.C) (Thermo Fisher - #15544034) and incubated for 1 hour at 225 rpm in a shaking incubator at 37ºC. Afterwards, 250 µL of the transformation was plated on pre-warmed Luria Broth (LB) (Thermo Fisher - #12795027) agar plates with ampicillin resistance (Sigma-Aldrich - #A5354) and incubated at 37ºC overnight.

3.1.2. Preparation of plasmid DNA

3.1.2.1. Small scale DNA preparation

Minipreparations, known as minipreps, were utilized to isolate a limited quantity of plasmid DNA (40 µg) from liquid bacterial cultures. This purification technique involves the precipitation of DNA in the presence of salts and isopropanol, effectively separating the plasmid DNA from other cellular components.

Bacterial colonies were picked and further grown in 3 mL of LB medium containing Ampicillin (100 µg/mL) at 37ºC overnight. On the following day, DNA was extracted

from bacterial cultures in exponential growth following the PureLink™ Quick Plasmid MiniPrep Kit protocol (Thermo Fisher - #K210011). With this kit, cells are lysed using an alkaline/SDS procedure, and the lysate was then applied to a silica membrane column, which selectively binds plasmid DNA. Contaminants were removed with wash buffer, and the isolated DNA was subsequently eluted in 50 µl Nuclease-free water (NFW). Prior to transitioning to large-scale production, the DNA obtained from the minipreps was digested with restriction enzymes (as explained in section 3.1.5.) to select the correct plasmids.

3.1.2.2. Large scale DNA preparation

In cases requiring larger quantities of DNA (500-850 µg), correct clones from minipreps were inoculated into 250 mL of LB medium with Ampicillin. After incubation overnight at 37ºC, LB containing the saturated bacteria was pelleted at 6000*g* for 15 minutes. DNA was isolated using the PureLink™ Quick Plasmid MaxiPrep Kit (Thermo Fisher - #K210006). Following cell lysis, DNA isolation was performed using anion exchange resin coupled with a lysate removal filter. The purified DNA was then recovered through elution and precipitation with isopropanol and 70% ethanol, and finally resuspended in 200 µL of NFW. Adjustment was made to have a stock with a final concentration of ~1000ng/mL. The eluted plasmid was sequenced (detailed in section 3.1.10.) to verify the absence of any mutations throughout the cloned construct sequence witih Genewiz® (from Azenta Life Sciences, Leipzig, Germany) and stored at -80°C for further use.

3.1.3. DNA isolation from eukaryotic cells

Genomic DNA from at least 100.000 cells was isolated to assess efficacy of CRISPR-Cas9-mediated KO (see section 3.3.4.) using the silica-based, phenol- and chloroform-free DNeasy Blood&Tissue kit (QIAGEN - #69504) following manufacturer's protocol. In short, samples were initially lysed using proteinase K, after which the lysate was loaded onto the DNeasy Mini spin column. During centrifugation, DNA was selectively bound to the DNeasy membrane as contaminants passed through.

Remaining contaminants and enzyme inhibitors were removed in two wash steps, and DNA was then eluted in 30-100 µL of NFW.

3.1.4. DNA quantification and purity assessment

The DNA quantification, obtained through the aforementioned techniques, was conducted by measuring absorbance at 260 nm in the NanoDrop™ 1000 spectrophotometer (Thermo Fisher). According to Beer-Lambert's law, the concentration of DNA can be directly calculated from absorbance values using the formula ($A = \varepsilon \cdot c \cdot l$), where:

A = absorbance

ε = absorption coefficient → for dsDNA at 260 nm, ε = 0.02 $(ng/\mu L)^{-1}cm^{-1}$

c = concentration (ng/µL)

l = optical path length (cm)

Besides concentration, to assess the presence of contaminants that absorb at 260 nm and could interfere with downstream applications, absorbance at 280 nm (indicative of phenol or proteins) and 230 nm (indicative of phenol or guanidine salts) were measured. $A_{260/280}$ ratios ~ 1.8 and $A_{260/230}$ ratios ranging from 2.0 to 2.2 are generally accepted as indicative of pure DNA samples.

3.1.5. DNA digestion

Purified DNA can be cleaved using bacterial endonucleases, also known as restriction enzymes, which recognize specific sequences on the DNA and introduce cuts at these sites. In this study, we used DNA digestion for cloning strategies, that is, to cleave specific DNA fragments from a plasmid vector and insert them into a new backbone previously cleaved with the same enzyme. Digestion products were analysed using agarose gel electrophoresis, and desired bands purified for subsequent cloning using commercial extraction kits (see Section 3.1.9). Additionally, identification of DNA digestion patterns was used to test fidelity of newly generated or purchased sequences after cutting with known restriction enzymes. The different vectors were digested with

the indicated µL of the corresponding New England Biolabs® enzymes of interest and CutSmart buffer (1X) in a final volume of 20-50 µl. According to the commercial protocol, digestion was allowed to proceed for 15 minutes to 16 hours of incubation at 37°C.

3.1.6. DNA ligation

Ligation is the process by which two double-stranded DNA fragments with either blunt or complementary cohesive ends, are fused together in a reaction catalyzed by an enzyme known as ligase, which uses ATP as an energy source to form a phosphodiester bond between the 5' phosphate group of one strand and the 3' hydroxyl group of another.

Ligations were performed using the Quick Ligation™ Kit (New England Biolabs, NEB - #M2200S) at 3:1 vector:insert ratio in a final volume of 20 µL reaction as follows:

Component	Quantity
Vector	50 ng
Insert	X ng
Quick Ligase Reaction Buffer	10 µL
Quick Ligase	1 µL
Nuclease-Free Water (NFW)	Up to 20 µL

To calculate the quantity (ng) of insert, the following formula from NEBioCalculator online tool (https://nebiocalculator.neb.com/#!/ligation, version 1.15.5) was used:

$$\text{Required mass insert (X)} = \text{desired}\frac{\text{insert}}{\text{vector}}\text{molar ratio} \cdot \text{mass vector} \cdot \text{ratio of insert to vector lengths}$$

The final reaction was gently mixed by pipetting up and down and incubated at room temperature (RT) for 30 minutes.

3.1.7. DNA amplification via Polymerase Chain reaction (PCR)

The Polymerase Chain Reaction (PCR) is a molecular biology technique which allows for the exponential amplification of specific DNA sequences *in vitro*. PCR is based on

the principle of DNA amplification, wherein a small segment of DNA is exponentially replicated through a series of temperature cycles. To initiate the amplification process, it is essential to have specific oligonucleotides, commonly referred to as primers, which match the sense and antisense strands of the target DNA sequences. These primers typically consist of 20-25 nucleotide sequences that precisely bind to the target sequences, enabling the extension of DNA fragments in the presence of deoxynucleotides triphosphates (dNTPs) by the DNA polymerase enzyme of *Thermophilus aquaticus* (Taq Polymerase), which functions optimally at elevated temperatures. The optimization of PCR reaction conditions relies on two pivotal factors: firstly, ensuring the effective functioning of primer pairs at a specific hybridization temperature, and secondly, considering that the length of the target DNA sequence directly impacts the duration of the elongation phase. The amplification rate using Taq Polymerase is 1 kilobase (kb) /minute.

The key components and steps of PCR include:

- **Denaturation**: The double-stranded DNA template is heated to a high temperature (typically around 94-98°C). This causes the DNA strands to separate or "denature" into two single strands, breaking the hydrogen bonds that hold them together.
- **Annealing**: The reaction mixture is cooled to a lower temperature (usually around 50-65°C). At this temperature, short DNA primers specifically designed to bind to complementary sequences on the target DNA anneal to their complementary sequences on the single-stranded DNA template.
- **Extension**: The temperature is raised to an intermediate level (usually around 72°C). At this temperature, a DNA polymerase enzyme synthesizes a new DNA strand by adding nucleotides to the primers, thus extending the DNA sequence complementary to the template strand.

PCRs for detecting mycoplasma contamination in the cell culture supernatant (SN) were done using the Taq Polymerase (Thermo Fisher - #EP0401) in a final volume of 20 µl with the following conditions:

PCR mix

Component	Volume (µL)
10X Taq Buffer	2 (1X)
50 mM $MgCl_2$	0.6
Forward Primer 10 µM	1
Reverse Primer 10 µM	1
dNTPs 10 mM	0.4
Cell culture SN	2
Taq Polymerase	0.15
NFW	Up to 20

The amplification process was performed in an Applied Biosystems 2720 Thermal Cycler adhering to the specified conditions:

	Temperature	Time
Initial denaturation	94°C	5 min
	94°C	1 min
35 cycles	60 °C	1 min
	72 °C	1 min 30s
Final extension	72 °C	10 min
	4 °C	Indefined

PCRs for amplifying the PD-1 region were performed using the Phusion® High-Fidelity DNA Polymerase (NEB - #M0530S) in a final volume of 50 µl as follows:

PCR mix

Component	Volume (µL)
5X Phusion GC Buffer	10 (1X)
Forward Primer 10 µM	2.5 (0,5 µM)
Reverse Primer 10 µM	2.5 (0,5 µM)
dNTPs 10 mM	1 (200 µM)
Template DNA	100-200 ng
Phusion DNA Polymerase	0.5 (1.0 units/50 µl PCR)
NFW	To 50

The amplification process was performed in an Applied Biosystems 2720 Thermal Cycler under the following conditions:

	Temperature	Time
Initial denaturation	98°C	30s
	98°C	10s
30 cycles	68 °C	20s
	72 °C	30s
Final extension	72 °C	10 min
	4 °C	Indefined

3.1.8. Preparation of Agarose Gels for Electrophoresis

The validation of PCR reactions and the isolation of target DNA by molecular weight were performed through agarose gels. To prepare these gels, 0.5-2 g of Agarose D1 Low EEO (Condalab - #8010) were dissolved in 50 mL of 1x Tris/Acetic acid/EDTA (TAE) buffer (BIO-RAD - #1610743) and heated in a microwave for 2 minutes. After cooling, 5 µl of SYBR™ Safe DNA Gel Stain (Thermo Fisher - #S33102) were added, and the gel was allowed to solidify. All samples were mixed with Gel Loading Dye Purple 6X, without SDS (NEB - #B7025S), and before running the gel, the 1 kb PlusLadder™ DNA molecular weight marker (Thermo Fisher - #10787018) was included as a control.

3.1.9. Purification of PCR products

PCR products and selected gel bands were cleaned up with a PureLink™ Quick PCR Purification Kit (Thermo Fisher - #K310001). The PureLink™ PCR Purification Kit utilizes silica-based membrane technology and chaotropic salts for selective binding of dsDNA, allowing purification of up to 40 µg of dsDNA. Initially, four volumes of PureLink™ Binding Buffer B2 with isopropanol were added to one volume of the PCR product (50 µL), loaded onto a PureLink™ Spin Column and centrifuged at RT at 10.000*g* for 1 minute, with the flow-through discarded. DNA washing was performed by adding 650 µL of Wash Buffer with ethanol to the column, followed by centrifugation at

RT at 10.000*g* for 1 minute. Finally, the column was centrifuged at maximum speed at RT for 3 minutes to remove any residual Wash Buffer and the purified PCR product was eluted in 50 µL of NFW and stored at –20°C.

3.1.10. DNA sequencing

Sanger sequencing of amplification products was performed by GeneWiz®. Primers used for PCR amplification and sequencing are indicated in Table 3.1. Sequences were analysed using Benchling® by alignment with the wild type or template sequence. To determine the percentage of insertions and deletions (INDELs) as well as the KO efficiency, samples were quantified by using Synthego software (version 3.0) as explained in section 3.3.4.

	Primer	Sequence (5' → 3')	T_m (ºC)	Product length (bp)
PCR	PD-1 Forward	TTTCCCTTCCGCTCACCTCC	58.2	444
	PD-1 Reverse	CAAAGAGGGGACTTGGGCCA	58.4	
Sequencing	pCCL 8F	GTGAATAGAGTTAGGCAGGG	50	
	EF1-α Forward	ATCTTGGTTCATTCTCAAGC	40	
	WPRE Reverse	GGGCCACAACTCCTCATAAA	53.9	
	CD8α Hinge Forward	CCCACCATCGCGTCGCAG	60.6	

Table 3.1. | Primer sequences used for PCR and sequencing. Abbreviations: CD8α, cluster of differentiation 8 alpha; EF1-α, Elongation factor 1-alpha; PD-1, programmed cell death ligand 1; WPRE, woodchuck hepatitis virus post-transcriptional regulatory element.

3.1.11. Molecular cloning

3.1.11.1. CAR construction

Single-chain variable fragments (scFv) used for targeting HER2 and FRβ with low or high affinity were previously described[254,259]. Similarly, scFv sequence M11 (targeting mesothelin) was extracted from patent WO2015090230A1[260]. All CAR sequences

(including the mentioned scFvs, signal peptide, CD8 hinge, CD28 or CD8 transmembrane regions and intracellular domains from CD28, 41BB or ICOS and CD3ζ), were synthesized by BaseClear B.V. (Leiden, Netherlands) or GenScript Biotech (New Jersey, United States of America) and cloned into the third-generation lentiviral vector pCCL (gently provided by Dr. Luigi Naldini)[261] under the control of EF1α promoter[262]. The 4D5-ICOS-CD3ζ construct was generated through molecular cloning using digested fragments from existing vectors, specifically from the 4D5-CD28-CD3ζ and 4D5.5-ICOS-CD3ζ as detailed in the Table 3.2.

pCCL-4D5.5-ICOS-CD3ζ

Component	Volume (µL)
AgeI (NEB)	1
NheI (NEB)	1
SalI HF (NEB)	1
DNA	3 µg
CutSmart Buffer (10X)	3
NFW	Up to 30

pCCL-4D5-41BB-CD3ζ

Component	Volume (µL)
BstXI (NEB)	1
NheI (NEB)	1
SalI HF (NEB)	1
DNA	3 µg
CutSmart Buffer (10X)	3
NFW	Up to 30

Table 3.2. | Restriction enzymes used in the digestions to obtain the pCCL-4D5-ICOS-CD3ζ. Abbreviations: DNA, desoxyribonucleic acid; HF, High fidelity; NEB, New England Biolabs: NFW: Nuclease-free water.

Then, pCCL-4D5-CD3ζ (vector) and ICOS (insert) were purified, ligated, transformed amplified and sequenced with the primer CD8 hinge forward to validate ICOS insertion before moving forward to maxiprep production. The final product was sequenced again with the primers EF1α Forward and woodchuck hepatitis virus post-transcriptional regulatory element (WPRE) reverse according to the methods described earlier.

3.1.11.2. Generation of PD-L1 constructs

To achieve high levels of PD-L1 expression, we utilized the pCCL-EF1α-PDL1 construct synthesized by GenScript. Additionally, for the generation of plasmids encoding for low levels of PD-L1 expression, we employed a strategy involving the digestion of the plasmid pCCL-pgk100-HER2t, generated by previous colleagues in the lab, along with

the pCCL-EF1α-PDL1 construct. The digestion of both vectors was performed as indicated in the Table 3.3.

Component	*Volume (µL)*
XbaI (NEB)	1
SalI HF (NEB)	1
DNA	4 µg
CutSmart Buffer (10X)	2
NFW	Up to 20

Table 3.3. | Restriction enzymes used in the cloning of pCCL-pgk100-PDL1. Abbreviations: DNA, desoxyribonucleic acid; HF, High fidelity; NEB, New England Biolabs: NFW: Nuclease-free water.

This process allowed for the isolation of the pCCL-pgk100 (vector) on one side and the PD-L1 gene (insert) on the other. Then, both elements were purified, ligated, transformed and amplified following the previously outlined procedures. Additionally, to validate the expected patterns before scaling up production, we conducted another digestion using the components outlined in Table 3.4.

Component	*Volume (µL)*
XbaI (NEB)	0.5
SalI HF (NEB)	0.5
EcoRI	0.5
DNA	4 µg
CutSmart Buffer (10X)	5
NFW	Up to 50

Table 3.4. | Restriction enzymes used for the validation of the pCCL-pgk100-PDL. Abbreviations: DNA, desoxyribonucleic acid; HF, High fidelity; NEB, New England Biolabs: NFW: Nuclease-free water.

Upon validation of the construct's fidelity, we proceeded with doing a maxiprep and sequencing it with the primer pCCL 8F (Gently provided by Dra. Beatriz Martínez) as detailed in sections 3.1.2.1. and 3.1.10., respectively.

3.2. RNA manipulation

3.2.1. RNA isolation from cells

Total RNA was isolated from sorted T-cells or tumour cells using the RNeasy Mini kit (QIAGEN - #74104) following the manufacturer's protocol with some optimizations done by Dr. Waugh, aimed at enhancing extraction efficiency, particularly when starting from a small number of sorted T-cells. In short, sorted cells were centrifuged at 350*g* for 20 minutes and pellets resuspended in 990 µL of freshly mixed RLT plus (QIAGEN - #1053393) with 10 µl undiluted Beta-mercaptoethanol (ß-ME) (Life Technologies - # 31350-010). Disruption and homogenization steps were performed in lysis buffer by vortexing using QIAshredder (QIAGEN - #79654) followed by centrifugation at maximum speed for 2.5 minutes at RT. The supernatant was carefully transferred to new low-binding tubes (Eppendorf - #022431021). Next, 70% ethanol was added and mixed vigorously. After centrifugation, the samples were loaded onto QIAGEN RNeasy MiniElute columns, spun, and the flow-through was discarded. This process was repeated for remaining samples. To avoid contamination of genomic DNA, purified RNA was treated with RNase-Free DNAse (QIAGEN - #79254) following 15 minutes of incubation at RT. Further washing steps were carried out with RWI and RPE solutions from the RNeasy Mini kit. Finally, elution was done by adding 14 µL RNAse-free H_2O to the column, incubating, and spinning. The elution step was repeated using the first eluate to ensure maximum yield. 1.5 µL were kept separately for quantification and purity assessment. The rest was stored at -80ºC until used for downstream applications to preserve integrity.

3.2.2. RNA quantification and purity assessment

Quantity and quality of the samples were assessed using the Nanodrop™ one/one spectrophotometry (Thermo Fisher) by 260 nm absorbance measurement as explained in Section 3.1.4. In this case, samples with $A_{260/280}$ ~ 2.0 and $A_{260/230}$ ~ 2.0-2.2 ratios were considered as "pure" RNA. A lower $A_{260/280}$ ratio indicates likely protein contamination, which may artificially inflate RNA quantity measurements. Samples with 260/230 ratios

below 2 typically have a significant amount of these contaminants that may interfere with downstream applications involving enzymes.

3.2.3. Gene expression analyses

3.2.3.1. Nanostring nCounter technology

Gene expression analysis was performed using the human CAR-T cell characterization panel, from Nanostring Technologies (Seattle, WA). NanoString employs its patented molecular barcodes, providing digital detection technology to perform highly multiplexed analyses. The CodeSet chemistry comprises a Reporter CodeSet and a Capture ProbeSet that specifically attach to the target molecules. Excess probes are subsequently eliminated, and the remaining hybridized probes securely adhere to the cartridge surface. This results in the immobilization and alignment of the target-probe complexes within the cartridge, where the barcodes are quantified through nCounter® systems.

Before transcriptomic analysis, CAR-T cells from three distinct healthy donors were co-cultured with SKOV3 tumour cells at a 1:3 effector-to-cell ratio for 48h. After this period, cells were labelled with anti-CD45 (for T-cell identification) and anti-HER2 (for tumour cell identification) antibodies. Subsequently, CD45+ cells were sorted by FACS, and total RNA was immediately extracted as explained in Section 3.2.1.

Samples were prepared according to the manufacturer's guidelines for the nCounter human CAR-T Characterization Panel (Nanostring). This comprehensive panel encompasses 780 human genes across eight critical components of CAR-T biology: metabolic fitness, phenotype, T-cell receptor (TCR) diversity, toxicity, activation, persistence, cell types and exhaustion. Briefly, for each sample, 3'mRNA gene expression profiling was generated from 280 ng of RNA. Next, the target RNA alongside the panel standard, a synthetic DNA oligonucleotide pool corresponding to the target sequences of the probe sets in the panel used for calibration, were hybridized together with the reporter and capture CodeSet at 65°C for 20 hours. Following hybridization, samples were loaded onto the fully automated nCounter Prep Station (NanoString Technologies, Seattle, WA), where they were purified and immobilized onto the internal surface of a sample cartridge for 2.5 hours. Once this step was completed, the sample

cartridges were transferred to the nCounter Digital Analyzer (NanoString Technologies, Seattle, WA) for image acquisition and data processing as per the manufacturer's protocol. The expression level of a gene was measured by counting the number of times the specific barcode for that gene was detected. The barcode counts were then tabulated in a comma-separated value (CSV) format. The raw digital count of expression was exported from nSolver v3.0 software for downstream analysis. Gene expression levels were normalized against the housekeeping genes, and data analysis was conducted using the Rosalind Platform (www.rosalind.bio/nanostring). Enrichr online software (https://maayanlab.cloud/Enrichr/) was used for the analysis of biological pathways and Gene Ontology (GO) terms associated with the differentially expressed genes by using the list of under- and over-expressed genes as input.

Transcriptomics data have been deposited in the Gene Expression Omnibus database under accession number GSE252036.

(https://www.ncbi.nlm.nih.gov/geo/query/acc.cgi?acc=GSE252036).

3.2.3.2. Reverse transcription-quantitative polymerase chain reaction (RT-qPCR)

Interesting candidates found in Nanostring analyses were validated by RT-qPCR. In order to be used as a template by DNA polymerases, mRNA was reverse transcribed before qPCR analysis. Briefly, 10 ng of total RNA was used for complementary DNA (cDNA) synthesis using the High-Capacity RNA-to-cDNA™ Kit (ThermoFisher - #4387406) in a final volume of 20 µL:

Component	+ RT reaction	-RT reaction
2X RT Buffer mix	10	10
20X RT Enzyme mix	1	-
RNA sample	up to 9*	up to 9
NFW	up to 20**	up to 20

Then, reactions were run in a thermal cycler as follows:

Setting	Step 1	Step 2	Step 3
Temperature	37	95	4
Time	60 min	5 min	infinite

cDNA is directly proportional to the amount of mRNA for a gene of interest in the sample analyzed, giving a direct measurement of its expression. A 1/10 dilution of cDNA with RNAse-free water was made before adding it to the PCR reaction mix.

This reaction was performed in 384-well plates in a thermocycler capable to detect fluorescence from samples (7900HT Real-Time PCR Fast System – Applied Biosystems). Evolution of fluorescence across the PCR cycles allowed for the calculation of the initial amount of cDNA of the gene of interest. This was quantified via the $2^{(-\Delta\Delta Ct)}$ method after relativization to a housekeeping gene (in our case, *ACTB*) that was stable across experimental conditions, and to a reference experimental condition. Normalized gene expression was $\log_2$ transformed for representation in a heatmap.

The reaction mixture was prepared for each gene as follows:

PCR reaction mix component	Single reaction
20X TaqMan GEA	1 µL
2X TaqMan MM	10 µL
cDNA template	4 µL
RNAse-free water	5 µL

Reactions were performed in duplicates with the following conditions:

	Temperature	Time
Hold	50°C	2:00
Hold	95°C	0:20
Cycle (40X)	95°C	0:01
	60°C	0:20

Probes used for RT-qPCR are listed in Table 3.5.

Gene	Assay identity	Chromosome location	Catalog #
TNFSF9	Hs00169409_m1	Chr.19: 6530999 - 6535928 on Build GRCh38	4448892
FOSB	Hs00171851_m1	Chr.19: 45467995 - 45475179 on Build GRCh38	4453320
ISG15	Hs00192713_m1	Chr.1: 1013467 - 1014540 on Build GRCh38	4453320
IFI35	Hs00413458_m1	Chr.17: 43006725 - 43014459 on Build GRCh38	4453320
IRF7	Hs00185375_m1	Chr.11: 612555 - 615999 on Build GRCh38	4453320
IFIT1	Hs01675197_m1	Chr.10: 89392546 - 89406487 on Build GRCh38	4453320
ACTB	Hs99999903_m1	Chr.7: 5527148 - 5530601 on Build GRCh38	4331182

Table 3.5. | List of Taqman probes used for gene expression analysis via qRT-PCR.

3.3. Clustered regularly interspaced short palindromic repeats (CRISPR)-Cas9 – mediated knock-out (KO)

In this work, we employed CRISPR/Cas9 technology for genetic editing of both tumour and CAR-T cells. This methodological approach relies on two primary components: a single-guide RNA (sgRNA), which binds to the targeted DNA sequence, and the endonuclease Cas9, which induces DNA double-strand breaks (DSBs) at the specified locus. Subsequently, error-prone endogenous DNA repair mechanisms facilitate the introduction of insertions or deletions (INDELs), potentially resulting in loss-of-function mutations within the targeted gene. To achieve this, we employed electroporation to deliver ribonucleoprotein (RNP) complexes, comprising Cas9 protein complexed with sgRNA, using the Invitrogen™ Neon™ transfection system (Thermo Fisher - # MPK5000).

3.3.1. Single guide RNA (sgRNA) design

sgRNAs play a critical role in conferring specificity to the CRISPR/Cas9 system. Each sgRNA is comprised of a single-strand RNA (ssRNA) sequence that is complementary to the target DNA sequence and a transactivating crRNA (tracrRNA) which binds to the Cas9 nuclease. This synergistic combination guides the Cas9 enzyme to the region of DNA complementarity, where both target recognition and the subsequent DNA cleavage take place. Because the tracrRNA component remains consistent across all sgRNAs, for the sake of simplicity, the specific ssRNA sequences are commonly referred to as sgRNAs.

sgRNAs were bioinformatically designed using the CRISPR Design Tool (Synthego, https://www.synthego.com/products/bioinformatics/crispr-design-tool). This tool uses a sequential algorithm to rank candidate guide RNA sequences that have a high chance of knocking out the gene of interest while minimizing off-target effects. To be suggested as candidates, guides need to accomplish the following features: (I) target a common exon in the primary transcript; (II) target an early region of the gene; (III) have an on-target score of > 0.5 based on the Azimuth 2.0 model; and (IV) have no off-target sites within the same genome that have 0, 1 or 2 mismatches compared to the guide RNA sequence. The chemically modified sgRNAs used in this study (detailed in Table 3.6.), which have shown to provide superior editing in most cell types (including T-cells), were purchased from Synthego (CRISPRevolution sgRNA EZ Kit, Synthego). Prior to use, sgRNAs (3 nmol) were rehydrated in 30 µL of the supplied nuclease-free 1x TE buffer.

sgRNA	Sequence (5' → 3')	Exon	On target score	Off-target sites
TRAC	AGAGTCTCTCAGCTGGTACA	Exon 3	0.632	0,0,2,2,23,254
PD-1	CGACTGGCCAGGGCGCCTGT	Exon 1	0.570	0,0,0,2,80
PD-L1	ATTTACTGTCACGGTTCCCA	Exon 2	0.632	0,0,0,9,85

Table 3.6. | List of sgRNA used to perform CRISPR/Cas9-mediated KO

3.3.2. CRISPR/Cas9-Mediated genetic editing in SKOV3 tumour cells

For the electroporation of the SKOV3 tumour cell line, RNP complexes were prepared by combining the sgRNA specific for PD-L1 with TrueCut™ Cas9 Protein v2 (ThermoFisher - #A36498) at a molar ratio of 3:1 in a final volume of 60 µL. The Cas9/sgRNA complex was then incubated at RT for 15-20 minutes. Concurrently, $5 \cdot 10^6$ SKOV3 cells were trypsinized, washed twice with PBS, and resuspended in 60 µL of buffer R on ice. After the incubation period, the 60 µL of Cas9/gRNA complex was added to the SKOV3 cell suspension and thoroughly mixed. Subsequently, 100 µL of the SKOV3 cells mixed with the Cas9/gRNA complexes was transferred into the Neon™ 100-µL tip (ThermoFisher - #MPP100) and electroporated under the following conditions: 1170V, 30 milliseconds, and 2 pulses, as recommended in the Neon Transfection System Cell Line Data and Transfection Parameters (https://www.thermofisher.com/es/es/home/life-science/cell-culture/transfection/neon-transfection-system/neon-transfection-system-cell-line-data.html). Electroporated cells were immediately transferred into a humidified 37ºC 5% CO_2 incubator, and editing efficiencies were assessed using flow cytometry as explained in section 3.6.

3.3.3. CRISPR/Cas9-Mediated genetic editing in primary human T cells

For most targets, gene editing can be done indistinctly two to four days after stimulation, when T cells have received sufficient activation from the CD3/CD28 beads and are actively proliferating. In our case, we performed the KO on day 4 of T-cell expansion. Briefly, T-cells were centrifuged at 300*g* for 7 minutes. Before removing the supernatant, the conditioned media required to maintain CAR-T cells at $1.5 \cdot 10^6$ cells/mL post-electroporation was added to their corresponding well/flask as explained in section 3.5.4.1, as it contained essential cytokines and factors secreted by T-cells necessary for proper T-cell expansion. Following this, T-cell pellets were washed twice with 20 mL of PBS and resuspended in Resuspension Buffer R at the desired concentration, aiming for $4–7 \cdot 10^6$ cells per reaction in a final volume of 60 µL, and kept on ice for no longer than 20 minutes to maintain cell viability and transfection

efficacy. It was noted that increasing the number of cells per reaction up to 8-10·10^6 reduced the KO efficiency. During T-cell centrifugation, RNP complexes were formed by combining 10 µg of Cas9 protein and 2.5 µg of sgRNA in 60 µL of Resuspension Buffer R per reaction, maintaining a 1:3.3 molar ratio of Cas9:gRNA. After incubating the RNP complex at RT for 10–20 minutes, it was added to the T-cells and thoroughly mixed. Next, 100 µL of the mixture were pipetted into the Neon™ 100-µL tip, ensuring no air bubbles were created, and finally electroporated using the program #24 (1600 V/10 ms/3 pulses). The electroporated cells were immediately transferred into the appropriate flask containing the previous calculated volume of conditioned medium (to adjust CAR-T cell concentration to 1.5·10^6 cells/mL) and placed in a humidified 37 °C, 5% CO_2 incubator. After 48 hours without disturbing the cells, CAR-T cell expansion was followed as explained in section 3.5.4.4.

A list of suggested experimental CRISPR/Cas9 controls to include as part of the expansion protocol is shown in Table 3.7.

Control	Description	Purpose
Positive control	CAR-T cells are electroporated with Cas9 complexed with sgRNAs that have demonstrated high editing efficiency (i.e., sgRNA for TRAC)	Ensures that all reagents, protocol, and equipment are functioning at optimal conditions This control might be used when optimizing a protocol or when trying a sgRNA for the first time
Negative control: Non-electroporated T cells	T cells are not electroporated and cultured in the absence of Cas9 and sgRNA	This control determines cell growth at basal conditions
Mock control: Electroporated T cells	CAR-T cells are electroporated with Cas9 complexed with a nontargeting sgRNA (i.e., scrb RNA), a sgRNA targeting a genomic safe harbour or an intron, or with no sgRNA CAR-T cells are electroporated with no Cas9 or sgRNA	It controls for toxicity from RNP (or Cas9), cell death from electroporation, or possible viability issues associated with editing the specific gene of interest. Ensures that the observed phenotype is due to the specific editing and not to the transfection process

Table 3.7. | Suggested experimental CRISPR/Cas9 controls. CAR: Chimeric antigen receptor; TRAC: T cell receptor alpha chain; RNP: Ribonucleoprotein; sgRNA: Single-guide RNA.

3.3.4. Knock-out quantification

Gene edited samples were quantified by using the inference of CRISPR Edits (ICE) CRISPR Analysis tool (Synthego), a free software tool which rely on Sanger sequencing to resolve indel size frequencies from edited cells by comparing and decomposing Sanger traces made from PCR products of targeted regions from unedited/mock and edited templates. ICE offers accurate results that correlate strongly with NGS-based analysis. Successfully analyzed samples will display the following parameters:

- **Sample Label**: This represents a unique identifier assigned to each sample.
- **Guide Target**: The 17-23 base pair sequence of the sgRNA(s) responsible for binding to the genomic DNA, excluding the PAM sequence.
- **PAM Sequence**: The Protospacer Adjacent Motif (PAM) sequence specific to the nuclease used. ICE is currently configured for the Cas9 nuclease from *Streptococcus pyogenes* (SpCas9) exclusively.
- **Indel Percentage**: This indicates the proportion of sequences within the sample that contain an indel. It encompasses all sequences that deviate from the wild type, whether they signify a knockout or knock-in mutation. The indel percentage serves as a measure of editing efficiency within a mixed cell population, providing insight into how effectively a particular sgRNA induces DNA cleavage under the existing transfection conditions.
- **Model Fit (R2)**: The R2 value, also known as the Pearson correlation coefficient, gauges how well the proposed indel distribution aligns with the Sanger sequence data obtained from the edited sample. The maximum R2 value is 1, with higher values reflecting increased confidence in both the indel percentage and KO Score. An R2 value of 0.8 or higher signifies a robust analysis.
- **KO Score**: This score reflects the portion of sequences that are likely to lead to the functional KO of a protein. It encompasses frameshift mutations and indels of 21 or more base pairs. The higher the KO Score, the greater the percentage of sequences that are anticipated to cause a KO of the target gene. KO cell pools comprise a mixture of both edited and unedited cells. Among the edited cells, various alleles of each cell may contain distinct indels produced through Non-Homologous End Joining (NHEJ). The KO Score for pools typically tends to be

lower than the Indel Percentage, offering a distinct perspective on the overall impact of the editing process.

Additionally, the relative representation of each sequence within the population, referred to as "Contribution," is shown. The Indel Distributions Tab presents a histogram overviewing the distribution of indel sizes across the edited population. Hovering over each bar reveals the size of the insertion or deletion and the percentage of sequences containing it. Finally, the Traces Tab displays edited and unedited control Sanger traces, focusing on the region around the sgRNA binding site. In the control sample, the sgRNA target sequence is underlined in black, and the PAM site is highlighted with a dashed red underline. The vertical dashed line on both traces indicates the cut site, with Non-Homologous End Joining (NHEJ) repair typically resulting in a diverse mix of bases downstream of the cut. An example of Trace Tab visualization is shown in Figure 3.1.

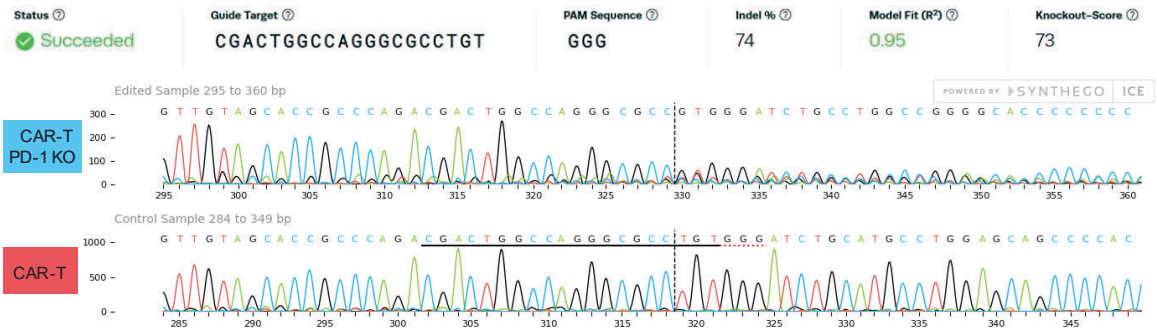

Figure 3.1 | Example of a Trace tab including all the parameters explained above of PD-1 KO obtained using the ICE analysis tool. The traces tab edited (CAR-T PD-1 KO) and control (CAR-T, bottom) Sanger traces in the region around the guide RNA binding site (horizontal black line) and the PAM site underlined with a red dotted line. The cut site is indicated with a vertical dotted line on both traces.

3.4. Supported lipid bilayers (SLBs)

3.4.1. Preparation of SLBs

Supported lipid bilayers (SLBs) were prepared as previously described by Axmann et al.[263] First, 1,2-dioleoyl-sn-glycero-3-[N(5-amino-1-carboxypentyl) iminodiacetic acid) succinyl] (nickel salt) (DGS-NTA(Ni)) and 1-palmitoyl-2-oleoyl-sn-glycero-3-phosphocholine were dissolved in chloroform and mixed in a 1:50 molar ratio. The

mixture was then dried under vacuum overnight and resuspended in 10 mL degassed PBS. Sonication was performed in a bath sonicator (Q700; Qsonica) under nitrogen at 120-170 W for at least 60 minutes until the suspension became clear. Nonunilamellar vesicles were pelleted through ultracentrifugation during 1 hour at 37.000 rpm (150.000*g*) at RT using a Sorvall RC M150GX ultracentrifuge with a S150AT-0121 rotor (Thermo Fisher). The clear supernatant was subjected to further centrifugation for 8 hours at 43.000 rpm (288.000*g*) at 4°C. The second supernatant was filtered (0,2 µm) and stored at 4°C for up to 6 months. Glass slides (22 x 64 mm^2 no. 1.5 borosilicate; Menzel-Gläser) were cleaned for 15 minutes using plasma (Zepto, Diener Electronic). Cleaned slides were attached to the bottom of an 12-well Nunc Lab-Tek chamber (Thermo Fisher) with Picodent twinsil extrahart (Picodent) until the glue had solidified. The lipid vesicle suspension was diluted 1:20 with PBS and filtered, and 100 µL of the diluted suspension were added to each well to form a continuous SLB. Excess vesicles were removed by washing the chambers with PBS. For functionalization, H12-tagged proteins were added to the SLBs and incubated for 60 min in the dark at RT. Finally, the chambers were rinsed twice with 15 ml PBS to remove unbound protein.

3.4.2. Microscopy setup

Microscopy was performed utilizing two distinctive inverted configurations. In one configuration, designed for TIR-based imaging, we employed an Eclipse Ti-E microscope body (Nikon Instruments), featuring a chromatically corrected 100× TIR objective (CFI SR Apo TIR 100× Oil, NA: 1.49; Nikon). A 647 nm diode laser (OBIS) served as the excitation source, while a custom-made Notch filter (Chroma Technology) effectively prevented the undesired reflection of 647 nm light from reaching the camera. This setup also included an ET700/75 emission bandpass filter (Chroma Technology) within the emission pathway, along with a dichroic (QUAD Cube). Data recording was accomplished using an iXon Ultra 897 EMCCD camera by Oxford Instruments. For seamless control and precise timing, an 8-channel DAQ-board (PCI-DDA08/16, National Instruments) integrated with the microscope automation and image analysis software MetaMorph (version 7.8.13.0, Molecular Devices) were used.

This combination facilitated the programming and application of timing protocols, allowing for precise orchestration of all microscope components.

3.4.3. Measurements of antigen densities on SLBs

The quantification of SLB antigen density was achieved through counting the diffraction-limited fluorescent events within a defined region of interest (ROI) or by dividing the fluorescence intensity value within the ROI relative to the single-molecule fluorescent intensity value. For bilayers that exhibited distinct and easily distinguishable diffraction-limited fluorescence events, 30 images were captured within a 100 x 100-pixel ROI. To ascertain the total number of molecules within each image's ROI, the Fiji Thunderstorm plugin (ImageJ/Fiji) was employed. The resulting count was then adjusted to account for pixel size and the number of images, enabling the determination of antigen density (with the conversion factor of 1 pixel≙0.0256μm^2, 100×100 pixels =10,000 pixels, or 256μm^2). To assess the antigen densities in SLBs, the average single-molecule fluorescence intensity value for a minimum of 300 molecules within the ROI was determined. This analysis was carried out using the Fiji Thunderstorm plugin, as previously described[263]. Subsequently, the average integrated intensity value for ROIs from 10 distinct images was computed, and this result was divided by the average single-molecule intensity value, yielding the number of molecules within the given ROI. To account for pixel size, the obtained value was adjusted. In the case of low antigen densities, which resulted in discernible diffraction-limited fluorescence events, the number of such events within a specific ROI across at least 30 images were counted and then the average count was divided by the ROI's area. The fluorophore densities were subsequently converted into antigen densities by taking into consideration the protein-to-dye ratio, a parameter determined through spectrophotometry.

3.5. Cell culture

3.5.1. Culture of commercial cells

3.5.1.1. Tumour cell lines

All human cancer cell lines were purchased from the American Type Culture Collection (ATCC) except from HEK 293FT (human embryonic kidney cells) and Jurkat Clon E6-1 (immortalized human lymphocytes from an acute T Cell Leukemia), which were obtained from Sigma Aldrich, and MDA-MB-468 (triple negative breast cancer), which was kindly provided by Dr. Aleix Prat from IDIBAPS-Hospital Clínic (Barcelona). HEK 293FT were cultured in DMEM-10 (Dubbeco's Modified Eagle's Medium, Gibco) supplemented with 1% GlutaMax and 1% non-essential amino acids (NEAA). SKOV3 (ovarian cystadenocarcinoma) were cultured in DMEM-10. CAPAN-2 (pancreatic carcinoma) and MDA-MB-468 were cultured in DMEM/F12 (Gibco), HCC1954 (breast ductal carcinoma) and Jurkat were cultured in RPMI-1640 (Roswell Park Memorial Institute, Gibco). All media was supplemented with 10% FBS (Merk, Lot #9669) and with penicillin-streptomycin (P/S) (100mg/mL) and all cell lines were grown at 37°C and 5% CO_2. All cells were regularly validated to be *Mycoplasma free* and authenticated in 2019 by IDEXX Bioanalytics using the Human 9-Marker STR Profile.

3.5.1.2. Human primary cells

Human Pulmonary Artery Smooth Muscle Cells (HPASMC), human Pulmonary Artery Endothelial Cells (HPAEC), human Renal Epithelial Cells (HREpC) and normal Human Epidermal Keratinocytes (NHEK) were purchased from Promocell and cultured according to manufacturer's protocols.

3.5.2. Genetically engineered tumour cell lines

To generate a cellular model expressing different PD-L1 densities, SKOV3 cells were genome edited to delete CD274 (PD-L1) using the CRISPR-Cas9 system as explained in the section 3.3.2. PD-L1 negative cell population was sorted by flow cytometry after treatment for 18 hours with 10UI of IFN-γ (BD Biosciences - # 554617). This treatment

induced PD-L1 expression, facilitating precise selection of the PD-L1 negative population. The SKOV3 PD-L1 KO cell line was then transduced with lentiviral vectors expressing PD-L1 under different promoters: EF1α (high) and pGK100 (low). Five days after transduction, tumour cells were trypsinized, washed two times with PBS and stained with L/D aqua (ThermoFisher - #L34957) and PD-L1 APC antibodies (BioLegend - #561787) and PD-L1+ tumour cells were collected separately using FacsAriaII cell sorter (BD). Copy numbers of PD-L1 molecules on cell surface were estimated using the Quantibrite™ Beads PE Fluorescence Quantitation Kit (BD Bioscience - #340495) according to the instructions of the manufacturer. Each BD Quantibrite™ PE tube contains a lyophilized pellet of beads conjugated with four levels of PE. Running a BD Quantibrite PE tube at the same instrument settings as the assay allows for conversion of the FL2 axis into the number of PE molecules bound per cell. By employing known ratios of PE to antibodies, this enables the conversion of PE molecules per cell to antibodies per cell.

SKOV3 PD-L1 KO and SKOV3 PD-L1 high cell lines were further modified to express folate receptor beta (FRβ) by using a lentiviral vector expressing FRβ under EF1α promoter. pCCL-EF1α-FRβ was synthesized by Genscript. After transduction, tumour cells were stained with an anti-FRβ antibody and FRβ+ tumour cells were collected using a FacsAriaII cell sorter (BD). MDA-MB-468 expressing high or low levels of HER2 were previously generated in the lab by Dra. Berta Marzal[262]. Both cell lines were further modified to express PD-L1 under the control of EF1α, as detailed for SKOV3 cells. For details on surface staining and sorting procedures, please refer to sections 3.6.1 and 3.6.3., respectively.

3.5.3. Lentiviral vector production

3.5.3.1. 293FT transfection

Lentiviruses are RNA viruses requiring a series of genes (Gag, Pol, Rev, Env, Tat) to be produced. Once lentivirus enters the cell, its RNA genome is retrotranscribed to dsDNA and this can integrate randomly inside the genome. To generate third-generation lentiviral particles, we conducted transfections on HEK293FT cells using our transfer

vector together with a pre-mixed combination of packaging plasmids (Fig. 3.2), which included:

- pMD2-VSV-G: This packaging plasmid encodes the lentiviral protein VSV-G, an envelope glycoprotein.
- pMDLg-pRRE: This packaging plasmid encodes the lentiviral proteins gag, which assembles the virus core, and pol, needed for the reverse transcription.
- pRSV-Rev: This packaging plasmid encodes the lentiviral protein REV, essential for the post-transcriptional transport.

Briefly, HEK293FT were seeded at $10{\cdot}10^6$ in a total volume of 18 mL of medium in a p150 culture plate. At the time of transfection, 18 µg of our pCCL transfer plasmid (containing the CAR) and the pre-mixed packaging plasmids mix containing 15 µg of pREV, 15 µg of pRRE and 7 µg of pVSV were diluted in serum-free DMEM (Tube 1). In parallel, linear PEI molecular weight (MW) 25,000 (Polysciences, 23966-1) mixed with medium (Tube 2) was added on the DNA mix drop-by-drop and incubated for 20 minutes at RT. Measures for 1 plate of 293FT are shown in Table 3.8.

MIX DNA + Medium (Tube 1)	MIX PEI + Medium (Tube 2)
18 µg interest vector	94,5 µL PEI (1X)
15 µg Rev 15 µg RRE 7 µg VSV-G 665 µL Medium	675 µL Medium
TOTAL VOLUME	
735 µL	769,5 µL

Table 3.8 | Amounts of DNA, PEI and medium to transfect one p150 plate.

During the incubation, 8 mL of medium per plate was removed, leaving the plate with only 10 mL before adding 1.5 mL of the PEI-DNA mixture carefully to each p150 plate to avoid disturbing the 293FT cells. After 4-6h of incubation, media was changed, and plates returned to the incubator. Viral supernatant was harvested at 48 and 72h post-transfection, 0.45 µm filtered and concentrated by LentiX™ as per manufacturer's protocol (Takara Bio - #631232). In short, one volume of LentiX™ concentrator was

gently mixed with three volumes of supernatant by inversion and incubated for 30 minutes at 4ºC before centrifugation at 1500*g* for 45 minutes at the same temperature. Finally, the off-white pellet was resuspended in complete media and frozen at −80 °C until use in 200 µL aliquots.

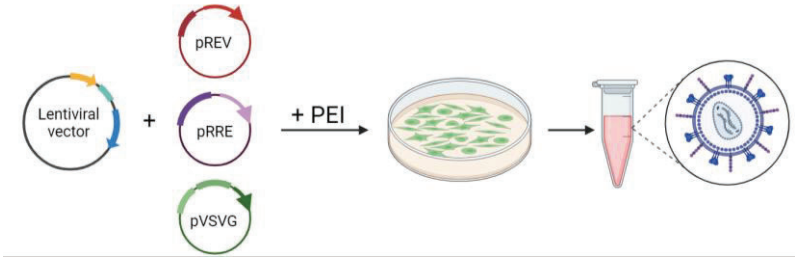

Figure 3.2 | Schematic Representation of lentiviral production on HEK293FT for the generation of lentiviral vectors containing the CAR.

3.5.3.2. Lentiviral vector titration

Lentiviral titration was done on Jurkat cells. The initial procedural stage was to determine the number of Jurkat cells required for the titration procedure, which depends on the quantity of vectors to be assessed (including the positive control). This calculation was performed in accordance with the following formula:

$$\text{Number of Jurkat cells} = [(\text{Number of virus to titer}) x\ 0.2^6] + 10^6$$

While lentiviral vectors were thawing on ice, both the Dilution Plate (96 well, round bottom) and the Titer Plate (96 well, flat bottom) were prepared. For the Dilution Plate, an initial 1/100 dilution was performed, combining 2 µL of vector with 18 µL of medium. Each vector was allocated to a dedicated column and 3-fold serial dilutions from Row A (with a dilution factor of 3) to Row H (with a dilution factor of 6561) were labelled for each sample. 60 µl of R10 medium to Rows A through H were added in each column, including a positive control well. Subsequently, 30 µL of the 1/100 diluted vector supernatant was applied to Row A, ensuring thorough mixing before transferring 30 µL from Row A to Row B. This process was repeated until each well contained a final volume of 60 µL. For the Titer Plate preparation, Jurkat cells were initially diluted to a concentration of $2{\cdot}10^5$ cells/mL. Using a multichannel pipette, 100 µL of Jurkat cells were dispensed into each well of the designated titer plate. Additionally, 100 µL of cells were allocated to one well reserved for untransduced cells (UTD) and another well

reserved for the unstained CAR control, used as a negative control. Following this, 50 µL of diluted vector supernatant were transferred from each well of the dilution plate into the corresponding well of the titer plate (Fig. 3.3). Finally, the titer plate was placed inside a 37°C, 5% CO_2 incubator and feeded with 100 µL of medium after a 24-hour incubation period.

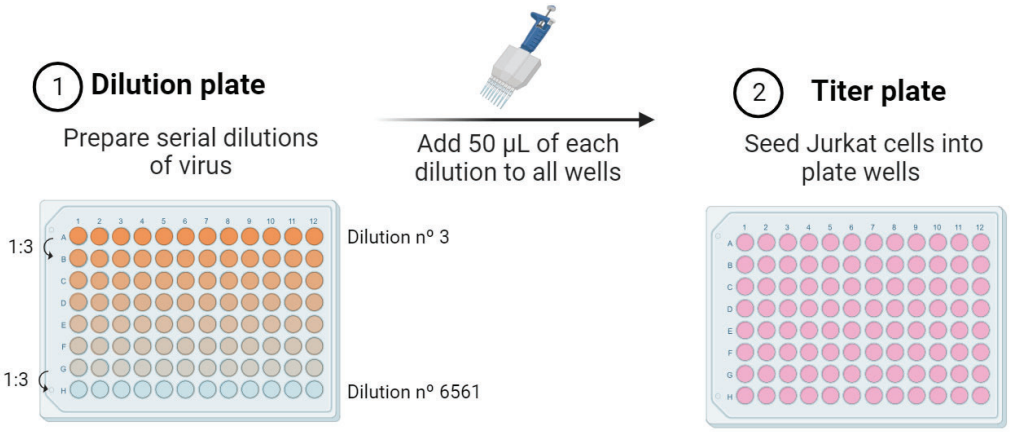

Figure 3.3 | Schematic Representation of lentiviral titration using the Jurkat tumour cell line.

3 days later, Jurkat cells were harvested, washed with PBS and stained with 2 µl of biotinylated Goat anti-mouse or anti-human $F(ab')_2$ (depending on the CAR construct origin) as explained in section 3.6.1. To calculate the viral titer, the following formula (for each vector at each dilution) was used:

$$\text{Titer}\left(\frac{\text{TU}}{\text{mL}}\right) = \frac{\%\ \text{positive}}{100} x\ 2^4 x\ 20\ x\ \text{dilution}$$

The first dilution at which the percentage of positive Jurkat cells was less than 20% was chosen because this dilution represents the most accurate limiting-dilution viral titer for the vector sample. Of note, the viral titer in T-lymphocytes is one-third of the titer in Jurkat cells, so to translate the calculated viral titer in Jurkat to a viral titer in T-cells the following formula was applied:

$$Viral\ titer\ in\ T-cells = \frac{Viral\ title\ in\ Jurkat\ cells}{3}$$

To transduce T-cells, a multiplicity of infection (MOI) between 3-10 viral particles/cell was used and calculated with this formula:

$$\text{Virus}\ (\mu\text{l}) = \frac{\text{nº cells x MOI}}{\text{nº viral particles}/\mu\text{l}}$$

3.5.4. CAR-T cell generation

3.5.4.1. Isolation and activation of primary human T-lymphocytes

Human T-cells were isolated from healthy donor buffy coats obtained from Banc de Sang i Teixits (Barcelona) under the Institutional Review Board approval and informed consent. The isolation of T-cells was done by Ficoll gradient (Lymphoprep, Stem Cell Technologies - #07851). Briefly, $CD4^+$ and $CD8^+$ T-cells were negatively isolated using RosetteSep™ Human $CD4^+$ or $CD8^+$ T-Cell Enrichment Cocktails (Stem Cell Technologies - #15022 and #15023, respectively) according to manufacturer's protocol. The buffy coat was mixed with isolation buffer and the enrichment kit and incubated at RT for 25 minutes. After this, isolation buffer was added to reach a final volume of 30 mL, and the mixture was overlaid on 15 mL of lymphocyte isolation solution. The tubes were centrifuged at 1200*g* for 25 minutes at RT with maximum acceleration and deceleration set to 1. The cell layer was carefully recovered using a sterile plastic Pasteur pipette and washed with isolation buffer. Erythrocytes were lysed using ACK lysing buffer, and the cells were subsequently washed and resuspended in CAR-T media (components detailed in Table 3.9.).

Component	Company	Catalog
RPMI 1640	Merck	R6504-10X1L
10% heat-inactivated FBS	Merck	F4135
1X Glutamax	ThermoFisher	35050-061
100 µg/mL Penicillin 100 U/mL streptomycin	ThermoFisher	15140122
10 mM HEPES	Sigma	H0887
10 ng/mL human recombinant IL-7	Miltenyi	130–095-362
10 ng/ mL human recombinant IL-15	Miltenyi	130–095-764

Table 3.9 | CAR-T cell media components

Cells were subsequently counted and stimulated separately with Dynabeads® Human T-Activator CD3/CD28 (Thermo Fisher - #11132D) at a 2:1 bead-to-cell ratio. $CD8^+$ T-cell groups included a 10% of $CD4^+$ T-cells to ensure its expansion. To support their growth and proliferation, human IL-7 and IL-15 was added every other day to a final

concentration of 10 ng/mL until day 8 of expansion. T-cells were left at $1 \cdot 10^6$ cells/mL concentration in the required plate/flask determined by the following formula together with Table 3.10.

$$N = \frac{Total\ milion\ cells}{0.35}$$

N	Well plate/flask type
2-5	24well plate
5-8	12well plate
8-20	6well plate
20-40	T25 flask-horizontal
40-112.5	T75 flask-horizontal
>112.5	T150 flask-horizontal

Table 3.10 | Plate or flask to culture T cells. Appropriate plate/flask to culture T-cells depending on the N value calculated with the indicated formula.

3.5.4.2. Transduction of T-cells with CAR-encoding lentiviral vectors

Following approximately 24 hours of activation, T-cells were transduced with the appropriate volume of CAR-encoding lentiviral vectors to reach a multiplicity of infection (MOI) of 2-10 (Fig. 3.4), in accordance with the formula below:

$$MOI = \frac{Viral\ titer \cdot Virus\ Volume}{T - cell\ number}$$

	MOI	T cell number ($\cdot 10^6$)	Virus ID	LV date	Viral Titer	Virus volume (µL)
CD4 UTD						
CD8 UTD						
CD4 Mov19 28z	3	10	Mov19-28Z	19/6/2023	4,79E+08	62,67
CD8 Mov19 28z	3	10	Mov19-28Z	19/6/2023	4,79E+08	62,67

Figure 3.4 | Representative table of T-cell transduction with CAR-encoding lentiviral vectors at day 1 of CAR-T cell expansion. ID, identification name; LV, lentivirus.

After 72 hours post-transduction, to avoid T-cells from remaining inactive for more than 2 days without replenishing media, half the volume of CAR-T medium was added.

3.5.4.3. Debeading and genomic edition of CAR-T cells

On the fourth day of culture, beads were removed in the morning. Concisely, T-cells were gently pipetted up and down to minimize air bubbles, and live T-cells were counted using trypan blue exclusion. CAR-T cell medium for each condition was calculated to adjust the cell concentration to $1{\cdot}10^6$ cells/ml. Samples were placed on a DynaMag-2 or Dynal 15-mL magnet magnet, depending on the volume (Thermo Fisher - #12321D and 12301D), allowing the beads to accumulate on the magnet-side walls for one minute. Without disturbing the beads, the sample was moved to the second tube for another minute, and then placed to the corresponding well/flask to ensure removal of all beads from the T-cell culture. Following the sequential process, the previously calculated medium was used to wash the beads after each transfer, and the cells were fed with the washing medium. Following a minimum incubation period of two hours after the debeading process, CAR-T cells were subjected to electroporation with either a control buffer (Mock CAR-T cells) or a mixture of Cas9 and a chemically synthesized sgRNA targeting *TRAC* or *PDCD1* using the CRISPR-Cas9 technology as explained in section 3.3.3.

3.5.4.4. Final expansion and freezing of CAR-T cells

After electroporation, CAR-T cells remained undisturbed for 24 hours and then were counted daily, maintained at $0{,}8{\cdot}10^6$ cells/mL to avoid cell overgrowth and transferred to the appropriate flask (Table 3.10) until day 10-11, when $CD4^+$ and $CD8^+$ T-cells were mixed at a 1:1 ratio, considering that the $CD8^+$ groups contain around a 10% of $CD4^+$ T-cells, and cryopreserved as explained in section 3.5.6. On day 7 or 8, the transduction efficiency was assessed by flow cytometry (section 3.6.1). For the experiments performed with the SLBs, CAR-T cells were sorted for CAR expression at day 7 of expansion as explained in section 3.6.3.

To confirm editing events in the *TRAC* locus, CAR-T cells were stained for CD3 at day 9 of T-cell expansion. For the PD-1 locus, DNA from CAR-T cells PD-1 KO edited pool was isolated as explained in section 3.1.3. The region surrounding the site of interest was

amplified, Sanger sequenced and quantified by using the ICE tool (Synthego) on day 8 and 10 of T-cell expansion as explained in section 3.3.4.

3.5.5. Cell counting

To determine cell numbers, trypan blue dying exclusion (Sigma - #T8154) was used. Adherent cells were detached by incubating them with TrypLE™ select (GIBCO - #12563029) for 5 minutes and resuspended in fresh medium containing FBS. A dilution in which up to 100 cells could be counted in each Neubauer chamber quadrant was made. Viable cells were counted and the number of cells per mL was calculated according to the following formula:

$$Number\ of\ \frac{\text{cells}}{\text{mL}} = Mean\ number\ of\ viable\ cells\ per\ quadrant\ x\ dilution\ factor\ x\ 10^4$$

3.5.5.1. Assessment of CAR-T cell population doublings

A successful primary T cell expansion is defined by population doubling reaching values ≥ 5. This number was calculated from day 4 until the end of the primary T cell expansion, relative to the number of cells stimulated on day 0 using the next formula: $Population\ doubling = (\log_2 \text{Total cells}_{\text{Day N}})$ - $(\log_2 \text{Total cells}_{\text{Day 0}})$

3.5.6. Cell freezing, cryopreservation and thawing

Cells were counted following the previously described method and were resuspended in cold freezing solution (comprising 80% FBS and 20% DMSO) to achieve a final concentration of 1-5·10^6 cells/mL for tumour cell lines and 20-50·10^6 cells/mL for primary T cells. The resulting cell suspension was distributed into cryotubes with 1 mL per tube, and subsequently placed in a freezing container at -80ºC for a 24-hour period. Following this initial freezing step, the cryotubes were stored within a liquid nitrogen tank. For cell thawing, cells were promptly transferred from the liquid nitrogen to a 37ºC water bath, diluted in pre-warmed medium and centrifuged at 300*g* for 5-7 minutes depending on the cell line. Finally, the resulting cell pellets were resuspended in fresh medium and plated at high confluence to maximize their recovery and viability.

3.5.7. Mycoplasma detection

All cell lines were routinely tested for mycoplasma contamination by PCR (explained in section 3.1.7.) using the primers shown in Table 3.11.

Primer	Sequence (5' → 3')	T_m (ºC)	Product length (bp)
Myco-1	GGCGAATGGGTGAGTAACACG	57,95	500
Myco-2	CGGATAACGCTTGCGACTATG	56,97	

Table 3.11. | Primers used for the detection of mycoplasma contamination.

Mycoplasma contamination was assessed in the SN of cell cultures that had been incubated for a minimum of 72 hours in the same medium. One mL of the SN was subjected to heating in a dry bath at 90ºC for 5 minutes, followed by centrifugation at 6000*g* for 5 minutes. The resulting pellet was removed, and only the clear supernatant was collected and stored at -20 ºC. In cases where the presence of mycoplasma was confirmed (evidenced by a band at 500bp), affected cells were either eliminated or, if feasible, treated with Plasmocin™ treatment (InvivoGen - #ant-mpt-1) at a concentration of 25 µg/mL for a minimum of two weeks. Subsequent testing was conducted until the mycoplasma test returned negative results. Plasmocin™ prophylactic (Invivogen - #ant-mpp) was added to the cells at a concentration of 5 µg/mL before sorting as a preventive measure against potential contaminations.

3.6. Flow cytometry and fluorescence activated cell sorting (FACS)

For suspension samples, cells were gently pipetted, followed by two PBS washes, before continuing with the staining process. As for adherent cells, they were washed with PBS, treated with trypsin for at least 3 minutes, and then washed twice with PBS prior to staining.

3.6.1. Surface staining

At least 200.000 T-cells were collected from wells and transferred into either a 96-well plate (U-bottom) or FACS tubes, followed by centrifugation at 2000 rpm for 3 minutes

and removal of the SN. Subsequently, cells were resuspended in 200 µl of PBS, and after another round of centrifugation, the supernatant was discarded. A single wash with 200 µl of PBS was performed to remove any residual FBS, critical for subsequent staining with viability dyes. Following this, cells were stained with Live and Dead (L/D) eFluor™ 450 (ThermoFisher - #48-4317-82) in the dark for 30 minutes RT and washed two times with PBS. Next, cells were resuspended in 100 µl of FACS buffer containing the desired antibodies against cell surface molecules. This was followed by a 30-minute incubation in the dark at 4ºC and two additional washes with FACS buffer. Finally, the cell pellet was fixed in 200 µl of PBS containing 2% paraformaldehyde (PFA).

For CAR-T cells obtained from *in vivo* experiments, 20 µl of murine Fc receptor (FcR) blocking reagent (Miltenyi - #130-092-575) was added to prevent nonspecific labelling for 10 minutes at RT prior to cell surface staining.

To detect CAR expression, cells were stained using goat anti-mouse IgG-biotin (Jackson ImmunoResearch). Due to its recognition of fragments from IgGs, the anti-Fc antibody cannot be combined with other surface antibodies (such as anti-CD4, CD8, etc.) as it poses a risk of nonspecific binding. Therefore, the anti-Fc antibody must be added separately and in advance of the other antibodies, in a separate step. To do this, cell pellets were resuspended with 100 µl of FACS buffer containing 2 µl of biotinylated anti-CAR antibodies. Following four washes with FACS buffer to ensure thorough removal of unbound antibodies, cells were resuspended in 100 µl of FACS buffer containing the antibodies against cell surface molecules and streptavidin.

3.6.2. Intracellular staining

For intracellular staining (ICS), cells were fixed and permeabilised using the True Nuclear and Foxp3/Transcription Factor Staining Buffer set (ThermoFisher - #00-5523-00) according to the manufacturer's instructions. Concisely, after the last wash from surface staining, cells were fixed by adding 200 µL of Fixation Buffer (Table 3.12.) to each well and incubated for 30 minutes at RT protected from light, centrifugated and washed with 200 µL of 1X Permeabilization buffer (Table 3.12). After fixation, T-cells sedimented at varying rates, necessitating higher centrifugation speeds and longer durations, for this

reason, all the centrifugation steps were performed at 500*g* at RT for 5 minutes. Cell pellets were then resuspended in 100 µL of 1X Permeabilization Buffer containing the appropriate directly conjugated antibody for detecting intracellular antigens, incubated for at least 30 minutes at RT under light protection and washed with 200 µL of 1X Permeabilization buffer two times. Finally, stained cells were resuspended in 200 µl of PBS containing 2% PFA and subjected to flow cytometric analysis.

Buffer	Composition
FACS Buffer	PBS 1X + 2% FBS
Fixation Buffer	Fixation/Permeabilization concentrate:diluent (1:3 ratio)
Permeabilization Buffer 1X	Permeabilization Buffer 10X (1:10 in distilled water)

Table 3.12 | List of buffers used in Intracellular Staining techniques.

All experiments were performed on a FacsCanto 3L, Fortessa 4L HT and Fortessa 5L (BD Biosciences). To ensure a high-quality analysis, 10.000 to 20.000 events of the population of interest were acquired and the data was analysed with FlowJo software (V.10, TreeStar). Antibodies listed on Table 3.13. were used for analysis.

Target	Fluorochrome	Clone	Dilution	Catalog #	Company
CD45	PerCP-Cy5.5	HI30	1:100	564105	BD Biosciences
CD45	APC	2D1	1:100	17-9459-42	Thermofisher
CD25	PECy7	4E3	1:50	25-0257-42	Thermofiher
CD4	AF488	RPA-T4	1:50	557695	BD Biosciences
CD4	PE	OKT-4	1:100	12-0048-42	ThermoFisher
CD8	APC	HIT8a	1:100	300912	BioLegend
CD8	APC-H7	SK1	1:100	566856	BD Biosciences
PD-1	PECy7	EH12.1	1:50	561272	BD Biosciences
PD-1	APC	J105	1:100	17-2799-42	Thermofisher
PD-1	BV711	EH12.2H7	1:50	329928	BioLegend
PD-L1	APC	29E.2A3	1:100	329708	BioLegend
PD-L1	PE	29E.2A3	1:50	329706	BioLegend
PD-L2	APC	24F.10C12	1:100	329608	BioLegend
TNF-α	PE	MAb11	1:50	554513	BD Biosciences

IFN-γ	PerCP-Cy5.5	B27	1:50	560704	BD Biosciences
CD107a	BV785	H4A3	1:50	328643	Biolegend
HER2	PE	24D2	1:100	324406	BioLegend
FRβ	PE	94b/FOLR2	1:5	391703	BioLegend
anti-mouse IgG, $F(ab')_2$ fragment specific	Biotin-SP (long spacer)	Polyclonal	1:50	115-065-072	Jackson ImmunoResearch
anti-human IgG, $F(ab')_2$ fragment specific	Biotin-SP (long spacer)	Polyclonal	1:50	109-066-006	Jackson ImmunoResearch
Isotype control Mouse IgG1 k	PE	MOPC-21	1:50	555749	BD Biosciences
Isotype control Mouse IgG1 k	APC	MOPC-21	1:100	555751	BD Biosciences
Related flow cytometry reagents:					
L/D Fixable viability dye	eFluor450	-	1:5000	65-0863-14	eBioscience
Streptavidin (SA)	PE	-	1:100	12-4317-87	ThermoFisher
SA	eFluor450	-	1:100	48-4317-82	ThermoFisher

Table 3.13 | List of antibodies and reagents used for Flow Cytometry techniques. AF, Alexa Fluor; APC, allophycocyanin; BV, brilliant violet; PE, phycoerythrin; Cy7 cyanine-7, PerCP, peridinin chlorophyll protein; Cy5.5, cyanine-5.5.

3.6.3. FACS sorting

In this work, SKOV3 tumour cells were sorted by PD-L1 expression levels: negative, low or high expression, respectively. Additionally, CAR-T cells were sorted based on the presence of CD45 for gene expression analyses, and on CAR expression on the seventh day of T-cell expansion for the experiments involving SLBs. Briefly, stained cells were sorted at 4ºC using a BD FACS Aria™ II or SORP cell separator by the personnel of the Cytometry and cell sorting facility of IDIBAPS. Gating strategies were employed based on forward and side scatter properties to exclude debris and doublets. Subpopulations

of interest were identified based on fluorescence intensity corresponding to specific markers. Sorted cells were collected into sterile tubes containing a 50:50 mixture of PBS and FBS buffer to enhance cell viability. After sorting, purity of sorted cells was assessed by reanalyzing sorted cells for marker expression using flow cytometry.

3.7. *In vitro* functional assays

3.7.1. Cytokine production

3.7.1.1. Enzyme-Linked ImmunoSorbent Assay (ELISA)

The fundamental principle of ELISA involves the immobilization of a target molecule, often an antigen or antibody of interest, onto a solid support. This immobilized molecule acts as a capture agent. Then, a secondary molecule, typically an enzyme-linked antibody, is applied. This secondary molecule binds specifically to the target molecule if present in the sample. After washing to remove unbound substances, a substrate for the enzyme is added. The enzyme, if bound to the target molecule, catalyses a reaction that produces a detectable signal, often a colour change or luminescence.

For the experiments with tumour cells, a total of $1{\cdot}10^5$ cancer cells were seeded in 48-well plates. Primary healthy cells ($1{\cdot}10^4$) were seeded in 96-well plates. After overnight incubation, T-cells were added at an effector/target ratio of 3:1. At indicated experiments, anti PD-L1 (Durvalumab) and anti PD-1 (Nivolumab) antibodies were added to CAR-T cells at a final concentration of 10 µg/mL. Supernatants were collected 24 hours after coculture, and interferon (IFN)-γ and interleukin (IL)-2 were analysed using the DuoSet® ELISA Development Kit (R&D Systems - #DY285B and DY202) as per the manufacturer's protocol.

For the experiments with the SLBs, CAR-T cells ($3{\cdot}10^5$) were resuspended in 100 µL of imaging buffer, seeded onto SLBs (containing different HER2 and PD-L1 densities) and incubated at 37°C for 15 minutes. Following incubation, 450 µL of RPMI 1640 medium supplemented with 25 mM HEPES, 10% FCS, 100 U/ml of P/S, 2 mM L-glutamine, and 50 µM of β-ME was added, and the cells were further incubated for 24 or 72 hours. The SN was collected and stored in 100 µL aliquots at -80°C until further use. The secretion

of IFN-γ was measured by ELISA using a commercially available kit (ELISA MAX™ Deluxe Set, BioLegend - #430104) as per manufacturer protocol.

Briefly, supernatants were incubated overnight on a plate coated with a capture antibody, and after the incubation, a detection antibody was added, followed by the addition of the Avidin-HRP solution. Subsequent addition of a colourless substrate solution led to an enzyme-substrate reaction, resulting in a colour change in positive wells. The intensity of the colour produced was directly proportional to the amount of target protein present in the sample. The reaction was terminated by the addition of a solution containing sulfuric acid, leading to the conversion of positive wells to a yellow coloration. Absorbance data was collected using Gen5 2.07 (Biotek) or iControl 2.0 (LifeSciences) software at 450 nm and 570 nm to correct for optical imperfections in the plate. Protein concentrations were determined by comparison to a standard curve generated from known concentrations of the target protein.

3.7.1.2. Bulk polyfunctionality assessment

For the intracellular detection of IFN-γ and tumour necrosis factor (TNF)-α, tumour cells ($5{\cdot}10^5$) were seeded in 12-well plates. After overnight incubation, T-cells were added at an effector/target ratio of 1:3. After 24 hours, GolgiPlug™ (BD Bioscience - #555029) was added to each well, along with a 1:500 dilution of a cocktail of phorbol 12-myristate 13-acetate (PMA) and ionomycin (Cell Stimulation Cocktail, Invitrogen - #00-4970-93) to the corresponding positive control wells. Four hours later, flow cytometry staining was performed as described in section 3.6.2.

3.7.1.3. Single-cell secretome (IsoLight polyfunctionality assay)

Co-cultures of CAR-T cells and SKOV3 tumour cells were established at a 1:3 effector:target ratio for 20 hours at 37°C, 5% CO_2. After incubation, cells were counted, checked for viability with trypan blue and further enriched using Anti-ErbB-2 MicroBeads (Miltenyi - #130-090-482) to deplete HER2+ tumour cells following manufacturer's instructions. Briefly, the erbB-2+ cells underwent magnetic labelling using Anti-ErbB-2 MicroBeads. Following this, the labelled cell suspension was

introduced into a MACS® Column, strategically positioned within the magnetic field of a MACS Separator. Herein, the magnetically tagged erbB-2+ cells were confined within the column, while unlabelled cells seamlessly passed through, leading to the depletion of erbB-2+ cells within this specific cell fraction.

Enriched T-cells were then stained with a cell membrane dye and an anti-CD8 AF647 antibody 10 minutes at RT for differentiation of $CD4^+$ and $CD8^+$ T-cell populations. Subsequently, 30.000 viable cells were loaded onto the 32-plex human IsoCode Single-Cell Adaptive Immune chip (IsoPlexis), and chips were inserted into the IsoLight machine.

A single-cell functional profile was established for each assessable product. These profiles were organized into distinct categories, including effector (comprising granzyme B [GrB], IFN-γ, macrophage inflammatory protein [MIP]-1α, perforin, TNF-α, TNF-β), stimulatory (encompassing granulocyte macrophage colony-stimulating factor, IL-2, IL-5, IL-7, IL-8, IL-9, IL-12, IL-15, IL-21), regulatory (including IL-4, IL-10, IL-13, IL-22, TGF-β1, sCD137, sCD40L), chemoattractive (featuring CCL-11, IP-10, MIP-1β, RANTES), and inflammatory (such as IL-1B, IL-6, IL-17A, IL-17F, MCP-1, MCP-4) functional groups. Polyfunctional CAR-T cells were characterized as cells simultaneously secreting a minimum of two proteins from the predefined panel per cell, with consideration given to the quantity of each produced protein (combining the number of secreted proteins and their intensity levels). Additionally, the Polyfunctional Strength Index (PSI) was calculated for each sample using a prespecified formula, defined as the percentage of polyfunctional cells, multiplied by mean fluorescence intensity (MFI) of the proteins secreted by those cells:

$$\text{PSI sample} = (\%\ \text{polyfunctional cells in sample}) \sum_{i=1}^{32} \text{MFI of secreted protein } i \text{ of the polifunction cells}$$

Data was analysed by using IsoSpeak software 2.9.0 (IsoPlexis, Branford, CT).

3.7.2. Proliferation assay

For T-cell proliferation assays, tumour cells ($1 \cdot 10^5$) were seeded in 48-well plates and after overnight incubation, T-cells were added at an effector/target ratio of 3:1. Absolute

numbers of live cells were calculated for each group using trypan blue exclusion before coculture and after 6 days of incubation with tumour cells.

3.7.3. Degranulation assay

In our study, we evaluated degranulation by measuring CD107α expression, a recognized marker for both T-cell activation and cytotoxic degranulation. For this assay, target cells ($1{\cdot}10^5$) were seeded in 48-well plates. After overnight incubation, T-cells were added (effector/target ratio of 1:1) and incubated for 2 hours at 37ºC. To enable the detection of the CD107α marker, a protein transport inhibitor containing brefeldin A, GolgiPlug™ (BD Bioscience - #555029) was added to each well along with 2 µL of the anti-CD107α antibody. The co-culture was extended for an additional 4 hours. Then, T-cell staining was analysed by flow cytometry as described in section 3.6.2.

3.8. *In vivo*

3.8.1. Animal manipulation

In this study, the NOD scid gamma mouse (NSG) was selected as the animal model due to its exceptionally high level of immunodeficiency. These mice exhibit a unique genetic makeup, with two critical mutations on the NOD/ShiLtJ background: one in the DNA repair complex protein Prkdc, known as the scid mutation, resulting in a deficiency of B and T-cells. Additionally, they carry a complete null allele of the IL-2 receptor common gamma chain (IL-2rgnull), preventing cytokine signalling through various receptors and causing a deficiency in functional natural killer (NK) cells. This remarkable level of immunodeficiency makes NSG mice a valuable choice for humanization through engraftment with various human cell lines.

3.8.1.1. Study approval

All mouse studies were performed under a protocol (184-20) approved by the Ethic Committee for Animal Experimentation (CEEA) of the University of Barcelona and Generalitat de Catalunya.

3.8.1.2. Animal housing

Mice were bred and maintained within the Animal Facility at the University of Barcelona, with a 12-hour light/dark cycle, a temperature range of 20-24ºC and a humidity range of 45-65%. Mice health status was regularly monitored by qualified personnel.

3.8.1.3. Tumour implantation

Tumour cell lines were amplified until the desired numbers to inoculate per mice, trypsinized, washed and resuspended in a solution of 1:1 PBS:Matrigel (Corning - #11543550) on ice. Matrigel is a solubilized extracellular matrix (ECM) generally used to facilitate tumour engraftment and growth especially in models with low take rates. It also helps to better mimic *in vivo* tumour environments. When working with Matrigel, cells were kept always on ice, as Matrigel solidifies between 22-35°C.

Female NSG mice were anesthetized by isoflurane inhalation (1-3%) prior to subcutaneous injection to reduce stress in the animals. 4-5·10^6 cells (SKOV3, HCC1954 or CAPAN2) cells were then implanted subcutaneously in a final volume of 100 µL per flank.

3.8.1.4. CAR-T cell treatment

On the day preceding the treatment, mice were subjected to randomization, considering tumour size, to ensure comparable baseline means. In parallel, CAR-T cells were thawed at 4·10^6 cells/mL. On the following day, the viable cells were counted via trypan blue exclusion, washed two times with PBS, strained through a 100-µm filter to eliminate any cellular aggregates and resuspended in PBS. Mice were treated intravenously with 2-5·10^6 control T-cells, mock CAR-T cells, or PD-1 KO CAR-T cells in

100 µL of PBS when tumours reached 150-250 mm^3. All mouse experiments included at least 4 mice per group (exact numbers are specified in figure legends). Tumour dimensions were measured weekly with a digital calliper and volumes were calculated using the formula $V = 6 \cdot \frac{(L \cdot W)^2}{\pi}$, where:

L = Length of tumour

W = Width of tumour

Mice were sacrificed when tumours reached 1500 mm^3, ensuring that no mice remained with tumour volumes above this threshold for longer than 5 days. PD-L1–blocking antibody (Durvalumab) was administered intraperitoneally (IP) at a dose of 10 mg/kg every 5 days during the specified experiment.

3.8.2. Peripheral Blood Persistence Analysis

Analysis of CAR-T cell persistence was conducted by assessing T-cell populations in the peripheral blood of treated animals using BD Trucount tubes (BD Bioscience® #663028). BD Trucount™ Tubes are equipped with a predetermined number of fluorescent beads, indicated on the pouch label. These beads serve as a reference for the flow cytometer software to compute absolute cell counts accurately.

The absolute number of human T-cells per µl of blood was determined by mixing whole blood with antibodies against T-cell markers in Trucount tubes. Approximately 100 µL of blood was collected via retro-orbital bleeding, placed into EDTA blood collection tubes and processed within a 24-hour window. Briefly, 20 µL of the antibody master mix, comprising the human lineage markers CD45-PerCyP5.5, CD4-PE and CD8-APC, was added to Trucount tubes. Following this, 50 µL of whole blood from treated animals were introduced to each Trucount tubes. A positive control was prepared using human PBMCs from healthy donors and added to untreated (or saline-treated) animal blood. After gentle vortexing and incubation in the dark at RT for 15 minutes, 450 µL of 1x BD FACS lysing solution was added to lyse red blood cells. Samples were then incubated again 15 minutes in the dark at RT. Compensation controls were used to set up voltages and adjust fluorescent compensation. Threshold adjustments were made to include

beads and cell populations of interest while minimizing debris. Flow cytometry analysis was performed by first gating on beads and $CD45^+$ cells, followed by further gating on specific T-cell populations (i.e., $CD4^+$ and $CD8^+$). 5.000 bead events per sample were recorded, and T-cell numbers were calculated using the following formula (the number of beads per test vary from lot to lot and are found on the Trucount tube foil bag):

$$\text{T} - \text{cell number (cells/µL blood)} = \frac{T\text{–}cell\ events}{Bead\ events} \text{ x } \frac{\text{Number of beads per test}}{\text{Volume of blood per test}}$$

3.8.3. Tissue processing

In the case of CAR-TILs obtained from *in vivo* experiments, cells were collected from xenograft mouse tumours at specified timepoints following T-cell treatment. Disaggregation of human tumours was done through an enzymatic method utilizing the Tumour Dissociation Kit for humans (Miltenyi - #130-095-929) as per-manufacturer's instructions. Briefly, the process began by wetting the fur around the tumour of the sacrificed mouse with 70% ethanol. The skin enclosing the tumour was then carefully cut, and the tumour was extracted using forceps. Subsequently, the tumour was rinsed in a well from a 6-well plate containing FBS-free medium placed on ice. Tumours were then sectioned into pieces measuring 2-4mm and transferred into a 15 mL tube containing the appropriate enzyme mix, detailed in Table 3.14.

Components	Volume
FBS-free RPMI	4.4 mL
Enzyme H	100 µL
Enzyme A	12.5 µL
Enzyme R	10 µl

Table 3.14 | Enzyme mix components for CAR-TILs isolation from tumours.

Then, tissue fragments were incubated for 30 minutes at 37°C with continuous rotation, using a rotor placed inside a cell incubator at the lowest speed after ensuring that the tubes were securely closed. The samples were then vigorously resuspended using a plastic pipette Pasteur and incubated for an additional 30 minutes at 37°C with continuous rotation. Following the incubation, samples were filtered through a 100 µm cell strainer, with gentle pressure applied using the rubber bottom of a 5 mL syringe. The

cell strainer was rinsed with 10 mL of RPMI media supplemented with 10% FBS. The processed tumour samples were kept on ice until analysis. Subsequently, the samples were centrifuged at 300*g* for 7 minutes at 4ºC, and the SN was discarded. The cell pellet was then resuspended in 1ml of ACK lysis buffer, and after pipetting to ensure thorough mixing, it was incubated for 1-2 minutes at RT (skipped if red blood cell contamination was minimal). Following this, 9 mL of RPMI with 10% FBS was added and mixed well. The sample was filtered again, through a 40 µm cell strainer, and rinsed with 10 mL of RPMI 10% FBS. Samples were centrifuged at 300*g* for 7 minutes at 4ºC, and the SN was discarded. For the analysis via flow cytometry, the processed samples were resuspended in PBS FBS-free, and the staining protocol explained in section 3.6.1.

3.9. Histological analyses

3.9.1. Immunohistochemistry (IHC)

Tumours were harvested at the experimental endpoint, fixed with PFA 4%, and embedded in paraffin. Immunohistochemistry stainings were performed by the Biobanc HCP-IDIBAPS Core according to standard protocols. Briefly, tumour sections were incubated with a 1:100 dilution of anti-PD-L1 antibody (Cell Signaling - #15165) followed by a rabbit specific IHC polymer detection kit HRP/DAB. Slides were counterstained with hematoxylin, dehydrated and mounted. Images were obtained using a Nikon Eclipse E600 inverted microscope and an Olympus DP72 camera.

3.10. Data representation and statistical analyses

All statistical analyses were performed using GraphPad Prism v9.4.1 (GraphPad Software Inc.). For comparisons of two groups, two-tailed t-tests or one-sample t-test were used. One-way analysis of variance (ANOVA) with Tukey post hoc test was used for the comparison of three or more groups in a single condition. For the analysis of multiple groups, a two-way ANOVA test with Sidak or Tukey's multiple comparisons correction were performed. Symbols indicate statistical significance as follows: *p<0.05; **p<0.01; ***p<0.001; ****p<0.0001; ns, not significant.

Results

4. Results

4.1. Generation of a tumour cell model with different levels of PD-L1 expression

To study the role of PD-1/PD-L1 axis on CAR-T cells under controlled conditions, we first generated a tumour model based on the ovarian cancer cell line SKOV3, which was engineered to express varying PD-L1 densities (negative, low or high). To this purpose, we knocked *CD274* (which encodes PD-L1) out from SKOV3 cells by using CRISPR/Cas9 technology. As PD-L1 is upregulated following exposure to IFN-γ, our initial objective was to achieve an IFN-γ concentration sufficient to induce PD-L1 upregulation in all cells in order to accurately select the desired cell populations. We determined that 10 International Units (IUs) of IFN-γ were adequate to attain 100% positive cells (Fig. 4.1a). With this knowledge, we conducted CRISPR gene editing targeting PD-L1 in SKOV3 cells, subsequently exposing them to 10 UIs of IFN-γ for 18 hours prior to sorting (Fig. 4.1b). As a result, we achieved an 86.6% depletion of PD-L1 expression within the targeted cell population, enabling us to proceed with sorting the PD-L1 negative population (Fig. 4.1c). To validate the complete absence of PD-L1 expression in the sorted cells, we exposed both SKOV3 WT and PD-L1 KO cell lines to IFN-γ treatment, subsequently assessing PD-L1 expression. In the case of the WT cell line, there was an observed upregulation of PD-L1 following IFN-γ treatment, whereas, in our KO cells, we could not detect PD-L1 expression (Fig. 4.1d). After generating the SKOV3 PD-L1 KO cells, we transduced them with LVs encoding PD-L1 under the control of constitutive promoters with either low (pgk100) or high (EF1α) intensity. Subsequently, we repeated the sorting process outlined earlier to obtain precise PD-L1 low and high expression populations. Cells transduced with the pgk100 promoter exhibited relatively lower PD-L1 expression, while those with the EF1α promoter displayed significantly higher levels of PD-L1 expression, thereby confirming that the patterns of PD-L1 expression correlated with the strength of the promoter used. In addition, we sought to confirm the representativeness of the generated model in terms of PD-L1 expression levels in wild-type cell lines, both at the basal level and during co-culture with CAR-T cells, known to release IFN-γ and

consequently induce PD-L1 expression[264,265]. In the case of SKOV3 WT cells, baseline (green) PD-L1 expression was situated between the negative and low populations, while SKOV3 WT cells treated with CAR-Ts (dark green) exhibit an expression level falling between the low and high populations (Fig. 4.1e). We also confirmed expected patterns of the SKOV3 PD-L1 model in terms of PD-L1 expression in xenograft tumours *in vivo*. Notably, SKOV3 WT cells displayed a baseline expression level positioned within between the negative and low ranges. Upon exposure to CAR-T cells, their PD-L1 expression exhibited a discernible transition from negative-low to low-high levels, as confirmed by immunohistochemistry (IHC) (Fig. 4.1f).

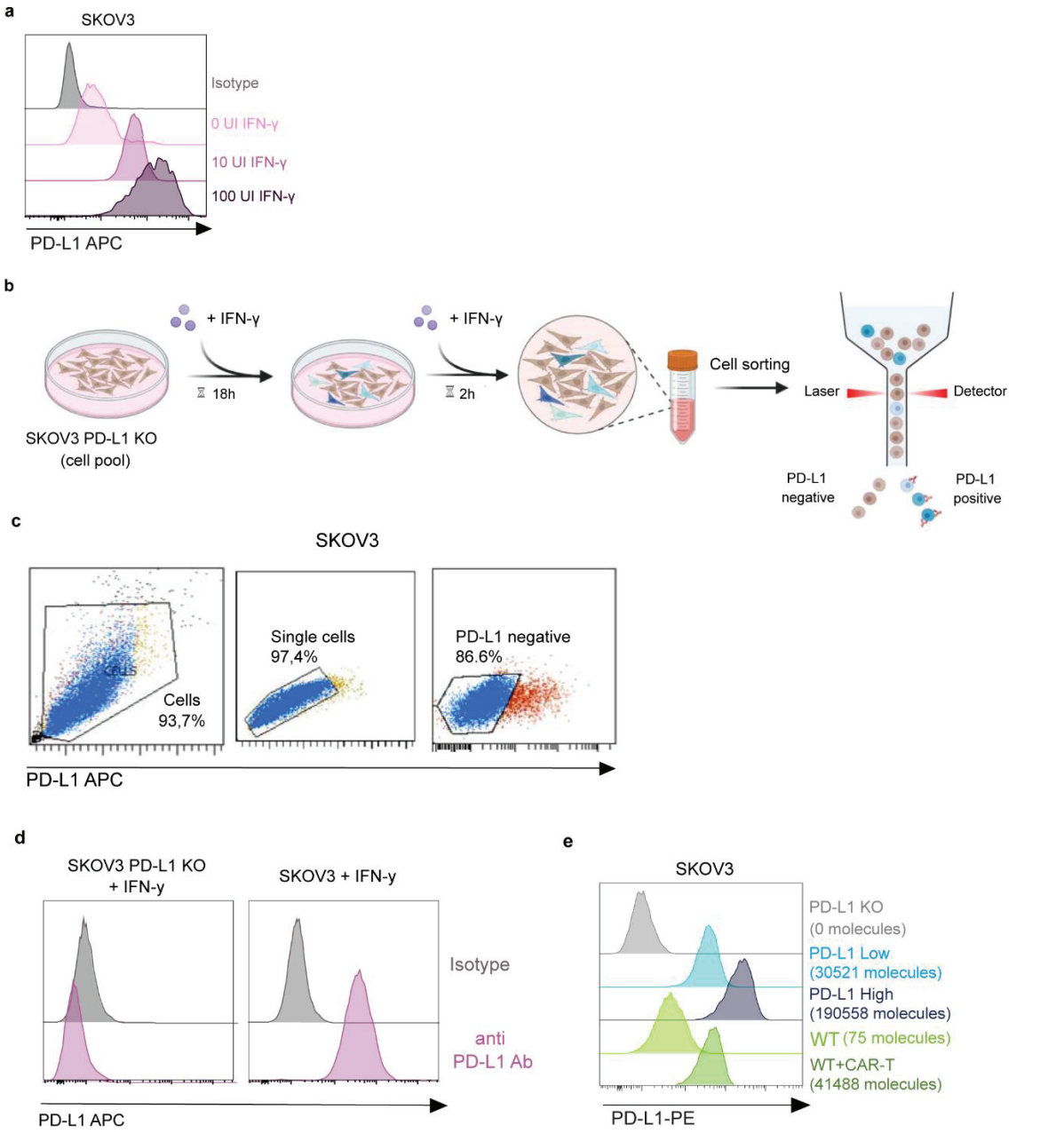

(continues on the next page)

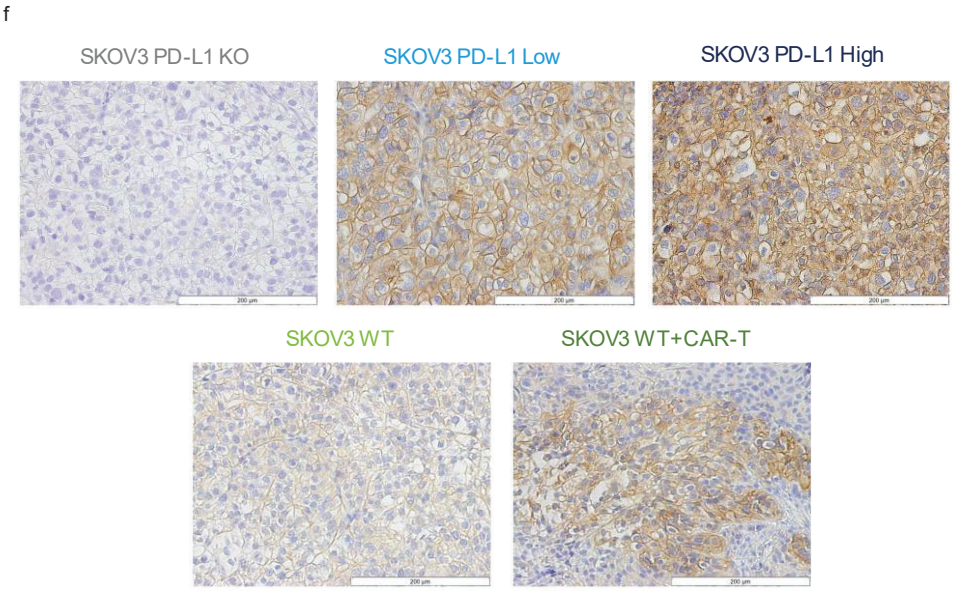

Figure 4.1 | Generation of a tumour cellular model with different PD-L1 densities. a PD-L1 expression by flow cytometry in SKOV3 WT cell line exposed to increasing international units (IU) of IFN-γ. **b** Workflow followed for sorting the desired PD-L1 negative, low or high cell lines. **c** Gating strategy followed during the sorting of PD-L1 negative SKOV3. **d** PD-L1 expression by flow cytometry of SKOV3 PD-L1 KO and SKOV3 tumour cells treated with IFN-γ. **e** Expression and quantification of PD-L1 molecules in SKOV3 cells expressing variable PD-L1 densities and compared to WT cells alone or co-cultured with CAR-T cells for 48 hours as assessed by flow cytometry. **f** Immunohistochemical staining of PD-L1 in SKOV3 PD-L1 KO, Low, High, and WT tumours treated with control T-cells or CAR-T cells at day 20-70 post-implantation in mice. Scale bar, 200 µm.

To determine the model's broader applicability, we investigated PD-L1 expression in a variety of tumour cell lines derived from different solid cancer types, such as pancreatic, breast, lung and colon, both under baseline conditions and during co-culture with CAR-T cells. We found that the majority of the cell lines tested fell within the range defined by our model (Fig. 4.2). This observation reinforced the model's capacity to accurately capture the natural diversity in PD-L1 expression across these distinct tumour cell lines.

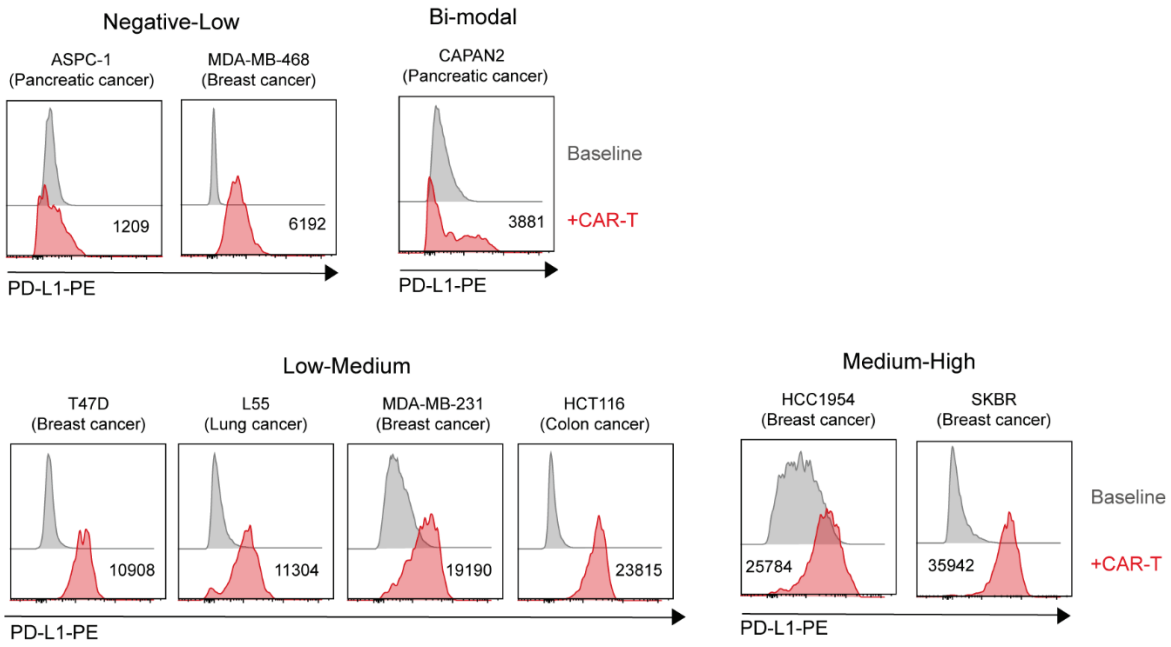

Figure 4.2 | Characterization of the SKOV3 tumour model in terms of PD-L1 expression. Expression and quantification of PD-L1 molecules on a panel of tumour cell lines at baseline (baseline, grey) or following coculture with CAR-T cells (red) for 48 hours assessed by flow cytometry.

4.1.1. PD-L1 exhibits higher expression than PD-L2 in SKOV3 cells both in vitro and in vivo.

To evaluate the possibility of PD-L2 influence in our model, we examined the expression profiles of PD-L1 and PD-L2 following treatment with CAR-T cells, considering both short-term and long-term expression patterns. Initially, an *in vitro* assessment was conducted after a 48-hour exposure to either IFN-γ or CAR-T cells. Our observations revealed a simultaneous upregulation of PD-L1 and PD-L2 within SKOV3 cells in response to both IFN-γ and CAR-T cell treatments, with PD-L1 exhibiting a more pronounced enhancement relative to PD-L2 (Fig. 4.3a). Another issue of concern was the possibility that knocking PD-L1 out might trigger an upregulation of PD-L2 as a compensatory mechanism in the PD-L1 negative tumour cells. For this reason, we also examined the PD-L2 expression in SKOV3 PD-L1 KO and WT cancer cells 24 hours after co-culturing with Control T-cells, mock CAR-T cells, and PD-1 KO CAR-T cells. Our analysis showed that the PD-L2 expression remained consistent in both tumour cell lines across all tested conditions, demonstrating no significant changes (Fig. 4.3b).

Subsequently, we proceed to evaluate the expression levels of both PD-L1 and PD-L2 expression at specified time-points (days 7, 14 and 21) after control T-cell or CAR-T cell treatments *in vivo* (Fig. 4.3c). A progressive increase in both PD-L1 expression and mean fluorescence intensity (MFI) was noted over time following treatment with CAR-T cells, although significance was only reached on day 21 (Fig. 4.3d-f, left panel). Conversely, for PD-L2, the values between the control and CAR-T-treated groups exhibited notable similarity, and no significant changes were observed in terms of expression levels or MFI (Fig. 4.3d-f, right panel). Collectively, these findings demonstrate that PD-L1, rather than PD-L2, undergoes upregulation in SKOV3 wild-type cells following CAR-T cell treatment. These observations support PD-L1 as the predominant ligand for PD-1 in our model.

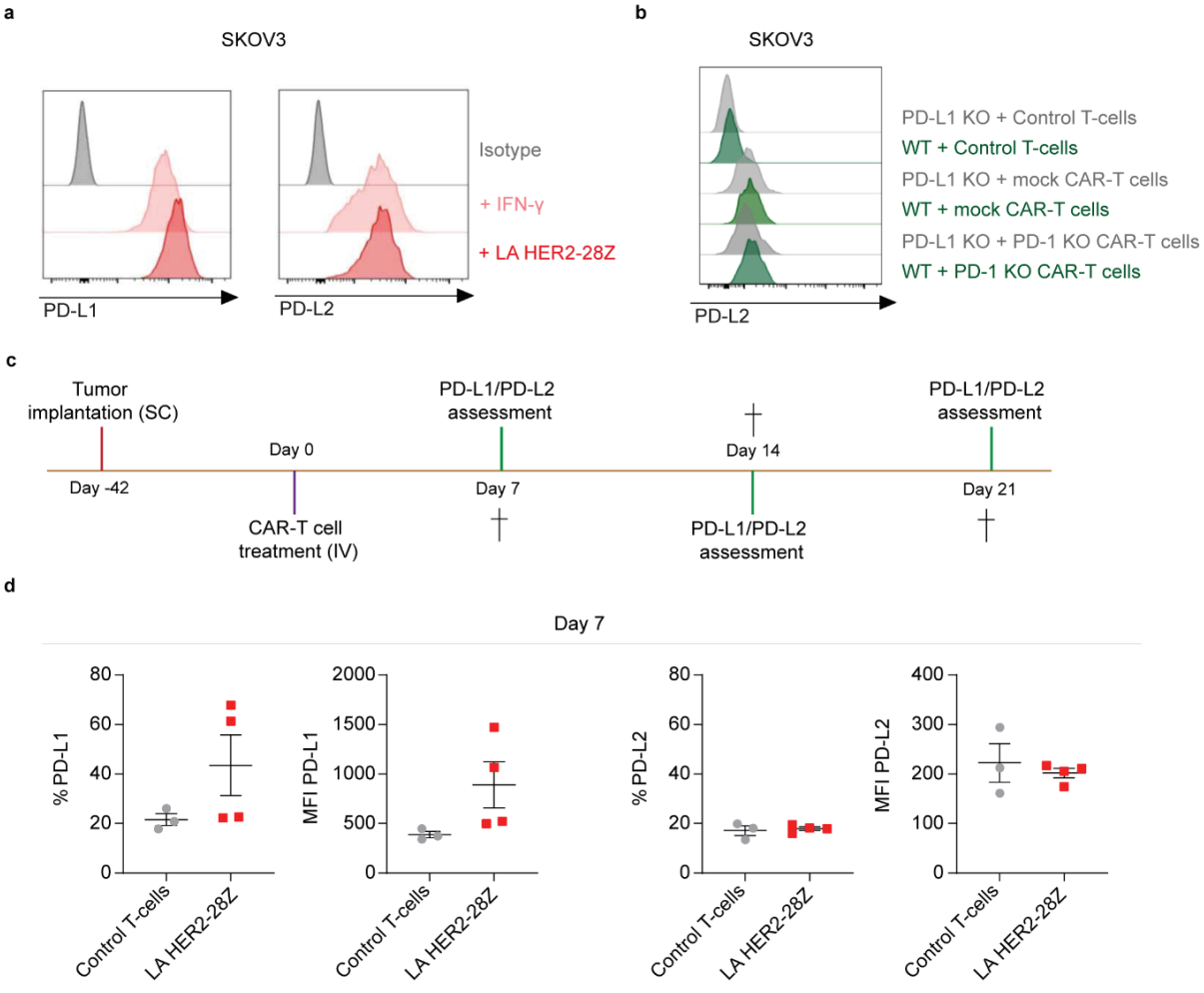

(continues on the next page)

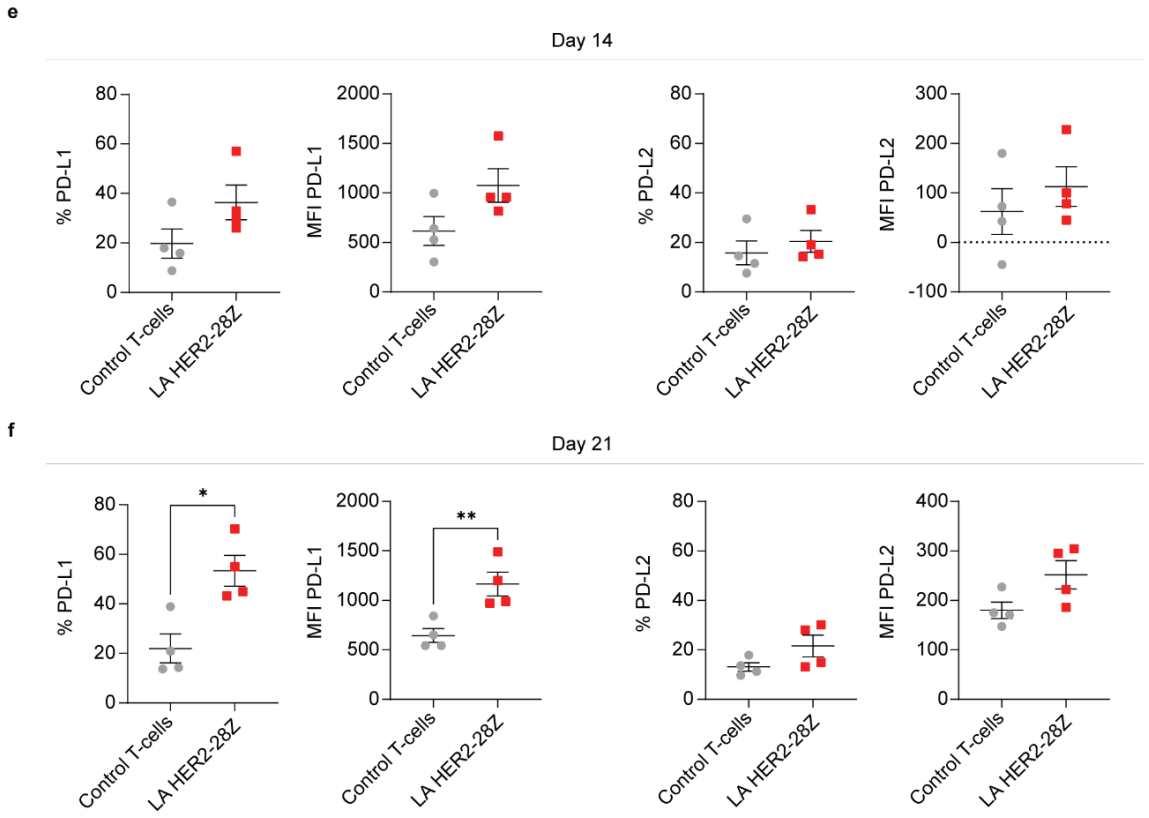

Figure 4.3 | Characterization of PD-L1 and PD-L2 upregulation *in vitro* and *in vivo*. **a** PD-L1 and PD-L2 expression on SKOV3 WT by flow cytometry after treatment for 48 hours with 10 IUs of IFN-γ or CAR-T cells. **b** PD-L2 expression on SKOV3 PD-L1 KO or SKOV3 WT by flow cytometry after treatment for 24 hours with control T-cells, mock CAR-T cells or PD-1 KO CAR-T cells. **c** Timeline of the *in vivo* experiment conducted. PD-L1 and PD-L2 expression and MFI in xenograft tumours at **d** day 7, **e** 14 or **f** 21 after control T or CAR-T cell treatment.

4.2. Generation of human PD-1 KO CAR-T cells targeting HER2 with low or high affinity

For the purpose of this study, we used CD28-costimulated CAR-T cells targeting HER2 either with high affinity (HA) by using the trastuzumab-based 4D5 scFv, or with low affinity (LA) by using a mutated version of the previous with a ~2000-fold reduced affinity, named 4D5.5[254] (Fig. 4.4a). Both CARs are of second-generation design, since they contain a fused CD28 and CD3ζ endodomain, and are under the control of the human EF1α promoter.

Because our group did not have experience in T-cell genome editing, we first optimized our protocol for the isolation, expansion and genetic modification of T-cells to include a

CRISPR-Cas9 gene editing step. Briefly, isolated T-cells were first stimulated with anti-CD3 and anti-CD28 magnetic beads and 24 hours following activation, they were transduced with LVs containing the CAR specific for HER2 either with LA or HA. On day 4 after stimulation, magnetic beads were removed from CAR-T cells and finally electroporated using the CRISPR/Cas9 system (Fig. 4.4b). As a first approach, we attempted to knock CD3 out from CAR-T cells using a published single guide RNA (sgRNA) targeting TCR-α chain constant region (TRAC)[243,266]. Because CD3 is constitutively expressed on the cell surface of T cells, the efficiency of CD3 KO can be easily detected by flow cytometry. CAR-T cells were electroporated with buffer alone (mock) or with Cas9 protein bound to the sgRNA specific for TRAC at 3.3:1 sgRNA:Cas9 ratio. Using this strategy, we were able to obtain a KO efficiency near to 100% (Fig. 4.4c). Therefore, we decided to apply a similar strategy to disrupt PD-1 using a chemically synthesized sgRNA targeting *PDCD1* exon 1 in CAR-T cells. We assessed the expression levels of surface CAR (Fig. 4.4d) and PD-1 on day eight of T-cell expansion. Both LA and HA mock CAR-T cells exhibited comparable levels of CAR and PD-1 expression of approximately 70%. This substantial PD-1 expression was indicative of a robust T-cell activation during primary expansion. Subsequently, by employing CRISPR/Cas9-mediated gene editing to KO PD-1, we observed a significant reduction in PD-1 expression levels (Fig. 4.4e). We consistently achieved ablation efficiencies of approximately 80% in all healthy donors used (Fig. 4.4f). To determine if the process of genome editing affected the *in vitro* expansion of CAR-T cells, we measured the number of times that T cells from different groups doubled since the activation through αCD3/CD28 stimulation, a parameter known as “population doublings”. We did not observe any differences in T cell growth between mock electroporated CAR-T cells and PD-1 KO CAR-T cells. However, when compared to control T-cells that did not go through the electroporation process, both transduced groups showed a decrease in the population doublings. This can be explained due to the toxicity induced during the electroporation step. Two days after electroporation, CAR-T cells recovered, and showed an exponential growth rate similar to control T cells (Fig. 4.4g). To test whether PD-1 deletion had any detrimental effect on CAR T cell activation, rested bulk PD-1 edited CAR T cells were re-stimulated with SKOV3 tumour cells and T cell activation was monitored by CD25 and PD-1 expression. PD-1 deletion did not impact CAR-mediated

activation, as evidenced by uniform CD25 up-regulation in both edited and mock CAR T cells following re-stimulation (Fig. 4.4h).

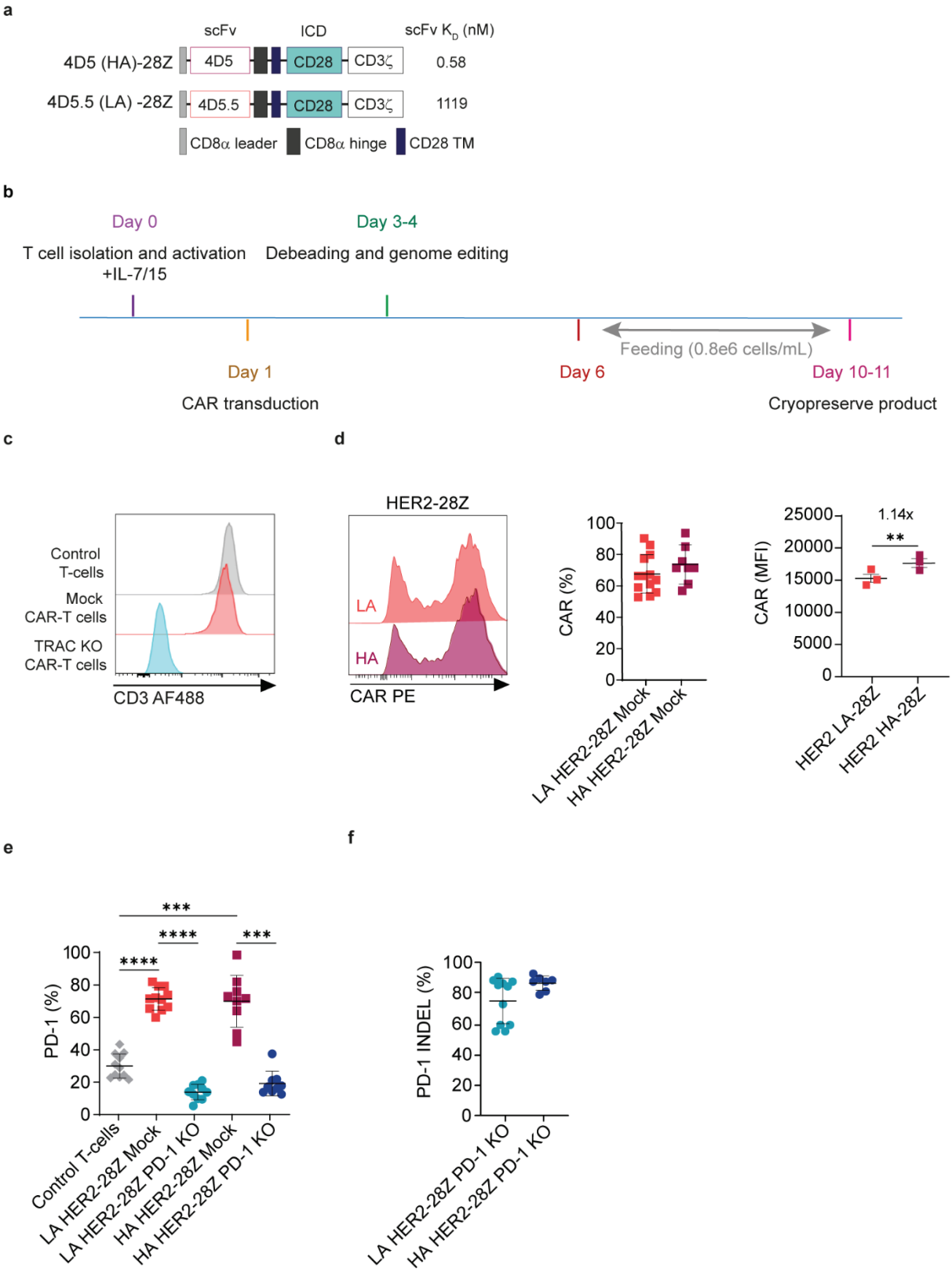

(continues on the next page)

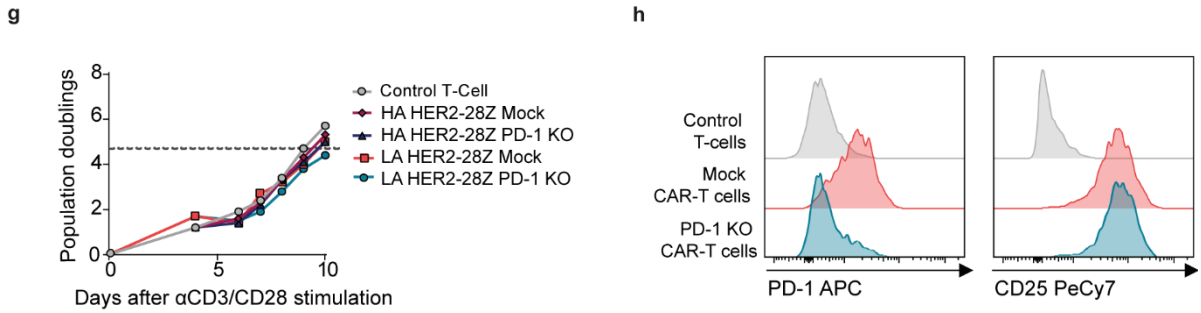

Figure 4.4 | Generation of PD-1 KO CAR-T cells. a Schematic overview of CAR constructs used with their corresponding affinity values. **b** Timeline of CRISPR-Cas9 editing and manufacturing in primary human CAR-T cells. **c** CD3 expression of control T-cells, LA HER2-28ζ mock and TRAC KO CAR-T cells by flow cytometry at day 9 of T-cell expansion. Flow cytometric analysis showing **d** CAR expression by representative histogram (left panel), percentage (middle panel) or MFI (right panel) or **e** PD-1 surface expression of indicated CAR-T cells at day 8 of T-cell expansion (n=11 donors for control T-cells and LA CAR-T cells, and 7 for HA CAR-T cells). Data plotted as mean ± SD. **, p<0.01; ****, p < 0.0001 by paired T-test. **f** CRISPR/Cas9 efficiency represented as mean frequency of indels at day 10 of T-cell expansion (n=10 donors for LA CAR-T cells and 7 for HA CAR-T cells). Data plotted as mean ± SD. **g** Representative population doubling of mock and PD-1 KO LA and HA HER2-28Z measured using trypan blue exclusion during CAR-T cell expansion (Representative of 5 donors). **h** PD-1 and CD25 expression gated on LA HER2-28ζ mock and PD-1 KO CAR+ T cells by flow cytometry at day 6 after co-culture with SKOV3 wt cells.

When we examined the percentage of PD-1 KO in T-cells during the primary expansion of CAR-T cells, a significant enrichment of both CD4+ and CD8+ T-cells lacking PD-1 was observed in LA CAR-T cells from day 8 to day 10 (Fig. 4.5a). However, this enrichment was not seen in HA CAR-T cells (Fig. 4.5b). This difference was intriguing, considering that these cells are not encountering PD-L1. While some publications affirm that T-cells themselves express PD-L1[267], we were unable to detect differences in expression that could account for this enrichment through flow cytometry analysis.

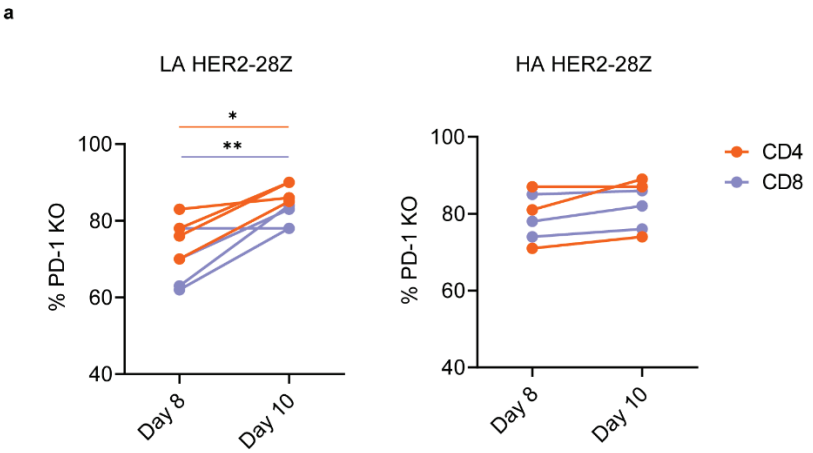

(continues on the next page)

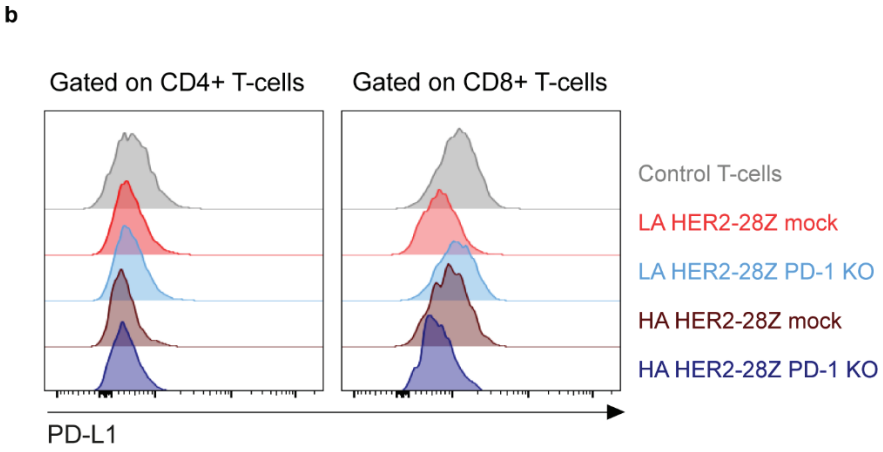

Figure 4.5 | Selective enrichment of PD-1 KO LA HER2-28ζ CAR-T Cells during the primary T cell expansion. a Percentage of PD-1 KO cells quantified using ICE (Synthego) at day 8 and day 10 of the primary expansion for LA (left panel) and HA HER2-28ζ (right panel). CD4+ T-cells are represented by orange lines, while CD8+ T-cells are indicated by purple lines. **b** PD-L1 expression on day 7 of the primary expansion, measured by flow cytometry in Control T cells, LA and HA HER2-28ζ mock and PD-1 KO. The results were plotted separately for CD4+ T-cells (left panel) and CD8+ T-cells (right panel).

4.3. PD-1/PD-L1 inhibition restores in vitro functionality of LA HER2-28ζ CAR-T cells, while it does not impact HA CARs

In our study, we propose that CAR-antigen affinity may influence T-cell susceptibility to the PD-1/PD-L1 axis. To explore this hypothesis, we conducted experiments to assess the impact of PD-1 ablation on the functionality of LA and HA CAR-T cells. Specifically, we co-cultured mock or PD-1 KO HER2-28ζ CAR-T cells with LA or HA using our PD-L1 cellular model and evaluated CAR-T cell activation by measuring cytokine secretion levels. In the absence of PD-L1 expression by tumour cells, both mock and PD-1 KO LA CAR-T cells released similar amounts of IFN-γ (Fig. 4.6a). This suggests that, in the absence of PD-L1, the presence or absence of PD-1 did not significantly affect the IFN-γ secretion of LA CAR-T cells. Conversely, when the tumour cells were engineered to express PD-L1 at either low or high levels, the expression of PD-L1 significantly suppressed the secretion of IFN-γ by mock HER2-28ζ CAR-T cells. This loss in cytokine release could be restored by genetic disruption of PD-1 in CAR-T cells (Fig. 4.6a). This implies that knocking out PD-1 in LA HER2-28ζ CAR-T cells can counteract the inhibitory effects of PD-L1 on cytokine secretion. In contrast, when PD-1 was knocked out in HA HER2-28ζ CAR-T cells and these modified CAR-T cells were co-cultured with PD-L1-

expressing tumour cells, there were only minor, non-significant increases in cytokine release as compared to mock CAR-T cells (Fig. 4.6b). Similar results were observed for the secretion of IL-2 (Fig. 4.6c, d).

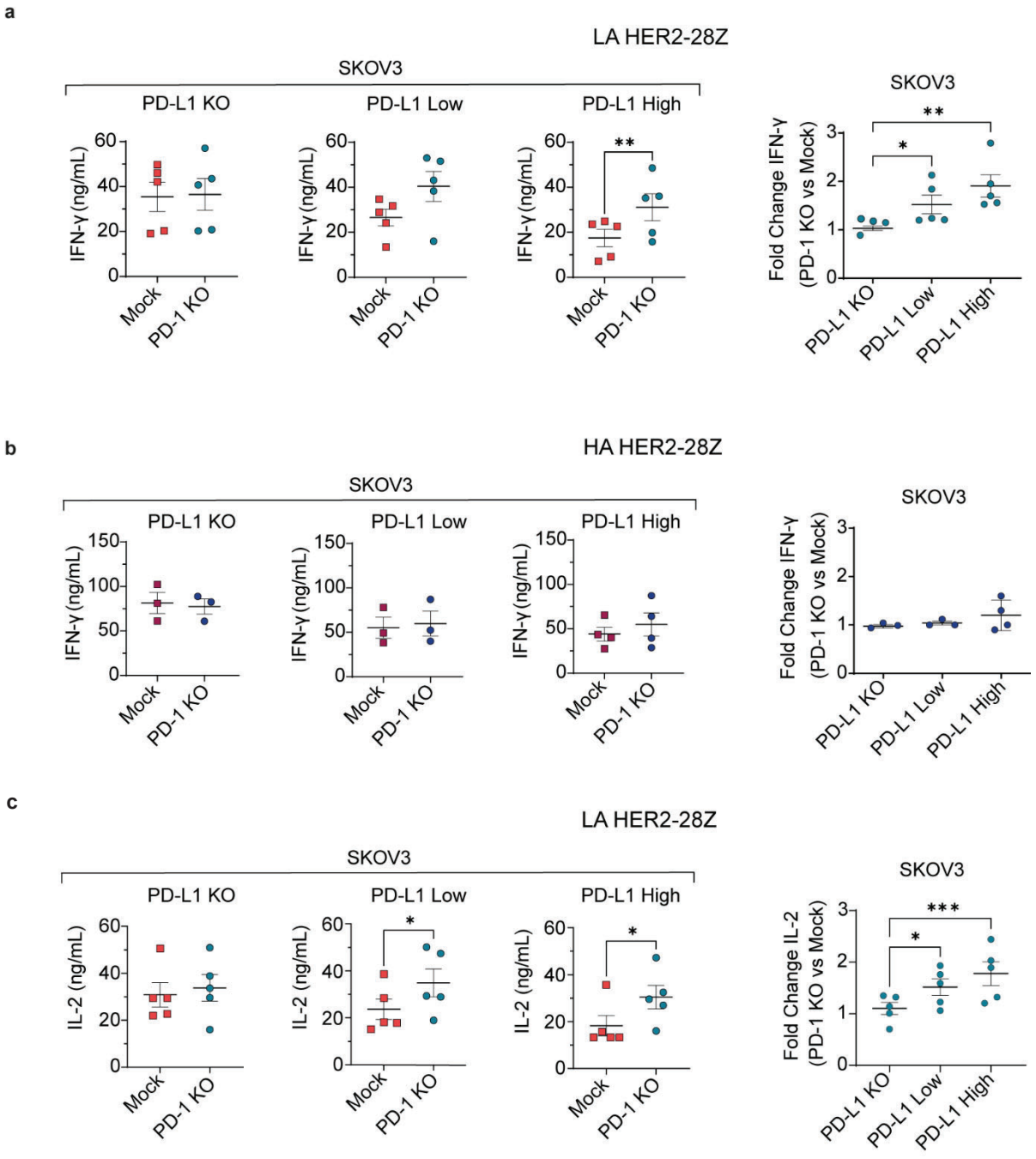

(continues on the next page)

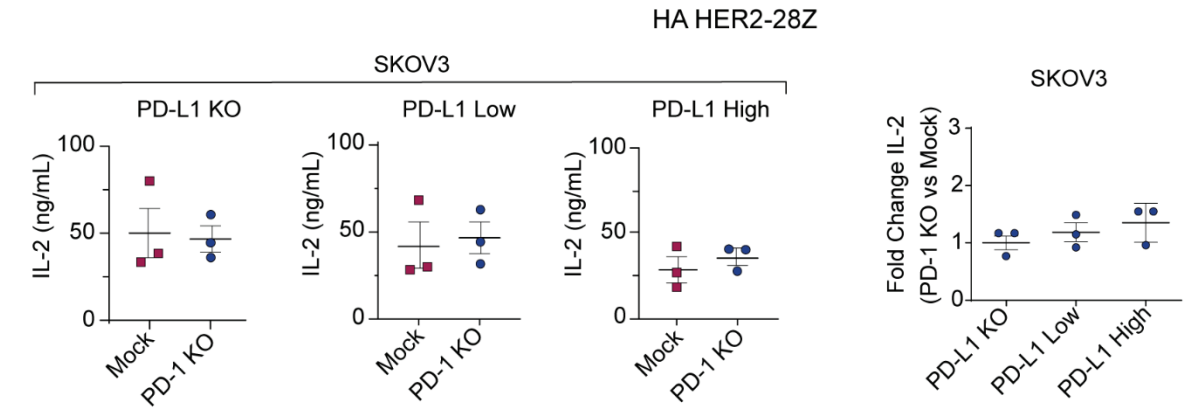

Fig 4.6 | PD-1 KO restores LA HER2-28ζ CAR-T cell cytokine secretion *in vitro* but does not affect HER2 HA-28ζ CAR-Ts. (**a-b**) IFN-γ (**c-d**) and IL-2 production by LA (**a, c**) or HA **(b, d)** CAR-T cells after 24 hours of co-culture with SKOV3 expressing variable PD-L1 densities (E:T=3:1) as quantified by ELISA. Cytokine secretion is represented as absolute levels (left panel) or as fold change versus mock (right panel) and plotted as mean ± SEM. Data are pooled from independent experiments where each dot represents CAR-T cells generated from different donors (n=3-5). *, $p < 0.05$; **, $p < 0.01$ by paired T-test.

4 | Results

We further validated these observations using an alternative pair of CARs designed to target FRβ with different affinities (Fig. 4.7a)[259]. It's noteworthy that the difference in affinity was less pronounced compared to the HER2-targeting CARs. Specifically, the dissociation constant (Kd) of the HA CAR was 21.89-fold lower than that of the LA CAR. LA and HA FRβ-28ζ based CARs with or without PD-1 KO were generated following the same methodology outlined for HER2-28ζ CAR-T cells. We assessed the expression levels of surface CAR (Fig. 4.7b) and PD-1 (Fig. 4.7c) on the eighth day of T-cell expansion. The percentage of CAR-positive cells was comparable between LA and HA-FRβ-28ζ CAR-T cells and, as expected, a significant reduction in PD-1 expression levels was observed between mock and PD-1 KO CAR-T cells following PD-1 KO. To assess the impact of PD-L1 on LA and HA FRβ-28ζ CAR-T cells, we overexpressed FRβ in our established SKOV3-based PD-L1 cellular model (Fig. 4.7b). After sorting based on FRβ and PD-L1 expression, we assessed CAR-T cell activation via cytokine secretion analysis. We found significantly higher levels of IFN-γ secreted by PD-1 KO LA CAR-T cells as compared to mock in the presence of PD-L1 (Fig. 4.7c, left panel). These differences were not observed in co-culture with the PD-L1 KO cell line or between PD-1 KO and mock HA CAR-T cells, which released similar levels of IFN-γ regardless of PD-

L1 presence (Fig. 4.7c, right panel). These findings align with our observations from the HER2 model, reinforcing the functional impact of PD-1 knockout across different CAR configurations targeting distinct antigens.

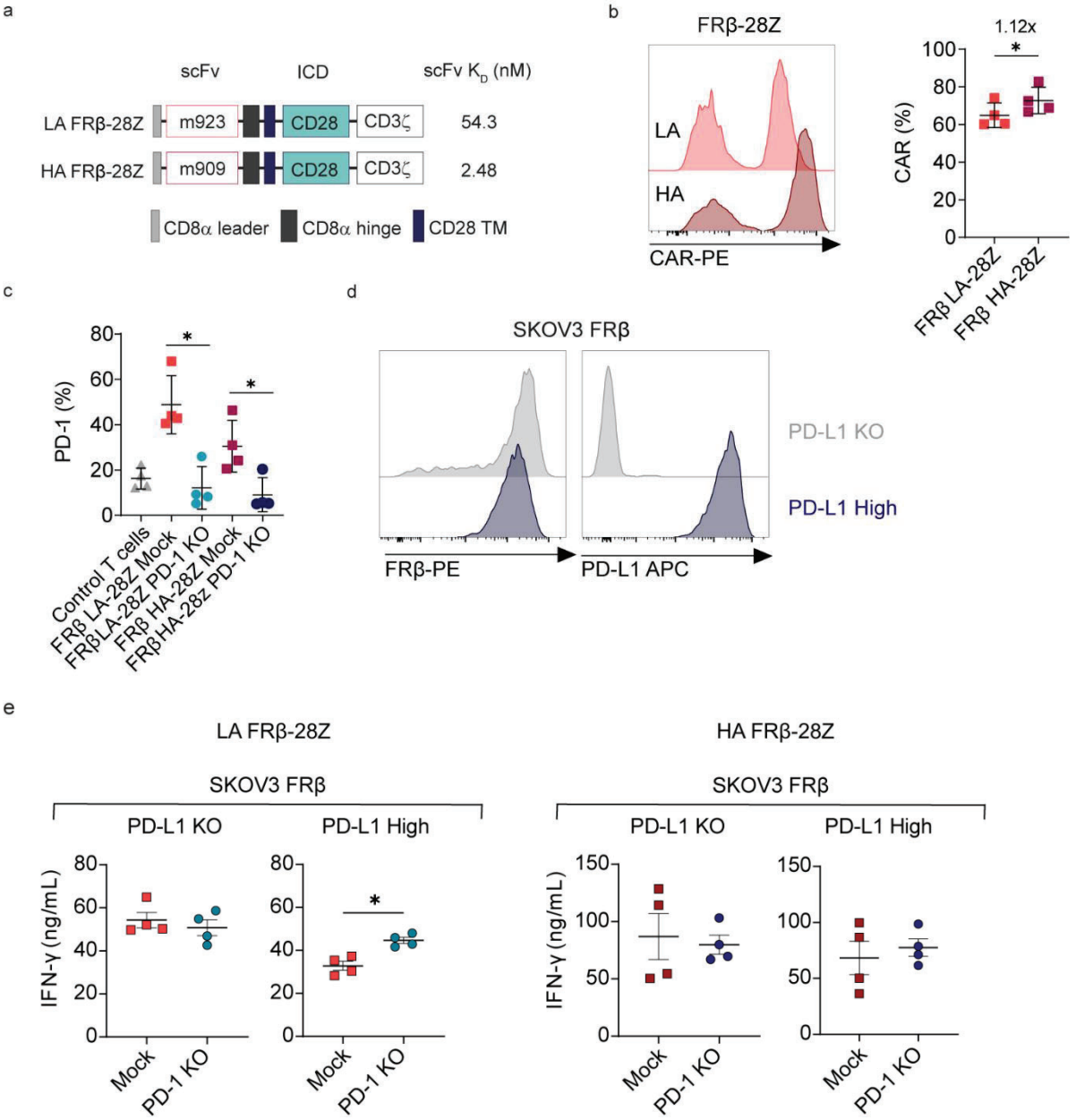

Fig 4.7 | PD-1 KO reestablishes IFN-γ secretion in LA FRβ-28ζ CAR-T cells, but not in HA FRβ-28ζ CAR-T cells, consistent with the observations of HER2-28ζ CAR-T cells. a Schematic overview of CAR constructs targeting FRβ used with their corresponding affinity values. Flow cytometric analysis showing **b** CAR by representative histogram (left panel) and percentage (right panel) or **c** PD-1 surface expression of indicated CAR-T cells at day 8 of T-cell expansion. Data plotted as mean ± SD (n=4 donors). *, $p < 0.05$ by paired T-test. **d** FRβ (left panel) and PD-L1 (right panel) expression by flow cytometry in indicated SKOV3 cell lines. **e** IFN-γ production by LA (left panel) or HA (right panel) FRβ-28Z CAR-T cells after 24 hours of co-culture with SKOV3.FRβ and indicated PD-L1 densities (E:T=3:1) as quantified by ELISA. Absolute levels are plotted as mean ± SEM (n=4 donors). *, $p < 0.05$ by paired T-test.

In light of the pivotal role that PD-1/PD-L1 blockade therapy has assumed in the field of immunotherapy during the recent years, our study sought to assess the cytokine secretion of CAR-T cells in combination with either Nivolumab (Opdivo®), an anti-PD-1 blocking antibody, or Durvalumab (Imfinzi®), an anti-PD-L1 blocking antibody, within the context of our PD-L1 tumour cell model. It is noteworthy that both immunotherapeutic agents have garnered approval from regulatory agencies, including the FDA and EMA, for the treatment of diverse solid tumour types[268]. Employing the same experimental methodology as that used in the comparison between mock and PD-1 KO CAR-T cells, we co-cultured CAR-Ts with either anti-PD-1 or anti-PD-L1 antibodies with SKOV3 tumour cells in the absence or presence of PD-L1 and analysed IFN-γ and IL-2 secretion after 24 hours. In the case of LA HER2-28ζ CAR-T cells, all groups released similar levels of IFN-γ and IL-2 in the lack of PD-L1 expression (Fig. 4.8a, left panel). Cytokine secretion by LA HER2-CAR-T cells gradually decreased as PD-L1 densities increased, and this loss was effectively reversed with the introduction of anti-PD-1 or anti-PD-L1 blocking antibodies (Fig. 4.8a, left panel and b). Conversely, when assessing the HA HER2-28ζ CAR, no discernible differences in cytokine secretion were observed after addition of anti-PD-1 or anti-PD-L1 blocking antibodies, not even in the presence of high PD-L1 densities (Fig. 4.8c and d). Altogether, these findings indicate that both anti-PD-1 and anti-PD-L1 treatments are capable of counteracting cytokine secretion in LA CAR-T cells, while showing no effect in HA CARs. These observations are in line with the previously observed higher resistance of HA CAR-T cells to the inhibitory effects of PD-L1-mediated immune suppression.

4 | Results

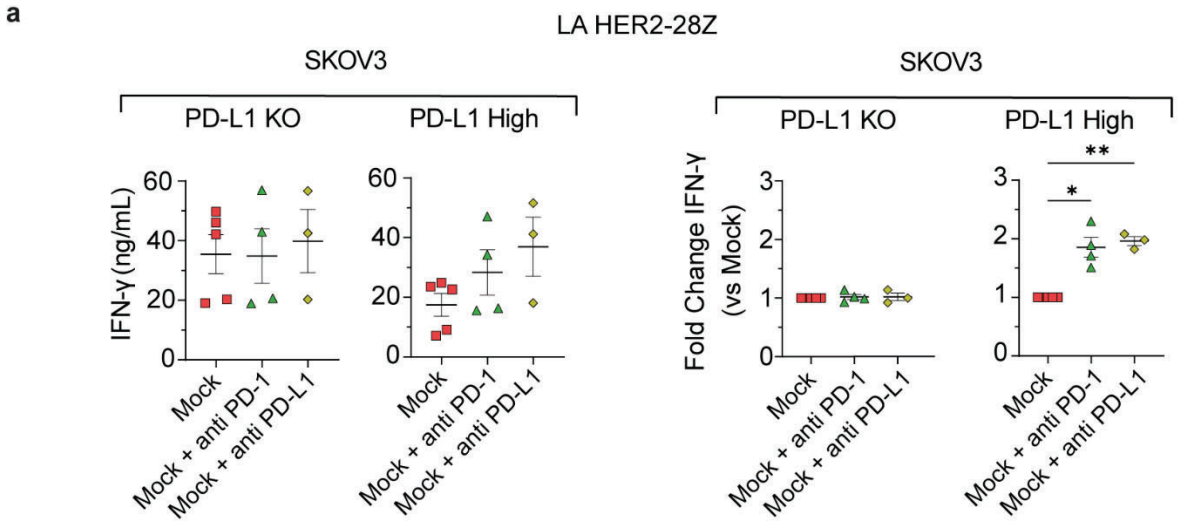

(continues on the next page)

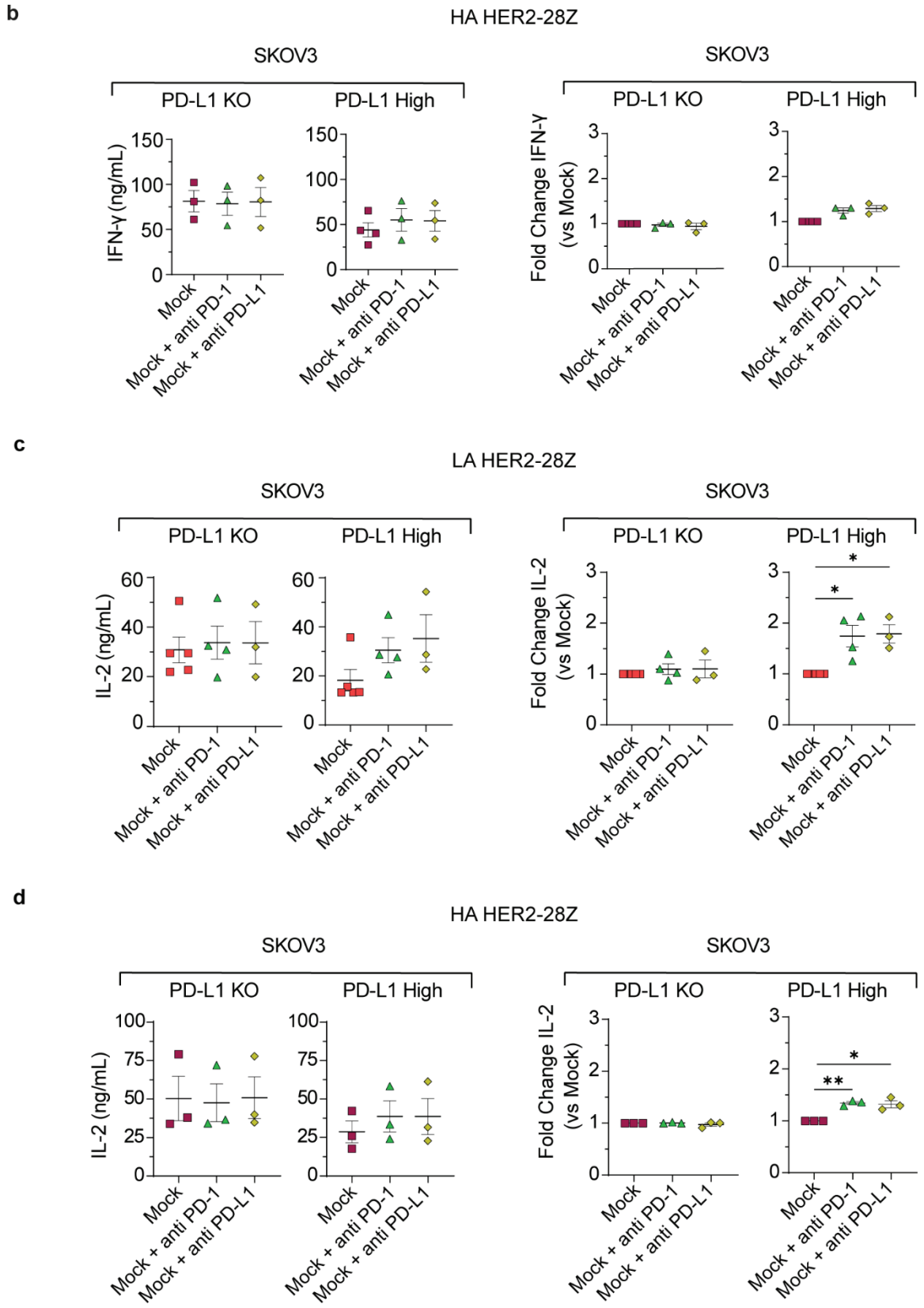

Fig. 4.8 | *In vitro* inhibition of PD-1/PD-L1 axis using blocking antibodies rescues cytokine secretion in LA HER2-28ζ CAR-T cells but not in HER2 HA-28Z CAR-T cells. (**a-b**) IFN-γ (**c-d**) and IL-2 production by LA (**a**) or HA **(b)** CAR-T cells alone or in combination with αPD-1 or αPD-

L1 antibodies after 24 hours of co-culture with SKOV3 expressing variable PD-L1 densities (E:T=3:1) as quantified by ELISA. Cytokine secretion is represented as absolute levels (left panel) or as fold change versus mock (right panel) and plotted as mean ± SEM. Data are pooled from independent experiments where each dot represents CAR-T cells generated from different donors (n=3-5). *, $p < 0.05$; **, $p < 0.01$ by paired T-test for absolute levels and ***, $p < 0.001$ by one-way ANOVA with Tukey post hoc test for fold-change.

We next tested the hypothesis that lack of PD-1 expression promotes enhanced proliferation in CAR-T cells. To this end, we co-cultured mock or PD-1 KO LA and HA CAR-T cells with the breast cancer cell line HCC1954, selected due to its high expression levels of HER2 and PD-L1 (Fig. 4.2a). Our findings revealed a two-fold increase in the proliferation of LA PD-1 KO CAR-T cells as compared to mock CAR-T cells 6 days after stimulation (Fig. 4.9a). In line with the cytokine secretion results, PD-1 KO did not provide a proliferative advantage to HA CAR-T cells (Fig. 4.9b).

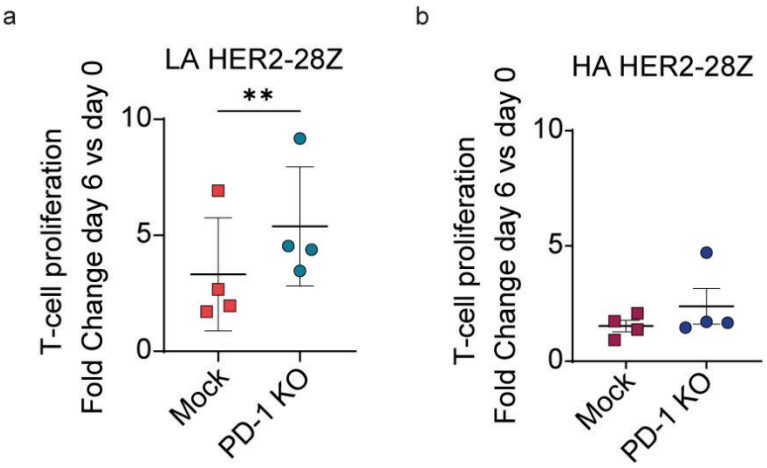

Fig. 4.9 | Differential impact of PD-1 KO on proliferation in LA HER2-28ζ CAR-T cells and HER2 HA-28ζ CAR-Ts. T-cell proliferation of **a** LA or **b** HA mock and PD-1-KO CAR-T cells following co-culture with HCC1954 (E:T=1:3). Fold change of absolute T-cell numbers at day 6 versus day 0 is represented. Data are plotted as mean ± SD (n=4 donors). **, $p < 0.01$ by paired T-test.

4.4. Sensitivity differences to T-cell inhibition via the PD-1/PD-L1 axis based on CAR affinity are maintained in lipid bilayers with controlled PD-L1 levels

To ensure that any disparities observed in the responses of LA and HA CAR-T cells following the genetic ablation of PD-1 were not attributed to inherent variations in tumour cells stemming from differential expression of PD-L1, we generated an

experimental setup involving the addition of CAR-T cells into a supported lipid bilayer (SLB) system. The lipid bilayer was engineered to include specific molecular components to serve distinct purposes. Firstly, ICAM-1 was incorporated, thereby facilitating the adhesion of CAR-T cells to the lipid bilayer through the binding to integrin lymphocyte function-associated antigen 1 (LFA-1) and the costimulatory molecule B7-1 found in the surface of T-cells. HER2 was added to the lipid bilayer at a fixed concentration (previously determined) to induce CAR-mediated T cell activation; and PD-L1 was also added at a range of titrated densities to represent various degrees of expression (Fig. 4.10a)[263,269] . Presence of PD-1 on the CAR-T cell membrane was confirmed by flow cytometry before adding the cells to the system to guarantee the subsequent interaction of PD-1 on CAR-T cells with the PD-L1 molecules incorporated within the lipid bilayer (Fig. 4.10b).

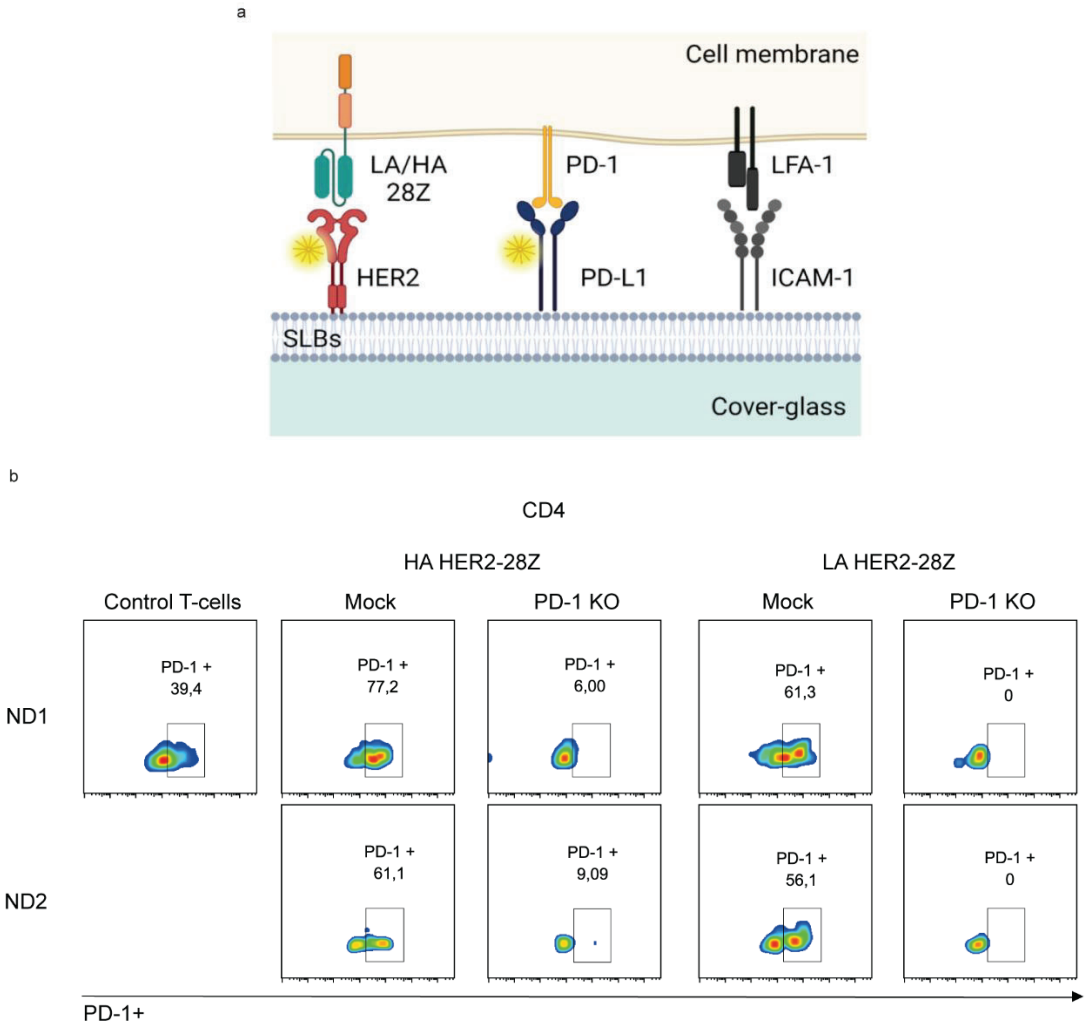

(continues on the next page)

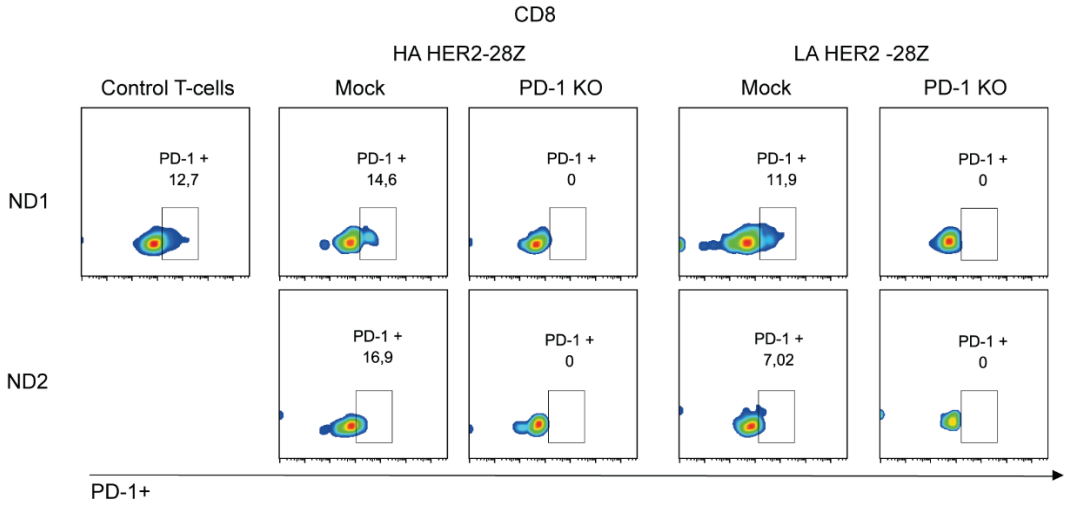

Fig 4.10 | Schematic outline of a SLB system and characterization of PD-1 expression in LA and HA HER2-28ζ CAR-T cells prior to exposure to the bilayers. a Schematic representation of an SLB featuring fluorescently labelled proteins (HER2 and PD-L1) and ICAM-1. Created with Biorender.com **b** Surface expression of PD-1 was assessed using flow cytometry on LA and HA HER2-28ζ mock and PD-1 KO CAR$^+$ T cells, 16 hours after thawing and just before their addition into the bilayers.

After exposing LA and HA mock or PD-1 KO CAR-T cells to the SLBs, we determined their respective activation levels via IFN-γ secretion. Consistent with the outcomes observed in our cellular model, we observed a reduction in IFN-γ release by LA mock CAR-T cells as they encountered increasing levels of PD-L1, and this inhibitory effect was reversed by PD-1 KO (Fig.4.11a left panel and 4.11b). In contrast, the secretion of IFN-γ by both mock and PD-1 KO HA CAR-T cells remained unaltered across the entire spectrum of PD-L1 concentrations that were tested (Fig. 4.11c right panel and 4.11d). These results underscored that the variances in IFN-γ secretion between LA and HA CAR-T cells in the presence of PD-L1 persisted within this system, thus confirming that the observed differences were indeed attributed to the presence of PD-L1.

a

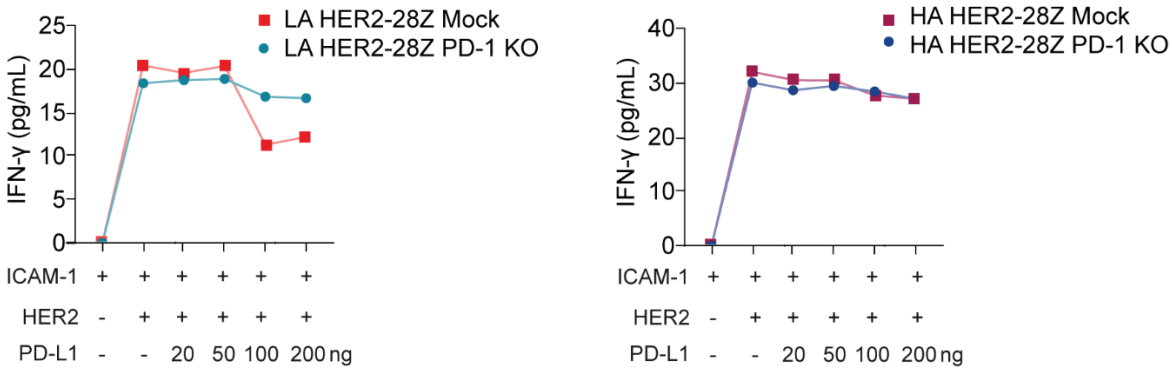

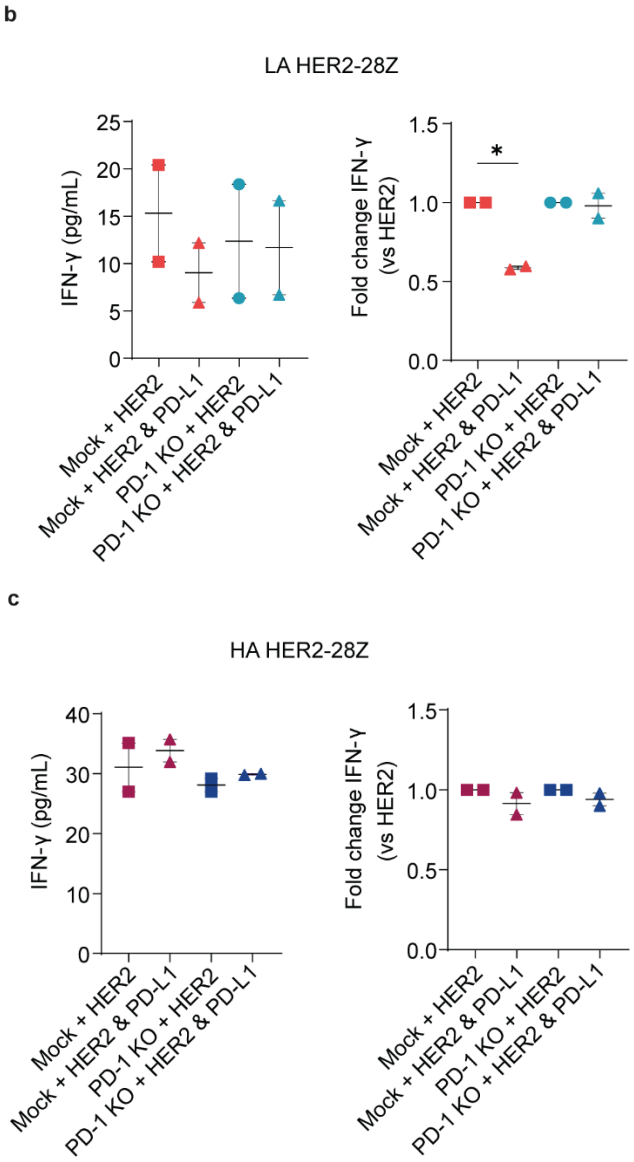

Fig 4.11 | Impact of PD-1/PD-L1 axis on CAR-T cell inhibition using a protein-functionalized planar glass SLB system with increasing amounts of PD-L1. a IFN-γ production by HER2-28ζ mock and PD-1-KO LA (left panel) or HA (right panel) CAR-T cells after 24 hours of co-culture with SLBs containing increasing concentrations of PD-L1. Data is representative of two different donors. HER2-28ζ mock and PD-1-KO **b** LA or **c** HA CAR-T cells were co-cultured for 24 hours with SLBs containing either HER2 alone or HER2 along with PD-L1 (200 ng). IFN-γ secretion measured by ELISA is represented as absolute levels (left panel) or fold change of the HER2 + PD-L1 condition compared to HER2 alone (right panel). Data are plotted as mean ± SEM (n= 2 donors). *, $p < 0.05$ by One sample T-test.

4.5. PD-1 KO increases the anti-tumour activity of LA but not HA HER2-28Z CAR-T cells in xenograft models with different PD-L1 densities

We next aimed to evaluate the impact of PD-1/PD-L1 axis on the therapeutic potential of HER2-28ζ CAR-T cells *in vivo*. In brief, female NOD SCID gamma mice (NSG), a strain

of immunodeficient laboratory mice that facilitate the engraftment of various human cell types, underwent subcutaneous implantation of $5x10^6$ tumour cells in both flanks. After a period of 40-50 days, once tumours were well-established, mice were treated with control T cells, mock CAR-T cells or PD-1 KO CAR-T cells. Subsequently, tumour size was measured every 4-5 days following treatment, and mice were ethically sacrificed upon reaching the predetermined tumour size limit (Fig 4.12a).

To begin, we assessed the antitumor efficacy of HER2-28ζ CAR-T cells in our PD-L1 cellular model. NSG mice bearing subcutaneous tumours expressing different PD-L1 densities (PD-L1 KO, PD-L1 Low or PD-L1 High) were treated with a single dose of $2\text{-}4{\cdot}10^6$ control T cells, mock or PD-1 KO CAR-T cells. As expected, both mock and PD-1 KO LA HER2-28ζ CAR-T cells showed similar anti-tumour activity and efficiently eliminated tumours that did not express PD-L1 (Fig. 4.12b, left panel). The presence of PD-L1 expression, even at low densities, impaired the anti-tumour efficacy of LA HER2-28ζ CAR-T cells. In tumours expressing either low or elevated levels of PD-L1, PD-1 ablation significantly enhanced anti-tumour responses, resulting in complete regressions in 90% of tumours (Fig. 4.12b, middle and right panels). Additionally, since it is still controversial whether PD-1 is required for long-term persistence of CAR-T cells, we assessed the T-cell persistence of LA HER2-28ζ mock and PD-1 KO CAR-T cells within tumours characterized by either null or high levels of PD-L1. Although a significant increased presence of PD-1 KO CAR-T cells in blood was noted compared to control T-cells, overall levels were notably low, and a comprehensive evaluation was not possible. Our findings suggest that this model may not be conducive to assessing persistence effectively. (Fig. 4.12c). We also validated the *in vivo* results with CAR-T cells in combination with anti-PD-L1 blocking antibodies in high PD-L1-expressing SKOV3 cells. Even though the combination with antibodies improved the anti-tumour effect of CAR-T cells alone, PD-1 KO CAR-T cells still showed the best efficacy (Fig. 4.12d and e). In the case of HA HER2-28ζ CAR-T cells, both mock and PD-1 KO showed remarkable efficacy, effectively eliminating all tumours with the highest PD-L1 expression. These results are in line with what we have previously observed *in vitro* and highlight the strong anti-tumour effects of HA HER2-28ζ CAR-T cells, suggesting their ability to target tumours independently of PD-L1 levels (Fig. 4.12f).

a

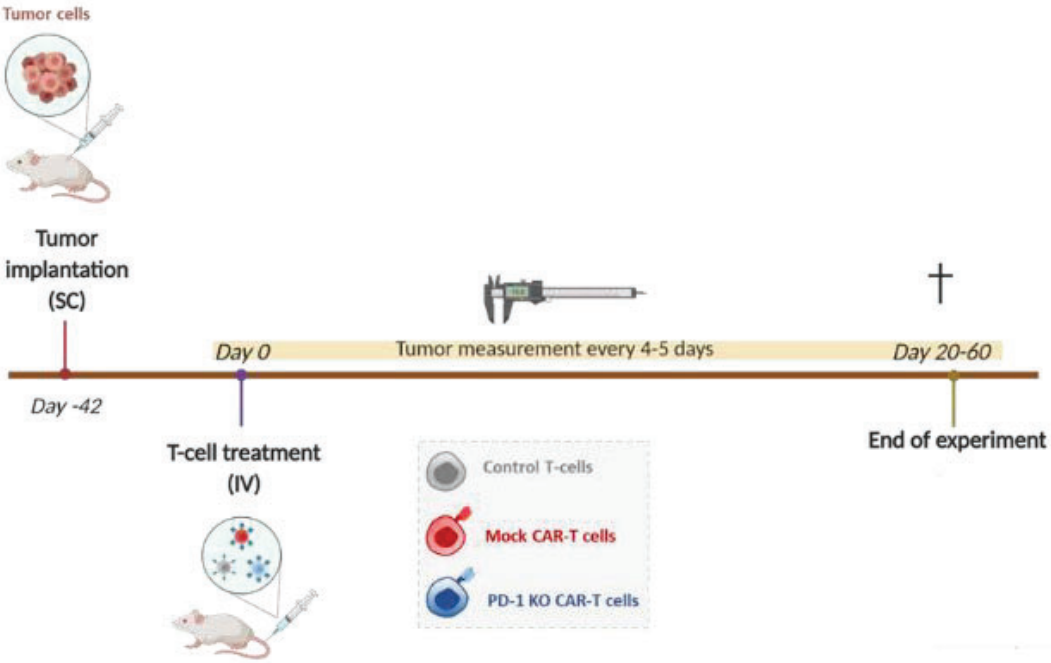

b

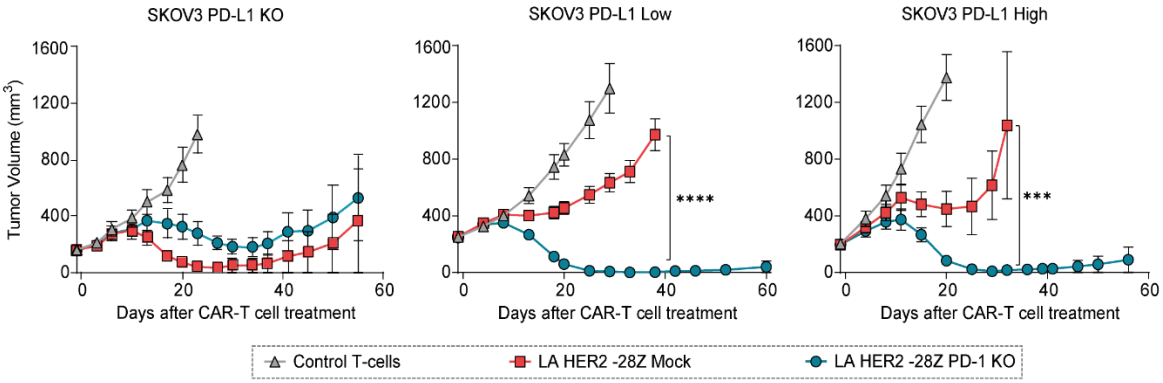

c

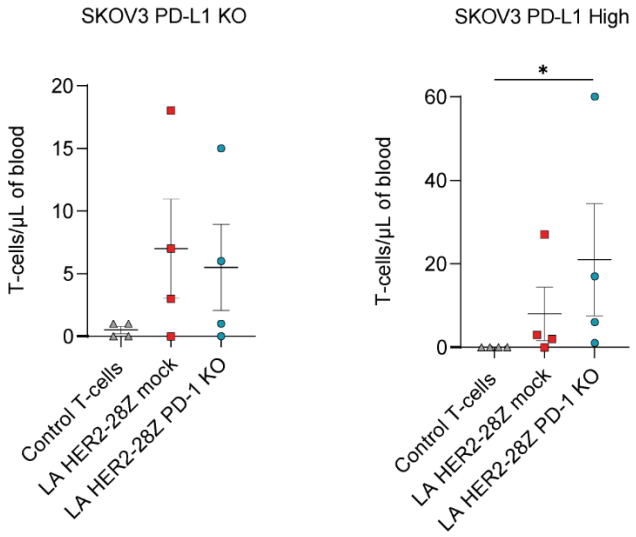

(continues on the next page)

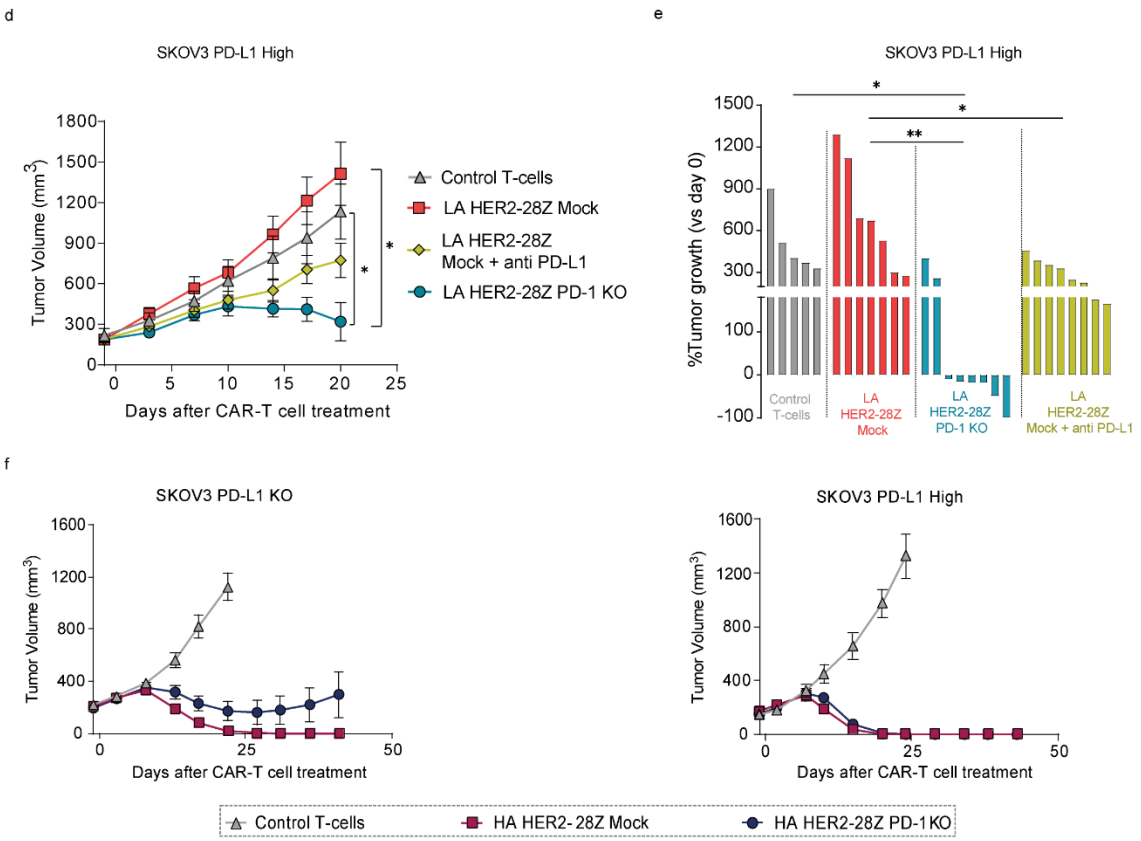

Fig. 4.12 | The disruption of the PD-1/PD-L1 axis signalling restores LA HER2-28ζ CAR-T cell function *in vivo* but does not affect HA HER2-28ζ CAR T-cells. a Schematic representation of the experimental design followed for the execution of *in vivo* experiments. Created with Biorender.com **b** Tumour measurements of NSG mice bearing SKOV3 tumours expressing indicated PD-L1 densities and treated with 3-4· 10^6 control T-cells, mock or PD-1 KO LA HER2-28ζ CAR^+-T cells (n = 8 for SKOV3 PD-L1 KO and PD-L1 High; n = 8, 13 or 12 for control, mock and PD-1 KO groups, respectively, for SKOV3 PD-L1 Low). **c** Concentration of CD45+ T cells for Control T-cells, mock and PD-1 KO LA HER2-28ζ CAR-T cells in the blood of treated animals 21 days after T cell injection. *p < 0.05 by Kruskal-Wallis multiple-comparisons test **d, e** NSG mice bearing SKOV3 PD-L1 High tumours were treated with 3 · 10^6 control T-cells (n = 5), mock (n = 7), mock + anti PD-L1 antibody (n = 7) or PD-1 KO (n = 8) LA HER2-28Z CAR+-T cells. **d** Tumour measurements and (**e**) percentage of tumour growth indicated as the change in tumour volume on day 20 versus baseline is shown. **f** Tumour measurements of NSG mice bearing SKOV3 tumours expressing indicated PD-L1 densities and treated with 3-4 · 10^6 control T-cells, mock or PD-1 KO HA HER2-28ζ CAR^+-T cells (n = 8, 13 and 12 for control, mock and PD-1 KO groups, respectively, for SKOV3 PD-L1 KO; n = 8 for SKOV3 PD-L1 High). Data in (**b**) and (**d-f**) are represented as mean tumour volume ±SEM and n indicates tumours per group. Error bars in (**c**) are represented by ± SEM and each dot represents a mouse (n = 4). (**c**) *, p < 0.05 by Kruskal Wallis multiple comparison test. (**b-d**) ***, p < 0.001; ****, p < 0.0001 by two-way ANOVA with Tukey's multiple testing correction. (**e**) *, p<0.05 and ****, p < 0.0001 by one-way ANOVA with Tukey post hoc test.

After analysing what happened in our PD-L1 cellular model, we sought to investigate the implications of PD-L1 levels more reflective of physiological conditions. Considering this, we measured the anti-tumour efficacy of control T-cells and LA or HA HER2-28ζ mock and PD-1 KO CAR-T cells in SKOV3 WT cells, expressing physiological levels of PD-L1. Again, PD-1 KO provided a significant advantage only to LA CAR-T cells (Fig. 4.13a), while the efficacy of HA CAR-T cells was not further improved (Fig. 4.13b). As HA mock CAR-T cells were able to eliminate tumours in all models tested, we repeated the *in vivo* experiment in SKOV3 WT cells line using more challenging conditions and treating larger tumours. We consistently found no significant differences between mock and PD-1 KO CAR-T cells, except for a noticeable reduction in overall efficacy observed in both groups (Fig. 4.13c). Next, we aimed to validate the anti-tumoral enhancement conferred by PD1 KO in an alternative HER2 expression model. Consistent results were noted in the breast cancer model HCC1954, highlighting the heightened anti-tumour efficacy of PD-1 KO LA HER2-28ζ CAR-T cells (Fig. 4.13d). Collectively, these findings indicate that genetic disruption of PD-1 enhances the anti-tumour effect of LA HER2-28ζ CAR-T cells in tumours expressing PD-L1, while it does not impact the efficacy of HA CAR-T cells.

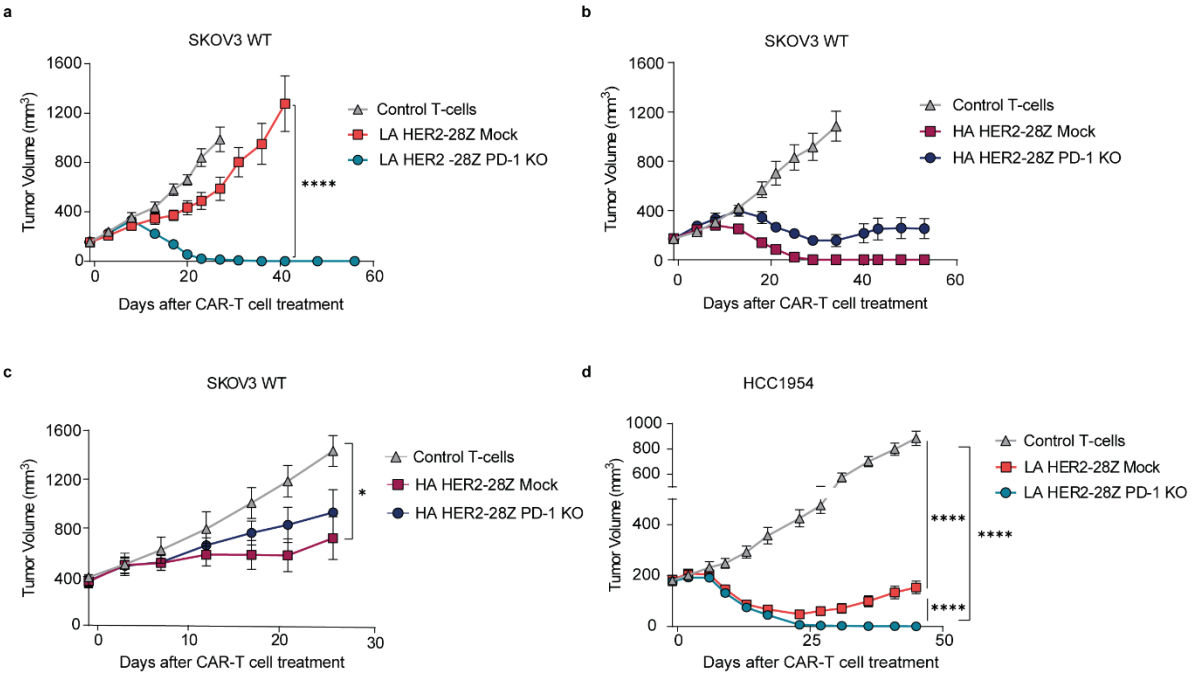

Fig 4.13 | PD-1 KO improves the *in vivo* functionality of LA HER2-28ζ CAR-T cells in different xenograft models, with no discernible impact on HA HER2-28ζ CAR-T cells. Tumour measurements of NSG mice bearing SKOV3 wild type tumours treated with $3 \cdot 10^6$ control T-cells, mock or PD-1 KO HER2−28ζ CAR$^+$-T cells of (**a**) LA (n = 8 for control and n = 10 for mock

and PD-1 KO groups) or (**b**) HA (n = 8 for all groups). **c** NSG mice bearing SKOV3 WT were treated with $3{\cdot}10^6$ control T-cells, mock or PD-1 KO HA HER2-28ζ CAR$^+$-T cells. (n=6 tumours for control and n=8 tumours for mock and PD-1 KO groups) **d** tumour measurements of NSG mice bearing HCC1954 tumours treated with $3 \cdot 10^6$ control T-cells (n = 9), mock (n = 10) or PD-1-KO (n = 10) LA HER2-28ζ CAR+-T cells. Data in (**a-d**) are represented as mean tumour volume ±SEM and n indicates tumours per group. *, p<0.05 and ****, p < 0.0001 by two-way ANOVA with Tukey's multiple testing correction.

Considering findings from previous studies[34,248,270] indicating that PD-1 ablation hampers memory cell formation and accelerates exhaustion, we aimed to see if there was a natural selection process *in vivo* between edited and non-edited cells within the same mouse. This was possible due to the administration of PD-1 KO cells as a bulk population, comprising both non-edited and edited cells, Genomic analyses showed that the levels of *PDCD 1* editing in CD4$^+$ and CD8$^+$ PD-1 KO cells, isolated 23 days after treatment (Fig. 4.14b) generally maintained similarity with the infused T cell product (Fig. 4.14c). Despite these variations among donors, the data suggest that PD-1 KO LA HER2-28ζ CAR-T cells were maintained over time.

a

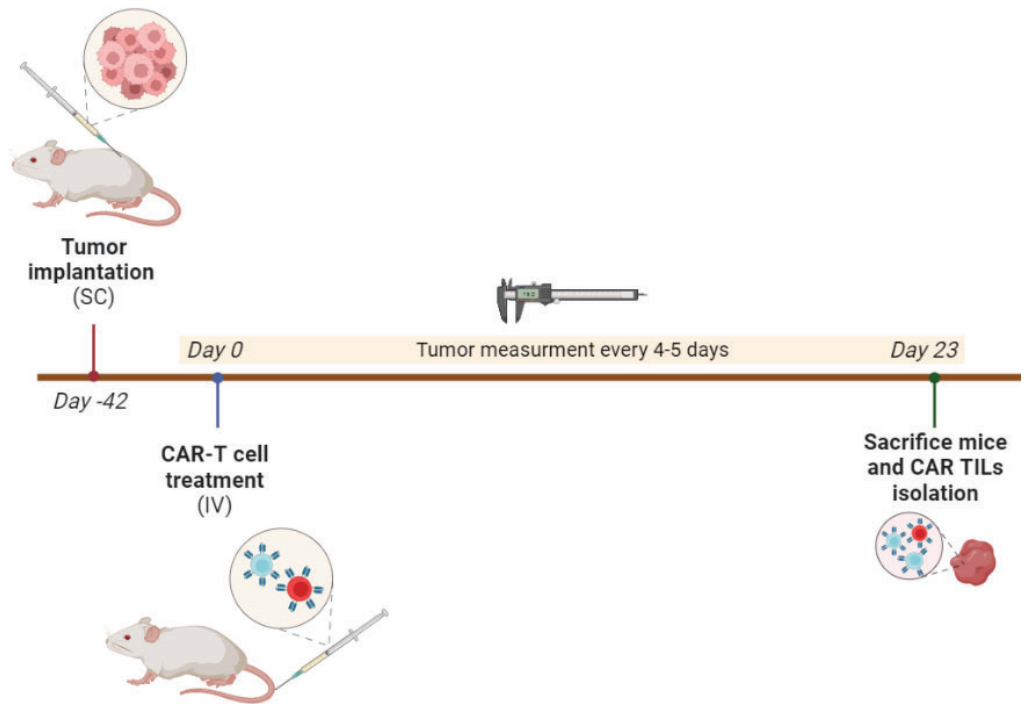

(continues on the next page)

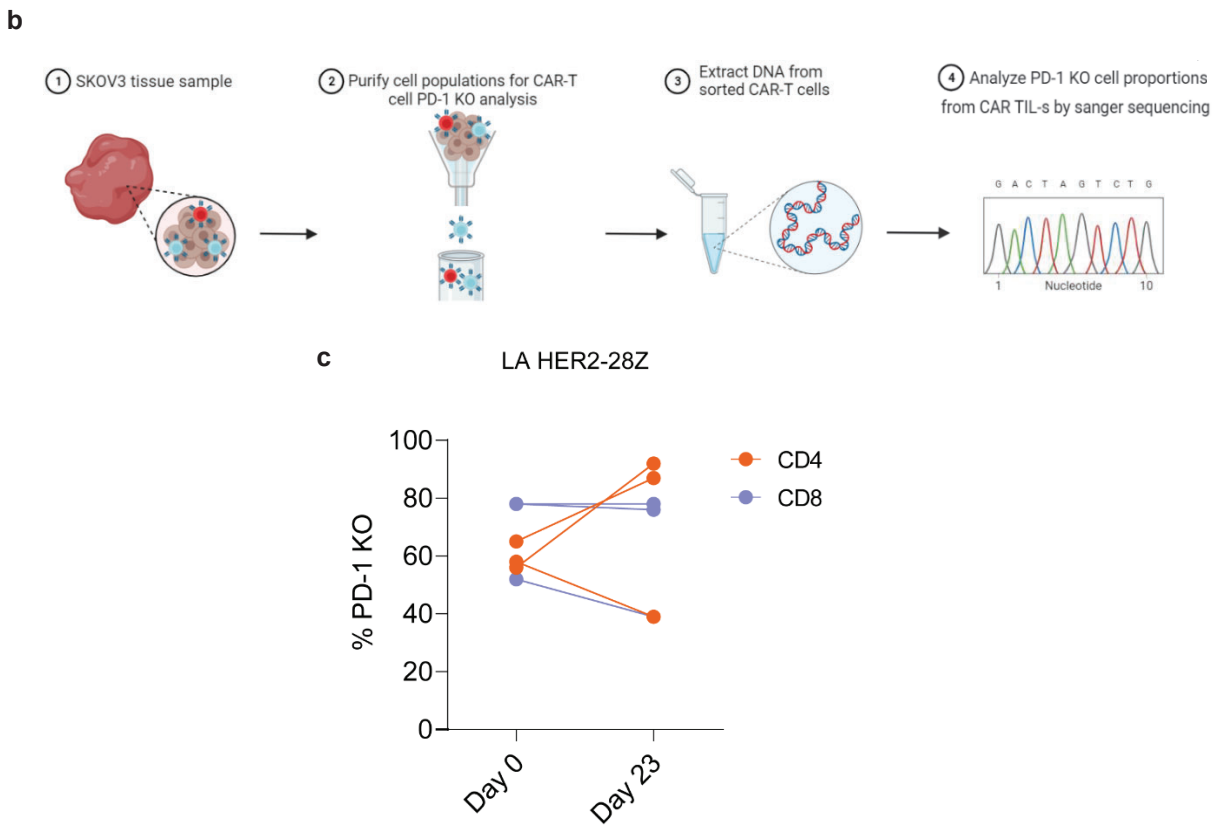

Figure 4.14 | PD-1 KO cell population is maintained in LA HER2-28ζ CAR TILs 23 days after treatment. a Schematic representation of the experimental design followed for the *in vivo* PD-1 KO enrichment. **b** Schematic representation of the steps followed for the quantification of PD-1 KO on CAR-T cells isolated from xenograft tumours *in vivo*. **c** Percentage of PD-1 KO cells quantified using the ICE tool from Synthego before and 23 days after treatment for LA HER2-28ζ. CD4+ T-cells are represented by orange lines, while CD8+ T-cells are indicated by purple lines. Each dot represents one independent healthy donor.

4.6. The benefits of PD-1 KO in LA HER2-28ζ CAR-T cells are confirmed in another CAR construct targeting a distinct antigen

Next, we aimed to explore if the higher sensitivity to PD-1/PD-L1 inhibitory pathway observed in LA HER2 CAR-T cells was extended to CAR-T cells directed against other antigens targeted with LA. To this end, we explored the effects of PD-1 KO in CAR-T cells targeting mesothelin with LA and containing the CD28 intracellular domain (Meso-28ζ)[260] (Fig. 4.15a). Using this CAR, we observed that in T-cells expressing an anti-mesothelin LA CAR, the inhibition of the PD-1/PD-L1 axis through either genetic disruption or the administration of PD-1 or PD-L1 blocking antibodies resulted both in elevated *in vitro* cytokine secretion (Fig. 4.15b) and enhanced *in vivo* anti-tumour effect

(Fig. 4.15c) against the CAPAN2 tumour cell line. We also evaluated the enrichment of the PD-1 KO CAR-T cell population, following the procedure outlined for the HER2 LA-28ζ CAR-T cells (Fig. 4.14b), after 83 days post-administration *in vivo*. We observed that both CD4+ and CD8+ populations of the edited cells remained sustained over time (Fig. 4.15d). These findings consistently validate the outcomes observed in LA HER2-28ζ CAR-T cells, underscoring the broad applicability and potential therapeutic significance of disrupting the PD-1/PD-L1 axis within the context of LA CAR-T cell therapies.

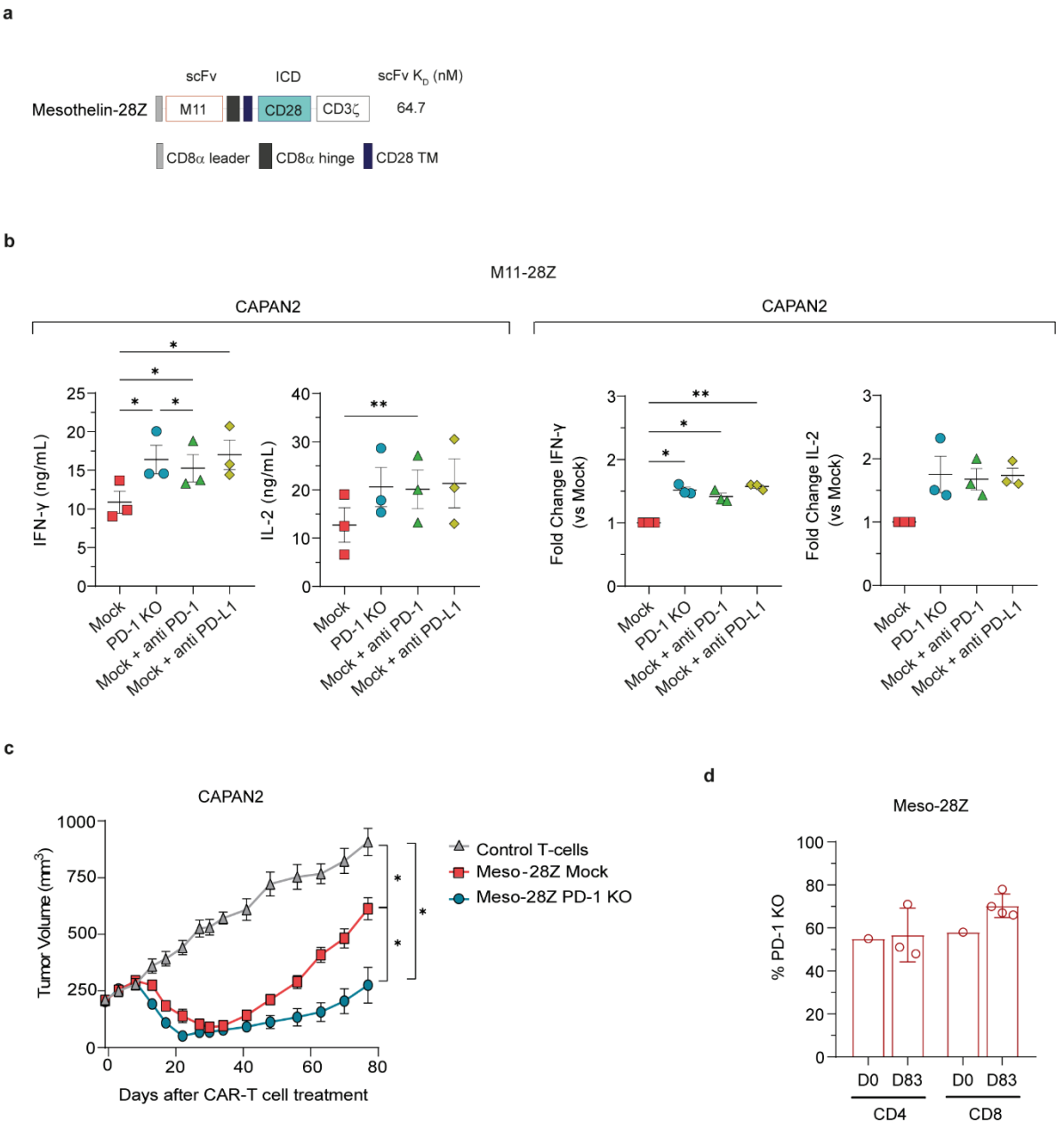

Figure 4.15 | Enhanced cytokine secretion and anti-tumour response in mesothelin-targeting LA CAR-T Cells through PD-1/PD-L1 axis modulation. a Schematic overview of the Meso-28ζ CAR construct used with its affinity. **b** Meso-28ζ mock, PD-1-KO, mock with anti PD-1

or anti PD-L1 CAR-T cells were co-cultured with CAPAN2 (E:T=3:1). IFN-γ and IL-2 release was analysed 24 hours later by ELISA. Cytokine secretion is represented by absolute levels (left panel) or by fold change of PD-1 KO CAR-T cells, mock CAR-T cells with anti PD-1 or anti PD-L1 as compared to mock CAR-T cells (right panel). Data are plotted as mean ± SEM. (n=3 donors). *, p = 0.01, **, p < 0.01, by one-way ANOVA with Tukey post hoc test. **c** NSG mice bearing CAPAN2 tumours were treated with $2{\cdot}10^6$ control T cells Meso-28ζ mock or PD-1 KO CAR-T cells. Mean tumour volume ± SEM is shown (n=12 tumours per group) *, p < 0.05 by two-way ANOVA with Tukey's multiple testing correction. **d** Percentage of PD-1 KO cells quantified using the ICE tool from Synthego before and 83 days after treatment for Meso-28ζ. Each dot represents one tumour. Data are plotted as mean ± SD.

4.7. PD-1 KO induces deeper changes in the transcriptome of LA HER2-28Z CAR-T cells as compared to HA CAR-T cells

In order to characterize the molecular mechanisms behind the different effects of PD-1 disruption in LA and HA HER2-28ζ CAR-T cells, we compared the transcriptomic profile of mock and PD-1 KO CAR-T cells following antigen recognition. For that, we used the nCounter® CAR-T Characterization Gene Expression Panel (Nanostring Technologies), which gives information about eight essential components of CAR-T biology relative to multiple subtypes of T-cells and their phenotypic changes, metabolic fitness, TCR diversity, toxicity, activation, persistence, cell types and exhaustion. Briefly, LA and HA HER2-28ζmock and PD-1 KO CAR-T cells were co-cultured with SKOV3 WT cells for 48-hours prior to the isolation of the CD45 population using flow sorting, and total RNA was immediately extracted for transcriptomic evaluation. Before proceeding with functional analyses, we verified the normalization of all samples, ensuring that gene counts were consistent across the board. Furthermore, we confirmed that both housekeeping genes and internal positive controls were consistently and uniformly represented in every sample. We then proceeded with differential gene expression analysis, first focusing on the comparison between PD-1 KO and mock in LA HER2-28ζ CAR-T cells. In this setting, the KO of PD-1 resulted in statistically significant downregulation of 20 genes and upregulation of 13 genes out of the 780 genes analysed in the panel (Fig. 4.16a). Within upregulated genes in PD-1 KO versus mock LA HER2 CAR-T cells we found FosB, a transcription factor that has been previously reported to be decreased in exhausted T cells during chronic viral infection [271] while increased in CAR-T cells from responding as compared to non-responding patients[272] . Other upregulated genes included T-cell

activation-related genes such as effector cytokines (IFN-γ, TNF, IL-2, CSF2/GM-CSF or CLCF1), chemokines (CCL3, CCL4, CCL20, XCL1/2) or co-stimulatory molecules (TNFSF9/4-1BBL). Genes that were downregulated in the PD-1 KO CAR-T cells included the transcription factor MAF, regulon driver of T cell exhaustion[273] ,genes related to type I and II IFN signalling (IRF9, ADAR, SP100, SOCS2, ISG15, STAT1, STAT2, IFIT1, IRF7, PML, IFI35), which have been recently linked to CAR-T cell dysfunction[274], CD68 (which is primarily a marker for macrophages but also found constitutively expressed on NK cells) and members of the B7 ligands family (CD86 and CD276/B7-H3). By contrast, only 7 genes were differentially expressed between mock and PD-1 KO in the HA HER2-28Z CAR-T cells, with the memory marker IL7R being the most relevant and upregulated in the PD-1 KO group (Fig. 4.16b). To provide deeper insight into the biological functions underlying the entire dysregulated gene expression signature pertaining to the comparison of mock and PD-1 KO LA CAR-T cells, we performed gene enrichment analysis (GEA)[275,276] . As anticipated, we observed a significant enrichment in categories related to cytokine signalling, two of which were related to type 1 IFN signalling pathways (Fig. 4.16c).

a

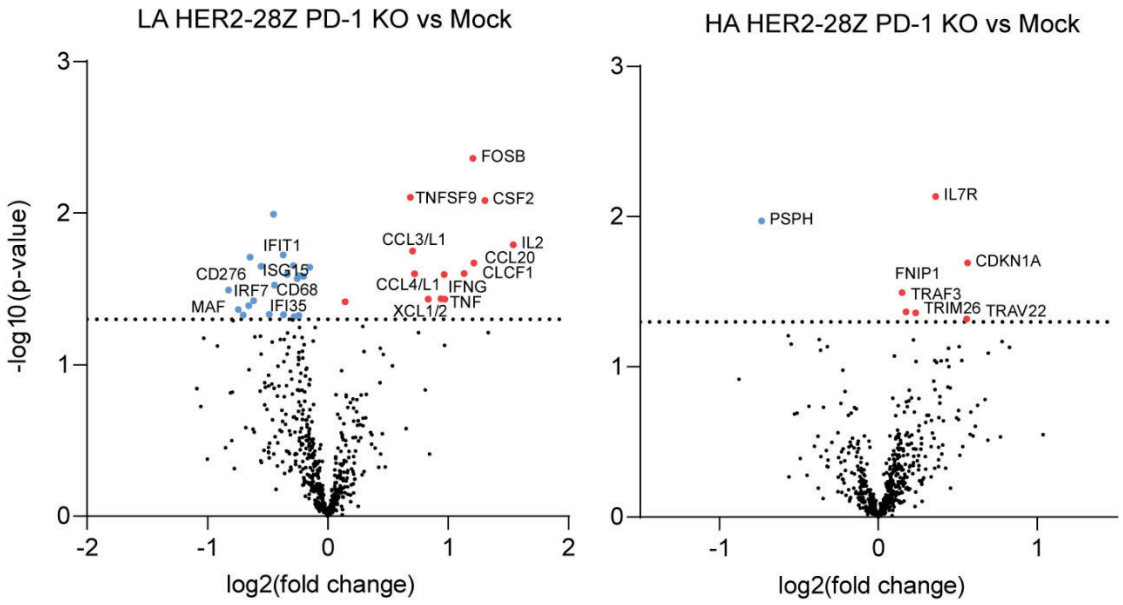

(continues on the next page)

b

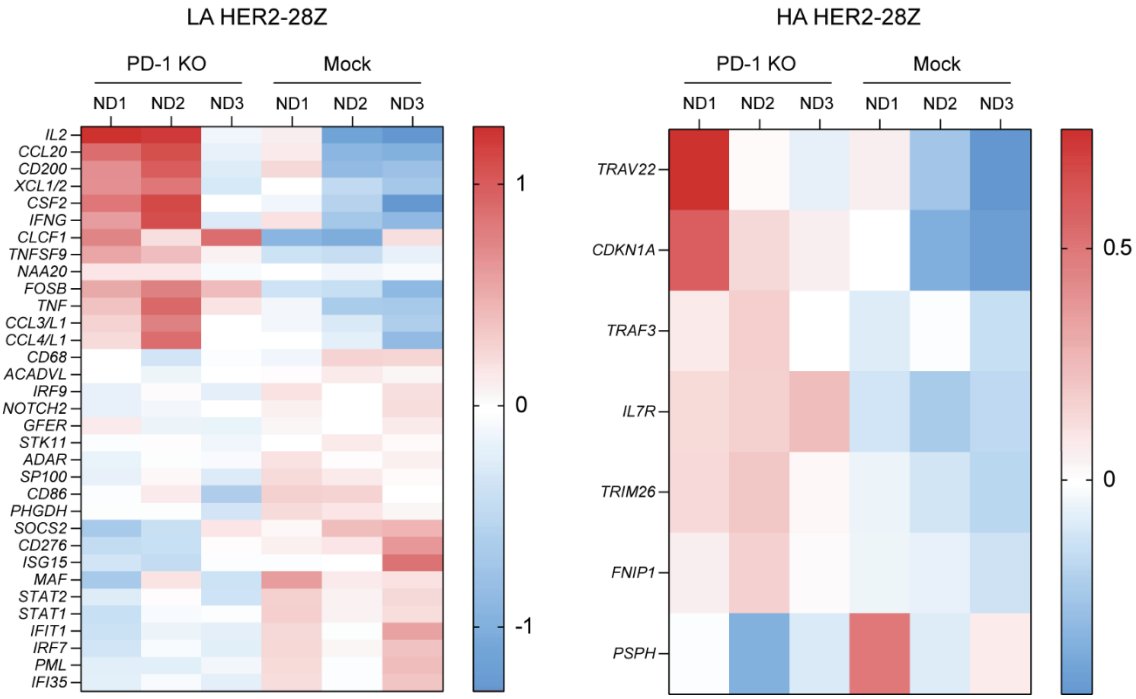

C

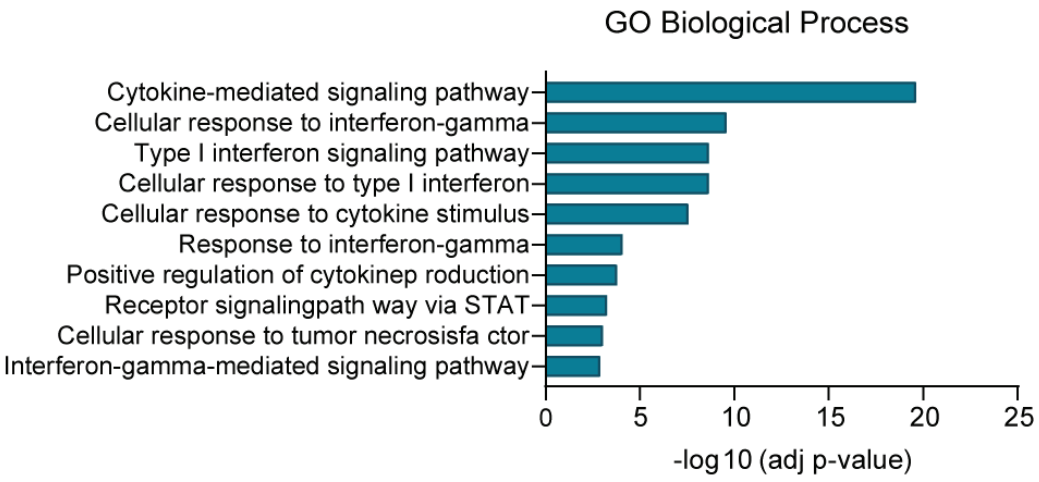

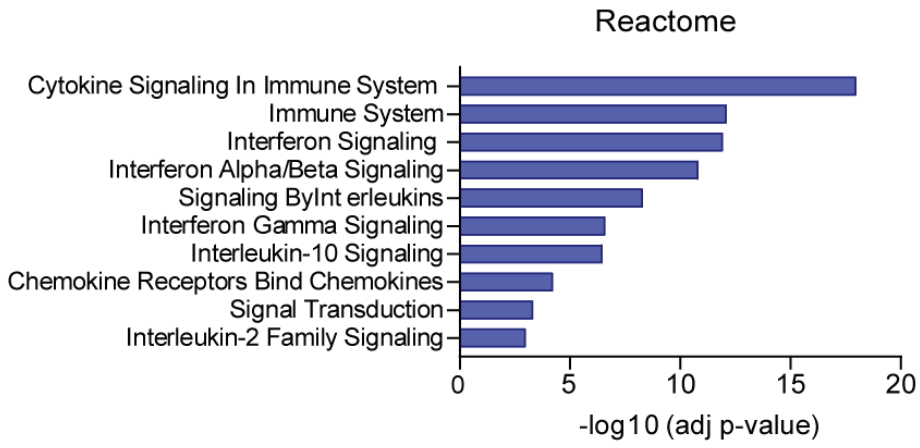

(continues on the next page)

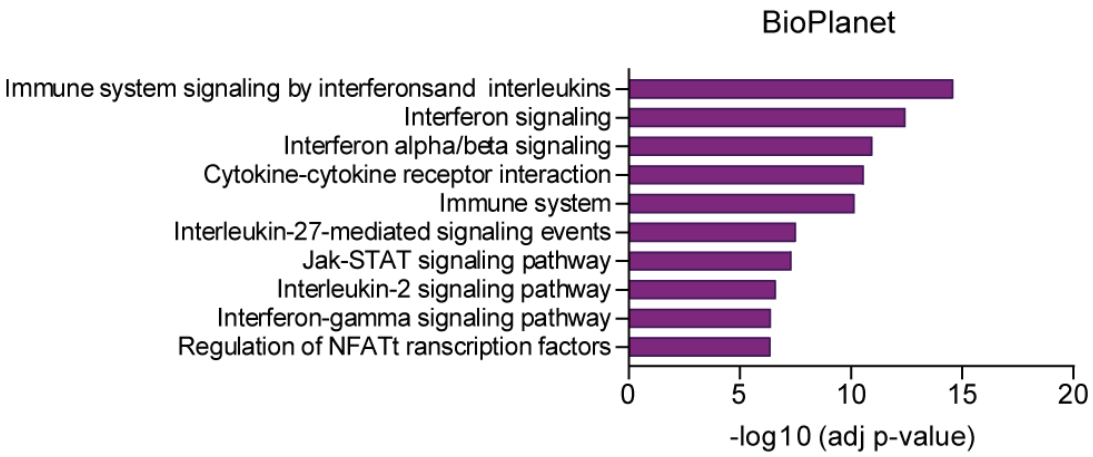

Fig. 4.16 | Differential transcriptomic response of HA and LA HER2-28Z CAR-T cells to PD-1 KO. a Volcano plots of differential expression between LA HER2-28Z PD-1 KO and mock CAR-T cells (left panel) or HA HER2-28Z PD-1 KO CAR-T cells vs mock (right panel) after stimulation with SKOV3 tumour cells for 48 hours. Red dots represent genes upregulated in PD-1 KO vs mock, blue dots represent genes downregulated genes in PD-1 KO vs mock and black dots represent genes not differentially expressed (n = 3 donors). **b** Heat map of statistically significant differentially expressed genes ($P \leqslant 0.05$) between LA HER2-28Z PD-1 KO CAR T cells and mock (left panel) or HA HER2-28Z PD-1 KO CAR-T cells vs mock (right panel) after stimulation with SKOV3 tumour cells for 48 hours (n = 3 donors). **c** Gene Ontology (GO) Biological process 2021 (left panel), Reactome 2022 (right panel) and Bioplanet (lower panel) pathway analysis of all significant differentially expressed genes between PD-1 KO and mock LA HER2-28Z CAR-T cells showing the top-10 enriched pathways. -log10 (adj p-value) was derived from Enrichr.

In light of these findings, we subsequently validated the expression of genes involved in this specific pathway. Selected candidates included IFIT1, IRF7, IFI35 and ISG15, while genes encoding cytokines were validated at the protein level using alternative methods (i.e., ELISA and Isoplexis), as shown in other sections. Additionally, we examined genes relevant to exhaustion and co-stimulation, such as FosB and TNFSF9/4-1BBL, respectively. To accomplish this, we employed Real-Time quantitative PCR (RT-qPCR). What we could observe was a similar gene expression pattern between the results obtained through RT-qPCR (Fig. 4.17a) and GEA (Fig. 4.17b), our earlier methodology, affirming the prior outcomes.

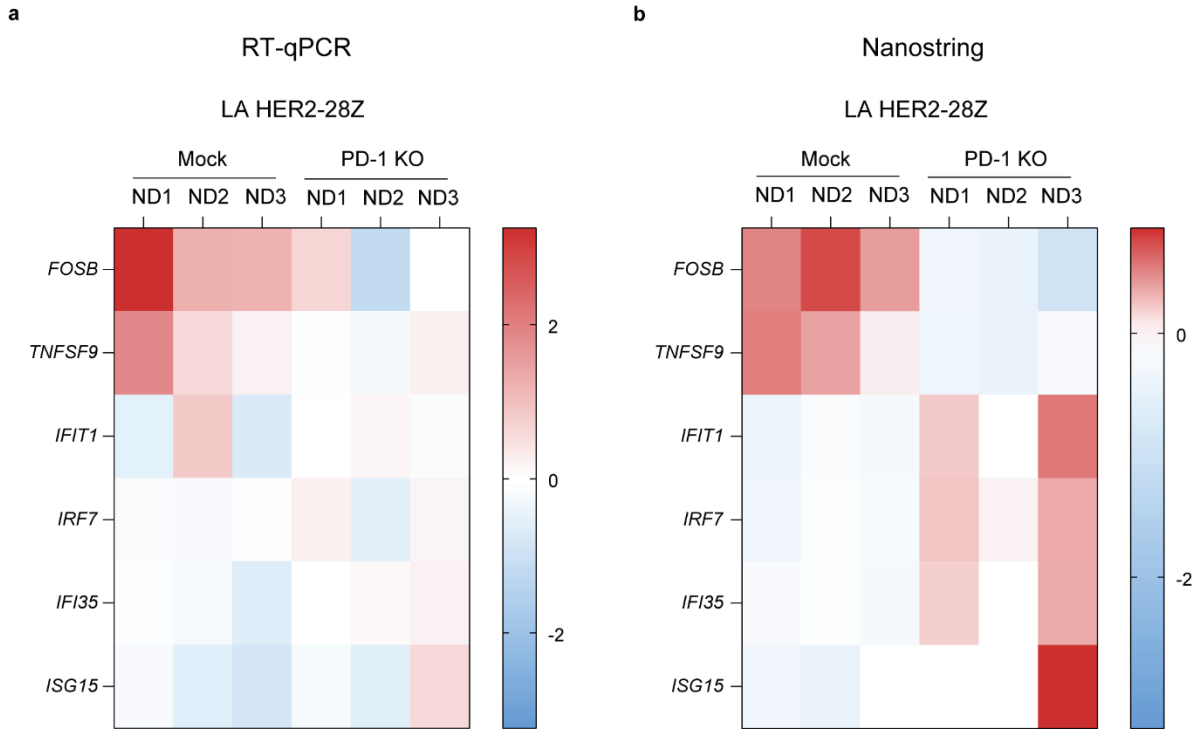

Figure 4.17 | Validation of relevant genes differentially expressed between LA HER2-28Z mock and PD-1 KO CAR-T cells by RT-qPCR. Heat map of the selected statistically significant differentially expressed genes ($P \leqslant 0.05$) between LA HER2-28Z PD-1 KO CAR T cells and mock obtained by **a** RT-qPCR or **b** by Nanostring.

To better understand the intrinsic differences between LA and HA CAR-T cells that could explain the differential sensitivity towards the PD-1/PD-L1 axis, we directly compared the transcriptomic profile of both groups. We found that LA HER2 CAR-T cells expressed preferentially genes associated with a more naïve phenotype such as TCF7, LEF1 and CD45RA[277–279],while HA CAR T-cells showed higher expression of gens associated with T-cell activation and/or exhaustion (CCL3, FOXP3, ICOS, TNFSF9, IL2, MAF) (Fig. 4.18a). We also found pathways related with T-cell differentiation and proliferation to be enriched in the HA versus LA CAR-T cells by gene enrichment analysis (Fig. 4.18b).

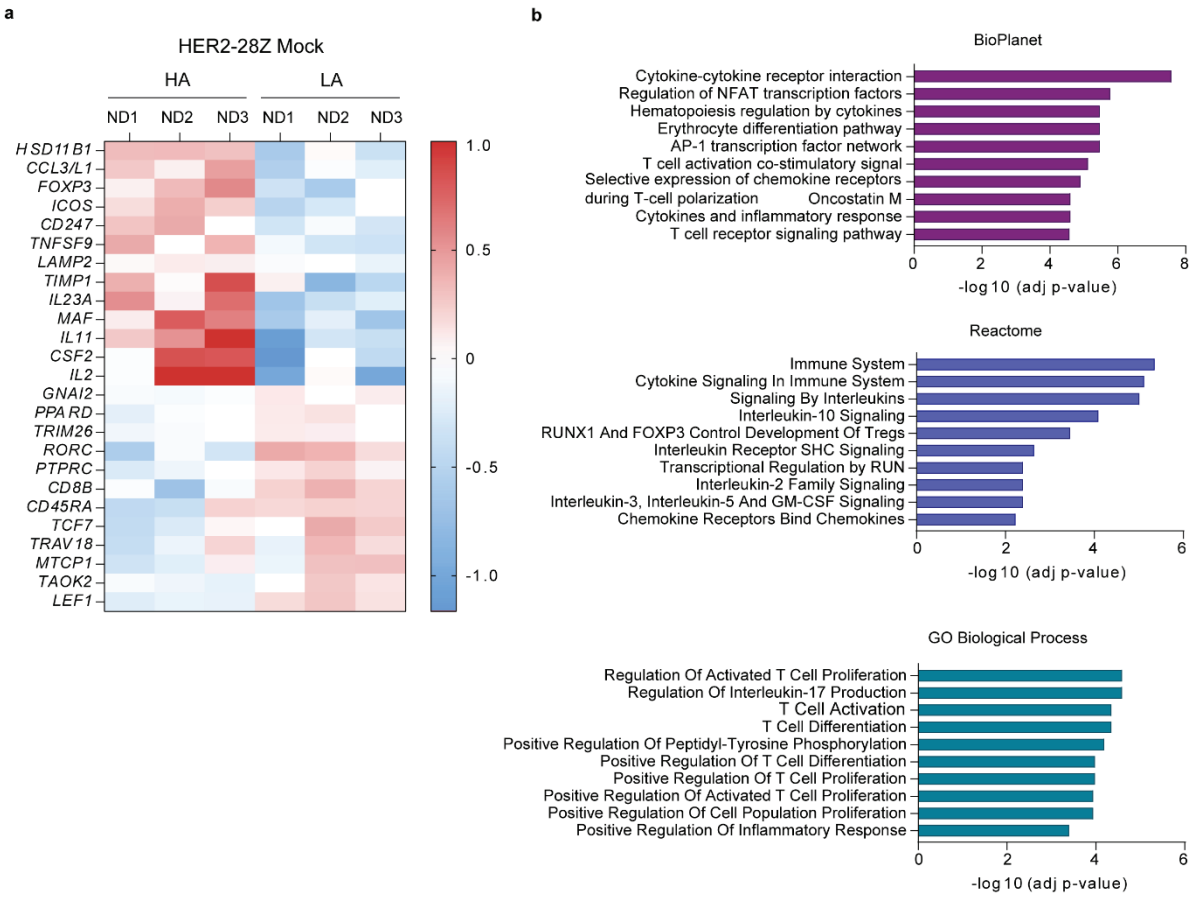

Figure 4.18 | Differential transcriptomic response of HA and LA HER2-28Z CAR-T cells. a Heat map of statistically significant (P⩽0.05) genes that define distinct transcriptional profiles between mock HA and mock LA HER2-28Z CAR T cells after stimulation with SKOV3 tumour cells for 48 hours (n = 3 donors). **b** Bioplanet 2019 (upper panel), Reactome 2022 (middle panel) and Gene Ontology (GO) Biological process 2023 (lower panel), pathway analysis of all significant differentially expressed genes between mock HA and mock LA HER2-28Z CAR-T cells showing the top-10 enriched pathways. -log10 (adj p-value) was derived from Enrichr.

Finally, we compared LA PD-1 KO CAR-T cells with HA CAR-T cells, both of which presented increased *in vitro* and *in vivo* performance compared to LA HER2-28ζ mock CAR-T cells. PD-1 KO LA HER CAR-T cells displayed a less exhausted phenotype with higher expression of *BCL6*, *FOSB* or *TCF7* and lower expression of genes related to exhaustion such as *IRF4*, *CTLA4*, *FAS, FOXO1* or *MAF* (Fig. 4.19a). During the GEA, we observed a substantial enrichment in pathways linked to apoptosis and programmed cell death, to interleukin-mediated signalling, specifically on the activities of IL-4, IL-13, and IL-2, to exhaustion and to T-regs (Fig. 4.19b). Overall, these findings suggest that PD-1 KO LA HER2-28Z cells exhibit a less exhausted phenotype when compared

to HA HER2-28ζ mock CAR-T cells, which have upregulated pathways associated with activation, inflammation and differentiation.

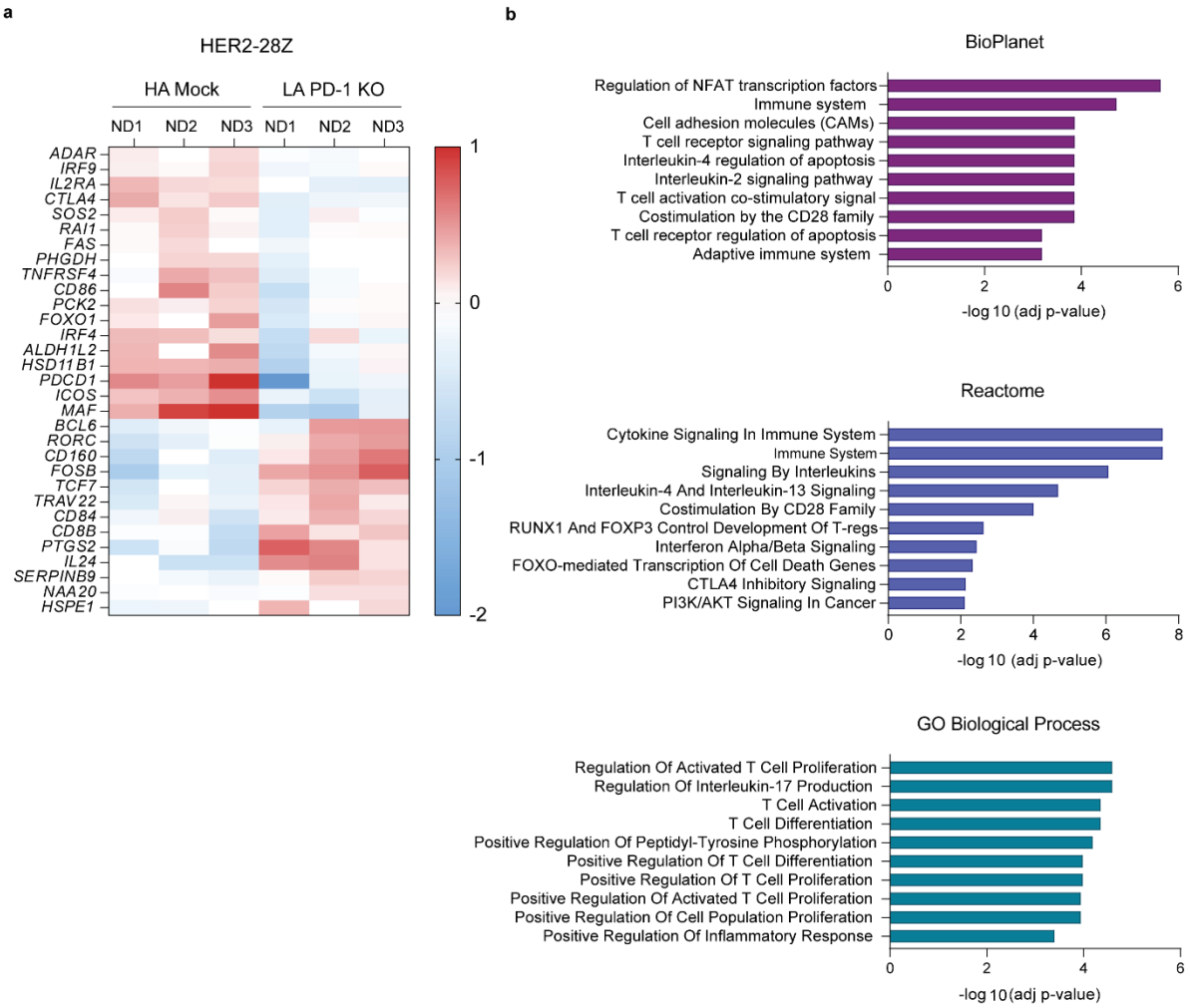

Figure 4.19 | Differential transcriptomic response of mock HA and PD-1 KO LA HER2-28Z CAR-T cells. **a** Heat map of statistically significant ($P \leqslant 0.05$) genes that define distinct transcriptional profiles between mock HA and PD-1 KO LA HER2-28Z CAR T cells after stimulation with SKOV3 tumour cells for 48 hours (n = 3 donors). **b** Bioplanet 2019 (upper panel), Reactome 2022 (middle panel) and Gene Ontology (GO) Biological process 2023 (lower panel), pathway analysis of all significant differentially expressed genes between mock HA and PD-1 KO LA HER2-28Z CAR-T cells showing the top-10 enriched pathways. -log10 (adj p-value) was derived from Enrichr.

4.8. PD-1 KO increases the polyfunctionality of LA but not HA HER2-28ζ CAR-T cells

Since a number of transcriptional changes involved genes encoding cytokines and because the polyfunctionality of CAR-T cells had been previously correlated with

improved clinical outcomes[280], we sought to assess whether genetic ablation of PD-1 increased the polyfunctionality of HER2-28Z CAR-T cells after antigen exposure. To this end, we performed a single-cell secretome analysis of low and high affinity HER2-28Z CAR-T cells after antigen exposure by using the Adaptive Immune cytokine panel (Isoplexis). We first observed in 3D t-SNE analysis that mock and PD-1 KO LA CAR-T cells segregated in separated clusters, revealing key functional differences between the groups (Fig. 4.20a). By contrast, in HA CAR-T cells, mock and PD-1 KO groups did not cluster separately, suggesting a more homogenous functional profile (Fig. 4.20b). These results are in agreement with the gene expression analysis (Fig. 4.16). In a more comprehensive analysis, when examining the percentages of polyfunctional cells secreting two, three, four, or five or more analytes, PD-1 KO in the LA HER2 CAR-T cells showed trends towards increased percentages of cells producing two or more cytokines both in $CD4^+$ and $CD8^+$ T cell populations, with statistical significance observed specifically in the $CD4^+$ subset for two analytes (Fig. 4.20c). We also measured the polyfunctional strength index (PSI), which accounts for levels and functional classification of the secreted cytokines. This analysis revealed an overall PSI increase by PD-1 disruption in LA HER2 CAR-T cells, with particular significance observed in effector cytokines within the $CD4^+$ populations (Fig. 4.20e). Conversely, the deletion of PD-1 in HA HER2-28Z CAR-T cells showed no significant enhancement in T-cell polyfunctionality or PSI (Fig. 4.20d and f), suggesting a less pronounced effect of PD-1 disruption.

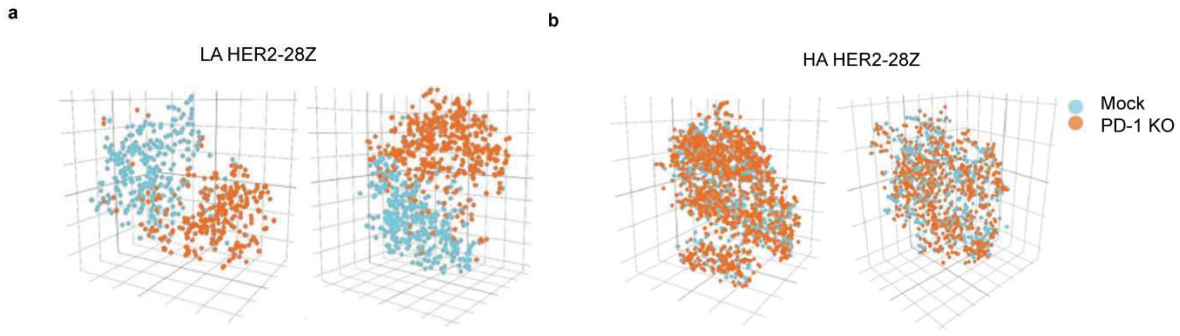

(continues on the next page)

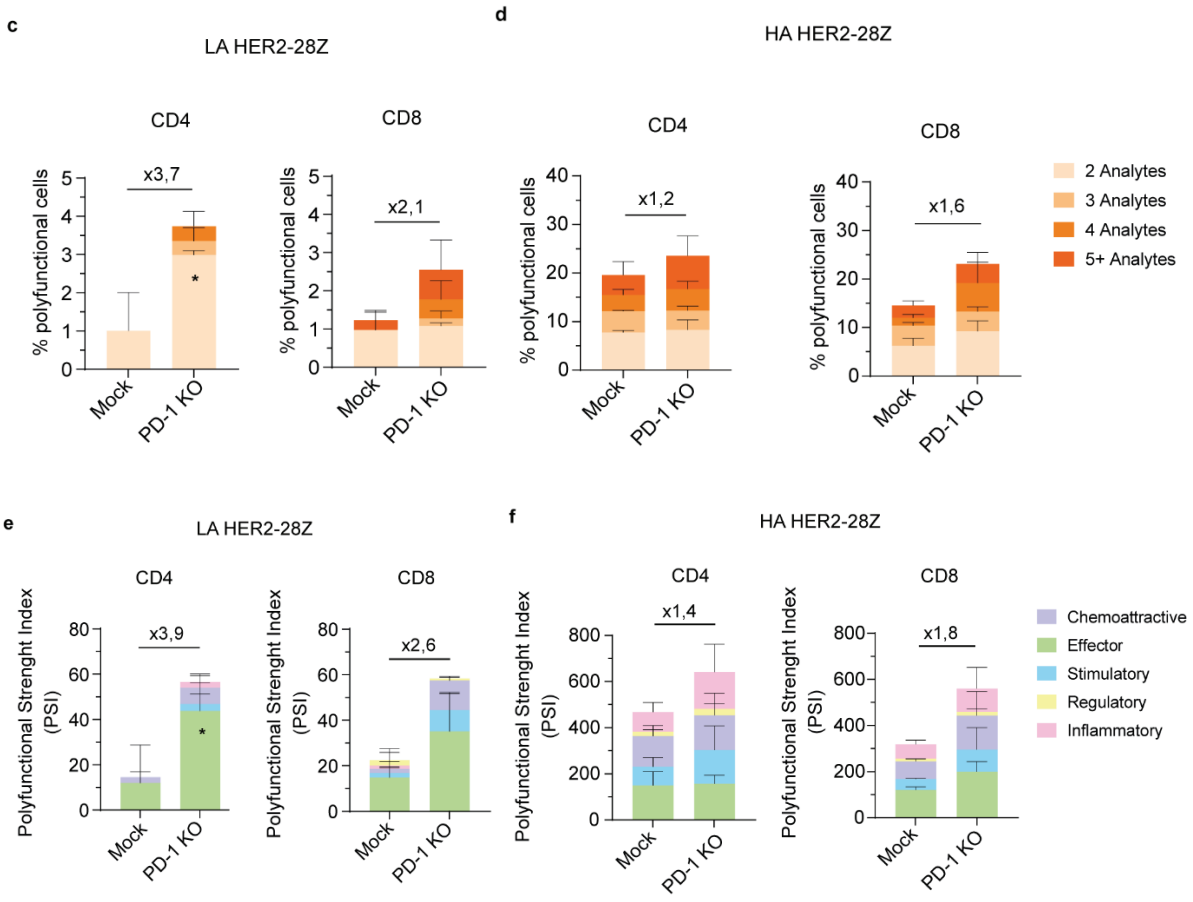

Figure 4.20 | Polyfunctional profiling of LA and HA HER2-28ζ CAR-T cells. Single-Cell Adaptive Immune panel (Isoplexis) of LA and HA HER2-28Z PD-1 KO versus mock CAR-T cells after co-culture with SKOV3 tumour cells (E:T=1:3). Three-dimensional t-SNE plots of **a** LA and **b** HA HER2-28Z PD-1 KO and mock CAR T cells by differentiating them based on their cytokine functional differences. Cell mapping stratifies data points from samples by PD-1 KO (orange) and mock (blue). Polyfunctionality comparison of **c** LA and **d** HA HER2-28Z PD-1 KO CAR T cells and LA and HA-28Z CAR T cells. Bar graphs depict mean % of polyfunctional cells ± SD (n=2 normal donors). *, $p < 0.05$ by two-way ANOVA with Šidák multiple comparisons correction. Polyfunctionality Strength Index (PSI) of **e** LA and **f** HA values. Bar graphs depict mean PSI ± SD (n=2 normal donors). *, $p < 0.05$ by two-way ANOVA with Šidák multiple comparisons correction.

In addition, single-cell secretome analysis suggested an upregulation in the secretion of IFN-γ and a reduced expression of regulatory cytokines such as IL-13, IL-22, and IL-4 by LA PD-1 KO CAR-T cells compared to LA mock CAR-T cells. Notably, PD-1 ablation had no discernible impact on the expression of these cytokines in HA CAR-T cells (Fig. 4.21). These findings are in concordance with the IFN-γ ELISA results, which also demonstrated increased secretion of IFN-γ by LA HER2-28ζ PD-1 KO CAR-T cells compared to mock CAR-T cells.

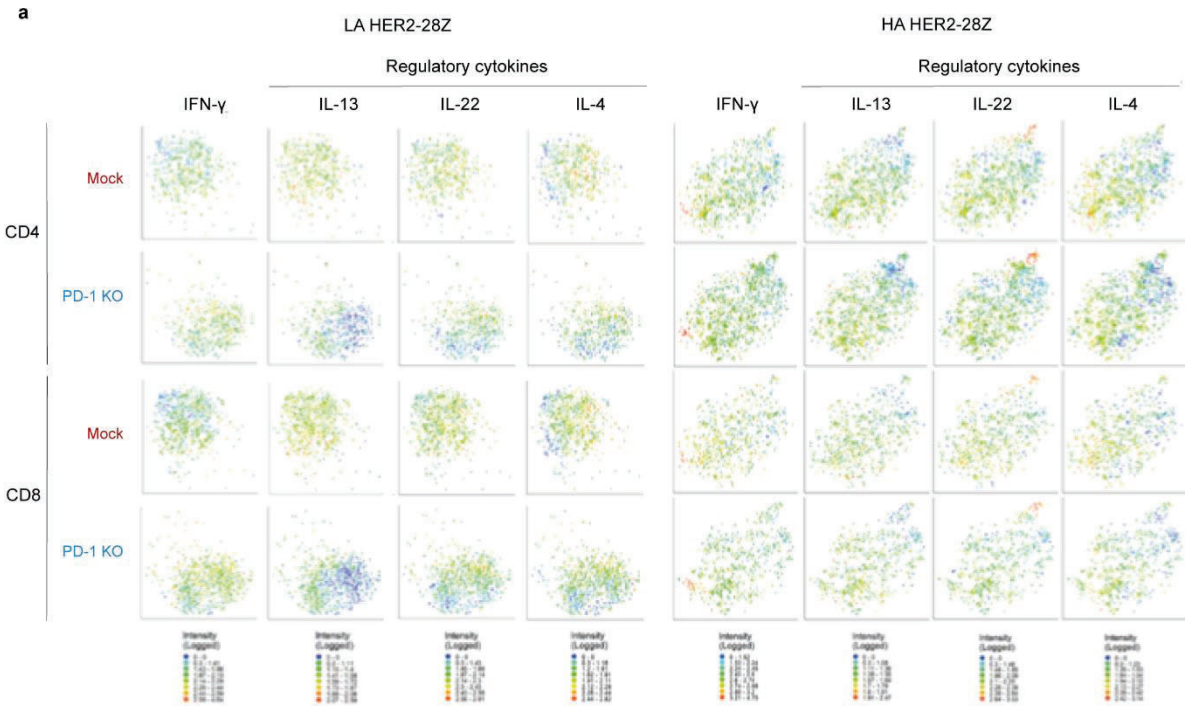

Figure 4.21 | PD-1 deletion differentially modulates regulatory cytokines in LA and HA HER2-28ζ CAR-T Cells / PD-1 deletion alters regulatory cytokines in LA but not HA HER2-28ζ CAR-T Cells. Single-Cell Adaptive Immune panel (Isoplexis) of LA and HA HER2-28Z PD-1 KO versus mock CAR-T cells after co-culture with SKOV3 tumour cells (E:T=1:3). a Single cell t-SNE plots of IFN-γ and regulatory cytokines (IL-13, IL-22 and IL-4) of LA HER2-28Z mock and PD-1 KO (right panel) or HA HER2-28Z mock and PD-1 KO (left panel). Density scale bar represents marker expression of cytokines for a given cell, ranging from low expression (blue) to high expression (red).

To validate the findings obtained from the polyfunctionality study, we performed an intracellular cytokine staining assay. In this assay, control T-cells or LA and HA mock and PD-1 KO CAR-T cells from five different healthy donors were co-cultured with SKOV3 WT. After 24 hours, we analysed the percentage of cells secreting both IFN-γ and TNF-α. We observed that the absence of PD-1 significantly enhanced the percentage of double-positive population of CAR-T cells when co-cultured with tumour cells in the context of LA CAR-T cells. However, there was no noticeable effect on HA CAR-T cells (Fig. 4.22a and b). Of note, frequencies of IFN-γ^+ TNF-α^+ T-cells in mock groups from LA and HA CAR-T cells were comparable (Fig 4.22a and b). As expected, no differences in the percentage of IFN-γ^+ TNF-α^+ secreting T-cells were observed across all experimental conditions in groups treated with PMA-Ionomycin, a T cell stimulation cocktail used as a positive control (Fig. 4.22c and d).

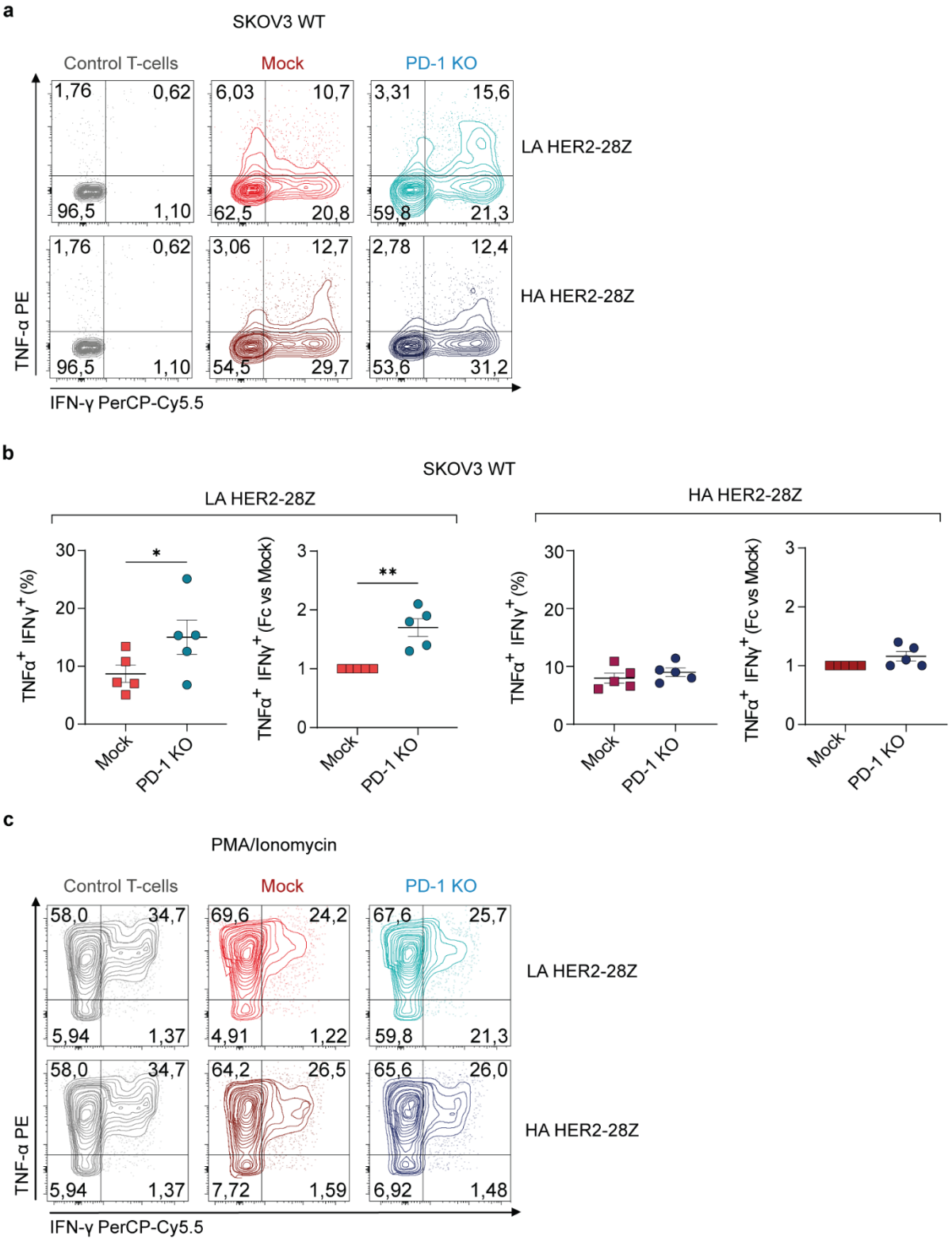

(continues on the next page)

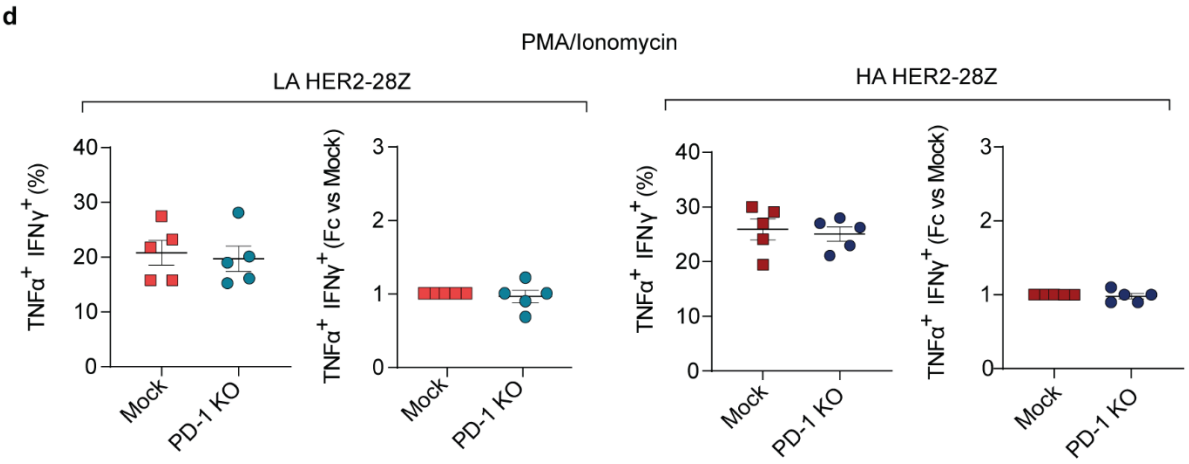

Figure 4.22 | PD-1 KO induces changes in the cytokine production profile of LA but not HA HER2-28ζ CAR-T cells. a Flow cytometry plots of intracellular cytokine staining for TNF-α and IFN-γ in indicated groups after co-culture with SKOV3 tumour cells for 24 hours. Data is pre-gated on CD45+ T-cells. **b** Frequency of IFN-γ$^+$ TNF-α$^+$ T-cells (gated on live/CD45$^+$) plotted as mean ± SEM (n=5 donors) are shown. *, p<0.05 by paired T-test. **, p<0.01 by one-sample T-test. **c** Flow cytometry plots of intracellular cytokine staining for TNF-α and IFN-γ in indicated groups after PMA ionomycin stimulation for 6 hours. Data is pre-gated on CD45+ T-cells. **d** Frequency of IFN-γ$^+$ TNF-α$^+$ T-cells (gated on live/CD45$^+$) plotted as mean ± SEM (n=5 donors) are shown.

Altogether, the upregulation of genes associated with T-cell activation alongside the augmented polyfunctionality could contribute to the heightened anti-tumour efficacy observed in LA HER2-28ζ PD-1 KO. Remarkably, the witnessed lack of distinguishable transcriptional changes at the transcriptomic level and in polyfunctionality supports the notion that PD-1 KO does not significantly impact the functional properties of HA HER2-28ζ CAR-T cells.

4.9. LA PD-1 KO display a safer toxicity profile as compared to HA HER2-28Z CAR-T cells

Using CAR-T cells resistant to the inhibition by the PD1-PDL1 axis may be an attractive strategy for the treatment of solid tumours. However, safety concerns arise when targeting tumour associated antigens using a high affinity CAR, as it may exhibit poor discrimination between tumour and healthy tissues expressing lower levels of the target antigen[218] . To address this concern, we first established co-cultures of LA or HA HER2-28Z CAR-T cells with or without PD-1 KO with a model of triple negative breast cancer cells (MDA-MB-468) engineered to express negative, low or high densities of HER2 previously developed in the lab. The HER2 densities expressed by the MDA-MB-468 HER2 Low cells are representative of HER2 densities found in some healthy tissues, while HER2 densities expressed by the MDA-MB-468 HER2 High cells represent HER2 overexpression in HER2+ tumours. In a second approach, we used a panel of human primary healthy cells including Epidermal Keratinocytes (NHEK), Renal Epithelial Cells (HREpC), Pulmonary Artery Endothelial Cells (HPAEC) and Pulmonary Artery Smooth Muscle Cells (HPASMC), all of which have been reported to express low but detectable HER2 densities[254]. As a readout of activation, we analysed the secretion of CD107α, IFN-γ and IL-2. Control T-cells were used as negative control.

In the context of the HER2 model (Fig. 4.23a), both LA and HA HER2-28Z CAR-T cells demonstrated comparable reactivity when confronted with the HER2 high-expressing cancer cell line. However, differences in activation emerged when these CAR-T cells encountered a cell line expressing lower levels of HER2. Only the HA HER2-28Z CAR-T cells displayed discernible expressions of the activation markers CD107α (Fig. 4.23b and c), IFN-γ (Fig. 4.23d) and IL-2 (Fig.4.23 e). Of note, none of the experimental groups showed reactivity towards tumour cells lacking HER2 expression. This observation further validates the specificity of HER2-targeted CAR-T cell therapy, as it specifically recognizes and engages with HER2-expressing cancer cells.

a

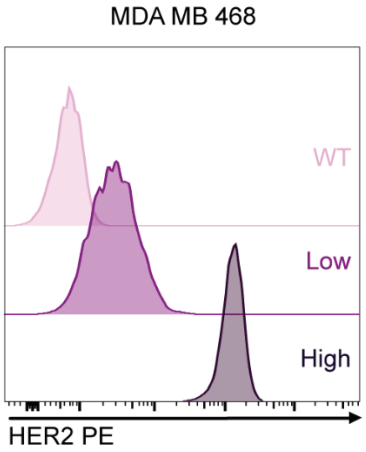

b

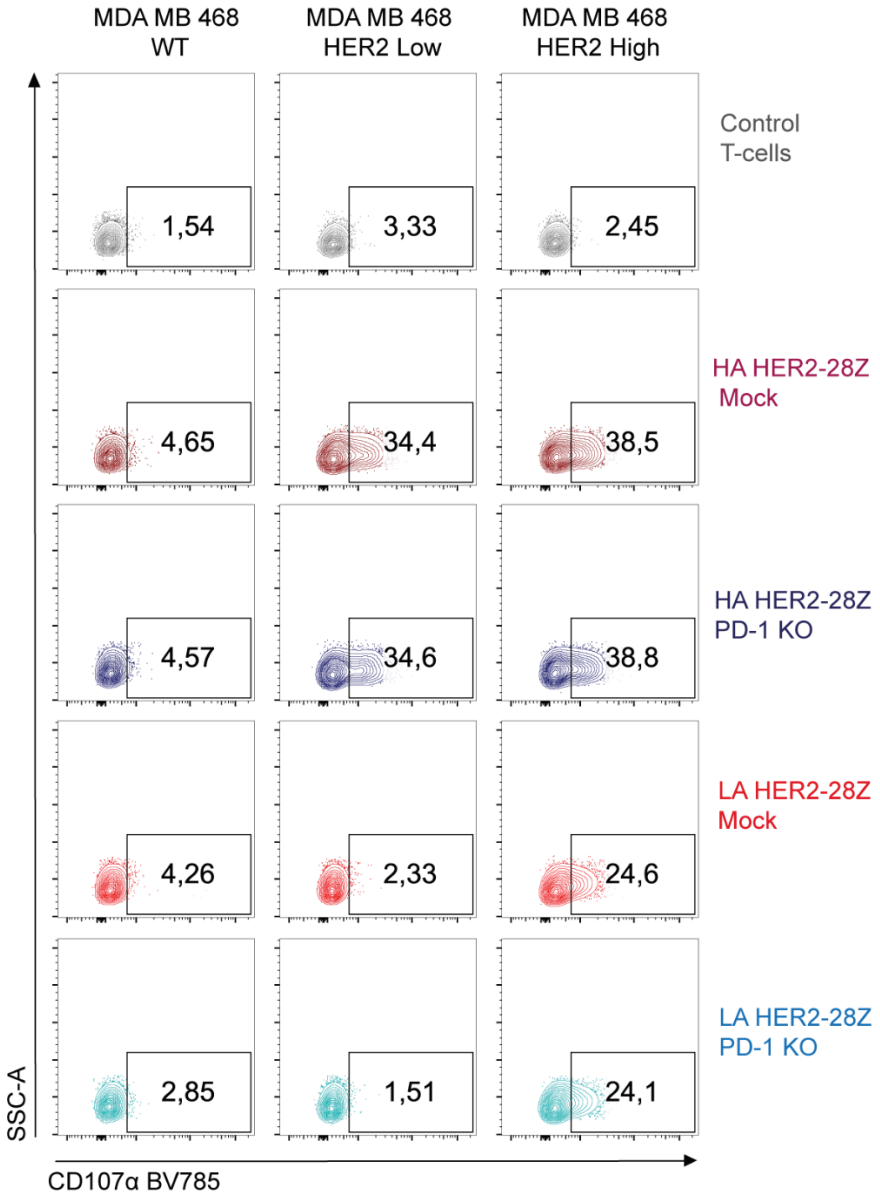

(continues on the next page)

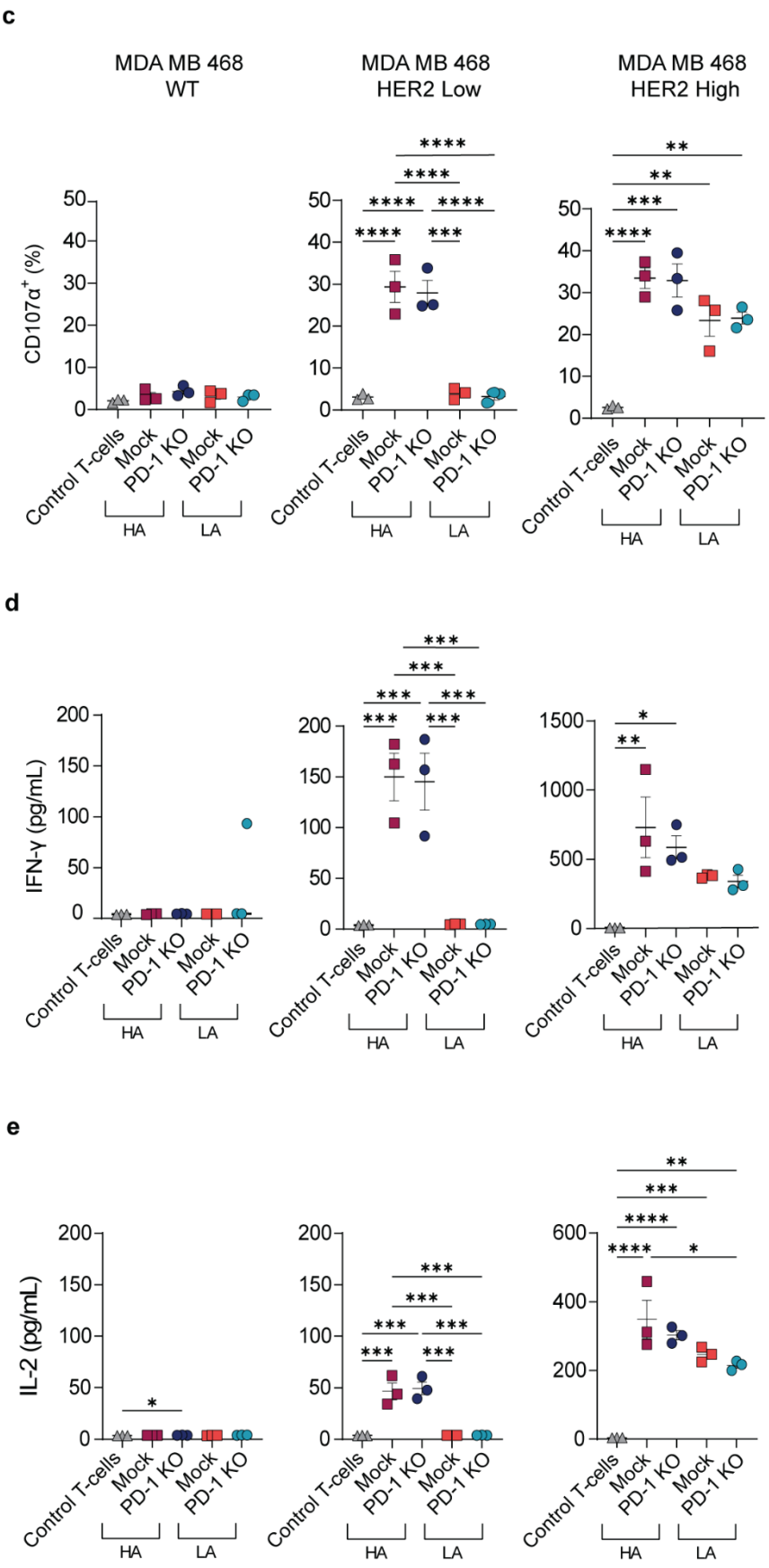

Figure 4.23 | Toxicity profile of mock and PD-1 KO LA and HA HER2-28Z CAR-T cells against a panel of tumour cells expressing variable HER2 densities. **a** HER2 expression by flow

cytometry in wild type MDA-MB-468 cells or MDA-MB-468 cells engineered to express low or high levels of HER2. Control T-cells, mock or PD-1 KO HER2-28Z CAR-T cells of LA or HA were co-cultured with indicated MDA-MB-468 cell lines. CD107α degranulation marker was measured after 6 hours of co-culture (E:T=1:1). **b** Representative flow cytometry plots and **c** percentage of cells producing CD107α (gated as live/CD45+) plotted as mean ± SEM (n=3 donors) are shown. **d** IFN-γ or **e** IL-2 production by control T-cells and mock or PD-1 KO HER2-28Z CAR-T cells of LA or HA after 24 hours of co-culture (E:T=3:1) as quantified by ELISA.

In line with these observations, only HA CAR-T cells were activated in response to co-culture with healthy cells as evidenced by increased production of CD107α (Fig. 4.24a and b), IFN-γ (Fig. 4.24c) and IL-2 (Fig. 4.24d). This differential response underscores the enhanced functionality and potency of the HA HER2-28Z CAR-T cells in recognizing and responding to cancer cells expressing diminished levels of HER2, raising safety concerns. Of note, PD-1 KO did not exacerbate the reactivity of LA HER2-28Z CAR-T cells against primary cells from healthy tissues, which showed a toxicity profile similar to non-tumour specific control T-cells.

a

(continues on the next page)

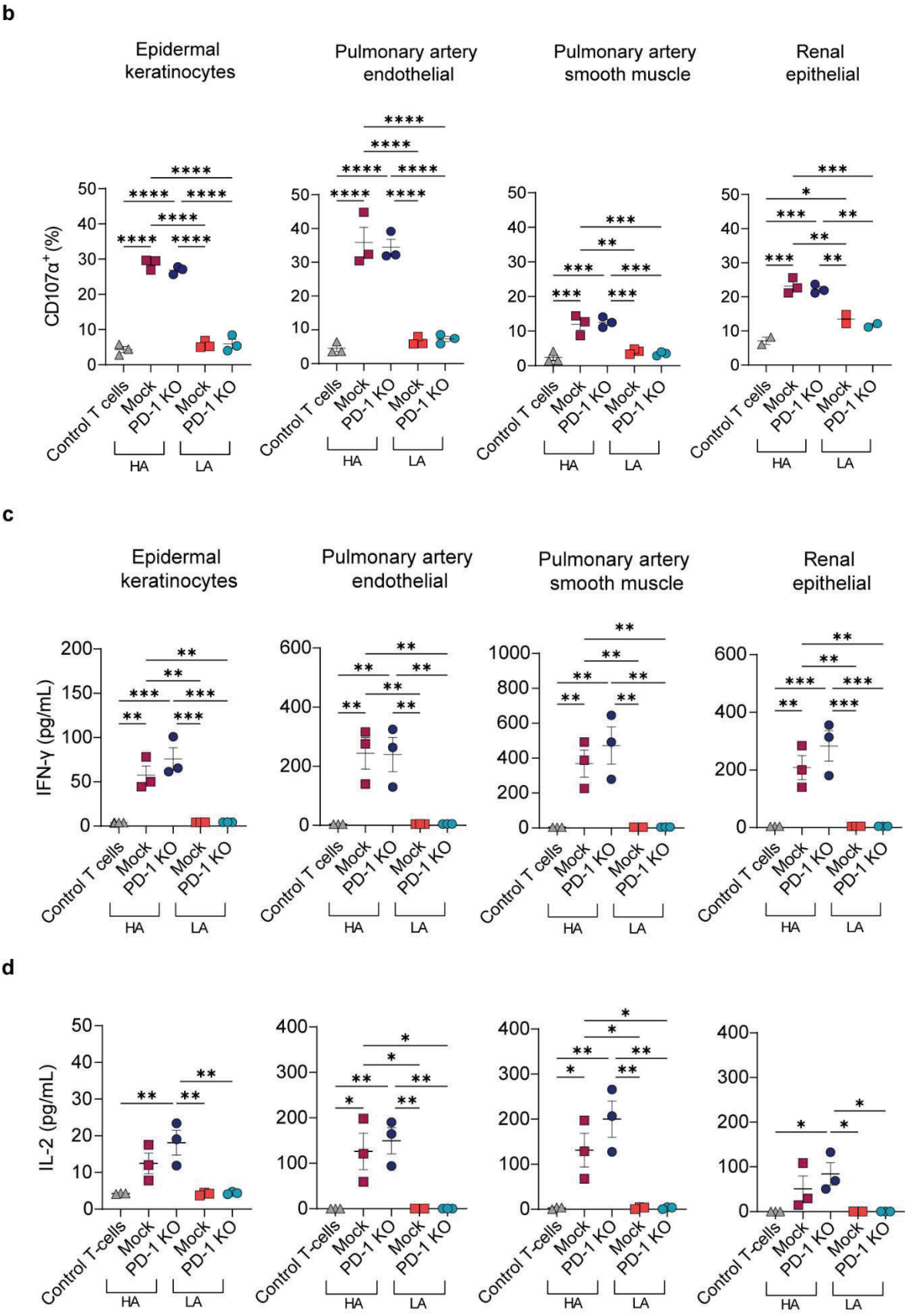

Figure 4.24 | HA HER2-28Z CAR-T cells demonstrate reactivity against a panel of primary healthy cells while LA CAR-T cells do not. Control T-cells, mock or PD-1 KO HER2-28Z CAR-T cells of LA or HA were co-cultured with a panel of human primary cells. CD107α degranulation

marker was measured after 6 hours of co-culture (E:T=1:1). **a** Representative flow cytometry plots and **b** percentage of cells producing CD107α (gated on live/CD45+) plotted as mean ± SEM (n=3 donors) are shown. **c** IFN-γ or **d** IL-2 production by control T-cells, mock or PD-1 KO HER2-28Z CAR-T cells of LA or HA after 24 hours of co-culture (E:T=3:1) as quantified by ELISA. Absolute levels are plotted as mean ± SEM (n=3 donors). *, p <0.05; **, p <0.01; ***, p <0.001; ****, p <0.0001 by one-way ANOVA with Tukey's multiple testing correction.

4.10. Target antigen densities and CAR expression play a role in determining sensitivity to PD-L1

We next sought to investigate how target antigen densities influence the heightened resistance of HA CAR-T cells to the PD-1/PD-L1 axis. We hypothesized that HA CAR-T cells might become susceptible to this inhibitory pathway under conditions of low antigen densities. To explore this, we took advantage of the lipid bilayer model outlined in Fig. 4.10a to titrate down HER2 densities while maintaining constant high levels of PD-L1. In this controlled environment, HA CAR-T cells remained unaffected by PD-L1, as indicated by comparable levels of IFN-γ released by mock CAR-T cells across all HER2 conditions. Of note, at the lowest antigen levels, mock and PD-1 KO exhibited similar behaviour, while as HER2 levels increased, PD-1 KO appeared to have a detrimental effect (Fig. 4.25b). In the LA setting, PD-1 KO conferred an advantage to CAR-T cells at all antigen density conditions tested (Fig. 4.25a). Next, we employed the cellular model based on a triple-negative breast cancer cell line, MDA-MB-468, but engineered to express either low or high levels of HER2 along with constitutive high levels of PD-L1 (Fig. 4.25c). Consistent with our previous observations in the SKOV3 model, we found that the absence of PD-1 led to an augmented production of cytokines by LA CAR-T cells when HER2 levels were high, while HA HER2-28Z CAR-T cells did not benefit from PD-1 KO (Fig. 4.25d-h). Conversely, in co-culture with HER2-low cells, PD-1 KO conferred an advantage to HA CAR-T cells under specific conditions. This increase was statistically significant in the IL-2 secretion (Fig. 4.25g) as well as the percentage of polyfunctional T cells producing both IFN-γ and TNF-α (Fig. 4.25h-j). Nonetheless, this effect was not observed in terms of IFN-γ levels measured via ELISA (Fig. 4.25e). As expected, we could not observe any differences among groups when treated with PMA/Ionomycin. In line with toxicity results in Fig. 4.24, LA HER2-28Z CAR-T cells did not exhibit reactivity in low

antigen conditions (Fig. 4.25e, g, j). These findings suggest that PD-1 knockout may potentiate the anti-tumour activity of HA CAR-T cells in environments where HER2 expression is low, but that the impact of PD-1 KO on cytokine production may vary depending on the specific cytokine measured, highlighting the complexity of the factors implied in the interactions between PD-1 and CAR-T cell function.

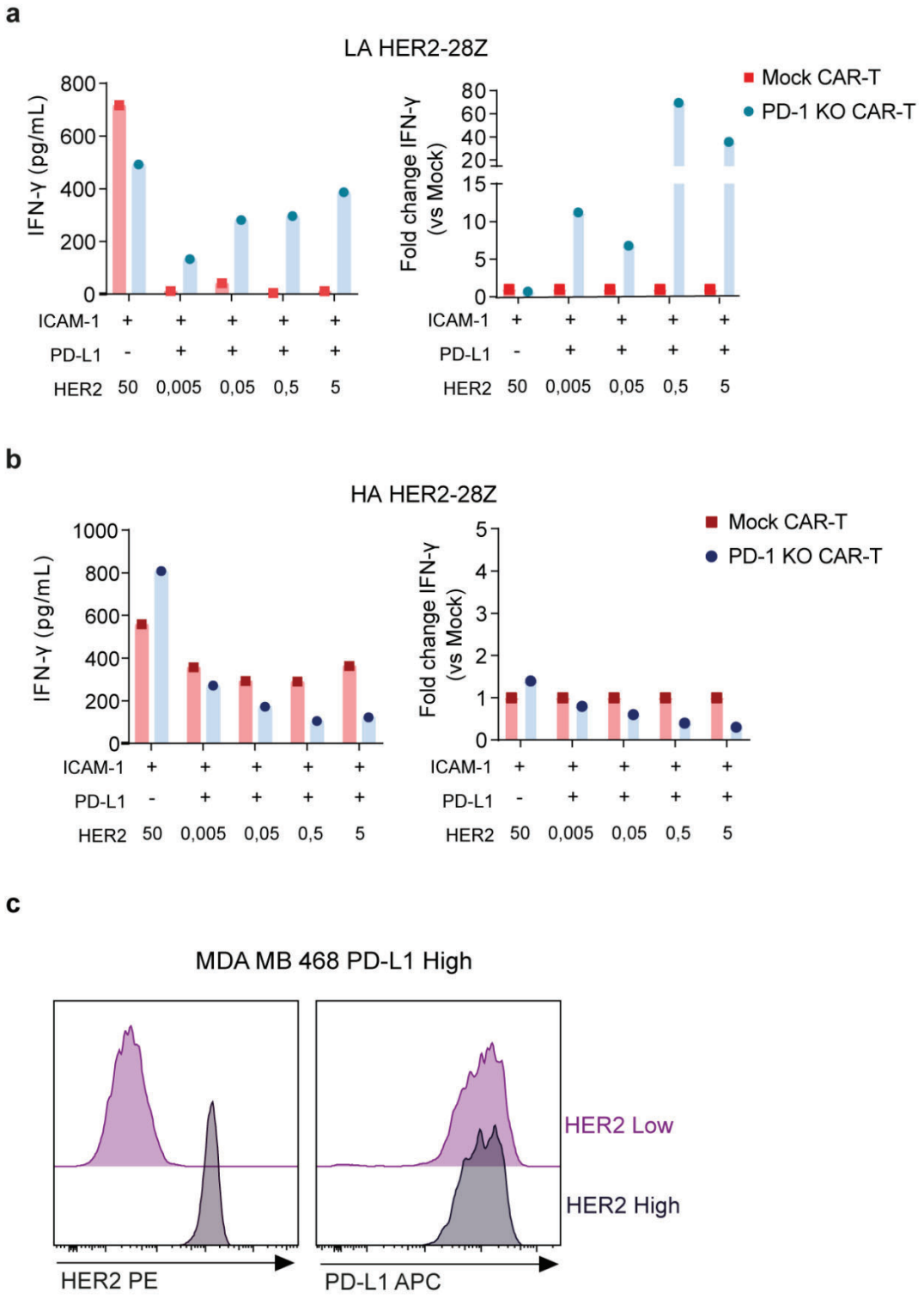

(continues on the next page)

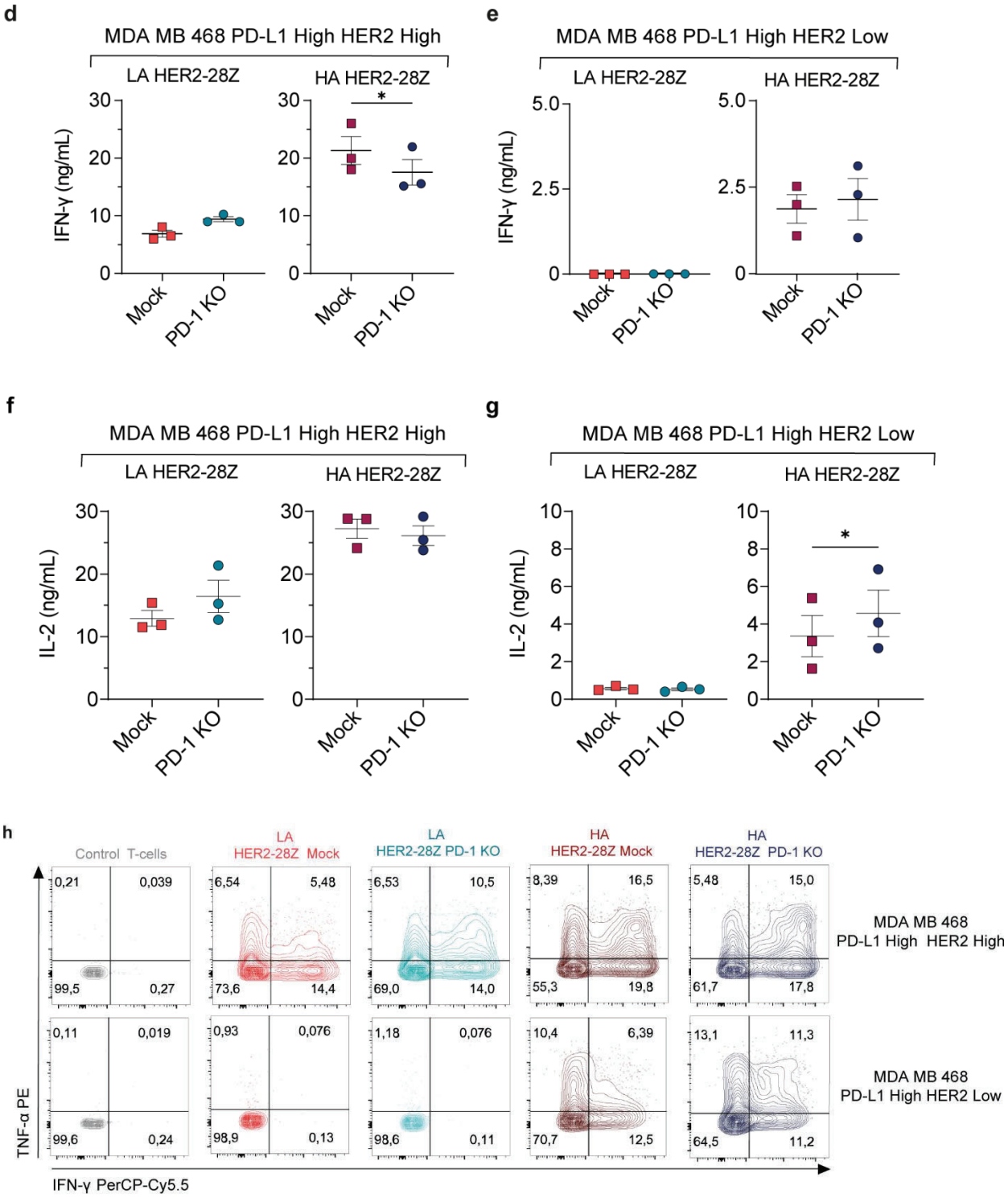

(continues on the next page)

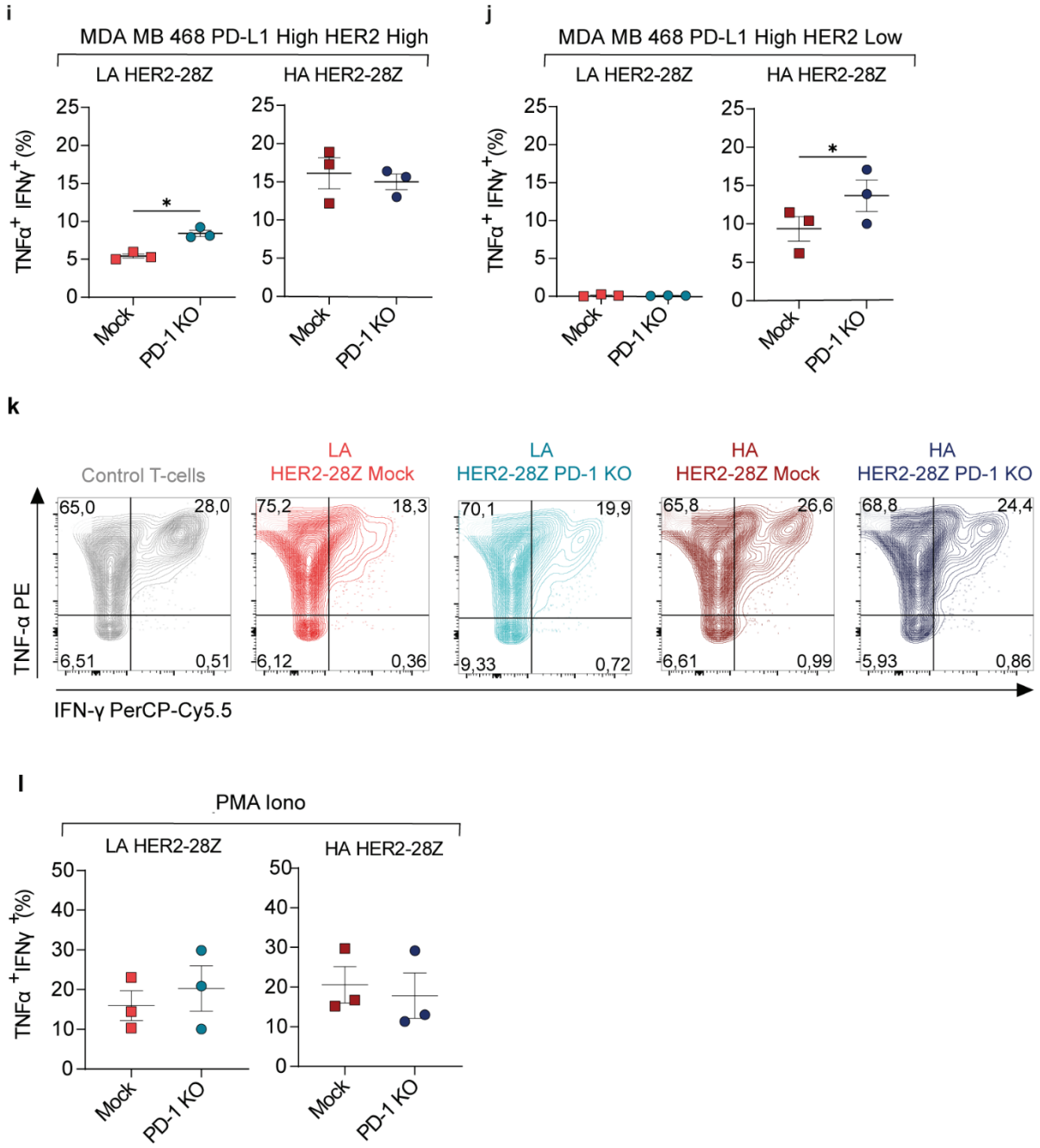

Fig. 4.25 | Target antigen levels are an influential factor in PD-L1 sensitivity. IFN-γ production by mock or PD-1-KO **a** LA or **b** HA HER2-28Z CAR-T cells after 72 hours of co-culture with SLBs containing either HER2 alone (50 ng) or increasing concentrations of HER2 along with PD-L1 (200 ng) as measured by ELISA. Data from one donor is represented as absolute levels (left panel) or fold change of IFN-γ by PD-1 KO versus mock HER2-28Z CAR-T cells (right panel). **c** HER2 (left panel) and PD-L1 (right panel) expression by flow cytometry in MDA-MB-468 cells engineered to overexpress PD-L1 and either low or high levels of HER2. IFN-γ production by mock or PD-1-KO LA (left panel) or HA (right panel) HER2-28Z CAR-T cells after 24 hours of co-culture with **d** MDA-MB-468 PD-L1 high HER2 high or **e** MDA-MB-468 PD-L1 high HER2 low (E:T=3:1) as measured by ELISA. Mean ± SEM is plotted (n=3 donors). IL-2 production by mock or PD-1-KO LA or HA HER2-28Z CAR-T cells after 24 hours of co-culture with **f** MDA-MB-468 PD-L1 high HER2 high or **g** MDA-MB-468 PD-L1 high HER2 low (E:T=3:1) as measured by ELISA. Mean

± SEM is plotted (n=3 donors). *, p<0.05 by paired T-test. Intracellular cytokine staining for TNF-α and IFN-γ in mock and PD-1 KO LA and HA HER2-28Z CAR-T cells after co-culture with MDA-MB-468 PD-L1 high HER2 high or HER2 low tumour cells for 24 hours (E:T=1:3). **h** Representative flow cytometry plots and **i-j** frequency of IFN-γ^+ TNF-α^+ T cells (gated on live/CD45+) plotted as mean ± SEM (n=3 donors). *, p<0.05 by paired T-test. k-l) Intracellular cytokine staining for TNF-α and IFN-γ in mock and PD-1 KO LA and HA HER2-28Z CAR-T cells after culture with PMA-ionomycin for 6 hours. **k** Representative flow cytometry plots and **l** frequency of IFN-γ^+ TNF-α^+ (gated on live/CD45+) T-cells plotted as mean ± SEM (n=3 donors) are shown.

Based on these results, we hypothesized that the inhibitory effects mediated by PD-L1 might be surmounted upon reaching a specific threshold of T-cell activation. We theorized that this threshold could also be achieved by utilizing T-cell products characterized by elevated levels of CAR expression. Specifically, we sought to investigate whether a CAR with low affinity for its target antigen but displaying a high densities of surface CAR expression could circumvent the inhibitory effects of this axis[86,281,282]. To address this question, we conducted studies with T-cell products containing either high (over 75%) or low (50-65%) levels of CAR on the T-cell surface (Fig. 4.26a). Among T-cells displaying lower CAR expression levels, the advantageous effects of PD-1 KO were evident in LA HER2-28Z CAR-T cells, whereas their HA counterparts, did not reach statistically significant changes in either total levels or fold change of IFN-γ secretion. Conversely, within the high CAR expression group, the benefits conferred by PD-1 KO in LA CAR-T cells were diminished (Fig. 4.26b), similar to our observations in the HA setting (Fig. 4.26c). These findings indicate that LA HER2-28Z CAR-T cells, characterized by high CAR density, demonstrate the ability to counteract the inhibitory effects of the PD-1/PD-L1 axis. Furthermore, irrespective of whether low or high CAR with high affinity is utilized, the resistance to PD-L1 inhibition persists.

Overall, our results demonstrate the significance of CAR affinity in dictating the sensitivity of CAR-T cells to the PD-1/PD-L1 axis. However, additional factors, such as antigen density and CAR expression levels, may also exert influence. These results emphasize the multifaceted nature of the interplay between CAR-T cells and tumour cells, providing valuable insights into the complexity of optimizing CAR-T cell therapy for enhanced anti-tumour efficacy.

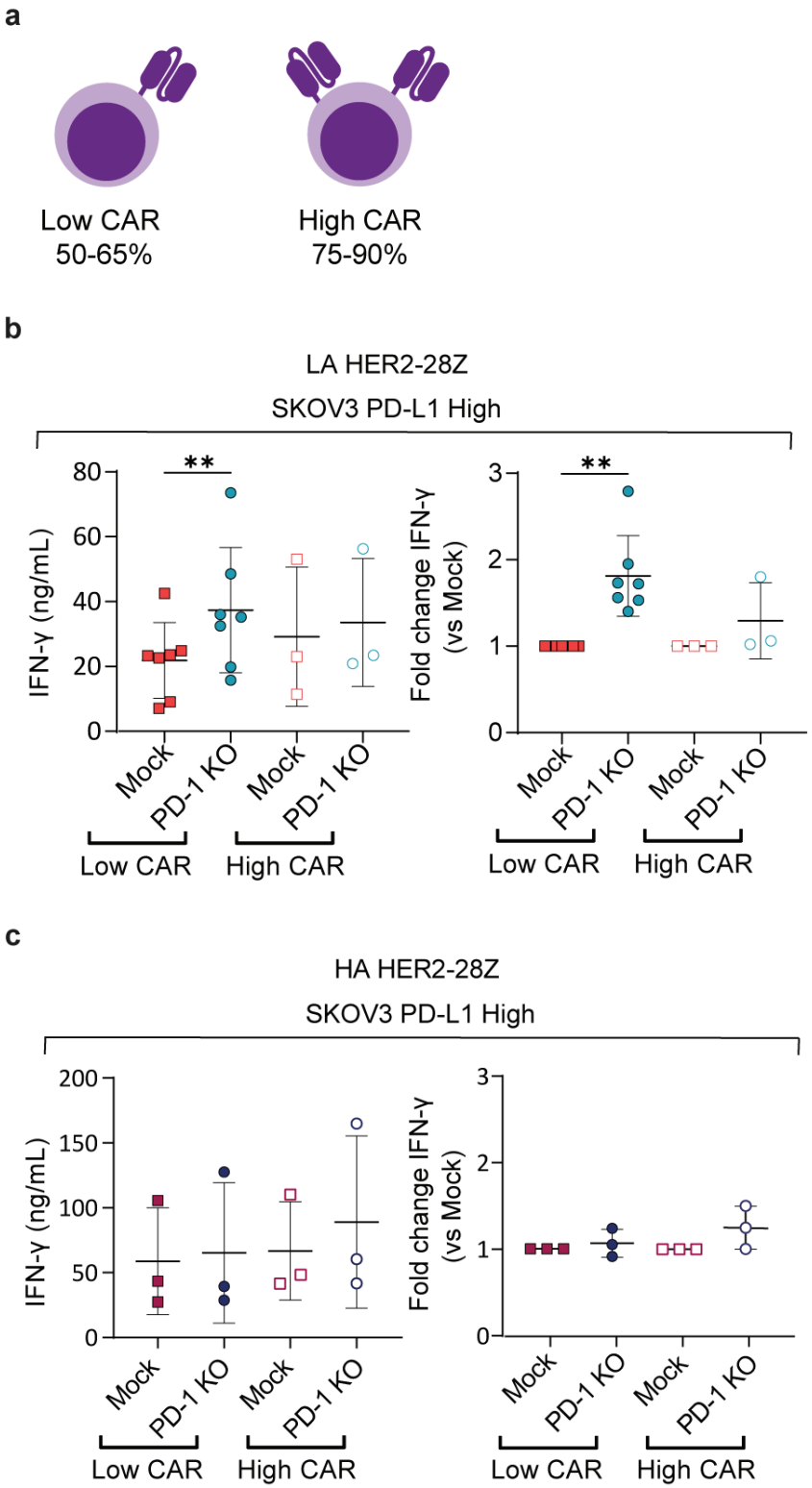

Figure 4.26 | Role of CAR expression in determining sensitivity to PD-L1. a Schematic representation of criteria to discriminate between Low CAR and High CAR-T cell products. IFN-γ production by mock or PD-1-KO (**b**) LA or (**c**) HA HER2-28Z CAR-T cells with either Low or High CAR frequencies after 24 hours of co-culture with SKOV3 PD-L1 High tumour cells (E:T=3:1). Mean ± SEM (n=3-8 donors) is represented for absolute levels (left panel) and fold change of PD-1 KO versus mock (right panel). **, p<0.01 by paired T-test (for absolute levels) or one-sample T-test (for fold change).

4.11. Advantages of PD-1 KO do not apply uniformly across different CAR constructs.

Given the influences of the other studied factors, namely target antigen levels and CAR expression, in addition to affinity in mediating the interaction between the PD-1/PD-L1 axis, we were prompted to investigate whether the co-stimulatory domain of the CAR would also play a role. Therefore, to determine the applicability of our observations with CD28-based HER2 CAR-T cells to other CAR constructs we evaluated CARs targeting HER2 but incorporating different co-stimulatory domains, including ICOS and 4-1BB, as (Fig. 4.27a). In a first approach, NSG mice containing SKOV3 wild-type tumours were treated with LA or HA HER2 CAR-T cells wherein the CD28 costimulatory domain had been replaced by ICOS (HER2-ICOSζ)[283]. We found PD-1 ablation to enhance anti-tumour efficacy of LA but not HA HER2 CAR-T cells, consistent with our earlier findings in CD28-based CAR-T cells (Fig. 4.27b). Since 4-1BB is a clinically relevant co-stimulatory domain, we also explored how the PD-1/PD-L1 axis impacted 4-1BB co-stimulated CAR-T cells (HER2-BBZ). We observed that neither PD-1 KO nor PD1/PD-L1 blockade by using antibodies increased cytokine secretion in vitro (Fig. 4.27c) or anti-tumour effect in vivo (Fig. 4.27d). This was also confirmed using CAR-T cells targeting mesothelin with LA (Meso-BBζ) (Fig. 4.27e). Differential CAR expression was ruled out as a potential reason for the differing sensitivity to PD-L1-mediated inhibition among constructs with distinct co-stimulatory domains, as ICOS-based CARs, despite being expressed at lower levels as compared to CD28, were still sensitive to PD-1/PD-L1 axis. In contrast, 4-1BB-based CARs exhibited comparable expression levels to CD28 but demonstrated greater resistance to inhibition by PD-L1 (Fig. 4.27f-g). These results can be explained, at least in part, by the lower expression levels of PD-1 when compared to that of CD28- or ICOS co-stimulated CARs (Fig. 4.27h) and are in line with previous studies showing that 4-1BB-based CARs are less sensitive to PD-1 mediated inhibition than CD28-based CARs[236,284].

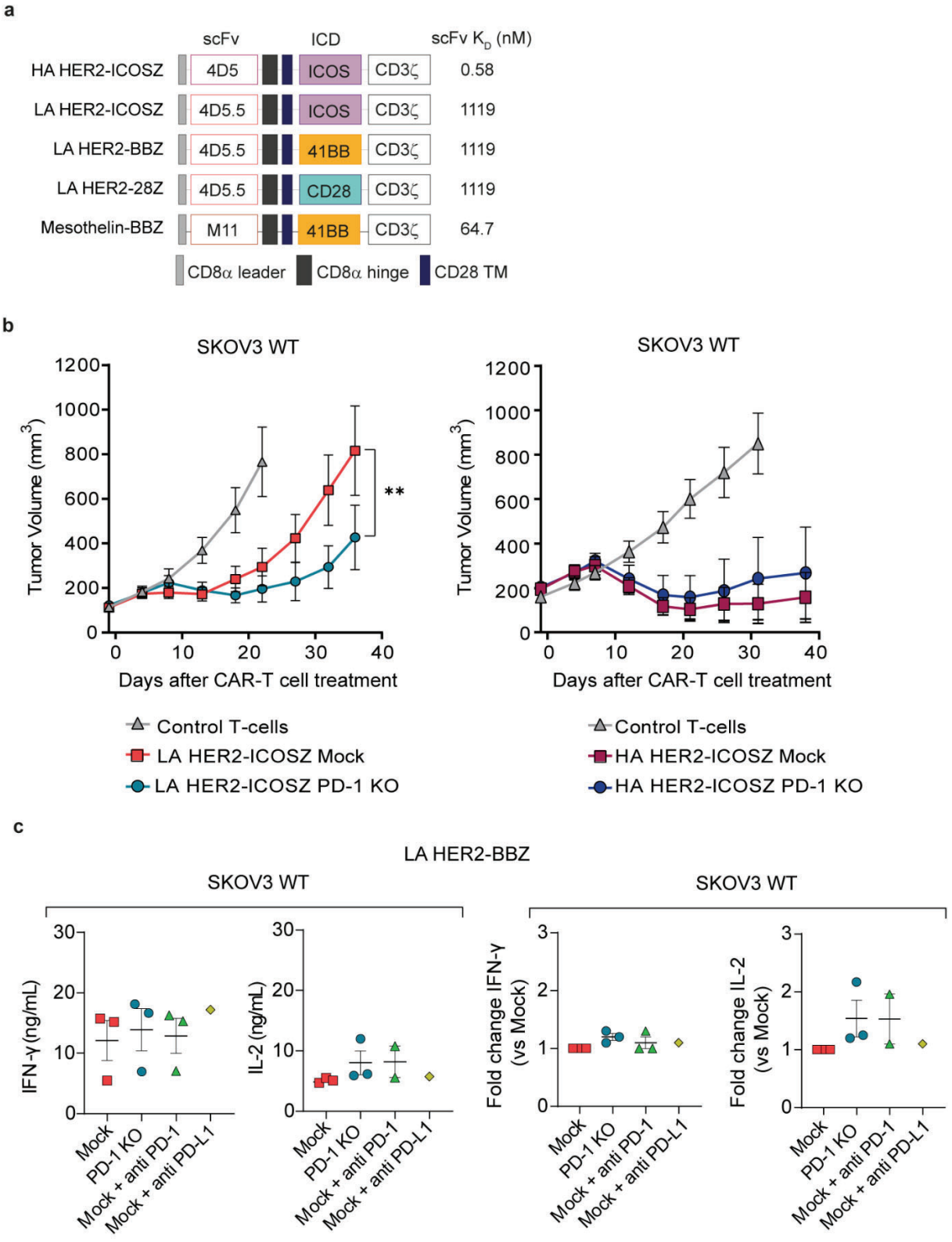

(continues on the next page)

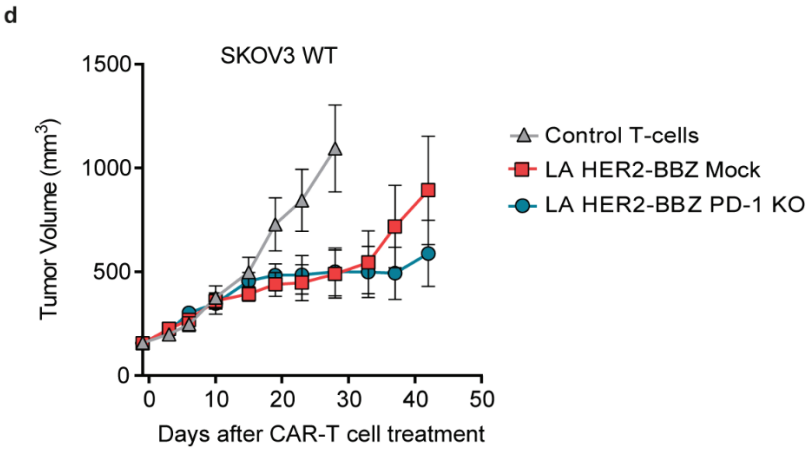
d
SKOV3 WT
Tumor Volume (mm3)
1500
1000
500
0
0
10
20
30
40
50
Days after CAR-T cell treatment
Control T-cells
LA HER2-BBZ Mock
LA HER2-BBZ PD-1 KO

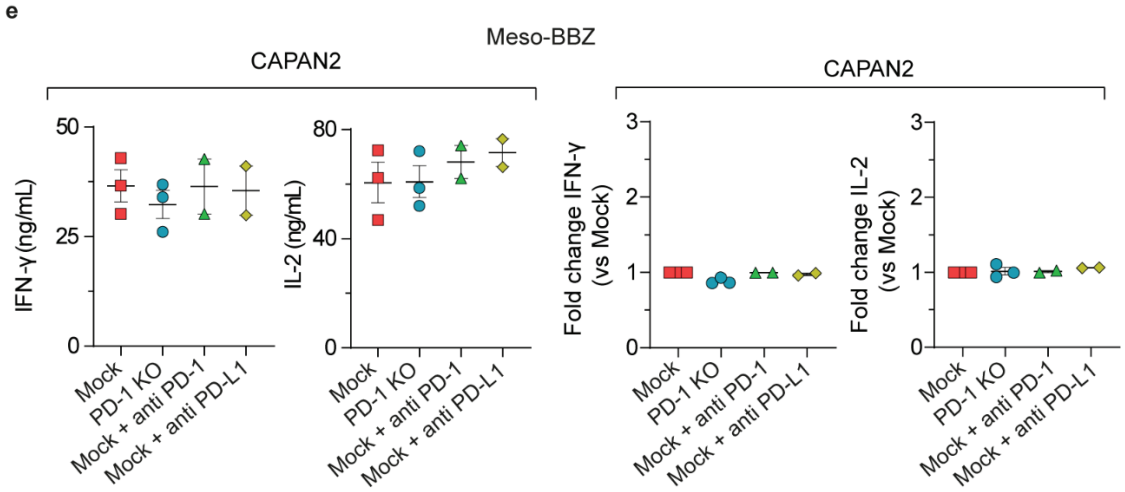
e
Meso-BBZ
CAPAN2
CAPAN2
IFN-γ (ng/mL)
IL-2 (ng/mL)
Fold change IFN-γ (vs Mock)
Fold change IL-2 (vs Mock)
Mock
PD-1 KO
Mock + anti PD-1
Mock + anti PD-L1

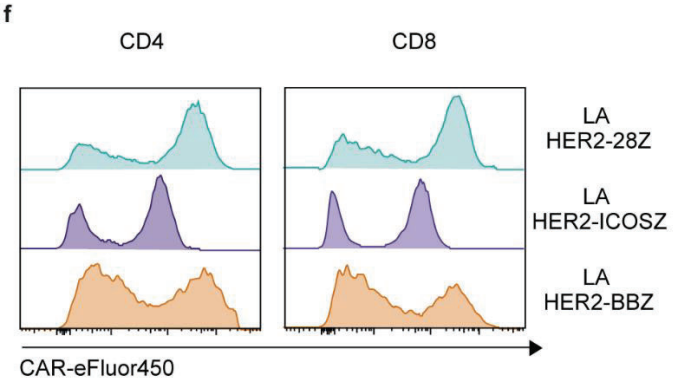
f
CD4
CD8
LA HER2-28Z
LA HER2-ICOSZ
LA HER2-BBZ
CAR-eFluor450

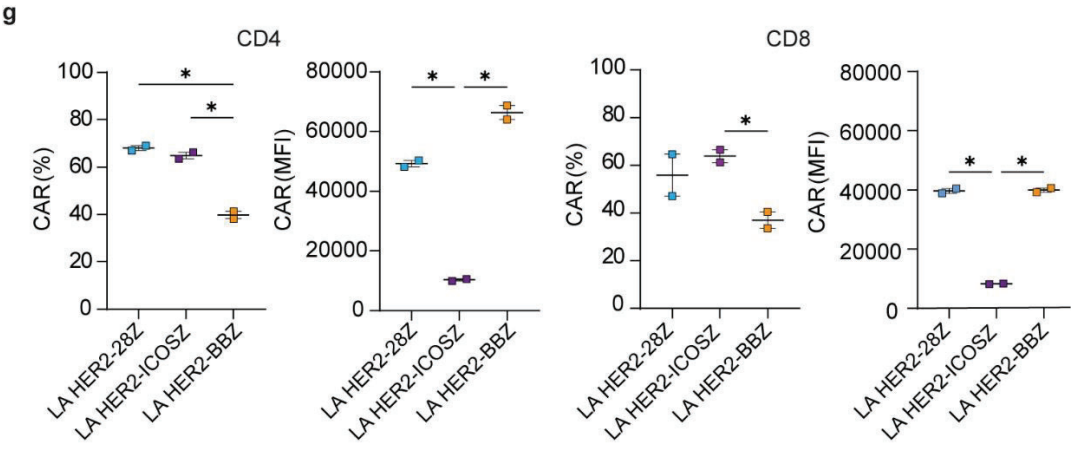
g
CD4
CD8
CAR (%)
CAR (MFI)
LA HER2-28Z
LA HER2-ICOSZ
LA HER2-BBZ

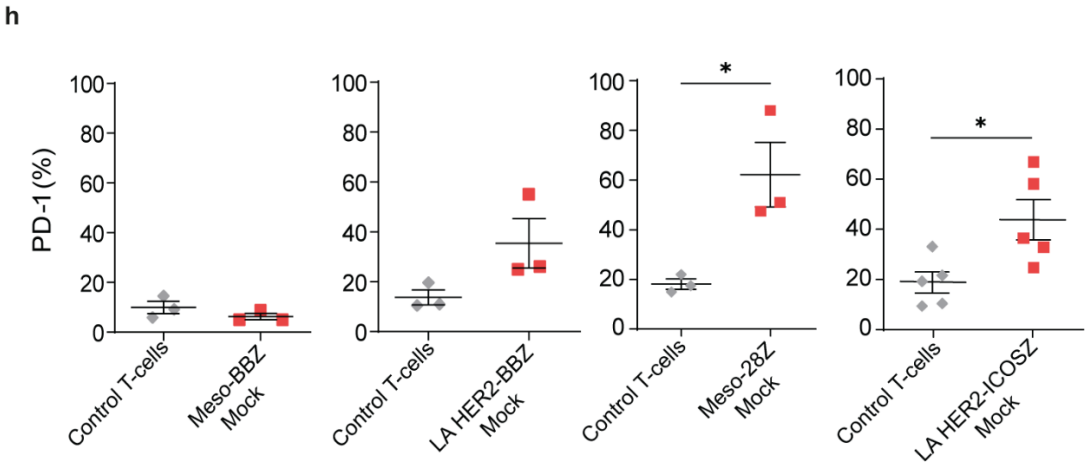

Figure 27 | Influence of co-stimulatory domains in PD-1/PD-L1 inhibition in CAR-T cells. a Schematic overview of CAR constructs used with their affinities **b** NSG mice bearing SKOV3 tumours were treated with $5{\cdot}10^6$ control T-cells, LA HER2-ICOSζ mock or PD-1 KO cells. (n = 10 tumours per group, left panel). NSG mice bearing SKOV3 tumours were treated with $3{\cdot}10^6$ control T-cells, HA HER2-ICOSζ mock or PD-1 KO cells. (n ≥ 6 tumours per group, right panel). Mean tumour volume ± SEM is shown. **, $p < 0.01$ by two-way ANOVA with Sidak multiple testing correction. **c** PD-1 KO or mock HER2-BBζ CAR-T cells, alone or in combination with anti PD-1 or anti PD-L1 antibodies CAR-T cells were co-cultured with SKOV3 tumour cells (E:T=3:1). IFN-γ and IL-2 release was analysed 24 h later by ELISA. Data are plotted as mean ± SEM (n =3 donors for all groups except mock+anti-PDL1 with one donor). **d** NSG mice bearing SKOV3 tumours were treated with $3{\cdot}10^6$ control T cells, LA HER2-BBζ mock or PD-1-KO cells CAR-T cells. Mean tumour volume ± SEM is shown (n ≥ 8 tumours per group). **e** Meso-BBζ mock, PD-1-KO, mock with anti PD-1 or anti PD-L1 CAR-T cells were co-cultured with CAPAN2 (E:T=3:1). IFN-y and IL-2 release was analysed 24 h later by ELISA. Cytokine secretion is represented by absolute levels (left panel) or by fold change of PD-1 KO CAR-T cells, mock CAR-T cells with anti PD-1 or anti PD-L1 as compared to mock CAR-T cells (right panel). Data are plotted as mean ± SEM (n=3 donors). **f** Representative flow cytometry plots depicting levels of CAR expression by LA HER2 CAR-T cells containing CD28, ICOS or 4-1BB as the co-stimulatory domain. CD4+ T cells (left panel) and CD8+ T cells (right panel). **g** Quantification of percentage of CAR positive cells (left panel) and MFI (right panel) of indicated CARs in CD4 or CD8 T cells. Data is represented as mean ± SEM (n=2 donors). *, $p < 0.05$ by one way ANOVA with Tukey post hoc test. **h** Percentage of PD-1 expression by flow cytometry of indicated CAR-T cells and their corresponding control T cells on day 8 of T-cell expansion (n=3-5 donors) *, $p < 0.05$ by paired T-test.

Discussion

5. Discussion

Clinical outcomes achieved until date with CAR-T cell therapy for the treatment of solid tumours are yet far from the unprecedented success witnessed in hematologic malignancies. The scientific community is now exhaustively exploring strategies to overcome some of the limitations that solid tumours present, including T cell inhibition within the suppressive TME.

One of the most prominent T-cell inhibitory axis is the PD-1/PD-L1 immune checkpoint pathway, which ultimately results in the suppression of effector T cell functions and can be detrimental to the effectiveness of therapies involving adoptive T cell transfer (i.e. TILs, TCR-T cells and CAR-T cells). Results reported herein unveil CAR affinity as a previously unexplored factor modulating the sensitivity of CAR-T cells to PD-1/PD-L1 axis, showing that low affinity CAR-T cells are more sensitive to PD-L1-mediated inhibition as compared to high affinity CARs. Accordingly, PD-1 genetic disruption only impacted positively on the functionality of low affinity CAR-T cells, while high affinity CAR-T cells remained unaltered. This behaviour holds true for CD28 and ICOS but not 4-1BB co-stimulated CAR-T cells, which are intrinsically less sensitive to PD-L1 inhibition.

The potential of disrupting PD-1/PD-L1 signalling as a strategy to overcome PD-L1-mediated T cell suppression and to boost the therapeutic index of CAR-T cells has been widely discussed. While most works report increased functionality of PD-1-ablated CAR-T cells[236,238,242,244,245,247,285], including preliminary results from clinical trials[192,193], some others suggest that PD-1 disruption accelerates T cell exhaustion and impairs long-term T-cell persistence[248,249]. We identified a lack of consistency within the different articles in terms of the tumour models used, ranging from cell lines engineered to constitutively express high PD-L1 densities to cell lines expressing physiological levels of PD-L1 in response to CAR-T cell activation. These conflicting results have also been observed with TCR-T cells, where knocking PD-1 out has been associated with long-term persistence and functionality[285], but also to increased exhaustion[34] and to diminished persistence in a clinical trial led by Carl June and colleagues from the

University of Pennsylvania[286]. Remarkably, in this study they did not detect high levels of PD-L1 in tumours, whereas the articles that have reported beneficial effects on PD-1 disruption generally used artificial models with high, constitutive PD-L1 levels, which might in part explain discrepancies in the reported results. Arising from this observation, and from the fact that currently available preclinical models often fail to predict clinical outcomes[287], the first goal of our project was the generation of robust preclinical models engineered to express different PD-L1 densities (absent, low or high) for systematic interrogation of different CAR configurations. Our cellular-based model demonstrated to be representative of the range of physiological PD-L1 expression levels observed in different tumour cell lines across cancer types. As an additional preclinical model to validate our findings, we developed glass-supported lipid bilayers (SLBs) mimicking the target cell membrane but containing precisely defined amounts of surface proteins, which supposed a valuable tool that allowed the determination of exact PD-L1 amounts required for T cell inhibition[288]. However, it would have been advantageous to correlate the PD-L1 expression levels of our model with biopsies from patients treated with CAR-T cells. Obtaining such biopsies is highly challenging, as there are still few clinical trials involving CAR-T cells in solid tumours, and access to biopsies from these trials is even more restricted. Furthermore, it would have been beneficial to validate the model with other more realistic models including other immunosuppressive cell types, such as tumour slices[289], patient-derived spheroids [290] or organoids[291] and patient-derived tumour-on-a-chip[292].

In addition, this study faces a significant limitation in its reliance on NSG mice, which are commonly used in cancer immunotherapy research. While NSG mice allow for the engraftment of both human tumour cells and immune cells, they possess inherent shortcomings. Firstly, NSG mice lack mature T-cells, B-cells and functional NK cells, impairing their ability to accurately replicate human immune responses. Additionally, the development and function of human immune cells within NSG mice are often suboptimal, potentially affecting the efficacy of immunotherapeutic agents. Importantly, the absence of a fully functional murine immune system can lead to alterations in the TME, failing to capture the complex interactions between CAR-T cells

and the real immunosuppressive milieu found in human tumours, where PD-L1 expression can be upregulated across various components of the environment[293].

To address some of these weaknesses, alternative models such as syngeneic or humanized mouse models have been proposed. While syngeneic models offer advantages like their easy establishment and possibility of interactions between tumour cells and a fully competent immune system, they often fail to recapitulate the chronic inflammatory environment and genetic complexity of human tumours[293]. These models could have been useful to address the effect of additional inhibitory interactions mediated by PD-L1 expressed by cells in the TME (e.g., MDSCs, TAMs, CAFs) on CAR-T cell fitness. Humanized mouse models, on the other hand, involve engrafting mice with functional human cells, tissues or organs to better mimic human physiology[294]. However, the occurrence of GVHD, incomplete immune reconstitution and engraftment failure remain an important challenge[295]. Thus, in the realm of immuno-oncology, the development of novel preclinical models that tackle these limitations is imperative for advancing basic and translational cancer research[296].

In the context of primary CAR-T cell expansion, we have observed an enrichment of the PD-1 KO cell population, despite CAR-T cells not being expected to encounter their antigen or the ligands of PD-1 at that point. Some researchers have shown that T-cells themselves can express PD-L1[297], which could offer a potential explanation, even though the expression of this molecule by T-cells is still being elucidated. However, we were unable to detect PD-L1 expression during the expansion of the CAR-T cells using flow cytometry. Furthermore, colleagues in our research group conducting other gene knockouts have also noted comparable enrichments during CAR-T cell expansion. Collectively, these observations suggest that the enrichment phenomenon occurs independently of the specific gene knockout, but further characterization is necessary to understand the relevance of these findings and the underlying mechanisms.

Solid tumours pose a unique challenge in identifying ideal target antigens compared to haematological malignancies. Unlike B cell malignancies or multiple myeloma, which commonly feature high and consistent expression of CD19 or BCMA, solid tumours frequently exhibit lower and more heterogeneous levels of antigen expression[91,214]. A

potential avenue to overcome the challenges associated with targeting antigens shared by solid tumours and normal tissues is to modify the affinity of the scFv. Affinity tuning via modification of the scFv of the CAR has emerged as an interesting approach, allowing for increased affinities sufficient for tumour cell recognition [282,298] that might permit better reactivity against tumour cells with a low density of antigen expression[299]. However, this approach also raises concerns regarding the potential recognition of target antigens present on healthy tissues. Conversely, low-affinity CAR-T cells might lack antitumour activity owing to their inability to sufficiently recognize and lyse tumour cells with lower expression levels of TAAs[298] but can help minimize possible toxicities derived from healthy cell recognition. However, whether CAR-T cells could have a different sensitivity to PD-1/PD-L1 blockade depending on their affinity had never been addressed. The most intriguing observation of our work, as observed in both preclinical models (tumour cells and SLBs), was that HA CAR-T cells were intrinsically more resistant to PD-L1-mediated inhibition as compared to their LA counterparts. Although we primarily used affinity-tuned HER2-specific CARs of low and high affinity[254] based on CD28 as co-stimulation domain, similar observations were made for CARs targeting FRβ or mesothelin and ICOS-co-stimulated CARs, suggesting that this effect is not unique for a specific targeted antigen or co-stimulatory domain. Supporting our data, a recent report explored PD-1/PD-L1 sensitivity dependent on TCR:pMHC affinity on T-cells. There, the authors found that subtle changes in TCR:pMHC affinity directly influence the inducibility and PD-1 sensitivity of genes during T cell activation, and that PD-1 preferentially inhibits the activation of low-affinity T cells[300].

Another aspect worthy of future exploration is the potential role of PD-1 within the context of cell avidity, which is the total intercellular force between multiple parallel interactions. Recent research highlights the significance of CAR-T cell avidity as a robust predictor of *in vivo* efficacy. Notably, studies by Mark B. Leick and colleagues at Harvard University have unveiled a correlation between different CAR-T cell avidity variants and their efficacy in tumour eradication *in vivo*[301]. Avidity outperformed traditional *in vitro* assessments of cytotoxicity and cytokine secretion in predicting *in vivo* results. Furthermore, investigations by Lydia Lee et al. have demonstrated the clinical relevance of cell avidity by elucidating underlying factors contributing to suboptimal outcomes

observed with the APRIL CAR in a phase I clinical trial for multiple myeloma, emphasizing the utility of cell avidity assessments in predicting CAR-T cell therapeutic outcomes in patients[302]. Interestingly, the level of PD-1 expression is linked to the strength of TCR signalling, and thus to the functional avidity of specific T cells[303]. In line with this, Ramona Schlenker et al. reported that engineering of low-avidity T cells recognizing a naturally processed and presented TAA with a chimeric PD-1:28 receptor increases effector function to levels seen with high-avidity T cells of identical specificity[304]. Therefore, avidity should be considered in future studies as a factor beyond affinity that could influence the effect of the PD-1/PD-L1 axis on CAR-T cell activity.

A more in-depth approach involving gene expression and single-cell polyfunctionality analyses of CAR-T cells after exposure to tumour cells expressing HER2 and physiological PD-L1 levels revealed that PD-1 KO induced a wider change in the LA HER2-28ζ CAR-T cell population than in HA HER2-28ζ CAR-T cells, which remained similar to mock-electroporated CAR-T cells in terms of gene expression. Most of the genes found upregulated in LA HER2-28ζ PD-1 KO CAR-T cells encoded cytokine-related factors, closely aligning with findings from a recent study by Shimizu et al using murine T lymphoma cells that recognize pMOG35–55/I-Ab with different affinities[305]. This study evidenced that genes associated with survival and proliferation exhibited greater resistance to PD-1-mediated inhibition upon TCR activation. In contrast, genes responsible for encoding cytokines and effector molecules, such as IFN-γ and IL-2, demonstrated heightened sensitivity to PD-1-mediated inhibition leading to a decreased efficiency in expression. This sensitivity appeared to be influenced by factors such as transcription factor (TF) binding motifs and CpG frequency within the promoter region. Genes showing more sensitivity to PD-1 inhibition harboured more binding sites of TFs such as RARγ, IRF1 and RARα, while those less affected by PD-1 signalling were enriched in NRF1, ATF1 or ERG1 motifs. Moreover, they observed that PD-1-sensitive genes displayed low CpG promoters, typical of genes related to differentiation that show spatiotemporally regulation expression, suggesting that genes mediating effector T cell functions might be more affected. The observations of this report are also supported by our findings at the protein level, with LA HER2-28ζ CAR-T cells having

increased cytokine secretion and polyfunctionality as a result of PD-1 KO. Not only this, but we also observed differences among cytokine functional categories, with effector cytokines being the most strongly upregulated by PD-1 disruption. Furthermore, in the article by Shimizu and colleagues it was hypothesized that T-cell clones exhibiting higher affinity to antigens might display increased resistance to PD-1 inhibition, as gene induction could take place at lower antigen levels. Notably, our observations with high-affinity CAR-T cells are in line with this hypothesis[305].

In this work, we emphasize CAR affinity as a central factor influencing sensitivity to PD-1/PD-L1 axis. Beyond this, we also explored the implications of both target antigen densities and CAR expression frequencies. Intriguingly, we observed that the enhanced resistance of HA CAR-T cells to PD-L1 was attenuated in the presence of low levels of CAR antigen. Conversely, the use of products with higher CAR frequencies appeared to mitigate the sensitivity of LA CAR-T cells to PD-L1-mediated suppression. These findings led us to postulate that inhibitory effects of PD-L1 on T cells can be overcome when T cell activation reaches a certain threshold. According to our results, this threshold of activation can be attainable not only through the utilization of a high affinity CAR but also by the presence of high CAR frequencies. However, in principle this latter strategy lacks the feasibility of being translated into the clinical setting due to the potential risk of genotoxicity, given the higher amounts of vector required. Moreover, the use of CAR-T cell products with high CAR expression can result in tonic signalling and has been correlated to worse clinical responses due to accelerated T cell exhaustion, both in preclinical studies[86] and clinical trials[306,307]. Interestingly, in apparent contradiction, one of the most successful CAR-T trials in solid tumours to date in term of response rates utilized products with >70% CAR transduction, potentially contributing to the success[158,214]. Despite the use of a third generation low-affinity CAR expressed from a retroviral vector makes it difficult to draw firm conclusions, this could be in line with our results showing that high CAR frequencies render LA CAR-T cells more insensitive to PD-1-mediated inhibition. Overall, our results highlight the complexity of CAR-T cell activity regulation, involving numerous interplaying factors from both target cells and therapeutic T cells themselves.

To achieve optimal T-cell activation, the formation of a productive IS is crucial. The predominant mediators in CAR-T cell IS formation are the CD3 complex, TCR or CAR interactions, CD28, LFA-1, PD-1, and adhesion molecules – ICAM-1 and VCAM-1 on tumour cells and CD2 and CD58 on T-cells[308]–. Recently, it has been described that the TCR localizes within micro-clusters within the IS along with PD-1, suggesting that positioning of molecules is also key for a functional IS. In line with this, there is proof that anti-PD-1 antibodies activate T cells by removing PD-1 away from the synapse, so changing the location of PD-1 or other immune receptors within the synapse could serve as an alternative approach to treat cancer[309]. Although not within the scope of this project, delving into the exploration of IS formed by HA and LA CARs both with and without PD-1 might provide valuable insights as it could also be involved in modulating the different sensitivities observed in PD-1/PD-L1-mediated inhibition. One of the essential molecules for IS formation, ICAM-1, has been shown to be instrumental for CAR-T cell effector function[310,311], and its upregulation has also been implicated in resistance to PD-1/PD-L1 pathway[312] , all in an IFN-γ-dependent manner. One could hypothesize that as HA CAR-T cells release higher levels of IFN-γ upon co-culture with tumour cells as compared to LA CAR-T cells, they can induce increased upregulation of ICAM-1 and therefore, increased resistance to PD-L1. Recently, another adhesion molecule, CD56, has been reported to play a role in CAR-T cell effectiveness in triple inhibitory receptor-resistant CAR-T cells (including TIM-3, LAG-3 and PD-1 knockdown)[313]. Considering these works, we cannot rule out the potential implication of alternative adhesion molecules in the resistance to PD-L1-mediated inhibition of HA CAR-T cells.

Moreover, the role of IFN-γ in the responses of CAR-T cells is complex and somewhat controversial[314] due to its diverse effects on the TME and T-cell function. IFN-γ has well-documented anti-tumour effects, including the promotion of tumour cell apoptosis[315] and inhibition of tumour cell proliferation. In addition, it can also stimulate stromal cells within the TME, such as fibroblasts and endothelial cells, leading to the production of chemokines and cytokines that recruit and activate immune cells[316]. On the other hand, it can also induce the expression of immunosuppressive molecules (like PD-L1 and PD-L2)[317], and chronic exposure to IFN-γ within the TME can induce further adaptive

resistance mechanisms, such as downregulation of antigen expression or alteration in antigen presentation machinery[318]. Regarding this, there is a recent publication showing that CAR-T cell killing requires the IFNγR pathway in solid but not liquid tumours, outlining an important mechanism of cell-intrinsic resistance to CAR-T cell cytotoxicity unique to solid tumours[311]. Despite this, and the fact that they generally lack a clearly defined immunosuppressive TME, the PD-1/PD-L1 axis still plays a role in haematological malignancies[319], so it would be interesting to assess the reproducibility of our findings in these cancers. In summary, understanding the complex interplay between IFN-γ signalling, the PD-1/PD-L1 axis, the TME and CAR-T cell responses is crucial for optimizing the efficacy of CAR-T cell therapy.

Another factor that may influence the different outcomes observed in PD-1 KO studies between pre-clinical and clinical trials is the differentiation stage of CAR-T cells used, which tend to be more naïve in preclinical studies compared to those derived from patients enrolled in clinical trials[76]. PD-1 has varying effects at different stages of T-cell differentiation, suggesting that its disruption could affect CAR-T cell responses differently depending on T-cell phenotypes [31,320]. Therefore, patient-derived CAR-T cells may exhibit different sensitivities to the PD-1/PD-L1 axis compared to CAR-T cells expanded from healthy donors.

PD-1 is a central regulator of CD8+ T cell exhaustion[34]. Concerns regarding accelerated T-cell exhaustion following PD-1 ablation have been raised in previous studies, both in the context of CAR-T cells for cancer treatment[248,249] and of virus-specific T cells in chronic infections[34]. Nevertheless, our gene expression analysis did not reveal a more exhausted phenotype of LA PD-1 KO CAR-T cells but rather the opposite. In fact, PD-1 KO CAR-T cells presented hallmarks of less exhausted T cells as compared to mock CAR-T cells. In this regard, we found that 11 out of 20 genes that were downregulated in PD-1 KO LA CAR-T cells were involved in the type I and II IFN signalling pathways, including IRF7, which is the main transcription factor regulating type I IFN pathway. Although IRF7 induction can potentiate CAR-T cell activation and induce antitumour activity[321], in certain contexts, type I IFN signalling can also orchestrate T cell immunosuppression[322,323] and induce apoptosis on CAR-T cells[324]. Recent papers identified chronic type I IFN signalling regulated by IRF7 to potentiate CAR-T cell

dysfunction[274] and to be predictive of poor CAR-T cell persistence in paediatric ALL patients[277]. Additionally, LA HER2-28ζ PD-1 KO CAR-T cells in our experiments expressed higher levels of *FOSB*, a transcription factor that is decreased in exhausted T cells in chronic viral infection[271], while increased in CAR-T cell products from responding patients as compared to non-responders[272]. However, it is important to note that our gene expression data was obtained after a single antigen stimulation *in vitro*, and further exploration of what would happen in the context of chronic antigen exposure might be required.

An additional source of current variability in the literature could come from the CAR construct used to generate therapeutic T cells. Importantly, CAR-T cells with different costimulatory domains (such as CD28, 4-1BB or ICOS) exhibit differential activity, phenotype and PD-1 expression[325]. Nevertheless, it is still unknown whether CARs containing different costimulatory domains are equally sensitive to PD-1 inhibition. Our study mainly focuses on knocking PD-1 out of 28ζ CAR-T cells, primarily due to their augmented expression of PD-1, enhanced cytotoxicity, and their low persistence[100,321]. However, we additionally performed a comparative analysis between CAR-T cells incorporating either ICOS or 4-1BB as a co-stimulatory domain. By using our preclinical model, we also observed that PD-1 KO does not increase the antitumor efficacy of LA CARs co-stimulated with 4-1BB, contrary to CARs featuring CD28 or ICOS as co-stimulatory domains. Our results are in line with previously published data[236,284] and might be partly attributed to the lower expression of PD-1 observed in 4-1BB co-stimulated CARs as compared to CD28 or ICOS.

Another factor potentially influencing the response to PD-1/PD-L1 inhibition is the structural similarity shared between PD-1, CD28, and ICOS. PD-1 consists of a single N-terminal IgV-like domain, an approximately 20 amino acid stalk separating the IgV domain from the plasma membrane, a transmembrane domain, and a cytoplasmic tail containing tyrosine-based signalling motifs. This structural arrangement, shared by CD28 and ICOS, implies potential functional similarities in their intracellular signalling pathways and interactions with downstream signalling molecules[26,326]. In fact, both CD28 and ICOS signal through the PI3K pathway, which is known to be inhibited by PD-

1 signalling [320,326,327]. Therefore, PD-1 blockade could potentially have a more significant impact on CD28 and ICOS-mediated signalling due to the relief of PI3K inhibition. Moreover, it is well-established that PD-1 activation by PD-L1 primarily suppresses T-cell function through the deactivation of CD28 signalling, further supporting a central role for co-stimulatory signalling pathways within the context of PD-1 therapy[284,326,327].4-1BB, on the other hand, primarily signals through the ERK pathway, which is not directly targeted by PD-1 inhibition [328]. As a result, PD-1 blockade may have less influence on 41BB-mediated signalling, leading to different sensitivities to PD-1 inhibition compared to CD28 and ICOS, although further experimental studies would be needed to elucidate underlying mechanisms and validate this hypothesis.

Considering the intrinsic differences between co-stimulatory domains, the selection of a specific one will depend on the distinct profiles of co-stimulatory and co-inhibitory ligand expressions within the tumour, as well as upon factors such as antigen expression level or density, the scFv's affinity for the tumour antigen, the proximity of the tumour epitope to the membrane, and other variations in construct design. For example, CD28-based CARs offer potent effector functions but limited cell expansion, potentially making them suitable for transient treatment of diseases requiring rapid tumour elimination and short-term CAR persistence. Conversely, 4-1BB-based CARs are better suited for diseases necessitating sustained T cell persistence to achieve complete responses[97,100,321].

Of note, it is relevant to highlight that even in the cases where PD-1 genetic deletion did not provide an advantage (i.e., HA and 4-1BB co-stimulated CAR-T cells), it never decreased CAR-T cell functionality in our hands. This observation offers the potential to repurpose the PD-1 locus as a site for targeted integration of transgenes such as IL-12 [329,330], capitalizing the kinetics of PD-1 expression after antigen encounter to restrict transgene expression to the TME while simultaneously disrupting PD-1.

Regarding affinity, in terms of clinical translation, the use of a HA CAR might be preferable as it exhibits greater efficacy and resistance to PD-L1-mediated inhibition without additional modifications. However, increased resistance to PD-L1 might, in the

context of HA CARs, come at the price of increased T-cell exhaustion and compromised safety by targeting shared antigens that can be expressed in healthy tissues.

Our gene expression data supports the notion of that HA CAR-T cells may be more prone to exhaustion, showing higher expression of the exhaustion-related transcription factor MAF, in contrast to the elevated expression of genes associated with a more naïve phenotype (*TCF7*, *LEF1* and *CD45RA*) by LA HER2-28ζ CAR-T cells. In the literature, a recent study demonstrated less exhausted and apoptotic phenotype and greater persistence of CAR-T cells targeting GPC3 with low affinity as compared to their high affinity counterparts[258]. In the same line, a CAR targeting CD19 with lower affinity than commercial products demonstrated greater persistence in preclinical mouse models and patients in a clinical study[252]. Importantly, polyfunctionality of CAR-T cells had been previously correlated with improved clinical outcomes, and a recent report has shown increased polyfunctionality index in LA CAR-T cells compared to their HA counterparts[331,332]. Moreover, advantageous effects observed with low affinity, as opposed to the ones observed with high affinity versions, have also been documented for TCRs[333]. Regarding safety concerns, a serious event occurred in the context of HER2-targeting CAR therapy when the use of a HA CAR (based on the scFv 4D5, as employed in our study) led to a fatal outcome in a patient with colon cancer metastatic to the lungs and liver. This was attributed to the high doses of CAR-T cells administered and to the potential CAR-mediated recognition of low levels of HER2 on lung epithelial cells[218]. In accordance, our findings evidence a more favourable toxicity profile of LA as compared to HA HER2-28ζ CAR-T cells when exposed to a collection of healthy tissue-derived primary cells, which was not altered by PD-1 KO regardless of scFv affinity. This underscores the necessity for caution and thorough investigation when employing HA CARs, emphasizing their potential for unintended activation in the presence of healthy cells expressing lower levels of the target antigen. Nevertheless, HA CAR-T cells may offer a promising solution when administered directly to the tumour site, mitigating the risk of off-target toxicities on healthy tissue, while LA CAR-T cells with PD-1 blockade could be a good option in carcinogen-induced cancers, where PD-L1 tends to be highly expressed in the TME[334] or as a second dose alternative to be administered once the first dose of CAR-T cells has reached the tumour, released IFN-γ and upregulated PD-L1[201].

A promising approach that has been evaluated in clinical trials and could broaden HA CAR-T cell applicability is the incorporation of suicide/elimination switches to deplete the adoptively transferred cell product when deemed necessary[157]. Interestingly, in terms of clinical efficacy, an analysis of available data from solid tumour CAR-T trials correlating clinical responses to CAR affinity concluded that the use of CARs targeting their antigens with moderate affinity led to better clinical responses as compared to high affinity CARs[307]. In line with this, two recent studies in solid tumours have demonstrated efficacy levels comparable to CD19-targeted CAR-T cell trials in lymphoma patients. One study used claudin18.2-specific CAR-T cells[190], while the other investigated third generation GD2-targeted CAR-T cells[158]. Certain methodological disparities between these trials pose challenges in drawing definitive conclusions, and the factors contributing to their higher success rates remain uncertain and warrant further investigation; nevertheless, both trials share common characteristics, including the use of CAR constructs with moderate to low affinity—36 to 83nM for claudin18.2 and 77nM for GD2[307]. Additionally, tumours in both studies expressed moderate to high levels of the target antigen across the majority of tumour cells, supporting the use of low to moderate-affinity CAR-T cells in these clinical situations[214].

There are several approaches to inhibit the PD-1/PD-L1 axis, which include blocking antibodies, shRNA- or peptide-mediated downregulation, DNR expression and genetic disruption. In this study, we showed that targeting the PD-1/PD-L1 axis is beneficial in LA CAR-T cells. Specifically, we employed CRISPR/Cas9 to knockout *PDCD1* as a proof of concept to disrupt the PD-1/PD-L1 axis, and we additionally validated some of our findings using CAR-T cells combined with anti-PD-L1 antibodies (durvalumab). The CRISPR/Cas9 system is highly efficient, enables multiplex editing of the human genome simultaneously, ensures sustained PD-1 blockade and, importantly, has demonstrated safety in the clinics[286,335]. Furthermore, it also circumvents some of the limitations of systemic PD-1 blockade using antibodies, which relies on the presence of a robust preexisting immunity, a fact that can limit its effectiveness in patients lacking high-avidity T-cells[285]. Additionally, due to the pivotal role of PD-1 in maintaining peripheral immune tolerance, systemic blockade of PD-1 can lead to heightened T-cell activation and autoreactivity[336]. Autoreactive T-cells, which tend to have low affinity to antigen, can

be efficiently supressed by PD-1, so inhibiting the axis could contribute to the frequent development of IrAEs[305]. Moreover, systemic administration of anti-PD-1 antibodies has been associated with the resurgence of immunosuppressive T-cells within the TME. This phenomenon is associated to cancer hyperprogression, caused by the reinvigoration of immunosuppressive T_{regs}[337]. However, combining CAR-T cells with immune checkpoint antibodies offers other advantages over the permanent ablation of the PD-1 signalling; it offers a more precise and flexible dosing regimen, eliminates the need for further genetic modifications on T cells and has the potential of reinvigorating endogenous T cells and CAR-T cells[201,338]. In fact, combination of CAR-T cells with PD-1 blocking antibodies has been explored in clinical trials with promising results[201,339]. We also provide data showing the feasibility of CAR-T cell combination with PD-1/PD-L1 blockade antibodies, even though our preclinical model does not allow for direct comparison between genetic PD-1 disruption and antibody-mediated blockade, mainly due to the absence of a mature immune system. Despite that, our results emphasize the applicability of our findings to diverse PD-1 disruption approaches in the pursuit of enhanced CAR-T cell therapy. Furthermore, the use of CRISPR/Cas9 to knock *PDCD1* out surpasses shRNA-based knock-down strategies in scenarios of constant PD-L1 over-expression, as even minimal levels of PD-1 expression through knockdown methods still exert a sustained and considerable inhibitory effect[249]. However, there are concerns regarding PD-1's role as a haplo-insufficient tumour suppressor *in vivo*[340], suggesting that PD-1-defficient cells, including those in adoptively transferred T-cells, may have an increased risk of unwanted malignant transformation, especially when coupled with additional oncogenic mutations triggered by sustained receptor activation. Nevertheless, a pre-clinical study from Sarah Dötsch et al. did not observe any instances of T-cell derived malignancy following PD-1 ablation, even after a 390-day period[285]. These results align with previous observations in patients treated with PD-1 KO TCR-engineered T-cells, who also showed no signs of T-cell genotoxicity during the monitoring period[286,335].

Another big concern within the field revolves around the potential for PD-1 KO to compromise the persistence of T-cells, a phenomenon already observed in clinical trials involving CARs and TCR-transgenic T-cells[192,286]. In our study, the assessment of

long-term persistence of PD-1 KO CAR-T cells faces significant limitations due to the inadequacy of NSG mouse models for this purpose. However, the study from Sarah Dötsch et al. demonstrated that adoptively transferred TCR-transgenic and CD19-targeting PD-1 KO T-cells retain their ability to differentiate into highly functional effector and memory T-cell subsets, which support long-term immunity. Moreover, they also robustly tracked functional PD-1 KO CAR-T cells for more than one year in a syngeneic immunocompetent mouse model with continuous antigen exposure[285].

Hospital Clínic-IDIBAPS is a pioneer European centre on developing academic CAR-T products and bringing them to the clinics. In 2021, an anti-CD19 CAR-T therapy developed in-house, ARI0001, was approved for the treatment of patients with r/r CD19+ B-cell ALL after a minimum of two lines of treatment or post-transplant relapse in adult patients older than 25 by the Spanish Agency of Medicines and Medical Devices (AEMPS), becoming the first treatment with genetically modified cells and fully developed in Europe to be approved by a regulatory agency [261,341]. Remarkably, this therapy has also received a PRIME designation by the European Medicines Agency (EMA). In addition, an anti-BCMA CAR-T therapy also developed at our institution, ARI0002h, has demonstrated clinical responses comparable to those obtained with commercial CARs in treating multiple myeloma[342] (NCT04309981). Finally, a third product, ARI0003, a dual CAR-T cell product targeting CD19 and BCMA is next to be tested in a first-in-human phase I clinical trial in r/r B cell aggressive lymphoma patients (NCT06097455). This extensive and accredited experience in CAR-T therapy development for hematologic malignancies will undoubtedly be instrumental in translating CAR-T cell therapies for solid tumour patient treatment, as discussed in the present work, into clinical practice. In fact, we are planning to start a phase I clinical trial for the treatment of patients with HER2+ solid tumours with CAR-T cells targeting HER2. Based on results from a previous doctoral thesis from the laboratory, 4-1BB co-stimulated CAR-T cells exhibit higher persistence and enhanced killing capacities as compared to CARs comprising other co-stimulatory domains. In the present study, we further demonstrate that 4-1BB CARs display increased resistance to PD-1/PD-L1 inhibition. For these reasons, LA HER2-BBζ CAR-T cells were selected as the clinical

candidate, as it obviates the need for further genetic modifications (i.e. PD-1 KO) and has a safer profile as compared to the HA HER2 CAR.

In conclusion, our study highlights the impact of CAR affinity and their co-stimulatory domains on the sensitivity of CAR-T cells to T-cell inhibition mediated by the PD-1/PD-L1 axis. We have demonstrated that CAR-T cells with HA inherently resist PD-L1-mediated inhibition, while those with LA CARs are more susceptible to this suppression. Furthermore, this higher resistance to the axis also holds true for LA CAR-T cells with high CAR expression and LA CAR-T cells harbouring the 4-1BB co-stimulatory domain. Conversely, LA CAR-T cells utilizing the ICOS or CD28 co-stimulatory domains show sensitivity to PD-1/PD-L1-mediated immunosuppression (Fig. 5.1). In essence, these findings provide valuable insights into the design and optimization of CAR-T cells for enhanced effectiveness in the treatment of solid tumours, and particularly shed light on how to target the PD-1/PD-L1 axis more effectively in combination with the use of CAR-T cells as the field moves forward to clinical applications.

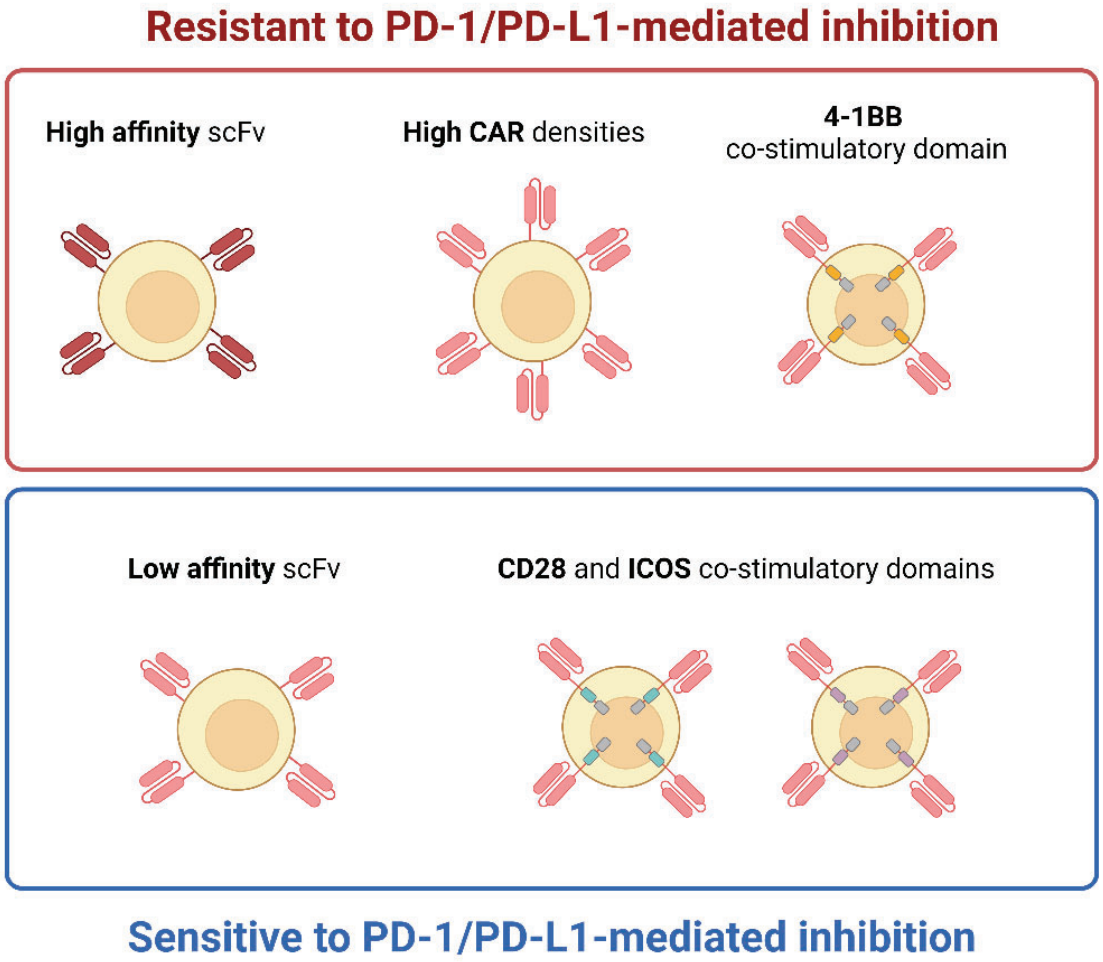

Figure 5.1 | Summary of identified responses to PD-1/PD-L1-mediated inhibition. In this work we found that CAR-T cells with HA scFvs (dark red), LA CAR-T cells with high CAR densities or LA CAR-T cells employing the 4-1BB co-stimulatory domain (orange) exhibited resistance to PD-1/PD-L1 axis inhibition. Conversely, CAR-T cells with LA scFvs (light red) and incorporating CD28 (turquoise) or ICOS (purple) co-stimulatory domains demonstrated sensitivity to the PD-1/PD-L1 axis. Abbreviations: CAR, chimeric antigen receptor; CD, cluster of differentiation; HA, high affinity; LA, low affinity; scFv, single chain fragment variable

Conclusions

6. Conclusions

1. Our cellular model with different PD-L1 expression levels is representative of the physiological range of PD-L1 densities observed across different tumour cell lines, both in vitro and in vivo.

2. PD-1 KO can be efficiently knocked-out from CAR-T cells using CRISPR-Cas9 without compromising their capacity to expand ex vivo.

3. In the presence of PD-L1, blocking the PD-1/PD-L1 axis enhances T cell effector functions, especially cytokine secretion, of LA-28ζ CAR-T cells with no discernible effect on HA HER2-28ζ CAR-T cells.

4. PD-1/PD-L1 inhibition restores in vivo antitumor effect of LA-28ζ CARs but does not impact HA-28ζ CAR-T cells in a context where PD-L1 is expressed.

5. Affinity-based differences to inhibition by PD-L1 are maintained in a lipid bilayer system functionalized with controlled amounts of PD-L1, HER2 and ICAM and in the absence of other potential inhibitors of CAR-T cell function.

6. PD-1 KO induces deeper changes in the transcriptome of LA as compared to HA HER2-28ζ CAR-T cells.

7. LA PD-1 KO CAR-T cells display a safer toxicity profile as compared to HA HER2-28ζ CAR-T cells, when exposed to a range of healthy tissue cells in vitro.

8. LA-28ζ CAR-T cells showing higher CAR expression levels exhibit greater resistance to PD-1/PD-L1-mediated inhibition compared to those with lower expression levels.

9. Low levels of the targeted antigen may increase the susceptibility of HA-28ζ CAR-T cells to inhibition via the PD-1/PD-L1 axis.

10. PD-1 KO improves the antitumour effect of LA HER2-specific CAR-T cells but not that of HA in ICOS-co-stimulated CARs, in line with results obtained with CD28-based CARs.

11. 4-1BB-based CARs are less sensitive to PD-1/PD-L1-mediated inhibition than CD28- or ICOS-based CARs.

12. Differences in PD-1/PD-L1-mediated inhibition between LA and HA CAR-T cells are maintained when using different scFvs targeting mesothelin and FRβ, suggesting that CAR affinity is an important factor modulating the sensitivity to PD-1/PD-L1 axis inhibition in CAR-T cell therapy.

References

7. References

1. Sung, H. et al.Global Cancer Statistics 2020: GLOBOCAN Estimates of Incidence and Mortality Worldwide for 36 Cancers in 185 Countries. *CA Cancer J Clin*. **71**, 209–249 (2021).
2. Hanahan, D. & Weinberg, R. A. The Hallmarks of Cancer. *Cell*. **100**, 57-70 (2000).
3. Hanahan, D. & Weinberg, R. A. Hallmarks of cancer: The next generation. *Cell*. **144**, 646–674 (2011).
4. Greten, F. R. & Grivennikov, S. I. Inflammation and Cancer: Triggers, Mechanisms, and Consequences. *Immunity*. **51**,27–41 (2019).
5. Grivennikov, S. I., Greten, F. R. & Karin, M. Immunity, Inflammation, and Cancer. *Cell*. **140**, 883–899 (2010).
6. Chen, D. S. & Mellman, I. Elements of cancer immunity and the cancer-immune set point. *Nature*. **541**,321–330 (2017).
7. Vinay, D. S. *et al*.Immune evasion in cancer: Mechanistic basis and therapeutic strategies. *Semin. Cancer Biol*. **35**,185–198 (2015).
8. Dunn, G. P., Old, L. J. & Schreiber, R. D. The three Es of cancer immunoediting. *Annu. Rev. Immunol*. **22**,329–360 (2004).
9. O'Donnell, J. S., Teng, M. W. L. & Smyth, M. J. Cancer immunoediting and resistance to T cell-based immunotherapy. *Nat. Rev. Clin. Oncol*. **16**,151–167 (2019).
10. Waldman, A. D., Fritz, J. M. & Lenardo, M. J. A guide to cancer immunotherapy: from T cell basic science to clinical practice. *Nat. Rev. Immunol*. **20**,651–668 (2020).
11. Chen, D. S. & Mellman, I. Oncology meets immunology: The cancer-immunity cycle. *Immunity*. **39**,1–10 (2013).

12. Korman, A. J., Garrett-Thomson, S. C. & Lonberg, N. The foundations of immune checkpoint blockade and the ipilimumab approval decennial. *Nat. Rev. Drug Discov*. **21**, 509–528 (2022).

13. Pardoll, D. M. The blockade of immune checkpoints in cancer immunotherapy. *Nature Reviews Cancer*. **12**, 252–264 (2012).

14. Topalian, S. L., Drake, C. G. & Pardoll, D. M. Immune checkpoint blockade: A common denominator approach to cancer therapy. *Cancer Cell*. **27**,450–461 (2015).

15. Ribas, A. & Wolchok, J. D. Cancer immunotherapy using checkpoint blockade. *Science* **359**,1350-1355(2018).

16. Wei, S. C., Duffy, C. R. & Allison, J. P. Fundamental mechanisms of immune checkpoint blockade therapy. *Cancer Discov* **8**,1069–1086 (2018).

17. Beaver Julia A. & Pazdur Richard. The Wild West of Checkpoint Inhibitor Development. *N. Engl. J. Med*. **386**, 1295–1297 (2022).

18. Beltra, J. C. *et al*. Developmental Relationships of Four Exhausted CD8+ T Cell Subsets Reveals Underlying Transcriptional and Epigenetic Landscape Control Mechanisms. *Immunity* **52**, 825-841.e8 (2020).

19. Ribas, A. Tumor Immunotherapy Directed at PD-1. *N. Engl. J. Med*. **366**, 2517–2519 (2012).

20. Kennedy, A. *et al*. Differences in CD80 and CD86 transendocytosis reveal CD86 as a key target for CTLA-4 immune regulation. *Nat Immunol* **23**, 1365–1378 (2022).

21. Sharma, P. & Allison, J. P. Immune checkpoint targeting in cancer therapy: Toward combination strategies with curative potential. *Cell* **161**,205–214 (2015).

22. Hodi, F. S. *et al*. Improved Survival with Ipilimumab in Patients with Metastatic Melanoma. *N. Engl. J. Med*. **363**, 711–723 (2010).

23. Perets, R. *et al*. Safety and efficacy of quavonlimab, a novel anti-CTLA-4 antibody (MK-1308), in combination with pembrolizumab in first-line advanced non-small-cell lung cancer. *Ann Oncol* **32**, 395–403 (2021).

24. Ishida, Y., Agata, Y., Shibahara, K. & Honjo, T. Induced expression of PD-1, a novel member of the immunoglobulin gene superfamily, upon programmed cell death. *EMBO J* **11**, 3887–3895 (1992).

25. Sharpe, A. H. & Pauken, K. E. The diverse functions of the PD1 inhibitory pathway. *Nat Rev Immunol* **18**, 153–167 (2018).

26. Patsoukis, N., Wang, Q., Strauss, L. & Boussiotis, V. A. *Revisiting the PD-1 Pathway*. *Sci. Adv*. **6**, eabd2712 (2020).

27. Paillon, N. *et al.*PD-1 inhibits T cell actin remodeling at the immunological synapse independently of its signaling motifs.*Sci. Signal.***16**, eadh2456(2023).

28. Sharpe, A. H. & Pauken, K. E. The diverse functions of the PD1 inhibitory pathway. *Nat Rev Immunol* **18**,153–167 (2018).

29. Sage, P. T. & Sharpe, A. H. T follicular regulatory cells. *Immunol Rev* **271**, 246–259 (2016).

30. Shi, J. *et al*. PD-1 Controls Follicular T Helper Cell Positioning and Function. *Immunity* **49**, 264-274.e4 (2018).

31. Ahn, E. *et al*. Role of PD-1 during effector CD8 T cell differentiation. *Proc Natl Acad Sci U S A* **115**, 4749–4754 (2018).

32. Amezquita, R. A. & Kaech, S. M. Immunology: The chronicles of T-cell exhaustion. *Nature* **543**, 190–191 (2017).

33. Wherry, E. J. & Kurachi, M. Molecular and cellular insights into T cell exhaustion. *Nat Rev Immunol* **15**, 486–499 (2015).

34. Odorizzi, P. M., Pauken, K. E., Paley, M. A., Sharpe, A. & Wherry, E. J. Genetic absence of PD-1 promotes accumulation of terminally differentiated exhausted CD8 + T cells . *J Exp Med* **212**, 1125–1137 (2015).

35. Abiko, K. *et al*. IFN-γ from lymphocytes induces PD-L1 expression and promotes progression of ovarian cancer. *Br J Cancer* **112**, 1501–1509 (2015).

36. Chen, S. *et al*. Mechanisms regulating PD-L1 expression on tumor and immune cells. *J Immunother Cancer* **7**, (2019).

37. Topalian, S. L. *et al*. Safety, Activity, and Immune Correlates of Anti–PD-1 Antibody in Cancer. *N. Engl. J. Med*. **366**, 2443–2454 (2012).

38. Brahmer, J. R. *et al*. Safety and Activity of Anti–PD-L1 Antibody in Patients with Advanced Cancer. *N. Engl. J. Med*. **366**, 2455–2465 (2012).

39. Reck, M. *et al*. Pembrolizumab versus Chemotherapy for PD-L1–Positive Non–Small-Cell Lung Cancer. *N. Engl. J. Med*. **375**, 1823–1833 (2016).

40. Kumagai, S. *et al*. The PD-1 expression balance between effector and regulatory T cells predicts the clinical efficacy of PD-1 blockade therapies. *Nat Immunol* **21**, 1346–1358 (2020).

41. Yin, Z. *et al*.Mechanisms underlying low-clinical responses to PD-1/PD-L1 blocking antibodies in immunotherapy of cancer: A key role of exosomal PD-L1. *J. Immunother. Cancer* **9**, e001698 (2021).

42. Baulu, E., Gardet, C., Chuvin, N. & Depil, S. TCR-Engineered T Cell Therapy in Solid Tumors: State of the Art and Perspectives. *Sci. Adv.* **9**, eadf3700 (2023).

43. Rosenberg, S. A., Restifo, N. P., Yang, J. C., Morgan, R. A. & Dudley, M. E. Adoptive cell transfer: A clinical path to effective cancer immunotherapy. *Nat Rev Cancer* **8**, 299–308 (2008).

44. Lafreniere, R., Rosenberg S. A. Adoptive immunotherapy of murine hepatic metastases with lymphokine activated killer (LAK) cells and recombinant interleukin 2 (RIL 2) can mediate the regression of both immunogenic and nonimmunogenic sarcomas and an adenocarcinoma. *J Immunol*.**135**(6), 4273–4280(1985).

45. Cameron, R. B., Spiess, P. J. & Rosenberg, S. A. Synergistic antitumor activity of tumor infiltrating lymphocytes, Interleukin 2 and local tumor irradiation. Studies on the mechanism of action. *J. Exp. Med.* **171**, 249-263(1990).

46. Rosenberg, S. A. & Restifo, N. P. Adoptive Cell Transfer as Personalized Immunotherapy for Human Cancer. *Science* **348**, 62-68(2015).

47. Guedan, S., Ruella, M. & June, C. H. Emerging Cellular Therapies for Cancer. *Annu Rev Immunol* **37**, 145–171 (2018).

48. Tran, E. *et al.* Cancer Immunotherapy Based on Mutation-Specific CD4+ T Cells in a Patient with Epithelial Cancer. *Science (1979)* **344**, 641–645 (2014).

49. Gros, A. *et al.* PD-1 identifies the patient-specific CD8+ tumor-reactive repertoire infiltrating human tumors. *J. Clin. Invest.* **124**, 2246–2259 (2014).

50. Parkhurst, M. *et al.* Isolation of T-cell receptors specifically reactive with mutated tumor-associated antigens from tumor-infiltrating lymphocytes based on CD137 expression. *Clin Cancer Res* **23**, 2491–2505 (2017).

51. Gros, A. *et al.* Prospective identification of neoantigen-specific lymphocytes in the peripheral blood of melanoma patients. *Nat Med* **22**, 433–438 (2016).

52. Tarhini, A. A. *et al.* Immune monitoring of the circulation and the tumor microenvironment in patients with regionally advanced melanoma receiving neoadjuvant ipilimumab. *PLoS One* **9**, (2014).

53. Sarnaik, A. A. et al. Lifileucel, a Tumor-Infiltrating Lymphocyte Therapy, in Metastatic Melanoma. *J Clin Oncol* **39**, 2656-2666 (2021).

54. Klebanoff, C. A., Chandran, S. S., Baker, B. M., Quezada, S. A. & Ribas, A. T cell receptor therapeutics: immunological targeting of the intracellular cancer proteome. *Nat Rev Drug Discov* **22**, 996–1017 (2023).

55. Blüthmann, H. *et al.*T-cell-specific deletion of T-cell receptor transgenes allow functional rearrangement of endogenous α and β-genes. *Nature* **334**, 156–159 (1988).

56. Holler, P. D., Chlewicki, L. K. & Kranz, D. M. TCRs with high affinity for foreign pMHC show self-reactivity. *Nat Immunol.* **4**, 55–62 (2003).

57. Holler, P. D. *et al. In Vitro* Evolution of a T cell receptor with high affinity for peptide/MHC. *Proc.Natl.Acad.Sci. USA*. **97**(10), 5387-5392 (2000).

58. Rosenberg, S. A. & Dudley, M. E. Cancer Regression in Patients with Metastatic Melanoma after the Transfer of Autologous Antitumor Lymphocytes. *Proc.Natl.Acad.Sci. USA.***101**, 14639-14645 (2004).

59. Robbins, P. F. *et al*. Tumor regression in patients with metastatic synovial cell sarcoma and melanoma using genetically engineered lymphocytes reactive with NY-ESO-1. *J Clin Oncol* **29**, 917–924 (2011).

60. Linette, G. P. *et al*. Cardiovascular toxicity and titin cross-reactivity of affinity-enhanced T cells in myeloma and melanoma. *Blood* **122**(6), 863-871(2013).

61. Morgan, R. A. *et al*. Cancer Regression and Neurological Toxicity Following Anti-MAGE-A3 TCR Gene Therapy. *J. Immunother.* **36**(2), 33-151 (2013).

62. Nathan, P. *et al*. Overall Survival Benefit with Tebentafusp in Metastatic Uveal Melanoma. *N. Engl. J. Med*. **385**, 1196–1206 (2021).

63. Hassel, J. C. *et al*. Three-Year Overall Survival with Tebentafusp in Metastatic Uveal Melanoma. *N. Engl. J. Med*. **389**, 2256–2266 (2023).

64. Gettinger, S. *et al*. Impaired HLA class I antigen processing and presentation as a mechanism of acquired resistance to immune checkpoint inhibitors in lung cancer. *Cancer Discov* **7**, 1420–1435 (2017).

65. Berrien-Elliott, M. M., Jacobs, M. T. & Fehniger, T. A. Allogeneic Natural Killer Cell Therapy. *Blood* **141** (8), 856-868 (2023).

66. Liu, E. *et al*. Use of CAR-Transduced Natural Killer Cells in CD19-Positive Lymphoid Tumors. *N. Engl. J. Med*. **382**, 545–553 (2020).

67. Klichinsky, M. *et al*. Human chimeric antigen receptor macrophages for cancer immunotherapy. *Nat Biotechnol* **38**, 947–953 (2020).

68. Qin, V. M., D'souza, C., Neeson, P. J. & Zhu, J. J. Chimeric antigen receptor beyond CAR-T cells. *Cancers* **13**,1–16 (2021).

69. June, C. H. & Sadelain, M. Chimeric Antigen Receptor Therapy. *N. Engl. J. Med. Rev.* **379**, 64–73 (2018).

70. Munshi, N. C. *et al*. Idecabtagene Vicleucel in Relapsed and Refractory Multiple Myeloma. *N. Engl. J. Med*. **384**, 705–716 (2021).

71. Labanieh, L. & Mackall, C. L. CAR immune cells: design principles, resistance and the next generation. *Nature* **614**, 635–648 (2023).

72. Eshhar, Z., Waks, T., Grosst, G. & Schindler, D. G. Specific Activation and Targeting of Cytotoxic Lymphocytes through Chimeric Single Chains Consisting of Antibody-Binding Domains and the y or C Subunits of the Immunoglobulin and T-Cell Receptors. *Proc.Natl.Acad.Sci.U S A*. **90**(2),720-724(1993).

73. June, C. H. & Sadelain, M. Chimeric Antigen Receptor Therapy. *N. Engl. J. Med. Rev.* **379**, 64–73 (2018).

74. June, C. H., O'Connor, R. S., Kawalekar, O. U., Ghassemi, S. & Milone, M. C. CAR T cell immunotherapy for human cancer. *Science* **359**, 1361–1365 (2018).

75. Sadelain, M., Brentjens, R. & Rivière, I. The basic principles of chimeric antigen receptor design. *Cancer Discov* **3**,388–398 (2013).

76. Salas-Benito, D., Berger, T. R. & Maus, M. V. Stalled CARs: Mechanisms of Resistance to CAR T Cell Therapies. *Annu.Rev. Can. Bio.***7** (1), 23-42(2023).

77. Guedan, S., Calderon, H., Posey, A. D. & Maus, M. V. Engineering and Design of Chimeric Antigen Receptors. *Mol Ther Methods Clin Dev* **12**, 145–156 (2019).

78. Rafiq, S., Hackett, C. S. & Brentjens, R. J. Engineering strategies to overcome the current roadblocks in CAR T cell therapy. *Nat. Rev. Clin. Oncol.* **17**,147–167 (2020).

79. Poorebrahim, M. *et al.* TCR-like CARs and TCR-CARs targeting neoepitopes: an emerging potential. *Cancer Gene Ther* **28**, 581–589 (2021).

80. Han, L. *et al.* Single VHH-directed BCMA CAR-T cells cause remission of relapsed/refractory multiple myeloma. *Leukemia* **35**, 3002–3006 (2021).

81. Drent, E. *et al.* A Rational Strategy for Reducing On-Target Off-Tumor Effects of CD38-Chimeric Antigen Receptors by Affinity Optimization. *Mol Ther* **25**, 1946–1958 (2017).

82. Sarén, T. *et al.* Complementarity-determining region clustering may cause CAR-T cell dysfunction. *Nat Commun* **14** (2023).

83. Gomes-Silva, D. *et al.* Tonic 4-1BB Costimulation in Chimeric Antigen Receptors Impedes T Cell Survival and Is Vector-Dependent. *Cell Rep* **21**, 17–26 (2017).

84. Calderon, H., Mamonkin, M. & Guedan, S. Analysis of CAR-Mediated Tonic Signaling. *Methods in Mol Biol* **2085**, 223–236 (2020).

85. Long, A. H. *et al.* 4-1BB costimulation ameliorates T cell exhaustion induced by tonic signaling of chimeric antigen receptors. *Nat Med* **21**, 581–590 (2015).

86. Chen, J. *et al.* Tuning charge density of chimeric antigen receptor optimizes tonic signaling and CAR-T cell fitness. *Cell Res* **33**, 341–354 (2023).

87. Hammill, J. A. *et al.* Designed ankyrin repeat proteins are effective targeting elements for chimeric antigen receptors. *J Immunother Cancer* **3**, (2015).

88. Brown, C. E. *et al.* Bioactivity and safety of IL13Rα2-redirected chimeric antigen receptor CD8+ T cells in patients with recurrent glioblastoma. *Clin Cancer Res* **21**, 4062–4072 (2015).

89. Shaffer, D. R. *et al.* T cells redirected against CD70 for the immunotherapy of CD70-positive malignancies. *Blood* **117**, 4304–4314 (2011).

90. Bajor, M. *et al.* PD-L1 CAR effector cells induce self-amplifying cytotoxic effects against target cells. *J Immunother Cancer* **10**, (2022).

91. Sterner, R. C. & Sterner, R. M. CAR-T cell therapy: current limitations and potential strategies. *Blood Cancer J* **11**, (2021).

92. Mazinani, M. & Rahbarizadeh, F. CAR-T cell potency: from structural elements to vector backbone components. *Biomark Res* **10** (2022).

93. Brocker, T. & Karjalainen, K. Signals through T Cell Receptor ζ Chain Alone Are Insufficient to Prime Resting T Lymphocytes. *J. Exp. Med.***181**, 1653–1659 (1995).

94. Savoldo, B. *et al.* CD28 costimulation improves expansion and persistence of chimeric antigen receptor-modified T cells in lymphoma patients. *J. Clin. Invest.***121**, 1822–1826 (2011).

95. Imai, C. *et al.* Chimeric receptors with 4-1BB signaling capacity provoke potent cytotoxicity against acute lymphoblastic leukemia. *Leukemia* **18**, 676–684 (2004).

96. Quintarelli, C. *et al.* Choice of costimulatory domains and of cytokines determines CAR T-cell activity in neuroblastoma. *Oncoimmunology* **7**, (2018).

97. Cappell, K. M. & Kochenderfer, J. N. A comparison of chimeric antigen receptors containing CD28 versus 4-1BB costimulatory domains. *Nat. Rev. Clin. Oncol.* **18**, 715–727 (2021).

98. Li, G. *et al.* 4-1BB enhancement of CAR T function requires NF-κB and TRAFs. *JCI Insight* **3** (18), e121322 (2018).

99. Philipson, B. I. *et al.* 4-1BB Costimulation Promotes CAR T Cell Survival through Noncanonical NF-KB Signaling. *Sci. Signal.***13**, eaay8248(2020).

100. Kawalekar, O. U. *et al.* Distinct Signaling of Coreceptors Regulates Specific Metabolism Pathways and Impacts Memory Development in CAR T Cells. *Immunity* **44**, 380–390 (2016).

101. Song, D. G. *et al.* CD27 costimulation augments the survival and antitumor activity of redirected human T cells in vivo. *Blood* **119**, 696–706 (2012).

102. Guedan, S. *et al.* Enhancing CAR T cell persistence through ICOS and 4-1BB costimulation. *JCI Insight* **3**, e96976 (2018).

103. Good, Z. *et al.* Post-infusion CAR TReg cells identify patients resistant to CD19-CAR therapy. *Nat Med* **28**, 1860–1871 (2022).

104. Boroughs, A. C. *et al.* Chimeric antigen receptor costimulation domains modulate human regulatory T cell function. *JCI Insight* **4**, (2019).

105. Tokarew, N., Ogonek, J., Endres, S., von Bergwelt-Baildon, M. & Kobold, S. Teaching an old dog new tricks: next-generation CAR T cells. *Br J Cancer* **120**, 26–37 (2019).

106. Koneru, M., O'Cearbhaill, R., Pendharkar, S., Spriggs, D. R. & Brentjens, R. J. A phase I clinical trial of adoptive T cell therapy using IL-12 secreting MUC-16ecto directed chimeric antigen receptors for recurrent ovarian cancer. *J Transl Med* **13**, (2015).

107. Jaspers, J. E. *et al.* IL-18-secreting CAR T cells targeting DLL3 are highly effective in small cell lung cancer models. *J. Clin. Invest.***133**, e166028 (2023).

108. Li, X., Daniyan, A. F., Lopez, A. V, Purdon, T. J. & Brentjens, R. J. Cytokine IL-36γ improves CAR T-cell functionality and induces endogenous antitumor response. *Leukemia* **35**, 506–521 (2021).

109. Adachi, K. *et al*. IL-7 and CCL19 expression in CAR-T cells improves immune cell infiltration and CAR-T cell survival in the tumor. *Nat Biotechnol* **36**, 346–351 (2018).

110. Ma, X. *et al*. Interleukin-23 engineering improves CAR T cell function in solid tumors. *Nat Biotechnol* **38**, 448–459 (2020).

111. Avanzi, M. P. *et al*. Engineered Tumor-Targeted T Cells Mediate Enhanced Anti-Tumor Efficacy Both Directly and through Activation of the Endogenous Immune System. *Cell Rep* **23**, 2130–2141 (2018).

112. Xie, Y. J. *et al*. Improved antitumor efficacy of chimeric antigen receptor T cells that secrete single-domain antibody fragments. *Cancer Immunol Res* **8**, 518–529 (2020).

113. Li, D. *et al*. Camel nanobody-based B7-H3 CAR-T cells show high efficacy against large solid tumours. *Nat Commun* **14**, (2023).

114. Kagoya, Y. *et al*. A novel chimeric antigen receptor containing a JAK-STAT signaling domain mediates superior antitumor effects. *Nat Med* **24**, 352–359 (2018).

115. Sadelain, M. CAR therapy: The CD19 paradigm. *J. Clin. Invest.* **125**,3392–3400 (2015).

116. Hammer, O. CD19 as an attractive target for antibody-based therapy. *mAbs* **4**,571–577 (2012).

117. Kochenderfer, J. N. *et al*. Eradication of B-lineage cells and regression of lymphoma in a patient treated with autologous T cells genetically engineered to recognize CD19. *Blood* **116**, 4099–4102 (2010).

118. Brentjens, R. J. *et al*. Safety and persistence of adoptively transferred autologous CD19-targeted T cells in patients with relapsed or chemotherapy refractory B-cell leukemias. *Blood* **118**, 4817–4828 (2011).

119. Porter, D. L., Levine, B. L., Kalos, M., Bagg, A. & June, C. H. Chimeric Antigen Receptor–Modified T Cells in Chronic Lymphoid Leukemia. *N. Engl. J. Med.* **365**, 725–733 (2011).

120. Grupp, S. A. *et al.* Chimeric Antigen Receptor–Modified T Cells for Acute Lymphoid Leukemia. *N. Engl. J. Med.* **368**, 1509–1518 (2013).

121. Lee, D. W. *et al.* T cells expressing CD19 chimeric antigen receptors for acute lymphoblastic leukaemia in children and young adults: A phase 1 dose-escalation trial. *The Lancet* **385**, 517–528 (2015).

122. Maude, S. L. *et al.* Chimeric Antigen Receptor T Cells for Sustained Remissions in Leukemia. *N. Engl. J. Med.* **371**, 1507–1517 (2014).

123. Maude, S. L. *et al.* Tisagenlecleucel in Children and Young Adults with B-Cell Lymphoblastic Leukemia. *N. Engl. J. Med.* **378**, 439–448 (2018).

124. Schuster, S. J. *et al.* Tisagenlecleucel in Adult Relapsed or Refractory Diffuse Large B-Cell Lymphoma. *N. Engl. J. Med.* **380**, 45–56 (2019).

125. Neelapu, S. S. *et al.* Axicabtagene Ciloleucel CAR T-Cell Therapy in Refractory Large B-Cell Lymphoma. *N. Engl. J. Med.* **377**, 2531–2544 (2017).

126. Park, J. H. *et al.* Long-Term Follow-up of CD19 CAR Therapy in Acute Lymphoblastic Leukemia. *N. Engl. J. Med.* **378**, 449–459 (2018).

127. Shah, N. N. *et al.* Long-Term Follow-Up of CD19-CAR T-Cell Therapy in Children and Young Adults With B-ALL. *J Clin Oncol* **39**, 1650–1659 (2021).

128. Awasthi, R., Maier, H. J., Zhang, J. & Lim, S. Kymriah® (tisagenlecleucel)–An overview of the clinical development journey of the first approved CAR-T therapy. *Hum Vaccin Immunother* **19**, (2023).

129. Wang, M. *et al.* KTE-X19 CAR T-Cell Therapy in Relapsed or Refractory Mantle-Cell Lymphoma. *N. Engl. J. Med.* **382**, 1331–1342 (2020).

130. Shah, B. D. *et al.* KTE-X19 for relapsed or refractory adult B-cell acute lymphoblastic leukaemia: phase 2 results of the single-arm, open-label, multicentre ZUMA-3 study. *The Lancet* **398**, 491–502 (2021).

131. Abramson, J. S. *et al*. Lisocabtagene maraleucel for patients with relapsed or refractory large B-cell lymphomas (TRANSCEND NHL 001): a multicentre seamless design study. *The Lancet* **396**, 839–852 (2020).

132. Neelapu, S. S. *et al*. Three-Year Follow-up Analysis of Axicabtagene Ciloleucel in Relapsed/Refractory Indolent Non-Hodgkin Lymphoma (ZUMA-5). *Blood* **143** (6), 496-506 (2024).

133. Berdeja, J. G. *et al*. Ciltacabtagene autoleucel, a B-cell maturation antigen-directed chimeric antigen receptor T-cell therapy in patients with relapsed or refractory multiple myeloma (CARTITUDE-1): a phase 1b/2 open-label study. *The Lancet* **398**, 314–324 (2021).

134. Fowler, N. H. *et al*. Tisagenlecleucel in adult relapsed or refractory follicular lymphoma: the phase 2 ELARA trial. *Nat Med* **28**, 325–332 (2022).

135. Locke, F. L. *et al*. Axicabtagene Ciloleucel as Second-Line Therapy for Large B-Cell Lymphoma. *N. Engl. J. Med*. **386**, 640–654 (2022).

136. Abramson, J. S. *et al*. Lisocabtagene Maraleucel as Second-Line Therapy for Large B-Cell Lymphoma: Primary Analysis of the Phase 3 TRANSFORM Study. *Blood* **141** (14), 1675-1684 (2023).

137. Neelapu, S. S. *et al*. Axicabtagene ciloleucel as first-line therapy in high-risk large B-cell lymphoma: the phase 2 ZUMA-12 trial. *Nat Med* **28**, 735–742 (2022).

138. Shah, N. N. *et al*. CD4/CD8 T-Cell Selection Affects Chimeric Antigen Receptor (CAR) T-Cell Potency and Toxicity: Updated results from a phase I Anti-CD22 CAR T-Cell Trial. *J Clin Oncol* **38**(17),1938–1950 (2020).

139. Baird, J. H. *et al*.Brief Report CD22-Directed CAR T-Cell Therapy Induces Complete Remissions in CD19-Directed CAR-Refractory Large B-Cell Lymphoma. *Blood***137** (17), 2321-2325(2021).

140. Ramos, C. A. *et al*. Anti-CD30 CAR-T Cell Therapy in Relapsed and Refractory Hodgkin Lymphoma. *J Clin Oncol*. **38**(32), 3794-3804(2020).

141. Pan, J. *et al*. Donor-Derived CD7 Chimeric Antigen Receptor T Cells for T-Cell Acute Lymphoblastic Leukemia: First-in-Human, Phase I Trial. *J Clin Oncol*. **39**(30), 3340-3351(2021).

142. Zhang, M. *et al*. Autologous Nanobody-Derived Fratricide-Resistant CD7-CAR T-cell Therapy for Patients with Relapsed and Refractory T-cell Acute Lymphoblastic Leukemia/Lymphoma. *Clin Cancer Res* **28**, 2830–2843 (2022).

143. Cui, Q. *et al*. CD38-directed CAR-T cell therapy: a novel immunotherapy strategy for relapsed acute myeloid leukemia after allogeneic hematopoietic stem cell transplantation. *J Hematol Oncol*. **14**, 82 (2021).

144. Ramos, C. A. *et al*. Clinical responses with T lymphocytes targeting malignancy-associated κ light chains. *J. Clin. Invest*.**126**, 2588–2596 (2016).

145. Zhang, W. Y. *et al*. Long-term safety and efficacy of CART-20 cells in patients with refractory or relapsed b-cell non-hodgkin lymphoma: 5-years follow-up results of the phase I and IIa trials. *Sig Transduct Target Ther* **2**, 17054 (2017).

146. Cappell, K. M. & Kochenderfer, J. N. Long-term outcomes following CAR T cell therapy: what we know so far. *Nat Rev Clin Oncol* **20**,359–371 (2023).

147. Bonifant, C. L., Jackson, H. J., Brentjens, R. J. & Curran, K. J. Toxicity and management in CAR T-cell therapy. *Mol Ther Oncolytics* **3**,16011 (2016).

148. Morris, E. C., Neelapu, S. S., Giavridis, T. & Sadelain, M. Cytokine release syndrome and associated neurotoxicity in cancer immunotherapy. *Nat Rev Immunol* **22**,85–96 (2022).

149. Brudno, J. N. & Kochenderfer, J. N. Recent advances in CAR T-cell toxicity: Mechanisms, manifestations and management. *Blood Rev* **34**,45–55 (2019).

150. Santomasso, B. D. *et al*. Clinical and biological correlates of neurotoxicity associated with car t-cell therapy in patients with B-cell acute lymphoblastic leukemia. *Cancer Discov* **8**, 958–971 (2018).

151. Van Der Stegen, S. J. C., Hamieh, M. & Sadelain, M. The pharmacology of second-generation chimeric antigen receptors. *Nat Rev Drug Discov* **14**,499–509 (2015).

152. Alexander I. Salter *et al.* Phosphoproteomic analysis of chimeric antigen receptor signaling reveals kinetic and quantitative differences that affect cell function. *Sci Signal* **11**, (2018).

153. Ying, Z. *et al.* A safe and potent anti-CD19 CAR T cell therapy. *Nat Med* **25**, 947–953 (2019).

154. Sommermeyer, D. *et al.* Fully human CD19-specific chimeric antigen receptors for T-cell therapy. *Leukemia* **31**, 2191–2199 (2017).

155. Lee, Y. G. *et al.* Regulation of CAR T cell-mediated cytokine release syndrome-like toxicity using low molecular weight adapters. *Nat Commun* **10**, (2019).

156. Lu, L., Xie, M., Yang, B., Zhao, W.-B. & Cao, J. Enhancing the Safety of CAR-T Cell Therapy: Synthetic Genetic Switch for Spatiotemporal Control. *Sci. Adv*. **10**, eadj6251(2024).

157. Stasi, A. Di *et al.* Inducible Apoptosis as a Safety Switch for Adoptive Cell Therapy. *N Engl J Med* **365**, 1673–83 (2011).

158. Del Bufalo, F. *et al.* GD2-CART01 for Relapsed or Refractory High-Risk Neuroblastoma. *N Engl J Med* **388**, 1284–1295 (2023).

159. Majzner, R. G. *et al.* GD2-CAR T cell therapy for H3K27M-mutated diffuse midline gliomas. *Nature* **603**, 934–941 (2022).

160. Parker, K. R. *et al.* Single-Cell Analyses Identify Brain Mural Cells Expressing CD19 as Potential Off-Tumor Targets for CAR-T Immunotherapies. *Cell* **183**, 126-142.e17 (2020).

161. Majzner, R. G. & Mackall, C. L. Tumor antigen escape from car t-cell therapy. *Cancer Discov* **8**,1219–26 (2018).

162. Furqan, F. & Shah, N. N. Annual Review of Medicine Multispecific CAR T Cells Deprive Lymphomas of Escape via Antigen Loss. *Annu Rev Med.***74**, 279-291(2023).

163. Wei, G. *et al.* CD19/CD22 dual-targeted car t-cell therapy for relapsed/refractory aggressive b-cell lymphoma: A safety and efficacy study. *Cancer Immunol Res* **9**, 1061–1070 (2021).

164. Spiegel, J. Y. *et al.* CAR T cells with dual targeting of CD19 and CD22 in adult patients with recurrent or refractory B cell malignancies: a phase 1 trial. *Nat Med* **27**, 1419–1431 (2021).

165. Shah, N. N. *et al.* Bispecific anti-CD20, anti-CD19 CAR T cells for relapsed B cell malignancies: a phase 1 dose escalation and expansion trial. *Nat Med* **26**, 1569–1575 (2020).

166. Huehls, A. M., Coupet, T. A. & Sentman, C. L. Bispecific T-cell engagers for cancer immunotherapy. *Immunol Cell Biol* **93**,290–296 (2015).

167. Choi, B. D. *et al.* CAR-T cells secreting BiTEs circumvent antigen escape without detectable toxicity. *Nat Biotechnol* **37**, 1049–1058 (2019).

168. Topp, M. S. *et al.* Phase II trial of the anti-CD19 bispecific T cell-engager blinatumomab shows hematologic and molecular remissions in patients with relapsed or refractory B-precursor acute lymphoblastic leukemia. *J Clin Oncol* **32**, 4134–4140 (2014).

169. Kuhn, N. F. *et al.* CD40 Ligand-Modified Chimeric Antigen Receptor T Cells Enhance Antitumor Function by Eliciting an Endogenous Antitumor Response. *Cancer Cell* **35**, 473-488.e6 (2019).

170. Narayan, V. *et al.* PSMA-targeting TGFβ-insensitive armored CAR T cells in metastatic castration-resistant prostate cancer: a phase 1 trial. *Nat Med* **28**, 724–734 (2022).

171. Hong, M., Clubb, J. D. & Chen, Y. Y. Engineering CAR-T Cells for Next-Generation Cancer Therapy. *Cancer Cell* **38**,473–488 (2020).

172. Sommermeyer, D. *et al.* Chimeric antigen receptor-modified T cells derived from defined CD8+ and CD4+ subsets confer superior antitumor reactivity in vivo. *Leukemia* **30**, 492–500 (2016).

173. Ghassemi, S. *et al.* Reducing ex vivo culture improves the antileukemic activity of chimeric antigen receptor (CAR) T cells. *Cancer Immunol Res* **6**, 1100–1109 (2018).

174. Sabatino, M. *et al*. Generation of clinical-grade CD19-specific CAR-modified CD8 1 memory stem cells for the treatment of human B-cell malignancies. *Blood* **128**(4), 519-528 (2015).

175. Turtle, C. J. *et al*. CD19 CAR-T cells of defined CD4+:CD8+ composition in adult B cell ALL patients. *J. Clin. Invest.* **126**, 2123–2138 (2016).

176. López-Cantillo, G., Urueña, C., Camacho, B. A. & Ramírez-Segura, C. CAR-T Cell Performance: How to Improve Their Persistence? *Front. Immunol.* **13** (2022).

177. Alizadeh, D. *et al*. IL15 enhances CAR-T cell antitumor activity by reducing mTORC1 activity and preserving their stem cell memory phenotype. *Cancer Immunol Res* **7**, 759–772 (2019).

178. Markley, J. C. & Sadelain, M. IL-7 and IL-21 are superior to IL-2 and IL-15 in promoting human T cell-mediated rejection of systemic lymphoma in immunodeficient mice. *Blood* **115**, 3508–3519 (2010).

179. Cieri, N. *et al*. IL-7 and IL-15 instruct the generation of human memory stem T cells from naive precursors. *Blood* **121**, 573–584 (2013).

180. Liu, Y. *et al*. Strategies to enhance CAR-T persistence. *Biomark Res* **10**, 86(2022).

181. Leone, R. D. *et al*. Glutamine Blockade Induces Divergent Metabolic Programs to Overcome Tumor Immune Evasion. *Science* **366**,1013-1021(2019).

182. Zheng, W. *et al*. PI3K orchestration of the in vivo persistence of chimeric antigen receptor-modified T cells. *Leukemia* **32**, 1157–1167 (2018).

183. Wang, Y. *et al*. Low-dose decitabine priming endows CAR T cells with enhanced and persistent antitumour potential via epigenetic reprogramming. *Nat Commun* **12** (2021).

184. Zhang, Z. *et al*. Metformin Enhances the Antitumor Activity of CD8+ T Lymphocytes via the AMPK–miR-107–Eomes–PD-1 Pathway. *J. Immunol.* **204**, 2575–2588 (2020).

185. Jin, L. *et al*. CXCR1- or CXCR2-modified CAR T cells co-opt IL-8 for maximal antitumor efficacy in solid tumors. *Nat Commun* **10**, (2019).

186. Lesch, S. *et al.* T cells armed with C-X-C chemokine receptor type 6 enhance adoptive cell therapy for pancreatic tumours. *Nat Biomed Eng* **5**, 1246–1260 (2021).

187. Lai, Y. *et al.* Toll-like receptor 2 costimulation potentiates the antitumor efficacy of CAR T Cells. *Leukemia* **32**, 801–808 (2018).

188. Ding, Z.-C. *et al.* Persistent STAT5 Activation Reprograms the Epigenetic Landscape in CD4 + T Cells to Drive Polyfunctionality and Antitumor Immunity. *Sci. Immunol* **5**, eaba5962(2020).

189. Seo, H. *et al.* BATF and IRF4 cooperate to counter exhaustion in tumor-infiltrating CAR T cells. *Nat Immunol* **22**, 983–995 (2021).

190. Qi, C. *et al.* Claudin18.2-specific CAR T cells in gastrointestinal cancers: phase 1 trial interim results. *Nat Med* **28**, 1189–1198 (2022).

191. Wang, Y. *et al.* CD133-directed CAR T cells for advanced metastasis malignancies: A phase I trial. *Oncoimmunology* **7**, (2018).

192. Lin, Y. *et al.* Phase I clinical trial of PD-1 knockout anti-MUC1 CAR-T cells in the treatment of patients with non-small cell lung cancer. *Ann. Oncol.* **30**, xi12 (2019).

193. Chen, S. & Lin, Y. Phase I Clinical Trial Using a Unique Immunotherapeutic Combination of MUC1-Targeted CAR-T Cells with PD-1-Knockout in the Treatment of Patients with Advanced Esophageal Cancer. *J. Clin. Oncol.* **41**, e16061(2023).

194. Louis, C. U. *et al.* Antitumor activity and long-term fate of chimeric antigen receptor-positive T cells in patients with neuroblastoma. *Blood* **118**(23), 6050-6056(2011).

195. Shi, D. *et al.* Chimeric Antigen Receptor-Glypican-3 T-Cell Therapy for Advanced Hepatocellular Carcinoma: Results of Phase I Trials. *Clin Cancer Res* **26**, 3979–3989 (2020).

196. Hegde, M. *et al.* Expansion of HER2-CAR T cells after lymphodepletion and clinical responses in patients with advanced sarcoma. *J Clin Oncol* **35**, 10508 (2017).

197. Ahmed, N. *et al*. HER2-specific chimeric antigen receptor–modified virus-specific T cells for progressive glioblastoma: A phase 1 dose-escalation trial. *JAMA Oncol* **3**, 1094–1101 (2017).

198. Brown, C. E. *et al*. Locoregional delivery of IL-13Rα2-targeting CAR-T cells in recurrent high-grade glioma: a phase 1 trial. *Nat Med* **30**, 1001–1012(2024)

199. Guo, Y. *et al*. Phase I study of chimeric antigen receptor–modified T cells in patients with EGFR-positive advanced biliary tract cancers. *Clin Cancer Res* **24**, 1277–1286 (2018).

200. Goff, S. L. *et al*. Pilot trial of Adoptive Transfer of Chimeric Antigen Receptor-transduced T cells targeting EGFRvIII in Patients with glioblastoma. *J Immunother*. **42**(4), 126-135 (2019).

201. Adusumilli, P. S. *et al*. A phase i trial of regional mesothelin-targeted car t-cell therapy in patients with malignant pleural disease, in combination with the anti–pd-1 agent pembrolizumab. *Cancer Discov* **11**, 2748–2763 (2021).

202. Haas, A. R. *et al*. Phase I Study of Lentiviral-Transduced Chimeric Antigen Receptor-Modified T Cells Recognizing Mesothelin in Advanced Solid Cancers. *Mol Ther* **27**, 1919–1929 (2019).

203. Shah, P. D. *et al*. Phase I Trial of Autologous RNA-electroporated cMET-directed CAR T Cells Administered Intravenously in Patients with Melanoma and Breast Carcinoma. *Cancer Res Commun* **3**, 821–829 (2023).

204. Katz, S. C. *et al*. HITM-SIR: phase Ib trial of intraarterial chimeric antigen receptor T-cell therapy and selective internal radiation therapy for CEA+ liver metastases. *Cancer Gene Ther* **27**, 341–355 (2020).

205. Katz, S. C. *et al*. HITM-SURE: Hepatic immunotherapy for metastases phase Ib anti-CEA CAR-T study utilizing pressure enabled drug delivery. *J Immunother Cancer* **8**, (2020).

206. Mackensen, A. *et al*. CLDN6-specific CAR-T cells plus amplifying RNA vaccine in relapsed or refractory solid tumors: the phase 1 BNT211-01 trial. *Nat Med* **29**, 2844–2853 (2023).

207. Finck, A. V., Blanchard, T., Roselle, C. P., Golinelli, G. & June, C. H. Engineered cellular immunotherapies in cancer and beyond. *Nat Med* **28**, 678–689 (2022).

208. Baker, D. J., Arany, Z., Baur, J. A., Epstein, J. A. & June, C. H. CAR T therapy beyond cancer: the evolution of a living drug. *Nature* **619**, 707–715 (2023).

209. Aghajanian, H., Rurik, J. G. & Epstein, J. A. CAR-based therapies: opportunities for immuno-medicine beyond cancer. *Nat Metabol* **4**, 163–169 (2022).

210. D'Aloia, M. M., Zizzari, I. G., Sacchetti, B., Pierelli, L. & Alimandi, M. CAR-T cells: The long and winding road to solid tumors. *Cell Death Dis* **9**(3), 288 (2018).

211. Donnadieu, E., Dupré, L., Pinho, L. G. & Cotta-de-Almeida, V. Surmounting the obstacles that impede effective CAR T cell trafficking to solid tumors. *J. Leukoc. Biol*. **108**,1067–1079 (2020).

212. Rodriguez-Garcia, A., Palazon, A., Noguera-Ortega, E., Powell, D. J. & Guedan, S. CAR-T Cells Hit the Tumor Microenvironment: Strategies to Overcome Tumor Escape. *Front Immunol* **11**, 1109(2020).

213. Hou, A. J., Chen, L. C. & Chen, Y. Y. Navigating CAR-T cells through the solid-tumour microenvironment. *Nat Rev Drug Discov* **20**, 531–550 (2021).

214. Albelda, S. M. CAR T cell therapy for patients with solid tumours: key lessons to learn and unlearn. *Nat Rev Clin Oncol* **21**, 47–66 (2024).

215. Watanabe, K., Kuramitsu, S., Posey, A. D. & June, C. H. Expanding the therapeutic window for CAR T cell therapy in solid tumors: The knowns and unknowns of CAR T cell biology. *Front Immunol* **9**, 1–12 (2018).

216. Garber, K. Driving T-cell immunotherapy to solid tumors. *Nat Biotechnol* **36**, 215–219 (2018).

217. Lamers, C. H. J. *et al*. Treatment of metastatic renal cell carcinoma with CAIX CAR-engineered T cells: Clinical evaluation and management of on-target toxicity. *Mol. Ther*. **21**, 904–912 (2013).

218. Morgan, R. A. *et al*. Case report of a serious adverse event following the administration of t cells transduced with a chimeric antigen receptor recognizing ERBB2. *Mol. Ther*. **18**, 843–851 (2010).

219. Ahmed, N. *et al*. Human epidermal growth factor receptor 2 (HER2) - Specific chimeric antigen receptor - Modified T cells for the immunotherapy of HER2-positive sarcoma. *J. Clin. Oncol*. **33**, 1688–1696 (2015).

220. Schmidts, A. & Maus, M. V. Making CAR T cells a solid option for solid tumors. *Front Immunol* **9**, 1–10 (2018).

221. Watanabe, K., Kuramitsu, S., Posey, A. D. & June, C. H. E Expanding the therapeutic window for CAR T cell therapy in solid tumors: The knowns and unknowns of CAR T cell biology. *Front Immunol* **9**, 1–12 (2018).

222. Beavis, P. A. *et al*. Reprogramming the tumor microenvironment to enhance adoptive cellular therapy. *Semin Immunol* **28**,64–72 (2016).

223. Schmittnaegel, M. & De Palma, M. Reprogramming Tumor Blood Vessels for Enhancing Immunotherapy. *Trends in Cancer* **3**, 809–812 (2017).

224. Sagnella, S. M. *et al*. Locoregional delivery of CAR-T cells in the clinic. *Pharmacol Res* **182**, 106329 (2022).

225. Gunderson, A. J. *et al*. TGFβ suppresses CD8+ T cell expression of CXCR3 and tumor trafficking. *Nat Commun* **11**, 1749 (2020).

226. Chakravarthy, A., Khan, L., Bensler, N. P., Bose, P. & De Carvalho, D. D. TGF-β-associated extracellular matrix genes link cancer-associated fibroblasts to immune evasion and immunotherapy failure. *Nat Commun* **9**, 4692 (2018).

227. Caruana, I. *et al*. Heparanase promotes tumor infiltration and antitumor activity of CAR-redirected T lymphocytes. *Nat Med* **21**, 524–529 (2015).

228. Rodriguez-Garcia, A. *et al*. CAR-T cell-mediated depletion of immunosuppressive tumor-associated macrophages promotes endogenous antitumor immunity and augments adoptive immunotherapy. *Nat Commun* **12** (2021).

229. Wang, L. C. S. *et al*. Targeting fibroblast activation protein in tumor stroma with chimeric antigen receptor T cells can inhibit tumor growth and augment host immunity without severe toxicity. *Cancer Immunol Res* **2**, 154–166 (2014).

230. Valkenburg, K. C., De Groot, A. E. & Pienta, K. J. Targeting the tumour stroma to improve cancer therapy. *Nat Rev Clin Oncol* **15**, 366–381 (2018).

231. Zarour, H. M. Reversing T-cell dysfunction and exhaustion in cancer. *Clin Cancer Res* **22**, 1856–1864 (2016).

232. McLane, L. M., Abdel-Hakeem, M. S. & Wherry, E. J. CD8 T Cell Exhaustion During Chronic Viral Infection and Cancer. *Annu Rev Immunol* **37**, 457–495 (2019).

233. Jiang, Y., Li, Y. & Zhu, B. T-cell exhaustion in the tumor microenvironment. *Cell Death Dis* **6**, 1–9 (2015).

234. Debattama R. Sen *et al*. The epigenetic landscape of T cell exhaustion. *Science* **354**, 1165–1169 (2016).

235. Robert, C. *et al*. Nivolumab in Previously Untreated Melanoma without BRAF Mutation. *N Engl J Med* **372**, 320–330 (2015).

236. Cherkassky, L. *et al*. Human CAR T cells with cell-intrinsic PD-1 checkpoint blockade resist tumor-mediated inhibition. *J. Clin. Invest.***126**, 3130–3144 (2016).

237. Bagley, S. J. *et al*. Repeated peripheral infusions of anti-EGFRvIII CAR T cells in combination with pembrolizumab show no efficacy in glioblastoma: a phase 1 trial. *Nat Cancer* **5**, 517-531(2024).

238. Rafiq, S. *et al*. Targeted delivery of a PD-1-blocking scFV by CAR-T cells enhances anti-tumor efficacy in vivo. *Nat Biotechnol* **36**, 847–858 (2018).

239. Harrasser, M. *et al*. Inducible localized delivery of an anti-PD-1 scFv enhances anti-tumor activity of ROR1 CAR-T cells in TNBC. *Breast Cancer Res* **24**, (2022).

240. Moon, Y. *et al*. Anti-PD-L1 peptide-conjugated prodrug nanoparticles for targeted cancer immunotherapy combining PD-L1 blockade with immunogenic cell death. *Theranostics* **12**, 1919–2014 (2022).

241. Menger, L. *et al*. TALEN-Mediated Inactivation of PD-1 in Tumor-Reactive Lymphocytes Promotes Intratumoral T-cell Persistence and Rejection of Established Tumors. *Cancer Res* **76**, 2087–2093 (2016).

242. Rupp, L. J. *et al*. CRISPR/Cas9-mediated PD-1 disruption enhances anti-Tumor efficacy of human chimeric antigen receptor T cells. *Sci Rep* **7**, 1–10 (2017).

243. Ren, J. *et al.* Multiplex genome editing to generate universal CAR T cells resistant to PD1 inhibition. *Clin Cancer Res* **23**, 2255–2266 (2017).

244. Hu, W. *et al.* CRISPR/Cas9-mediated PD-1 disruption enhances human mesothelin-targeted CAR T cell effector functions. *Cancer Immunol Immunother* **68**, 365–377 (2018).

245. Guo, X. *et al.* Disruption of PD-1 enhanced the anti-tumor activity of chimeric antigen receptor T cells against hepatocellular carcinoma. *Front Pharmacol* **9**, 1–15 (2018).

246. Liu, X. *et al.* A chimeric switch-receptor targeting PD1 augments the efficacy of second-generation CAR T cells in advanced solid tumors. *Cancer Res* **76**, 1578–1590 (2016).

247. Choi, B. D. *et al.* CRISPR-Cas9 disruption of PD-1 enhances activity of universal EGFRvIII CAR T cells in a preclinical model of human glioblastoma. *J Immunother Cancer* **7**, (2019).

248. Kalinin, R. S. *et al.* Engineered Removal of PD-1 From the Surface of CD19 CAR-T Cells Results in Increased Activation and Diminished Survival. *Front Mol Biosci* **8**, (2021).

249. Wei, J. *et al.* PD-1 silencing impairs the anti-tumor function of chimeric antigen receptor modified T cells by inhibiting proliferation activity. *J Immunother Cancer* **7**, (2019).

250. Agarwal, S. *et al.* Deletion of the inhibitory co-receptor CTLA-4 enhances and invigorates chimeric antigen receptor T cells. *Immunity* **56**, 2388-2407.e9 (2023).

251. Chmielewski, M., Hombach, A., Heuser, C., Adams, G. P. & Abken, H. T Cell Activation by Antibody-Like Immunoreceptors: Increase in Affinity of the Single-Chain Fragment Domain above Threshold Does Not Increase T Cell Activation against Antigen-Positive Target Cells but Decreases Selectivity. *J Immunol.* **173** (2004).

252. Ghorashian, S. *et al*. Enhanced CAR T cell expansion and prolonged persistence in pediatric patients with ALL treated with a low-affinity CD19 CAR. *Nat Med* **25**, 1408–1414 (2019).

253. Gardner, R. A. *et al*. Intent-to-treat leukemia remission by CD19 CAR T cells of defined formulation and dose in children and young adults. *Blood* **129**, 3322–3331 (2017).

254. Liu, X. *et al*. Affinity-tuned ErbB2 or EGFR chimeric antigen receptor T cells exhibit an increased therapeutic index against tumors in mice. *Cancer Res* **75**, 3596–3607 (2015).

255. Shabaneh, T. B. *et al*. Systemically administered low-affinity HER2 CAR T cells mediate antitumor efficacy without toxicity. *J Immunother Cancer* **12**, (2024).

256. Wang, Y. *et al*. Affinity fine-tuning anti-CAIX CAR-T cells mitigate on-target off-tumor side effects. *Mol Cancer* **23**, (2024).

257. Park, S. *et al*. Micromolar affinity CAR T cells to ICAM-1 achieves rapid tumor elimination while avoiding systemic toxicity. *Sci Rep* **7**, (2017).

258. Caraballo Galva, L. D. *et al*. Novel low-avidity glypican-3 specific CARTs resist exhaustion and mediate durable antitumor effects against HCC. *Hepatology* **76**, 330–344 (2022).

259. Lynn, R. C. *et al*. High-affinity FRβ-specific CAR T cells eradicate AML and normal myeloid lineage without HSC toxicity. *Leukemia* **30**, 1355–1364 (2016).

260. Beatty, G., Engels, B., et al. Human mesothelin chimeric antigen receptors and uses thereof (International application, Patent No WO2015090230A1). Novartis AG, The Trustees of the University of Pennsylvania (2015).

261. Castella, M. *et al*. Development of a Novel Anti-CD19 Chimeric Antigen Receptor: A Paradigm for an Affordable CAR T Cell Production at Academic Institutions. *Mol Ther Methods Clin Dev* **12**, 134–144 (2019).

262. Marzal Martí, B. Receptor Antigénico Quimérico en linfocitos T para el tratamiento del cáncer de mama HER2+. PhD thesis, Universitat de Barcelona, Barcelona (2023).

263. Axmann, M., Schütz, G. J. & Huppa, J. B. Single molecule fluorescence microscopy on planar supported Bilayers. *J. Vis. Exp.***104**, e53158 (2015).

264. Abiko, K. *et al.* IFN-γ from lymphocytes induces PD-L1 expression and promotes progression of ovarian cancer. *Br J Cancer* **112**, 1501–1509 (2015).

265. Blank, C. *et al.* PD-L1/B7H-1 Inhibits the Effector Phase of Tumor Rejection by T Cell Receptor (TCR) Transgenic CD8 T Cells. *CancerRes* **64**(3),1140–1145(2004).

266. Ren, J. *et al.* A versatile system for rapid multiplex genome-edited CAR T cell generation. *Oncotarget* **8**, 17002–17011 (2017).

267. Diskin, B. *et al.* PD-L1 engagement on T cells promotes self-tolerance and suppression of neighboring macrophages and effector T cells in cancer. *Nat Immunol* **21**, 442–454 (2020).

268. Ribas, A. & Wolchok, J. D. Cancer immunotherapy using checkpoint blockade. *Science* **359**, 1350–1355 (2018).

269. Gudipati, V. *et al.* Inefficient CAR-proximal signaling blunts antigen sensitivity. *Nat Immunol* **21**, 848–856 (2020).

270. Ogando, J. *et al.* PD-1 signaling affects cristae morphology and leads to mitochondrial dysfunction in human CD8+ T lymphocytes. *J Immunother Cancer* **7**, (2019).

271. Wherry, E. J. *et al.* Molecular Signature of CD8+ T Cell Exhaustion during Chronic Viral Infection. *Immunity* **27**, 670–684 (2007).

272. Beider, K. *et al.* Molecular and Functional Signatures Associated with CAR T Cell Exhaustion and Impaired Clinical Response in Patients with B Cell Malignancies. *Cells* **11**, (2022).

273. Giordano, M. *et al.* Molecular profiling of CD8 T cells in autochthonous melanoma identifies Maf as driver of exhaustion. *EMBO J* **34**, 2042–2058 (2015).

274. Jung, I. Y. *et al.* Type I Interferon Signaling via the EGR2 Transcriptional Regulator Potentiates CAR T Cell–Intrinsic Dysfunction. *Cancer Discov* **13**, 1636–1655 (2023).

275. Chen, E. Y. *et al*. Enrichr: interactive and collaborative HTML5 gene list enrichment analysis tool. *BMC Bioinforma*.**14**, 128 (2013).

276. Kuleshov, M. V. *et al*. Enrichr: a comprehensive gene set enrichment analysis web server 2016 update. *Nucleic Acids Res* **44**, W90–W97 (2016).

277. Chen, G. M. *et al*. Integrative bulk and single-cell profiling of premanufacture t-cell populations reveals factors mediating long-term persistence of car t-cell therapy. *Cancer Discov* **11**, 2186–2199 (2021).

278. Good, C. R. *et al*. An NK-like CAR T cell transition in CAR T cell dysfunction. *Cell* **184**, 6081-6100.e26 (2021).

279. Willinger, T. *et al*. Human Naive CD8 T Cells Down-Regulate Expression of the WNT Pathway Transcription Factors Lymphoid Enhancer Binding Factor 1 and Transcription Factor 7 (T Cell Factor-1) Following Antigen Encounter In Vitro and In Vivo. *J Immunol* **176**(3),1439–1446 (2006).

280. Rossi, J. *et al*. Preinfusion Polyfunctional Anti-CD19 Chimeric Antigen Receptor T Cells Are Associated with Clinical Outcomes in NHL. *Blood* **32** (8), 804-814(2018)

281. Hudecek, M. *et al*. Receptor affinity and extracellular domain modifications affect tumor recognition by ROR1-specific chimeric antigen receptor T cells. *Clin Cancer Res* **19**, 3153–3164 (2013).

282. Majzner, R. G. *et al*. Tuning the antigen density requirement for car T-cell activity. *Cancer Discov* **10**, 702–723 (2020).

283. Guedan, S. *et al*. ICOS-based chimeric antigen receptors program bipolar TH17/TH1 cells. *Blood* **124**, 1070–1080 (2014).

284. Zolov, S. N., Rietberg, S. P. & Bonifant, C. L. Programmed cell death protein 1 activation preferentially inhibits CD28.CAR–T cells. *Cytotherapy* **20**, 1259–1266 (2018).

285. Dötsch, S. *et al*. Long-term persistence and functionality of adoptively transferred antigen-specific T cells with genetically ablated PD-1 expression. *Proc Natl Acad Sci U S A* **120**, (2023).

286. Stadtmauer, E. A. *et al.* CRISPR-engineered T cells in patients with refractory cancer. *Science* **367**, (2020).

287. Guedan, S. *et al.* Time 2EVOLVE: predicting efficacy of engineered T-cells -how far is the bench from the bedside? *J Immunother Cancer* **10**, e003487(2022).

288. Peters, T. *et al.* TCR/CD3-based synthetic antigen receptors (TCC) convey superior antigen sensitivity combined with high fidelity of activation. *bioRxiv*2023.03.16.532775

289. Laforêts, F. *et al.* Semi-supervised analysis of myeloid and T cell behavior in ex vivo ovarian tumor slices reveals changes in cell motility after treatments. *iScience* **26**, (2023).

290. Faria, C. *et al.* Patient-derived lymphoma spheroids integrating immune tumor microenvironment as preclinical follicular lymphoma models for personalized medicine. *J Immunother Cancer* **11**, (2023).

291. Neal, J. T. *et al.* Organoid Modeling of the Tumor Immune Microenvironment. *Cell* **175**, 1972-1988.e16 (2018).

292. Haque, M. R. *et al.* Patient-derived pancreatic cancer-on-a-chip recapitulates the tumor microenvironment. *Microsyst Nanoeng* **8**, (2022).

293. Guil-Luna, S., Sedlik, C. & Piaggio, E. Humanized Mouse Models to Evaluate Cancer Immunotherapeutics *Annu. Rev. Can. Bio.* **5**, 119-136 (2021).

294. Cogels, M. M. *et al.* Humanized Mice as a Valuable Pre-Clinical Model for Cancer Immunotherapy Research. *Front. Oncol.* **11**, 784947 (2021).

295. Park, N. *et al.* Preclinical platform for long-term evaluation of immuno-oncology drugs using hCD34+ humanized mouse model. *J Immunother Cancer* **8**, e001513 (2020).

296. Guedan, S. *et al.* Time 2EVOLVE: predicting efficacy of engineered T-cells - how far is the bench from the bedside? *J Immunother Cancer*. **10**(5), e003487(2022).

297. Latchman, Y. E. *et al.* PD-L1-Deficient Mice Show That PD-L1 on T Cells, Antigen-Presenting Cells, and Host Tissues Negatively Regulates T Cells. *Proc Natl Acad Sci U S A*. **101 (**29), 10691-10696(2004).

298. Harrer, D. C. *et al.* Fine-tuning the antigen sensitivity of CAR T cells: emerging strategies and current challenges. *Front Immunol*.**14**, 1321596(2023).

299. Heitzeneder, S. *et al.* GPC2-CAR T cells tuned for low antigen density mediate potent activity against neuroblastoma without toxicity. *Cancer Cell* **40**, 53-69.e9 (2022).

300. Shimizu, K. *et al.* PD-1 preferentially inhibits the activation of low-affinity T cells. *Proc Natl Acad Sci U S A*. **118** (35), e2107141118 (2021).

301. Leick, M. B. *et al.* Non-cleavable hinge enhances avidity and expansion of CAR-T cells for acute myeloid leukemia. *Cancer Cell* **40**, 494-508.e5 (2022).

302. Lee, L. *et al.* Limited efficacy of APRIL CAR in patients with multiple myeloma indicate challenges in the use of natural ligands for CAR T-cell therapy. *J Immunother Cancer* **11**, (2023).

303. Pauken, K. E. & Wherry, E. J. Overcoming T cell exhaustion in infection and cancer. *Trends in Immunol* **36**, 265–276 (2015).

304. Schlenker, R. *et al.* Chimeric PD-1:28 receptor upgrades low-avidity T cells and restores effector function of tumor-infiltrating lymphocytes for adoptive cell therapy. *Cancer Res* **77**, 3577–3590 (2017).

305. Shimizu, K. *et al.* PD-1 Imposes Qualitative Control of Cellular Transcriptomes in Response to T Cell Activation. *Mol Cell* **77**, 937-950.e6 (2020).

306. Rodriguez-Marquez, P. *et al.* CAR Density Influences Antitumoral Efficacy of BCMA CAR T Cells and Correlates with Clinical Outcome. *Sci. Adv.* **8**, eabo0514(2022).

307. Mao, R., Kong, W. & He, Y. The affinity of antigen-binding domain on the antitumor efficacy of CAR T cells: Moderate is better. *Front Immunol* **13** (2022).

308. Espie, D. & Donnadieu, E. New insights into CAR T cell-mediated killing of tumor cells. *Front Immunol* **13**, 1016208 (2022).

309. Hao, L. Y. *et al.* Exclusion of PD-1 from the immune synapse: a novel strategy to modulate T cell function. *bioRxiv*. 2023;2023.11.16.566907.

310. Kantari-Mimoun, C. *et al.* CAR T-cell Entry into Tumor Islets Is a Two-Step Process Dependent on IFNg and ICAM-1. *Cancer Immunol Res* **9**, 1425–1438 (2021).

311. Larson, R. C. *et al.* CAR T cell killing requires the IFNγR pathway in solid but not liquid tumours. *Nature* **604**, 563–570 (2022).

312. Dong, E. *et al.* IFN-γ surmounts PD-L1/PD1 inhibition to CAR-T cell therapy by upregulating ICAM-1 on tumor cells. *Signal Transduct. Target Ther.***6**, 20 (2021).

313. Zou, F. *et al.* Engineered triple inhibitory receptor resistance improves anti-tumor CAR-T cell performance via CD56. *Nat Commun* **10**, (2019).

314. López-Soto, A., Gonzalez, S. & Folgueras, A. R. IFN Signaling and ICB Resistance: Time is on Tumor's Side. *Trends in Cancer* **3**,161–163 (2017).

315. Boulch, M. *et al.* Tumor-intrinsic sensitivity to the pro-apoptotic effects of IFN-γ is a major determinant of CD4+ CAR T-cell antitumor activity. *Nat Cancer* **4**, 968–983 (2023).

316. Alizadeh, D. *et al.* IFNγ is critical for CAR T cell–mediated myeloid activation and induction of endogenous immunity. *Cancer Discov* **11**, 2248–2265 (2021).

317. Garcia-Diaz, A. *et al.* Interferon Receptor Signaling Pathways Regulating PD-L1 and PD-L2 Expression. *Cell Rep* **19**, 1189–1201 (2017).

318. Zaretsky, J. M. *et al.* Mutations Associated with Acquired Resistance to PD-1 Blockade in Melanoma. *N Engl J Med* **375**, 819–829 (2016).

319. Andersen, M. H. The targeting of immunosuppressive mechanisms in hematological malignancies. *Leukemia***28**, 1784–1792 (2014)

320. Riley, J. L. PD-1 signaling in primary T cells. *Immunol Rev* **229**,114–125 (2009).

321. Zhao, Z. *et al.* Structural Design of Engineered Costimulation Determines Tumor Rejection Kinetics and Persistence of CAR T Cells. *Cancer Cell* **28**, 415–428 (2015).

322. John R. Teijaro *et al.* Persistent LCMV Infection Is Controlled by Blockade of Type I Interferon Signaling. *Science* **340**, 207–2011 (2013).

323. Wilson, E. B. *et al*. Blockade of chronic type I interferon signaling to control persistent LCMV infection. *Science* **340**, 202–207 (2013).

324. Evgin, L. *et al*. Oncolytic virus-derived type I interferon restricts CAR T cell therapy. *Nat Commun* **11**, (2020).

325. Hui, E. *et al*. The T cell costimulatory receptor CD28 is a primary target of PD-1 mediated inhibition. *Science* **4**, 1–14 (2016).

326. Hui, E. *et al*. T cell costimulatory receptor CD28 is a primary target for PD-1-mediated inhibition. *Science* **355**, 1428–1433 (2017).

327. Kamphorst, A. O. *et al*. Rescue of exhausted CD8 T cells by PD-1-targeted therapies is CD28-dependent. *Science* **355**, 1423–1427 (2017).

328. Sanchez-Paulete, A. R. *et al*. Deciphering CD137 (4-1BB) signaling in T-cell costimulation for translation into successful cancer immunotherapy. *Eur J Immunol* **46**, 513–522 (2016).

329. Sachdeva, M. *et al*. Repurposing endogenous immune pathways to tailor and control chimeric antigen receptor T cell functionality. *Nat Commun* **10**, (2019).

330. Kim, S., Park, C. I., Lee, S., Choi, H. R. & Kim, C. H. Reprogramming of IL-12 secretion in the PDCD1 locus improves the anti-tumor activity of NY-ESO-1 TCR-T cells. *Front Immunol* **14**, (2023).

331. Michelozzi, I. M. *et al*. Activation priming and cytokine polyfunctionality modulate the enhanced functionality of low-affinity CD19 CAR T cells. *Blood Adv* **7**, 1725–1738 (2023).

332. Rossi, J. *et al*. Preinfusion polyfunctional anti-CD19 chimeric antigen receptor T cells are associated with clinical outcomes in NHL.*Blood***132**, 804–814 (2018).

333. Zhong, S. *et al*. T-cell receptor affinity and avidity defines antitumor response and autoimmunity in T-cell immunotherapy. *Proc Natl Acad Sci U S A* **110**, 6973–6978 (2013).

334. Yi, M., Niu, M., Xu, L., Luo, S. & Wu, K. Regulation of PD-L1 expression in the tumor microenvironment. *J Hematol Oncol***14**, 10(2021).

335. Lu, Y. *et al*. Safety and feasibility of CRISPR-edited T cells in patients with refractory non-small-cell lung cancer. *Nat Med* **26**, 732–740 (2020).

336. Sullivan, R. J. & Weber, J. S. Immune-related toxicities of checkpoint inhibitors: mechanisms and mitigation strategies. *Nat RevDrug Discov* **21**,495–508 (2022).

337. Kamada, T. *et al*. PD-1+ regulatory T cells amplified by PD-1 blockade promote hyperprogression of cancer. *Proc Natl Acad Sci U S A* **116**, 9999–10008 (2019).

338. Grosser, R., Cherkassky, L., Chintala, N. & Adusumilli, P. S. Combination Immunotherapy with CAR T Cells and Checkpoint Blockade for the Treatment of Solid Tumors. *Cancer Cell* **36**, 471–482 (2019).

339. Zhou, Y. *et al*. Ray of dawn: Anti-PD-1 immunotherapy enhances the chimeric antigen receptor T-cell therapy in Lymphoma patients. *BMC Cancer* **23**, (2023).

340. Wartewig, T. *et al*. PD-1 is a haploinsufficient suppressor of T cell lymphomagenesis. *Nature* **552**, 121–125 (2017).

341. Ortíz-Maldonado, V. *et al*. CART19-BE-01: A Multicenter Trial of ARI-0001 Cell Therapy in Patients with CD19+ Relapsed/Refractory Malignancies. *Mol Ther* **29**, 636–644 (2021).

342. Oliver-Caldés, A. *et al*. Fractionated initial infusion and booster dose of ARI0002h, a humanised, BCMA-directed CAR T-cell therapy, for patients with relapsed or refractory multiple myeloma (CARTBCMA-HCB-01): a single-arm, multicentre, academic pilot study. *Lancet Oncol* **24**, 913–924 (2023).

Appendix

8. Appendix

Related publications directly linked to the research conducted in this doctoral thesis.

Appendix 8.1 - Scientific publications

nature communications

Article

https://doi.org/10.1038/s41467-024-47799-z

CAR affinity modulates the sensitivity of CAR-T cells to PD-1/PD-L1-mediated inhibition

Received: 6 October 2023

Accepted: 12 April 2024

Published online: 26 April 2024

Check for updates

Irene Andreu-Saumell[1,5], Alba Rodriguez-Garcia[1,5] ✉, Vanessa Mühlgrabner[2], Marta Gimenez-Alejandre[1], Berta Marzal[1], Joan Castellsagué[1], Fara Brasó-Maristany[1], Hugo Calderon[1], Laura Angelats[1,3], Salut Colell[1], Mara Nuding[1], Marta Soria-Castellano[1], Paula Barbao[1], Aleix Prat[1,3,4], Alvaro Urbano-Ispizua[1,3], Johannes B. Huppa[2] & Sonia Guedan[1] ✉

Chimeric antigen receptor (CAR)-T cell therapy for solid tumors faces significant hurdles, including T-cell inhibition mediated by the PD-1/PD-L1 axis. The effects of disrupting this pathway on T-cells are being actively explored and controversial outcomes have been reported. Here, we hypothesize that CAR-antigen affinity may be a key factor modulating T-cell susceptibility towards the PD-1/PD-L1 axis. We systematically interrogate CAR-T cells targeting HER2 with either low (LA) or high affinity (HA) in various preclinical models. Our results reveal an increased sensitivity of LA CAR-T cells to PD-L1-mediated inhibition when compared to their HA counterparts by using in vitro models of tumor cell lines and supported lipid bilayers modified to display varying PD-L1 densities. CRISPR/Cas9-mediated knockout (KO) of PD-1 enhances LA CAR-T cell cytokine secretion and polyfunctionality in vitro and antitumor effect in vivo and results in the downregulation of gene signatures related to T-cell exhaustion. By contrast, HA CAR-T cell features remain unaffected following PD-1 KO. This behavior holds true for CD28 and ICOS but not 4-1BB co-stimulated CAR-T cells, which are less sensitive to PD-L1 inhibition albeit targeting the antigen with LA. Our findings may inform CAR-T therapies involving disruption of PD-1/PD-L1 pathway tailored in particular for effective treatment of solid tumors.

Clinical outcomes achieved until date with CAR-T cell therapy for the treatment of solid tumors are yet far from the unprecedented success witnessed in hematologic malignancies[1]. In spite of this, recent works provide clear evidence of objective antitumor responses in patients with hard to treat solid tumors[2–4]. These results are highly encouraging and provide proof of the potential of CAR-T cells in this setting. Nevertheless, several obstacles remain to be addressed, including T cell inhibition within the suppressive tumor microenvironment (TME)[5].

One of the most prominent and well-studied T cell inhibitory axis is the PD-1/PD-L1 immune checkpoint pathway. T cell activation

[1]Oncology and Hematology Department, Fundació Clínic Recerca Biomédica- IDIBAPS, Barcelona, Spain. [2]Medical University of Vienna, Center for Pathophysiology, Infectiology and Immunology, Institute for Hygiene and Applied Immunology, Vienna, Austria. [3]Department of Medicine, University of Barcelona, Barcelona, Spain. [4]Institute of Cancer and Blood Diseases, Hospital Clínic de Barcelona, Barcelona, Spain. [5]These authors contributed equally: Irene Andreu-Saumell, Alba Rodriguez-Garcia. ✉e-mail: rodriguez6@recerca.clinic.cat; sguedan@recerca.clinic.cat

following antigen recognition results in PD-1 upregulation, along with an intracellular signaling cascade that leads to the release of Th1 cytokines. These cytokines, in turn, induce the upregulation of the inhibitory ligand PD-L1 on tumor cells but also on other cell populations within the TME. The interaction between PD-1 on T cells and PD-L1 on tumors ultimately leads to T cell suppression[6,7]. As these activated T cells are potentially tumor-specific infiltrating T cells (either endogenous or adoptively transferred T cells modified to express tumor-specific TCR or CARs), preventing the binding between PD-1 and PD-L1 might rescue antitumor T cell cytotoxicity and result in increased efficacy of cell-based immunotherapies.

A variety of methodologies including immune checkpoint blockade antibodies (in combination or secreted by the CAR-T cells themselves), downregulation of PD-1 (by shRNA or by relocating PD-1 to Golgi/ endoplasmic reticulum (ER) using retention peptides), genetic disruption (by TALEN or CRISPR/Cas9) or dominant negative receptors (DNR) have been used to increase the potency of CAR-T cells. Although the majority of reports demonstrate an advantage of targeting the PD-1/PL1 axis in terms of increased anti-tumor properties[8–17], it is worth noting that some studies have raised concerns about adverse effects associated with long-term PD-1 disruption, including induction of T cell exhaustion and impaired persistence[18,19], implying certain discrepancies in the field. Conflicting findings observed in these investigations can be attributed to several factors, including variability in (i) PD-1 disruption methodology, (ii) preclinical models and (iii) CAR constructs employed.

In this work, we hypothesize that CAR affinity is a key underexplored factor modulating T cell sensitivity to PD-1/PD-L1 axis. To address the model variability issue and gain deeper understanding on how CAR affinity for the targeted antigen might influence this pathway, we develop a preclinical model of tumor cell lines engineered to express different PD-L1 densities (absent, low, or high) for systematic interrogation of different CAR configurations both in vitro and in vivo. We also develop a synthetic model of glass-supported lipid bilayers (SLBs) with controlled amounts of both target antigen and PD-L1 molecules. Using these preclinical models, we explore the effects of inhibiting the PD-1/PD-L1 axis on CAR-T cells targeting their cognate antigen with either low (LA) or high affinity (HA) and comprising different co-stimulatory domains (CD28, ICOS, and 4-1BB). We find that LA CAR-T cells are more sensitive to PD-1/PD-L1 axis-mediated inhibition compared to HA CARs. Consequently, PD-1 disruption enhances the functionality of LA CAR-T cells, while it does not provide an advantage to HA CAR-T cells. This is true for CD28 and ICOS co-stimulation domains, while 4-1BB co-stimulated CAR-T cells are intrinsically more resistant to PD-L1-mediated inhibition regardless of the affinity for the targeted antigen.

Results

PD-1/PD-L1 inhibition restores in vitro functionality of LA but does not impact HA CAR-T cells

To study the role of PD-1/PD-L1 axis on CAR-T cells under controlled conditions, we first generated a tumor model based on the ovarian cancer cell line SKOV3, which was engineered to express varying PD-L1 densities (negative, low or high). We validated HER2 expression across all generated cell lines (Supplementary Fig. 1a) and confirmed expected patterns of PD-L1 expression both in vitro (Fig. 1a) and in xenograft tumors in vivo (Fig. 1b). Moreover, we compared them to those found in wild-type (WT) tumor cell lines from different tissues, including SKOV3, either at basal levels or after co-culture with CAR-T cells (Supplementary Fig. 1b, c). We validated that our model is representative of the various densities of PD-L1 found physiologically in different tumor cell lines. In parallel, we generated CD28-costimulated CAR-T cells targeting HER2 either with high affinity (HA) by using the trastuzumab-based 4D5 scFv, or with low affinity (LA) by using a mutated version of the previous with a ~2000-fold reduced affinity, named 4D5.5 (Fig. 1c)[20].

We assessed the expression levels of surface CAR (Fig. 1d and Supplementary Fig. 1d) and PD-1 (Fig. 1e). Both LA and HA mock CAR-T cells exhibited comparable levels of CAR and PD-1 expression of approximately 70%. This substantial PD-1 expression was indicative of a robust T-cell activation during primary expansion. Subsequently, by employing CRISPR/Cas9-mediated gene editing to KO PD-1, we observed a significant reduction in PD-1 expression levels (Fig. 1e). We consistently achieved ablation efficiencies of approximately 80% in all normal donors used (Fig. 1f). PD-1 deletion did not impact T-cell expansion (Supplementary Fig. 1f) or CAR-mediated activation, as evidenced by similar population doublings and uniform CD25 upregulation in both edited and mock CAR-T cells following re-stimulation (Supplementary Fig. 1g).

To determine the effects of PD-1 ablation on CAR-T cell function, we co-cultured mock or PD-1 KO HER2-28Z CAR-T cells of LA or HA with our PD-L1 cellular model and measured cytokine secretion. In the absence of PD-L1 expression by tumor cells, both mock and PD-1 KO LA CAR-T cells released similar amounts of IFN-γ. Conversely, PD-L1 expressed by SKOV3 either at low or high levels suppressed IFN-γ secretion by mock CAR-T cells. This loss in cytokine release was restored by genetic disruption of PD-1 (Fig. 1g). In contrast, PD-1 KO in HA CAR-T cells led to non-significant increases in cytokine release, implying a higher resistance of HA CAR-T cells to PD-L1 mediated inhibition (Fig. 1h). Similar results were observed when the PD-1/PD-L1 axis was targeted in LA and HA CAR-T cells using blocking antibodies against PD-1 or PD-L1 (Fig. 1i, j) and for the secretion of IL-2 (Supplementary Fig. 2a–d). We validated these findings in an alternative pair of CARs targeting FRβ with different affinities (Fig. 1c and Supplementary Fig. 3a–c)[21]. By using the SKOV3-based PD-L1 cellular model in which we overexpressed FRβ (Supplementary Fig. 3d), we found significantly higher levels of IFN-γ secreted by PD-1 KO LA CAR-T cells as compared to mock in the presence of PD-L1 (Fig. 1k, left panel). These differences were not observed in co-culture with the PD-L1 KO cell line or between PD-1 KO and mock HA CAR-T cells, which released similar levels of IFN-γ regardless of PD-L1 presence (Fig. 1k, right panel). While the differences in affinity were less pronounced for the FRβ-targeting CAR pair (21.89-fold), these findings align with our observations from the HER2 model.

We next tested the hypothesis that lack of PD-1 expression promotes enhanced proliferation in CAR-T cells. To this end, we co-cultured mock or PD-1 KO LA and HA HER2-28Z CAR-T cells with the breast cancer cell line HCC1954, selected due to its high expression levels of HER2 and PD-L1 (Supplementary Fig. 1c, d). Our findings revealed a two-fold increase in the proliferation of LA PD-1 KO CAR-T cells as compared to mock CAR-T cells 6 days after stimulation. In line with the cytokine secretion results, PD-1 KO did not provide a proliferative advantage to HA CAR-T cells (Fig. 1l).

PD-1 KO increases efficacy of LA but not HA HER2-28Z CAR-T cells in vivo

We next aimed to evaluate the impact of PD-1/PD-L1 axis on the therapeutic potential of HER2-28Z CAR-T cells in vivo. NSG mice bearing SKOV3 subcutaneous tumors expressing different levels of PD-L1 were treated with a single dose of control T cells, mock or PD-1 KO CAR-T cells. In line with cytokine release data obtained in vitro, both mock and PD-1 KO LA CAR-T cells showed similar anti-tumor activity and efficiently eliminated tumors that did not express PD-L1 (Fig. 2a, left panel). However, even low levels of PD-L1 expression impaired the anti-tumor efficacy of LA HER2 CAR-T cells. PD-1 ablation significantly enhanced anti-tumor responses, resulting in complete regressions in 90% of tumors expressing either low or high levels of PD-L1 (Fig. 2a, middle and right panels). We validated these results with CAR-T cells in combination with anti-PD-L1 blocking antibodies in high PD-L1-

https://doi.org/10.1038/s41467-024-47799-z

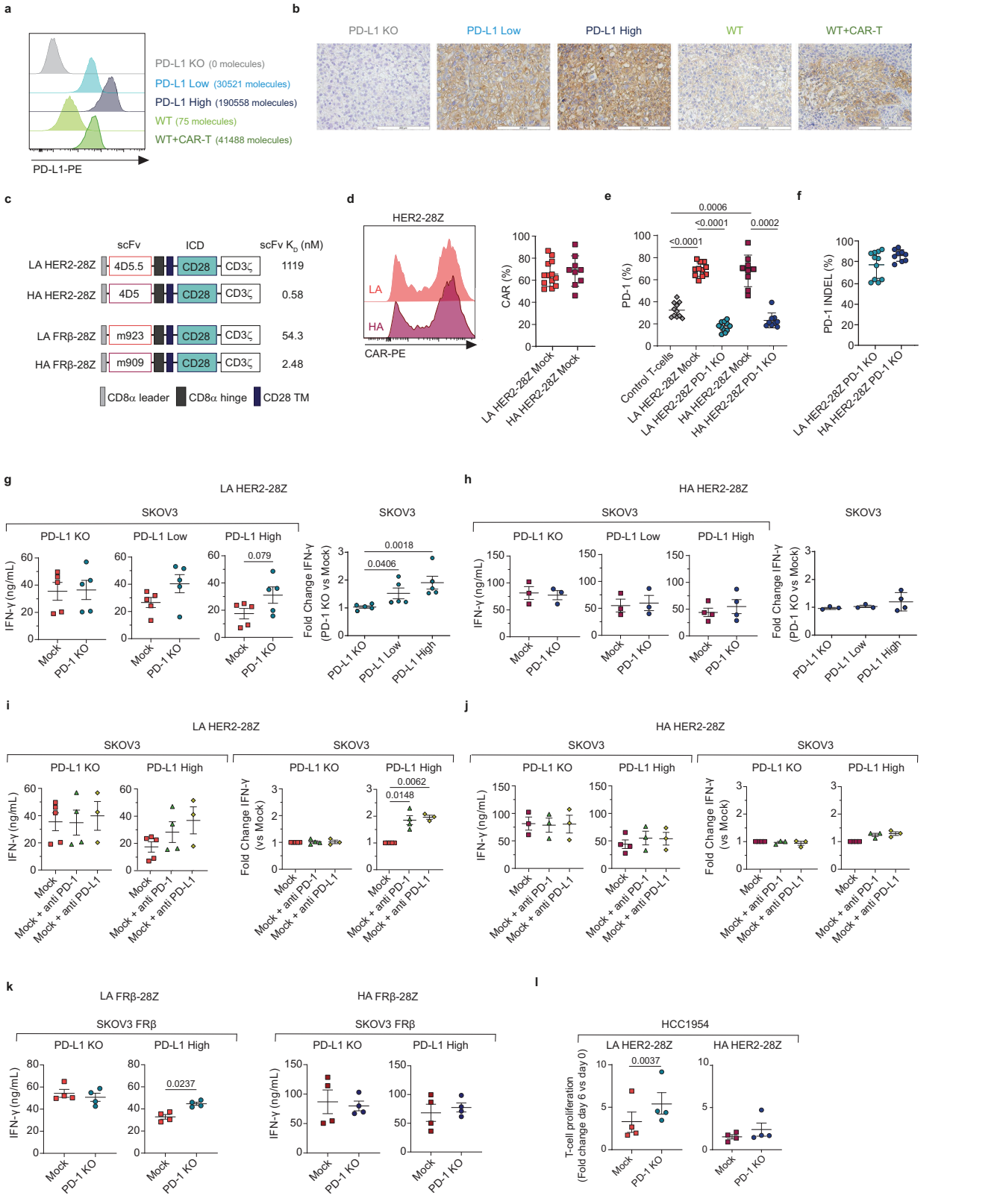

expressing SKOV3 cells. Even though the combination with antibodies improved the anti-tumor effect of CAR-T cells alone, PD-1 KO CAR-T cells still showed the best efficacy (Fig. 2b, c). Regarding HA CAR-T cells, both mock and PD-1 KO were able to eliminate nearly all tumors, including those with the highest PD-L1 expression levels (Fig. 2d). We then measured the anti-tumor efficacy in WT SKOV3 cells, expressing physiological levels of PD-L1. Again, PD-1 KO provided a significant advantage only to LA CAR-T cells (Fig. 2e), while the efficacy of HA CAR-T cells was not further improved (Fig. 2f). As HA mock CAR-T cells were able to eliminate tumors in all models tested, we repeated the in vivo experiment in SKOV3 WT cell line using more challenging conditions and treating larger tumors. We consistently found no significant differences between mock and PD-1 KO CAR-T cells, except for a noticeable reduction in overall efficacy observed in both groups

Fig. 1 | PD-1 KO restores LA HER2-28Z CAR-T cell function in vitro but does not affect HA HER2-28Z CAR-Ts. a Expression and quantification of PD-L1 molecules in SKOV3 cells expressing variable PD-L1 densities and compared to wild type (WT) cells alone or co-cultured with CAR-T cells for 48 h as assessed by flow cytometry. **b** Immunohistochemical staining of PD-L1 in SKOV3 PD-L1 KO, Low, High, and WT tumors treated with control T-cells or CAR-T cells at day 20–70 post-implantation in mice. Representative images from $n = 2$ tumors per group are shown. Scale bar, 200 μm. **c** Schematic overview of CAR constructs used with their corresponding affinity values. HER2-28Z CAR-T cells with LA or HA and with or without PD-1 genome editing were generated from 9 to 13 healthy donors. CAR (**d**) and PD-1 (**e**) expression were quantified by flow cytometry and the efficiency of PD-1 knock-out (**f**) was quantified by using ICE tool (Synthego). LA (**g**, **i**) or HA (**h**, **j**) HER2-28Z CAR-T cells were co-cultured with indicated SKOV3 cells for 24 h. The PD-1/PD-L1 axis was inhibited by knocking out PD-1 (**g**, **h**) or by addition of blocking antibodies (**i**, **j**). IFN-γ production was analyzed by ELISA ($n = 3–5$). Data is represented as absolute levels (left panel) or as fold change versus mock (right panel). **k** LA (left panel) or HA (right panel) FRβ−28Z CAR-T cells were co-cultured with SKOV3 expressing FRβ and indicated PD-L1 densities. IFN-γ production was quantified by ELISA ($n = 4$). **l** T-cell proliferation of LA (left panel) or HA (right panel) HER2-28Z CAR-T cells following co-culture with HCC1954. Fold change of absolute T-cell numbers at day 6 versus day 0 is represented ($n = 4$). Data in (**d**–**l**) are pooled from independent experiments where each dot represents CAR-T cells generated from a different donor (n) and represented as mean ± SD (in **d**–**f**) or mean ± SEM (in **g**–**l**). p values by a two-tailed paired T test (**e**, **g**, **h** for absolute levels graphs, **k**, **l**), one-way ANOVA (**g**, **h** for fold change graphs) or two-tailed one sample T test (**i**) are indicated. Source data and exact n values for each group in (**d**–**j**) are provided as a Source Data file.

(Supplementary Fig. 4). Similar results in terms of enhanced anti-tumor activity by PD-1 KO LA HER2-28Z CAR-T cells were observed in the breast cancer model HCC1954 (Fig. 2g). Collectively, these findings indicate that genetic disruption of PD-1 enhances the anti-tumor effect of LA HER2-28Z CAR-T cells in tumors expressing PD-L1, while it does not impact the efficacy of HA CAR-T cells.

Affinity-based differences to inhibition by PD-L1 are maintained in a lipid bilayer system

To ensure that differences observed between LA and HA CAR-T cells upon PD-1 ablation were not due to intrinsic changes in tumor cells derived from differential expression of PD-L1, we utilized a supported lipid bilayer system (SLB) functionalized with the intercellular adhesion molecule 1 (ICAM-1) to facilitate cell attachment, HER2 for CAR recognition and PD-L1 at titrated densities (Fig. 3a)[22,23]. Presence of PD-1 on the CAR-T cell membrane was confirmed by flow cytometry before adding the cells to the system, ensuring its interaction with the PD-L1 in the bilayer (Supplementary Fig. 5). After exposing LA and HA mock or PD-1 KO CAR-T cells to the SLBs, we determined their respective activation levels via IFN-γ secretion. In line with results obtained in the cellular model, IFN-γ release by LA mock CAR-T cells was reduced in the presence of high densities of PD-L1, and this inhibition was reversed by PD-1 KO (Fig. 3b, left panel and 3c). In contrast, secretion of IFN-γ by both mock and PD-1 KO HA CAR-T cells remained unaltered at all PD-L1 concentrations tested (Fig. 3b, right panel and 3d). Overall, differences in IFN-γ secretion between LA and HA HER2-28Z CAR-T cells in the presence of PD-L1 persisted in this system, thereby confirming that they were indeed attributable to PD-L1.

PD-1 KO induces deeper changes in the transcriptome of LA as compared to HA HER2-28Z CAR-T cells

In order to characterize the molecular mechanisms behind the different effects of PD-1 disruption in LA and HA HER2-28Z CAR-T cells, we compared the transcriptomic profile of mock and PD-1 KO CAR-T cells following antigen recognition by using the nCounter® CAR-T Characterization Gene Expression Panel (Nanostring Technologies). Knocking PD-1 out of LA HER2-28Z CAR-T cells resulted in statistically significant downregulation of 20 genes and upregulation of 13 genes out of the 780 genes analyzed in the panel (Fig. 4a, b, left panels). Within upregulated genes in PD-1 KO versus mock LA HER2 CAR-T cells we found FosB, a transcription factor that has been previously reported to be decreased in exhausted T cells during chronic viral infection[24] while increased in CAR-T cells from responding as compared to non-responding patients[25]. Other upregulated genes included T-cell activation-related genes such as effector cytokines (IFN-γ, TNF, IL-2, CSF2/GM-CSF or CLCF1), chemokines (CCL3, CCL4, CCL20, XCL1/2) or co-stimulatory molecules (TNFSF9/4-1BBL). Genes that were downregulated in the PD-1 KO CAR-T cells included the transcription factor MAF, regulon driver of T cell exhaustion[24,26], genes related to type I and II IFN signaling (IRF9, ADAR, SP100, SOCS2, ISG15, STAT1, STAT2, IFIT1, IRF7, PML, IFI35), which have been recently linked to CAR-T cell dysfunction[27–29], CD68 (which is primarily a marker for macrophages but also found constitutively expressed on NK cells) and members of the B7 ligands family (CD86 and CD276/B7-H3). By contrast, only 7 genes were differentially expressed between mock and PD-1 KO in the HA HER2-28Z CAR-T cells, with the memory marker IL7R being the most relevant and upregulated in the PD-1 KO group (Fig. 4a, b, right panels). To provide deeper insight into the biological functions underlying the entire dysregulated gene expression signature pertaining to the comparison of mock and PD-1 KO LA CAR-T cells, we performed gene enrichment analysis[30,31]. As anticipated, we observed a significant enrichment in categories related to cytokine signaling, two of which were related to type 1 IFN signaling pathways (Fig. 4c and Supplementary Fig. 6a).

To better understand the intrinsic differences between LA and HA CAR-T cells that could explain the differential sensitivity towards the PD-1/PD-L1 axis, we directly compared the transcriptomic profile of both groups. We found that LA HER2-28Z CAR-T cells expressed preferentially genes associated with a more naïve phenotype such as TCF7, LEF1 and CD45RA[28,32,33], while HA CAR T-cells showed higher expression of the exhaustion-related transcription factor MAF (Supplementary Fig. 6b). We also compared the transcriptome of PD-1 KO LA HER2-28Z CAR-T cells with that of HA CAR-T cells, as both presented with similar anti-tumor activity. Regardless, PD-1 KO LA HER2-28Z CAR-T cells displayed a less exhausted phenotype with higher expression of BCL6, FOSB or TCF7 and lower expression of genes related to exhaustion such as IRF4, CTLA4, FAS or MAF (Supplementary Fig. 6c).

PD-1 KO increases the polyfunctionality of LA but not HA HER2-28Z CAR-T cells

Since a number of transcriptional changes involved genes encoding cytokines and because the polyfunctionality of CAR-T cells had been previously correlated with improved clinical outcomes[34], we sought to assess whether genetic ablation of PD-1 increased the polyfunctionality of HER2-28Z CAR-T cells after antigen exposure. To this end, we performed a single-cell secretome analysis of low and high affinity HER2-28Z CAR-T cells after antigen exposure by using the Adaptive Immune cytokine panel (Isoplexis). We first observed in 3D t-SNE analysis that mock and PD-1 KO LA CAR-T cells segregated in separated clusters, revealing key functional differences between the groups (Fig. 5a). By contrast, in HA CAR-T cells, mock and PD-1 KO groups did not cluster separately, suggesting a more homogenous functional profile (Fig. 5b). These results are in agreement with the gene expression analysis (Fig. 4). In a deeper analysis, PD-1 KO in the LA HER2-28Z CAR-T cells showed trends towards increased percentages of cells producing two or more cytokines both in $CD4^+$ and $CD8^+$ T cell populations (Fig. 5c). We also measured the polyfunctional strength index (PSI), which accounts for levels and functional classification of the secreted cytokines. This analysis revealed an overall PSI increase by PD-1 disruption in LA HER2 CAR-T cells and a predominance of effector cytokines in all groups (Fig. 5e). In contrast, knocking out PD-1 in HA HER2-28Z CAR-T cells did not significantly increase T-cell polyfunctionality or PSI,

https://doi.org/10.1038/s41467-024-47799-z

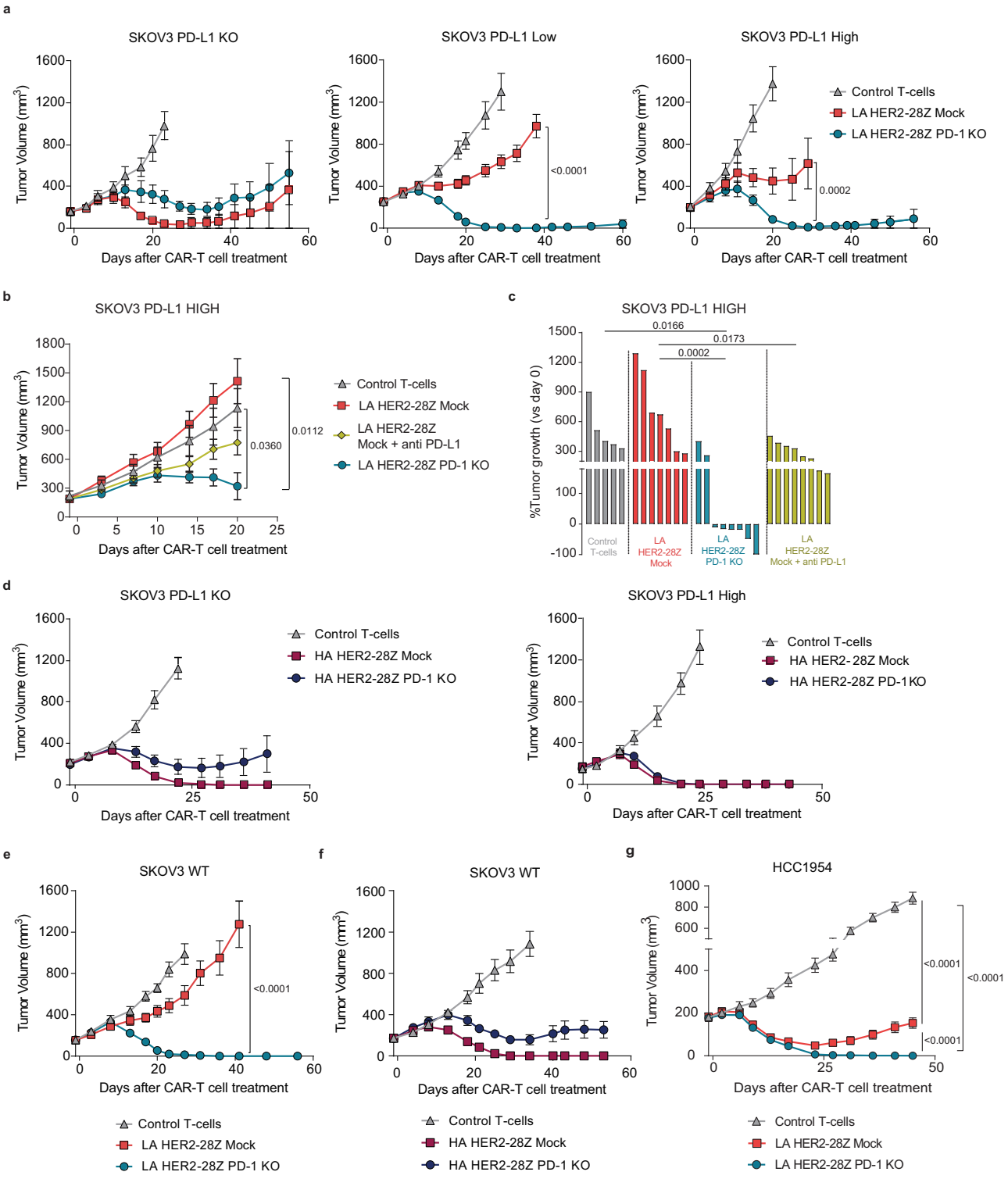

implying a less profound impact of PD-1 disruption (Fig. 5d, f). In addition, single-cell secretome analysis suggested a reduced expression of regulatory cytokines such as IL-13, IL-22 or IL-4 by LA PD-1 KO CAR-T cells, while PD-1 ablation did not alter the expression of these cytokines in HA CAR-T cells (Supplementary Fig. 7a).

To confirm the results obtained in the polyfunctionality study, we performed an intracellular cytokine staining (ICS) assay. While the PMA-Ionomycin-treated groups exhibited consistent outcomes across all experimental conditions (Supplementary Fig. 7b, c), PD-1 KO enhanced the frequency of CAR-T cells concurrently releasing IFN-γ and TNF-α during co-culture with HER2+ tumor cells in the context of LA CAR-T cells. Conversely, no discernible effect between mock and PD-1 KO groups on HA CAR-T cells was observed (Fig. 5g, h). Of note, frequencies of IFN-γ^{+}TNF-α^{+} T cells in mock groups from LA and HA CAR-T cells were comparable.

Altogether, the upregulation of genes associated with T-cell activation alongside the augmented polyfunctionality could contribute to the heightened anti-tumor efficacy observed in LA HER2-28Z PD-1 KO.

Fig. 2 | PD-1 KO restores LA HER2-28Z CAR-T cell function in vivo but does not affect HA HER2-28Z CAR T-cells. a Tumor measurements of NSG mice bearing SKOV3 tumors expressing indicated PD-L1 densities and treated with 3–4 × 10^6 control T-cells, mock or PD-1 KO LA HER2-28Z CAR$^+$-T cells (n = 8 for SKOV3 PD-L1 KO and PD-L1 High; n = 8, 13 or 12 for control, mock and PD-1 KO groups, respectively, for SKOV3 PD-L1 Low). **b**, **c** NSG mice bearing SKOV3 PD-L1 High tumors were treated with 3 × 10^6 control T-cells (n = 5), mock (n = 7), mock + anti PD-L1 antibody (n = 7) or PD-1 KO (n = 8) LA HER2-28Z CAR$^+$-T cells. **b** Tumor measurements and (**c**) percentage of tumor growth indicated as the change in tumor volume on day 20 versus baseline is shown. **d** Tumor measurements of NSG mice bearing SKOV3 tumors expressing indicated PD-L1 densities and treated with 3–4 × 10^6 control T-cells, mock or PD-1 KO HA HER2-28Z CAR$^+$-T cells (n = 8, 13 and 12 for control, mock and PD-1 KO groups, respectively, for SKOV3 PD-L1 KO; n = 8 for SKOV3 PD-L1 High). Tumor measurements of NSG mice bearing SKOV3 wild type tumors treated with 3 × 10^6 control T-cells, mock or PD-1 KO HER2–28Z CAR$^+$-T cells of (**e**) LA (n = 8 for control and n = 10 for mock and PD-1 KO groups) or (**f**) HA (n = 8 for all groups). **g** Tumor measurements of NSG mice bearing HCC1954 tumors treated with 3 × 10^6 control T-cells (n = 9), mock (n = 10) or PD-1-KO (n = 10) LA HER2-28Z CAR$^+$-T cells. Data in (**a**, **b**) and (**d**–**g**) are represented as mean tumor volume ±SEM and n indicates tumors per group. p values by (**c**) one-way ANOVA with Tukey post-hoc test or (**a**, **b**, **d**–**g**) two-way ANOVA with Tukey's multiple testing correction are indicated. Source data are provided as a Source Data file.

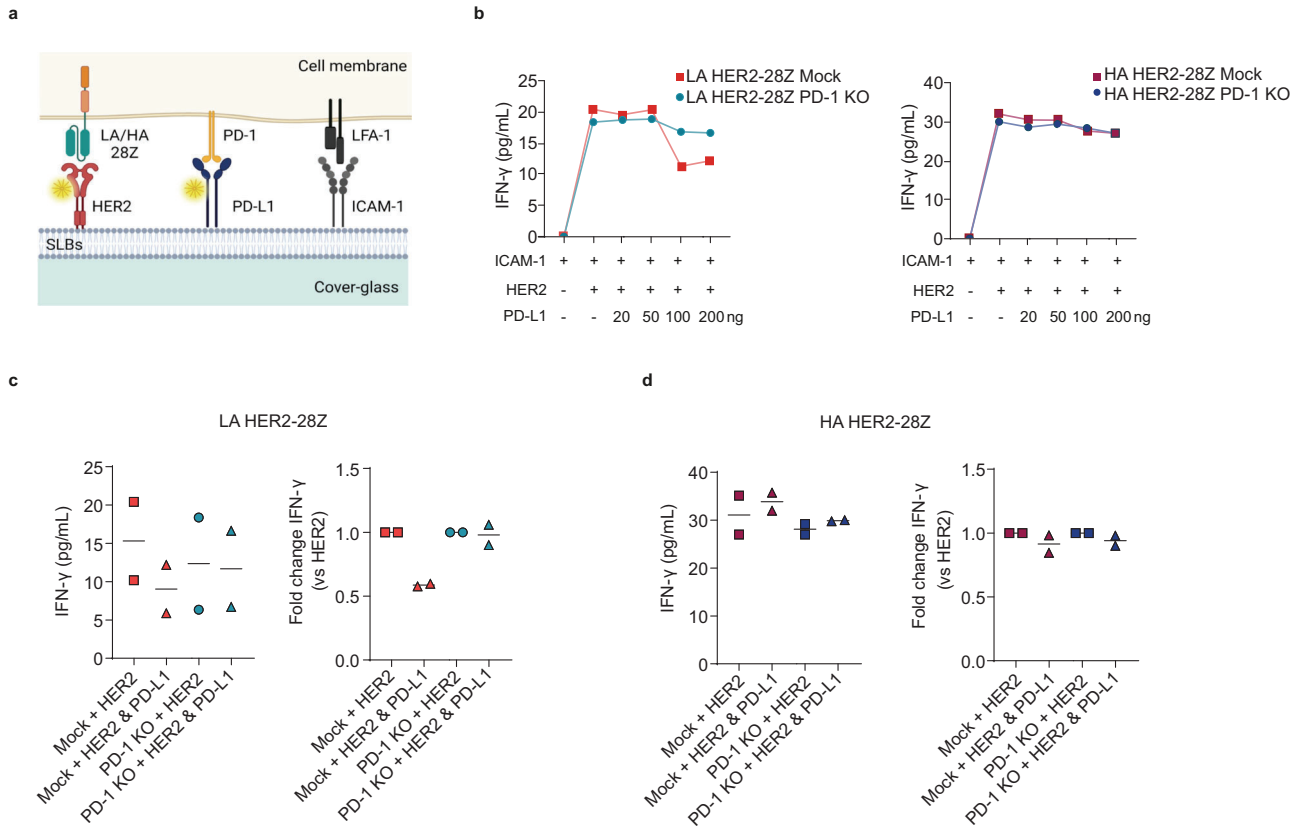

Fig. 3 | HA HER2-28Z CAR-T cells are more resistant to inhibition by increasing amounts of PD-L1 in a protein-functionalized planar glass SLB system. **a** Schematic representation of an SLB featuring fluorescently labeled proteins (HER2 and PD-L1) and ICAM-1. Created with Biorender.com. **b** IFN-γ production by HER2-28Z mock and PD-1-KO LA (left panel) or HA (right panel) CAR-T cells after 24 h of co-culture with SLBs containing increasing concentrations of PD-L1. HER2-28Z mock and PD-1-KO (**c**) LA or (**d**) HA CAR-T cells were co-cultured for 24 h with SLBs containing either HER2 alone (2 ng) or HER2 along with PD-L1 (200 ng). IFN-γ secretion as measured by ELISA is represented as absolute levels (left panel) or fold change of the HER2 + PD-L1 condition compared to HER2 alone (right panel). Data in (**b**) is representative of two different donors and in (**c**, **d**) is shown as mean of two different donors (n = 2). Source data are provided as a Source Data file.

Remarkably, the witnessed lack of distinguishable transcriptional changes at the transcriptomic level and in polyfunctionality supports the notion that PD-1 KO does not significantly impact the functional properties of HA HER2-28Z CAR-T cells.

LA PD-1 KO display a safer toxicity profile as compared to HA HER2-28Z CAR-T cells

Using CAR-T cells resistant to the inhibition by the PD-1/PD-L1 axis may be an attractive strategy for the treatment of solid tumors. However, safety concerns arise when targeting tumor associated antigens using a high affinity CAR, as it may exhibit poor discrimination between tumor and healthy tissues expressing lower levels of the target antigen. To address this concern, we established co-cultures of LA or HA HER2-28Z CAR-T cells with or without PD-1 KO and a panel of human primary healthy cells including Epidermal Keratinocytes (NHEK), Renal Epithelial Cells (HREpC), Pulmonary Artery Endothelial Cells (HPAEC) and Pulmonary Artery Smooth Muscle Cells (HPASMC), all of which have been reported to express low but detectable HER2 densities[20]. Both LA and HA HER2-28Z CAR-T cells demonstrated comparable reactivity against a control cancer cell line expressing high HER2 levels (Supplementary Fig. 8a–e). However, only HA CAR-T cells were activated in response to co-culture with healthy cells as evidenced by increased production of CD107-α, IFN-γ and IL-2 (Fig. 6a, b, c, and Supplementary Fig. 8f, respectively), raising safety concerns. Of note, PD-1 KO did not exacerbate the reactivity of LA HER2-28Z CAR-T cells against primary cells from healthy tissues, which showed a toxicity profile similar to non-tumor specific control T cells.

Target antigen densities and CAR expression play a role in determining sensitivity to PD-L1

We then investigated how target antigen densities influence the heightened resistance of HA CAR-T cells to the PD-1/PD-L1 axis. We

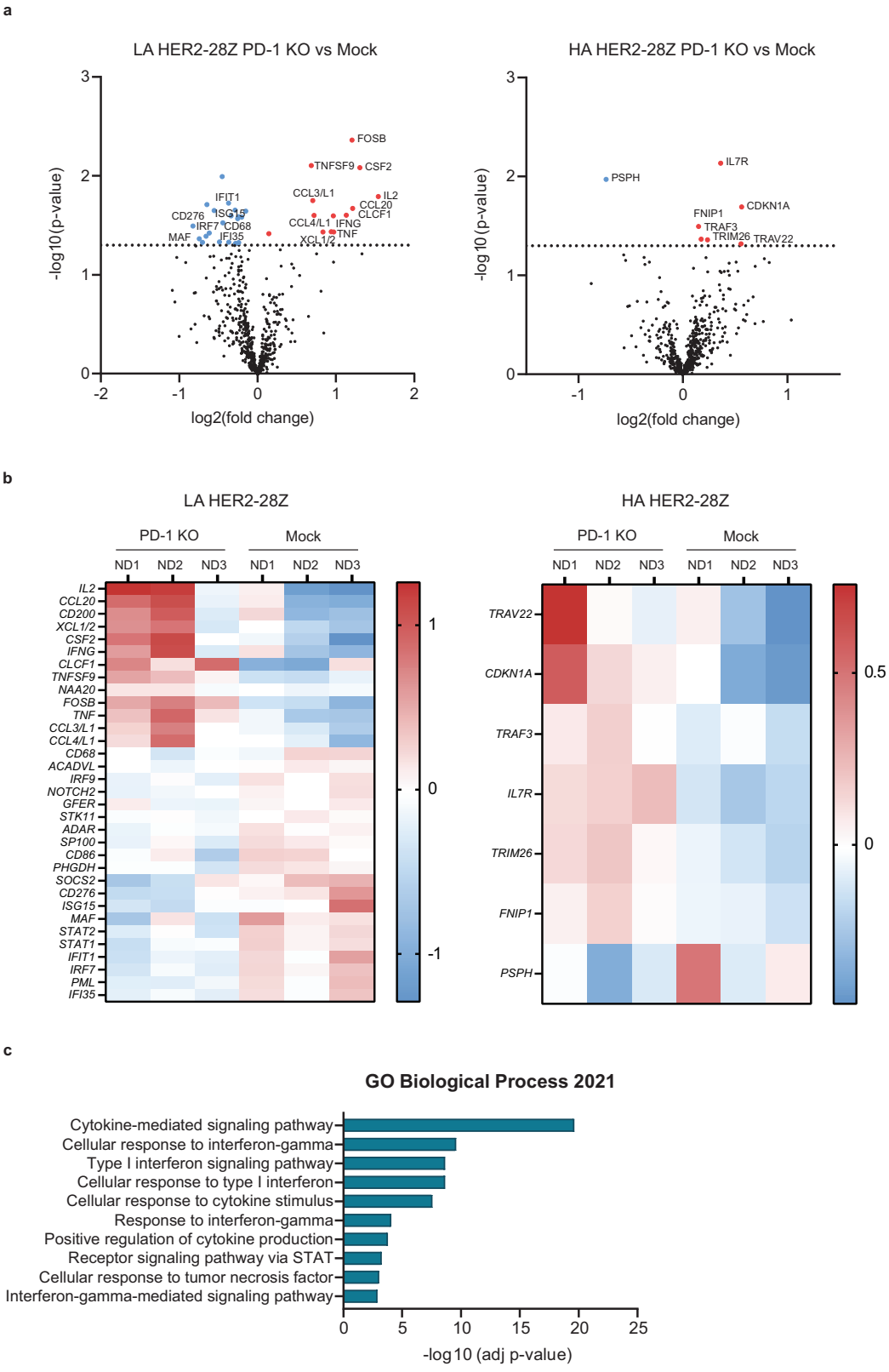

hypothesized that HA CAR-T cells might become susceptible to this inhibitory pathway under conditions of low antigen densities.

To explore this, we took advantage of the lipid bilayer model outlined in Fig. 3a to titrate down HER2 densities while maintaining constant high levels of PD-L1. In this controlled environment, HA CAR-T cells remained unaffected by PD-L1, as indicated by comparable levels of IFN-γ released by mock CAR-T cells across all HER2 conditions. Of note, at the lowest antigen levels, mock and PD-1 KO exhibited similar behavior, while as HER2 levels increased, PD-1 KO appeared to have a detrimental effect (Fig. 7b). In the LA setting, PD-1 KO conferred an advantage to CAR-T cells at all antigen density conditions tested (Fig. 7a).

Next, we employed a cellular model based on a triple-negative breast cancer cell line, MDA-MB-468, engineered to express either low

Fig. 4 | Differential transcriptomic response of HA and LA HER2-28Z CAR-T cells to PD-1 KO. Transcriptomic analysis of mock and PD-1 KO LA or HA HER2-28Z CAR-T cells was performed after stimulation with SKOV3 WT tumor cells for 48 h. **a** Volcano plots of differential expression between mock and PD-1 KO in LA (left panel) or HA (right panel) HER2-28Z CAR-T cells. Red dots represent genes upregulated in PD-1 KO vs mock, blue dots represent genes downregulated genes in PD-1 KO vs mock and black dots represent genes not differentially expressed. Differentially expressed genes are annotated. The horizontal line is at an adjusted *p* value of 0.05. **b** Heat map of differential expression between mock and PD-1 KO in LA (left panel) or HA (right panel) HER2−28Z CAR-T cells. **c** Gene Ontology (GO) Biological process of differentially expressed genes between PD-1 KO and mock LA HER2-28Z CAR-T cells. Data in (**a**–**c**) is represented as mean of $n = 3$ donors. In (**a**, **b**) *p* value thresholds ($p < 0.05$) were derived from Rosalind and adjusted using the Benjamini–Hochberg method. In (**c**) *p* value thresholds ($p < 0.05$) were derived from Enrichr by a Fisher exact test and adjusted using the Benjamini–Hochberg method. All tests were two-sided. Source data are provided as a Source Data file.

or high levels of HER2 along with constitutive high levels of PD-L1 (Supplementary Fig. 9a). Consistent with our observations in the SKOV3 model, PD-1 KO provided an advantage to LA CAR-T cells when HER2 levels were high. However, under conditions of high antigen densities, HA HER2-28Z CAR-T cells did not benefit from PD-1 KO (Fig. 7c, e–f). Conversely, in co-culture with HER2-low cells, PD-1 KO conferred an advantage to HA CAR-T cells under certain settings, reaching statistical significance in terms of increased percentage of polyfunctional T cells producing both IFN-γ and TNF-α (Fig. 7e, g and Supplementary Fig. 9c, d) and IL-2 secretion (Supplementary Fig. 9b), but not in IFN- γ as measured by ELISA (Fig. 7d). In line with toxicity results in Fig. 6, LA HER2-28Z CAR-T cells did not exhibit reactivity in low antigen conditions.

Based on these results, we hypothesized that PD-L1-mediated inhibition could potentially be overcome at a certain threshold of T-cell activation, and that this could also be achieved by utilizing T-cell products with high percentage of CAR transduction. To validate this hypothesis, we conducted studies with T-cell products containing more than 75% CAR^+ T cells (High CAR) as compared to products containing 50-65% CAR^+ T cells (Low CAR) (Fig. 7h). In this scenario, the advantage provided by PD-1 KO in the LA CAR-T cells was lessened (Fig. 7i), similar to our observations in the HA setting (Fig. 7j).

Overall, our results demonstrate that although CAR affinity is pivotal in determining sensitivity of CAR-T cells to PD-1/PD-L1 axis, other factors such as antigen density and CAR expression levels may also play a role.

Advantages of PD-1 KO do not apply uniformly across different CAR constructs

To determine whether our observations with CD28-based HER2 CAR-T cells could be applied to CARs containing different co-stimulation domains we first interrogated CARs targeting HER2 with either LA or HA and containing ICOS as a co-stimulatory domain in vivo (Fig. 8a)[35]. As shown in Fig. 8b, we found that PD-1 ablation enhanced the anti-tumor efficacy of LA but not HA HER2 CAR-T cells in mice containing SKOV3 wild-type tumors, consistent with our earlier findings in CD28-based CAR-T cells. Since 4-1BB is a clinically relevant co-stimulatory domain, we also explored how the PD-1/PD-L1 axis impacted 4-1BB co-stimulated LA CAR-T cells (HER2-BBZ, Fig. 8a). We observed that neither PD-1 KO nor PD-1/PD-L1 blockade by using antibodies increased cytokine secretion in vitro (Fig. 8c) or anti-tumor effect in vivo (Fig. 8d). Higher resistance of 4-1BB-based CARs to PD-L1 was also confirmed in vitro by using CAR-T cells targeting mesothelin also with LA (Mesothelin-BBZ, Fig. 8a and Supplementary Fig. 10c). Differential CAR expression was ruled out as a potential reason for the differing sensitivity to PD-L1-mediated inhibition among constructs with distinct co-stimulatory domains, as ICOS-based CARs, despite being expressed at lower levels as compared to CD28, were still sensitive to PD-1/PD-L1 axis. In contrast, 4-1BB-based CARs exhibited comparable expression levels to CD28 but demonstrated greater resistance to inhibition by PD-L1 (Supplementary Fig. 10a, b). These results can be explained, at least in part, by the lower expression levels of PD-1 when compared to that of CD28- or ICOS co-stimulated CARs (Supplementary Fig. 10d) and are in line with previous studies showing that 4-1BB-based CARs are less sensitive to PD-1 mediated inhibition than CD28-based CARs[8,36].

Finally, we explored if the higher sensitivity to PD-1/PD-L1 inhibitory pathway observed in LA HER2 CAR-T cells was also maintained in CAR-T cells targeting other antigens with LA. To this end we explored the effects of PD-1 KO in CAR-T cells targeting mesothelin with LA and containing the CD28 intracellular domain (Mesothelin-28Z, Fig. 8a)[37]. Interestingly, we observed that in T-cells expressing an anti-mesothelin LA CAR, blocking the PD-1/PD-L1 axis through genetic disruption or with the use of PD-1 or PD-L1 blocking antibodies resulted both in elevated in vitro cytokine secretion (Fig. 8e) and enhanced in vivo anti-tumor effect (Fig. 8f), confirming results obtained with LA HER2-28Z CAR-T cells.

Discussion

The findings reported herein unveil CAR affinity as a factor modulating the sensitivity of CAR-T cells to PD-1/PD-L1 axis. By using a preclinical model of tumor cells expressing varying PD-L1 densities, we found that low affinity CAR-T cells are more sensitive to PD-L1-mediated inhibition as compared to high affinity CARs. Accordingly, PD-1 disruption only impacted positively on the functionality of low affinity CAR-T cells, while high affinity CAR-T cells remained unaltered.

The potential of disrupting PD-1/PD-L1 signaling as a strategy to overcome PD-L1-mediated T cell suppression and to boost the therapeutic index of CAR-T cells has been widely discussed. While most works report increased functionality of PD-1-ablated CAR-T cells[8–17], some others suggest that PD-1 disruption accelerates T cell exhaustion and impairs long-term T cell persistence[18,19]. We identified a lack of consistency within the different articles in terms of the tumor models used, ranging from cell lines engineered to constitutively express high levels of PD-L1 to cell lines expressing physiological levels of PD-L1 in response to CAR-T cell activation. This might in part explain discrepancies in the reported results. Arising from this observation, and by the fact that currently available preclinical models often fail to predict clinical outcomes[38], the first goal of our project was the generation of robust preclinical models for systematic interrogation of different CARs. Our cellular-based model demonstrated to be representative of the range of physiological PD-L1 expression levels observed in different tumor cell lines across cancer types. As an additional preclinical model to validate our findings, we developed glass-supported lipid bilayers (SLBs) mimicking the target cell membrane but containing precisely defined amounts of surface proteins, which supposed a valuable tool that allowed the determination of exact PD-L1 amounts required for T cell inhibition[22].

The most intriguing observation of our work, as observed in both preclinical models, was that HA CAR-T cells were intrinsically more resistant to PD-L1-mediated inhibition as compared to their LA counterparts. Although we primarily used affinity tuned HER2-specific CARs of low and high affinity[20] based on CD28 as co-stimulation domain, similar observations were made for CARs targeting FRβ or mesothelin and ICOS-co-stimulated CARs, suggesting that this effect is not unique for a specific targeted antigen or co-stimulatory domain. More in-deep gene expression and single-cell polyfunctionality analysis after exposure to tumor cells expressing HER2 and physiological PD-L1 levels revealed that whether PD-1 KO induced a significant change in the LA CAR-T cell population at the transcriptomic and functional level, HA CAR-T cells after PD-1 KO remained similar to the mock-electroporated CAR-T cells. In this work, we emphasize CAR affinity as a central factor

https://doi.org/10.1038/s41467-024-47799-z

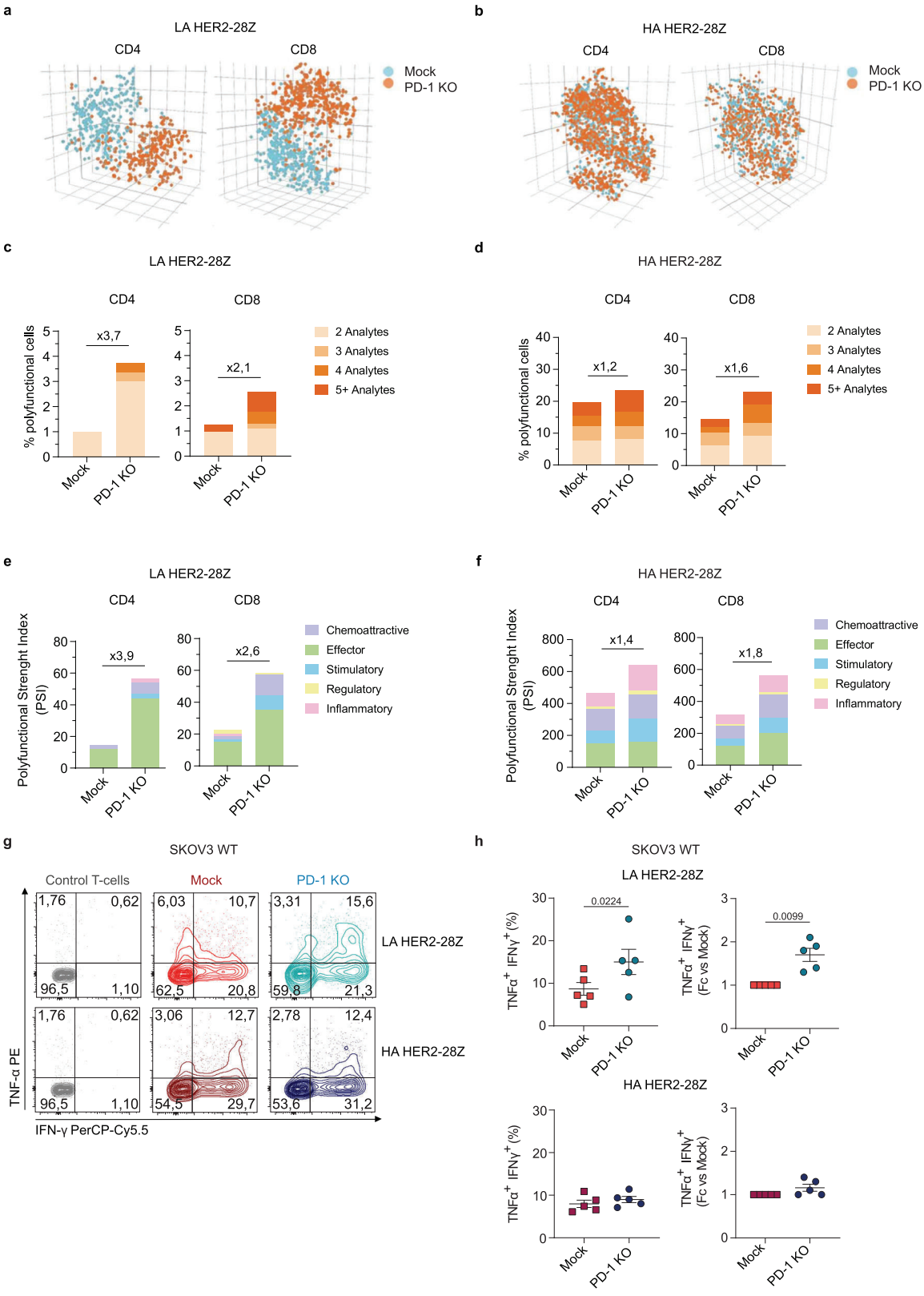

influencing sensitivity to PD-1/PD-L1 axis. Beyond this, we also explored the implications of both target antigen densities and CAR expression frequencies. Intriguingly, we observed that the enhanced resistance of HA CAR-T cells to PD-L1 was attenuated in the presence of low levels of CAR antigen. Conversely, the use of products with higher CAR frequencies appeared to mitigate the sensitivity of LA CAR-T cells to PD-L1-mediated suppression. These findings lead us to postulate that inhibitory effects of PD-L1 on T cells can be overcome when T cell activation reaches a certain threshold. According to our results, this threshold of activation can be attainable not only through the utilization of a high affinity CAR but also by the presence of high CAR frequencies. However, in principle this latter strategy lacks the potential of being translated into the clinical setting due to risk of genotoxicity, given the higher amounts of vector required. Moreover, the use of

Fig. 5 | Polyfunctional profiling of PD-1 KO LA and HA HER2-28Z CAR-T cells. Single-Cell Adaptive Immune panel (Isoplexis) of mock and PD-1 KO LA and HA HER2-28Z CAR-T cells after co-culture with SKOV3 tumor cells for 24 h (E:T = 1:3). Three-dimensional t-SNE plots of (**a**) LA and (**b**) HA mock (blue) and PD-1 KO (orange) HER2-28Z CAR-T cells by differentiating them based on their cytokine functional differences. Frequencies of polyfunctional cells of mock and PD-1 KO (**c**) LA and (**d**) HA HER2-28Z CAR-T cells. Polyfunctionality Strength Index (PSI) of mock and PD-1 KO (**e**) LA and (**f**) HA HER2-28Z CAR-T cells. Fold-change values for PD-1 KO versus mock are indicated. **g** Representative flow cytometry plots of intracellular cytokine staining for TNF-α and IFN-γ in mock and PD-1 KO LA and HA HER2−28Z CAR-T cells after co-culture with SKOV3 tumor cells for 24 hours (E:T = 1:3) (gated on live/CD45$^+$). **h** Frequencies of IFN-γ$^+$TNF-α$^+$ T-cells represented as absolute numbers and fold change of PD-1 KO versus mock are shown. In (**a**–**f**), data is shown as mean from $n = 2$ donors. In (**h**), data is pooled from four independent experiments where each dot represents CAR-T cells generated from a different donor ($n = 5$), and is represented as mean ± SEM. p values by a two-tailed paired T test for absolute numbers or by two-tailed one-sample T test for fold-change graphs are indicated. Source data are provided as a Source Data file.

CAR-T cell products with high CAR expression has been correlated to worse clinical responses due to accelerated T cell exhaustion[39]. Interestingly, in apparent contradiction to this, one of the most successful CAR-T trials in solid tumors to date in term of response rates, utilized products with >70% CAR transduction, potentially contributing to the success[2,40]. Overall, our results highlight the complexity of CAR-T cell activity regulation, involving numerous interplaying factors.

The formation of a productive immune synapse (IS) is crucial to achieve optimal T-cell activation, and adhesion molecules are crucial players in IS formation[41]. One of those is ICAM-1, which has been shown to be instrumental for CAR-T cell effector function[42,43], and its upregulation has also been implicated in resistance to PD-1/PD-L1 pathway[44], all in an IFN-γ-dependent manner. One can hypothesize that as HA CAR-T cells release higher levels of IFN-γ upon co-culture with tumor cells as compared to LA CAR-T cells, they can induce increased upregulation of ICAM-1 and therefore, increased resistance to PD-L1. Recently, another adhesion molecule, CD56, has been reported to play a role in CAR-T cell effectiveness in triple inhibitory receptor-resistant CAR-T cells (including PD-1 knockdown)[45]. Considering these works, we cannot rule out the potential implication of alternative adhesion molecules in the resistance to PD-L1-mediated inhibition of HA CAR-T cells.

Concerns regarding accelerated T-cell exhaustion following PD-1 ablation have been raised in previous studies, both in the context of CAR-T cells for cancer treatment[18,19] and in virus-specific T cells in chronic infections[46]. Our transcriptomic analysis did not reveal a more exhausted phenotype of LA PD-1 KO CAR-T cells but rather the opposite. In fact, PD-1 KO CAR-T cells presented hallmarks of less exhausted T cells as compared to mock CAR-T cells. In this regard, we found that 11 out of 20 genes that were downregulated in PD-1 KO LA CAR-T cells were genes involved in the type I and II IFN signaling pathways, including IRF7 which is the main transcription factor regulating type I IFN pathway. Although IRF7 induction can potentiate CAR-T cell activation and induce antitumor activity[47], in certain contexts, type I IFN signaling can also orchestrate T cell immunosuppression[48,49] and induce apoptosis on CAR-T cells[50]. Recent papers identified chronic type I IFN signaling regulated by IRF7 to potentiate CAR-T cell dysfunction[27] and to be predictive of poor CAR-T cell persistence in pediatric acute lymphoblastic leukemia (ALL) patients[28]. By contrast, PD-1 KO CAR-T cells in our experiments expressed higher levels of FosB, a transcription factor that is decreased in exhausted T cells in chronic viral infection[24] while increased in CAR-T cell products from responding patients as compared to non-responders[25]. However, it is important to note that our transcriptomic data was obtained after a single antigen stimulation in vitro, and further exploration of what would happen in the context of repeated stimulations might be required.

In broader terms, by using our preclinical model, we also observed that PD-1 KO does not increase the antitumor efficacy of LA CARs co-stimulated with 4-1BB, contrary to CARs featuring CD28 or ICOS as co-stimulatory domains. Our results are in line with the previously described by others[8,36] and might be attributed in part to the PD-1 low phenotype but also to the distinct pathway that 4-1BB signal through as compared to CD28 and ICOS. It is well-established that PD-1 activation by PD-L1 primarily suppresses T-cell function through the deactivation of CD28 signaling, suggesting the central role played by co-stimulatory pathways within the context of PD-1 therapy[51,52].

Of note, it is relevant to highlight that even in the cases where PD-1 genetic deletion does not provide an advantage (i.e., HA and 4-1BB co-stimulated CAR-T cells) it never decreases CAR-T cell functionality in our hands. This observation offers the potential to repurpose PD-1 as a site for targeted integration of therapeutic transgenes, capitalizing the kinetics of PD-1 expression after antigen encounter to restrict transgene expression to the tumor microenvironment while simultaneously disrupting PD-1[53,54].

In terms of clinical translation of our findings, the use of a high affinity CAR might be preferable as it exhibits greater efficacy and resistance to PD-L1-mediated inhibition without additional modifications. However, increased resistance to PD-L1 might come at the price of increased T-cell exhaustion and diminished safety. Our transcriptomic data supports the notion of that HA CAR-T cells may be more prone to exhaustion. In the literature, a recent study demonstrated less exhausted and apoptotic phenotype and greater persistence of CAR-T cells targeting GPC3 with low affinity as compared to their high affinity counterparts[55]. In the same line, a CAR targeting CD19 with lower affinity than commercial products demonstrated greater persistence in preclinical mouse models and patients in a clinical study[56]. Regarding safety concerns, a serious event occurred in the context of HER2-targeting CAR therapy where the use of a HA CAR (based on the scFv 4D5, as employed in our study) led to a fatal outcome in a patient with colon cancer metastatic to the lungs and liver. This was attributed to the high doses of CAR-T cells administered and to the potential CAR-mediated recognition of low levels of HER2 on lung epithelial cells[57]. Our findings evidence a more favorable toxicity profile of LA PD-1 KO as compared to HA HER2-28Z CAR-T cells. This underscores the necessity for caution and thorough investigation when employing HA CARs, emphasizing their potential for unintended activation in the presence of healthy cells expressing lower levels of the target antigen. Interestingly, in terms of efficacy, an analysis of available data from solid tumor CAR-T trials correlating clinical responses to CAR affinity concluded that the use of CARs targeting their antigens with moderate affinity led to best clinical responses as compared to high affinity CARs[58].

Regarding the methodology employed for PD-1/PD-L1 disruption, our study utilized CRISPR/Cas9 to knockout *pdcd1* as a proof of concept. This method is highly efficient, ensures sustained PD-1 blockade, circumvents toxicities associated with systemic PD-1 blockade and has demonstrated safety in the clinics[59,60]. However, we also provide data showing the feasibility of CAR-T cell combination with PD-1/PD-L1 blockade antibodies. Combining CAR-T cells with immune checkpoint antibodies offers other advantages such as more precise and flexible dosing regimen, eliminates the need for further genetic modifications on T cells, and can impact both endogenous T cells and CAR-T cells. In fact, combination of CAR-T cells with PD-1 blocking antibodies has also been explored in clinical trials[61]. This broadens the scope of therapeutic possibilities, emphasizing the adaptability of our findings to diverse PD-1 disruption approaches in the pursuit of enhanced CAR-T cell therapy.

In conclusion, our study reveals that CAR affinity plays a role in determining the sensitivity of CAR-T cells to T-cell inhibition mediated by the PD-1/PD-L1 axis. We have demonstrated that HA CAR-T cells

https://doi.org/10.1038/s41467-024-47799-z

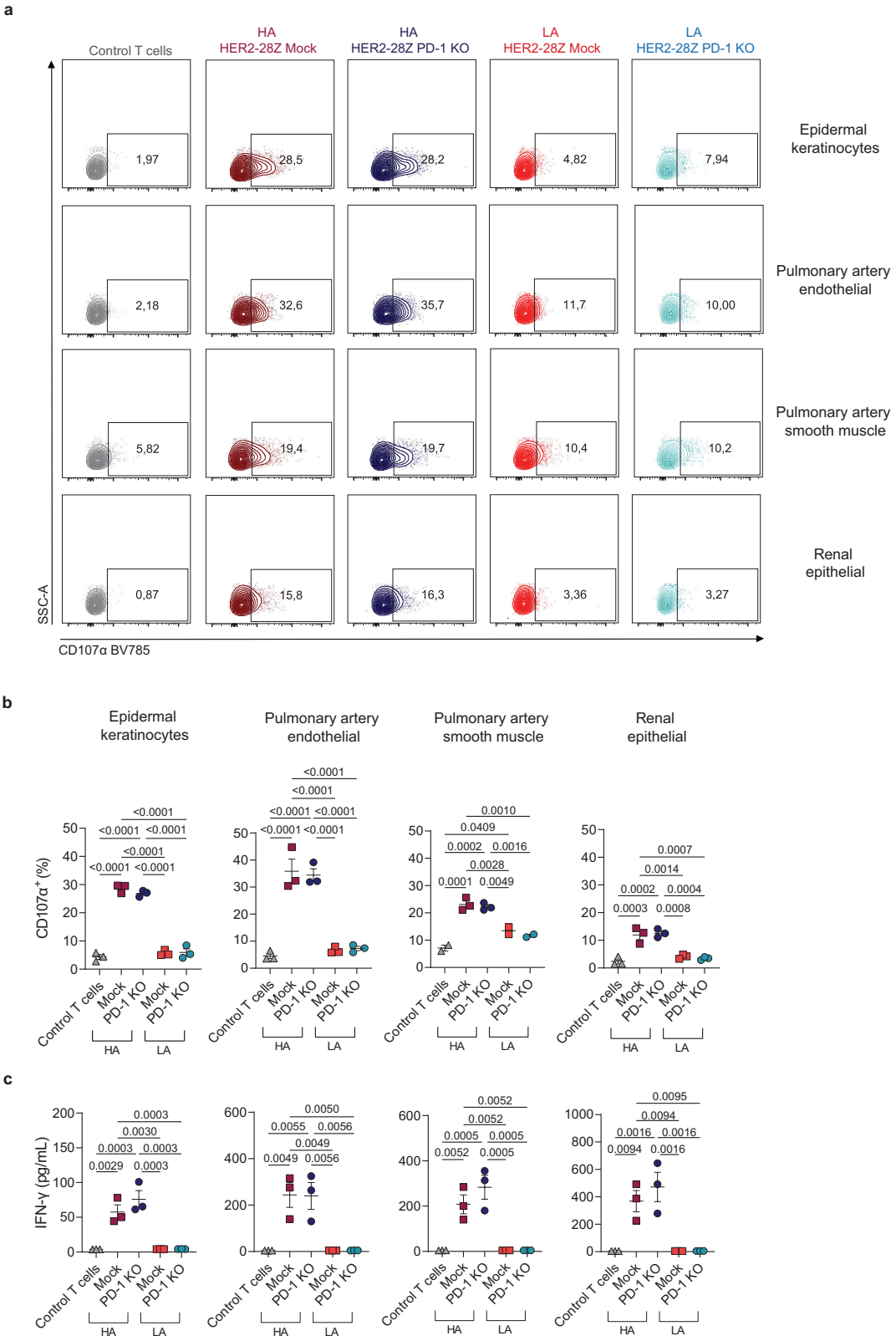

Fig. 6 | HA HER2-28Z CAR-T cells demonstrate reactivity against a panel of primary healthy cells while LA CAR-T cells do not. Mock or PD-1 KO HER2-28Z CAR-T cells of LA or HA were co-cultured with a panel of human primary cells. **a**, **b** CD107-α degranulation marker was measured after 6 h of co-culture (E:T = 1:1). **a** Representative flow cytometry plots and (**b**) percentage of cells producing CD107-α (gated on live/CD45$^+$) are shown. **c** IFN-γ production by HER2-28Z CAR-T cells after 24 h of co-culture (E:T = 3:1) as quantified by ELISA. Data in (**b**, **c**) are plotted as mean ± SEM ($n = 3$ donors). p values by one-way ANOVA with Tukey's multiple testing correction are indicated. Source data are provided as a Source Data file.

https://doi.org/10.1038/s41467-024-47799-z

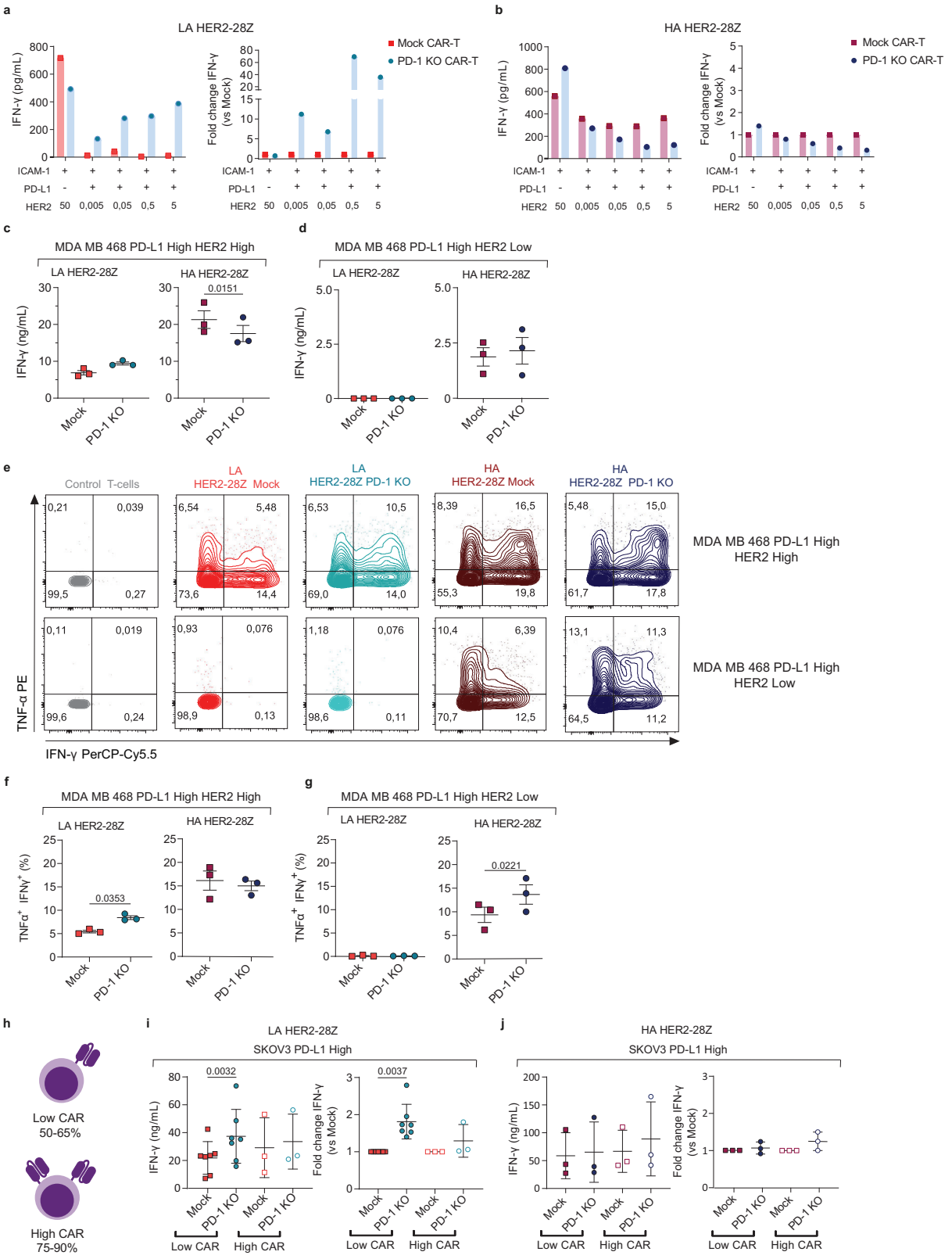

exhibit inherent resistance to PD-L1-mediated inhibition, whereas LA CARs are more susceptible to this suppression. In essence, these findings provide valuable insights into the design and optimization of CAR-T cells for enhanced effectiveness in the treatment of solid tumors, and particularly shed light on how to target the PD-1/PD-L1 axis more effectively in combination with the use of CAR-T cells as the field moves forward to clinical applications.

Methods

Study approval

Human T cells are isolated from buffy coats obtained from the Barcelona Public Blood and Tissue Bank. All samples are deidentified prior to receipt and no protected health information is transferred from the blood bank to our team or institution. Therefore, informed consent is not required from our side. Specific approval for this project was

Fig. 7 | Role of target antigen and CAR expression in determining sensitivity to PD-L1. IFN-γ production by mock or PD-1-KO (**a**) LA or (**b**) HA HER2-28Z CAR-T cells after 72 h of co-culture with SLBs containing either HER2 alone (50 ng) or increasing concentrations of HER2 along with PD-L1 (200 ng) as measured by ELISA. Data from one donor is represented as absolute levels (left panel) or fold change of IFN-γ by PD-1 KO versus mock HER2-28Z CAR-T cells (right panel). IFN-γ production by mock or PD-1-KO LA (left panel) or HA (right panel) HER2-28Z CAR-T cells after 24 h of co-culture with (**c**) MDA-MB-468 PD-L1 high HER2 high or (**d**) MDA-MB-468 PD-L1 high HER2 low (E:T = 3:1) as measured by ELISA. **e** Representative flow cytometry plots and frequencies of IFN-γ$^+$TNF-α$^+$ T-cells (gated on live/CD45$^+$) of intracellular cytokine staining for TNF-α and IFN-γ in mock and PD-1 KO LA and HA HER2-28Z CAR-T cells after co-culture with MDA-MB-468 PD-L1 high HER2 high (**f**) or MDA-MB-468 PD-L1 high HER2 low (**g**) tumor cells for 24 h (E:T = 1:3). **h** Schematic representation of criteria to discriminate between Low CAR and High CAR-T cell products. Created with Adobe Illustrator. IFN-γ production by mock or PD-1-KO (**i**) LA or (**j**) HA HER2-28Z CAR-T cells with either Low ($n = 7$ donors for LA and $n = 4$ for HA) or High ($n = 3$ donors) CAR frequencies after 24 h of co-culture with SKOV3 PD-L1 High tumor cells (E:T = 3:1). Data in (**c**, **d**, **f**, **g**) is represented as mean ± SEM ($n = 3$ donors) and p values by a two-tailed paired T-test are indicated. Data in (**i**) and (**j**) is pooled from nine and five independent experiments, respectively, where each dot represents CAR-T cells generated from different donors (n) and represented as mean ± SEM for absolute levels (left panel) and fold change of PD-1 KO versus mock (right panel). p values by a two-tailed paired T test (for absolute levels) or a two-tailed one-sample T-test (for fold change) are indicated. Source data are provided as a Source Data file.

obtained from the local ethic committee (Comité de Ética de la investigación con medicamentos CEIm).

All mouse studies were performed under a protocol (184-20) approved by the Ethic Committee for Animal Experimentation (CEEA) of the University of Barcelona and Generalitat de Catalunya.

Cell line culture

Details of all cell lines used in this study are listed in Supplementary Table 1. All cell lines were grown at 37 °C and 5% CO_2 and were regularly validated to be *Mycoplasma free* and authenticated in 2019 by IDEXX Bioanalytics using the Human 9-Marker STR Profile.

Generation of cancer cell lines

SKOV3 cells were genome edited to delete CD274 (PD-L1) using the CRISPR-Cas9 system. Single guide targeting CD274 (A*U*U*UACUGUCACGGUUCCCA) was synthetized by Synthego. Ribonucleoprotein (RNP) complexes were formed by mixing the sgRNA and the TrueCut™ Cas9 Protein v2 (ThermoFisher) at a ratio of 3:1 and incubated for 10–15 min at room temperature following the per manufacturer's protocol (ThermoFisher). RNP complexes where then added to 5×10^6 SKOV3 and the cells were electroporated with the following conditions: 1170 V, 30mseg and 2 pulses using the Neon transfection system (ThermoFisher). PD-L1 negative cell population was sorted by flow cytometry after treatment with IFN-γ to induce PD-L1 expression and to allow accurate selection of the PD-L1 negative population. The SKOV3 PD-L1 KO cell line was then transduced with lentiviral vectors expressing PD-L1 under different promoters: EF1α (high expression) and PGK100 (low). pCCL-EF1α-PD-L1 was synthetized by Genscript. To generate pCCL-PGK100-PD-L1, an already created plasmid in the lab pCCL-PGK100-HER2t and pCCL-EF1α-PD-L1 were digested with XbaI and SalI-HF (From NEB) to obtain pCCL-PGK100 and PD-L1 fragments. Then, the backbone with the promoters and the PD-L1 sequence were purified using QIAquick PCR Purification Kit (QIAGEN), ligated, and transformed in Stbl3 (ThermoFisher). Five days after transduction, tumor cells were stained with L/D aqua and PD-L1 APC antibodies, and PD-L1$^+$ tumor cells were collected separately using FacsAriaII cell sorter (BD). Copy numbers of PD-L1 molecules on cell surface were estimated using the Quantibrite™ Beads PE Fluorescence Quantitation Kit (ref. 340495, BD) according to the instructions of the manufacturer. SKOV3 PD-L1 KO and SKOV3 PD-L1 high cell lines were further modified to express folate receptor beta (FRβ) by using a lentiviral vector expressing FRβ under EF1α promoter. pCCL-EF1α-FRβ was synthesized by Genscript. After transduction, tumor cells were stained with an anti-FRβ antibody and FRβ+ tumor cells were collected using a FacsAriaII cell sorter (BD). Triple negative breast cancer cells (MDA-MB-468) were transduced with lentiviral vectors expressing a truncated version of HER2 lacking the intracellular domain under different promoters: EF1α (high expression) and PGK100 (low). After transduction, tumor cells were stained with an anti-HER2 antibody, and HER2+ tumor cells were collected using a FacsAriaII cell sorter (BD). MDA-MB-468 HER2 low and MDA-MB-468 HER2 high were further modified to express PD-L1 under the control of EF1α, as detailed for SKOV3 cells.

Preparation of SLBs

Supported lipid bilayers (SLBs) were prepared as previously described[23]. First, 1,2-dioleoyl-sn-glycero-3-[N(5-amino-1-carboxypentyl) iminodiacetic acid succinyl] (nickel salt) (DGS-NTA(Ni)) and 1-palmitoyl-2-oleoyl-sn-glycero-3-phosphocholine were dissolved in chloroform and mixed in a 1:50 molar ratio. The mixture was then dried under vacuum overnight and resuspended in degassed PBS. Sonication was performed under nitrogen until the suspension became clear. Nonunilamellar vesicles were pelleted through ultracentrifugation, and the clear supernatant was subjected to further centrifugation. The second supernatant was filtered and stored under nitrogen. Glass slides were cleaned for 15 min using plasma (Zepto, Diener Electronic). Cleaned slides were attached to the bottom of an 12-well Nunc Lab-Tek chamber (Thermo Fisher Scientific) with Picodent twinsil extrahart (Picodent) until the glue had solidified. The lipid vesicle suspension was diluted 1:20 with PBS and filtered, and 100 µL of the diluted suspension were added to each well to form a continuous SLB. Excess vesicles were removed by washing the chambers with PBS. H12-tagged proteins were added to the SLBs and incubated for 60 min in the dark at room temperature. Finally, the chambers were rinsed with PBS to remove unbound protein.

CAR construction and lentiviral production

Single-chain variable fragments (scFv) used for targeting HER2 or FRβ with low or high affinity were previously described[20,21,62]. Similarly, scFv sequence of M11 (targeting mesothelin) was extracted from patent WO2015090230A1 (Human mesothelin chimeric antigen receptors and uses thereof)[37]. All CAR sequences (including the mentioned scFvs, signal peptide, CD8 hinge, CD28 or CD8 transmembrane regions and intracellular domains from CD28, 41BB or ICOS and CD3Z), were synthesized by BaseClear B.V. or Genscript and cloned into the third-generation lentiviral vector pCCL under the control of EF1α promoter[63,64]. Lentiviral vectors were produced after transfection of 293FT and tittered in Jurkat cells as previously described[35]. Briefly, 293FT cells were seeded at 10×10^6 in a total volume of 18 mL of medium in a p150 culture plate. Eighteen hours later, 293FT cells were transfected with 18 µg of pCCL transfer plasmid (containing CAR) and a pre-mixed packaging mix containing 15 µg of pREV, 15 µg of pRRE and 7 µg of pVSV using PEI® (Polysciences). The viral supernatant was harvested at 48 and 72 h post-transfection, 0.45 µm filtered, concentrated by LentiX as per manufacturer's protocol (Clontech) and frozen at −80 °C until use.

Isolation, transduction, electroporation and expansion of primary human T lymphocytes

Human T cells were isolated from healthy donor buffy coats obtained from the Barcelona Public Blood and Tissue Bank and expanded as

https://doi.org/10.1038/s41467-024-47799-z

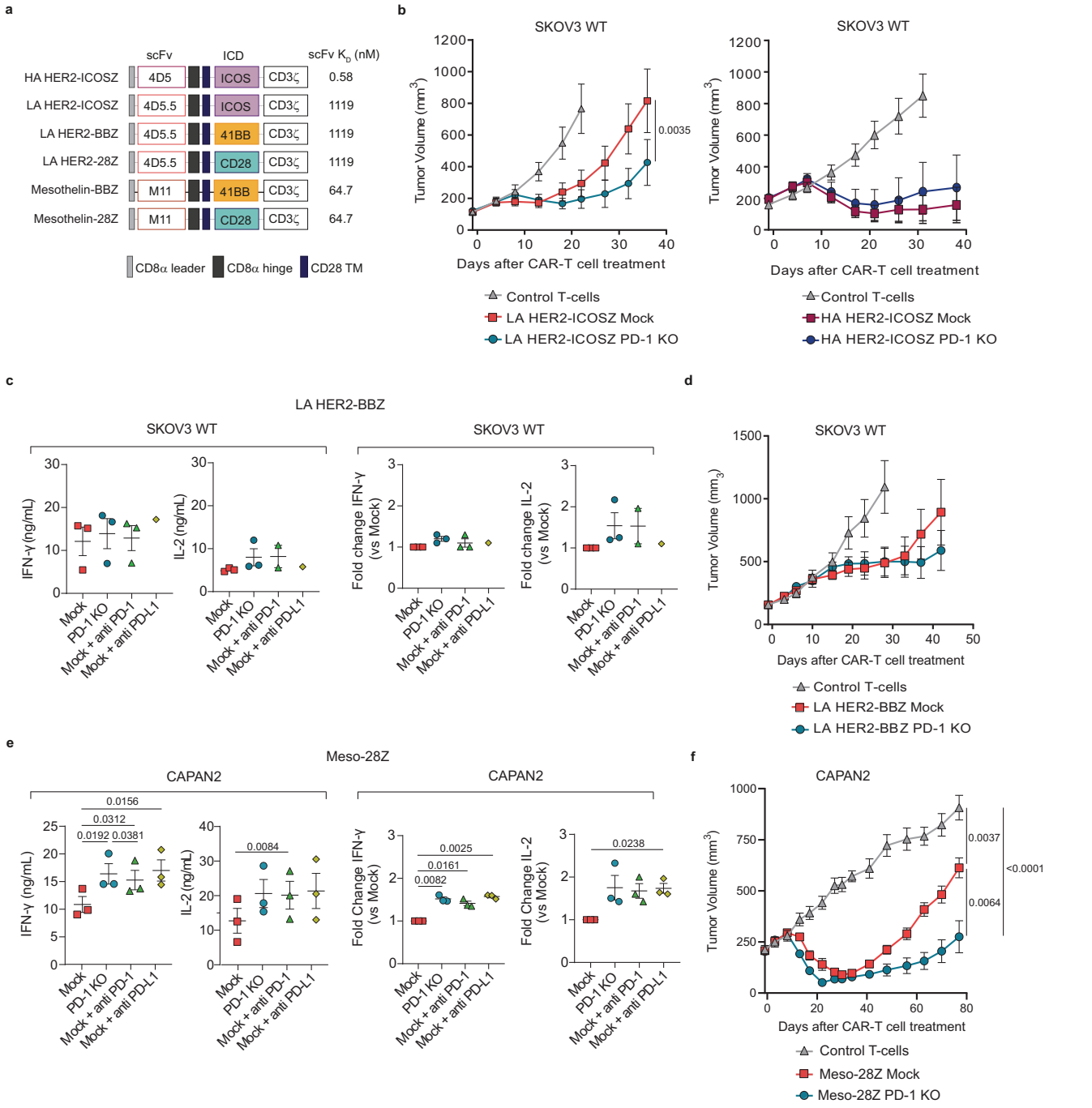

Fig. 8 | Influence of scFv and co-stimulatory domains in PD-1/PD-L1-mediated inhibition of CAR-T cells. a Schematic overview of CAR constructs used with their corresponding affinity values. **b** Tumor measurements of NSG mice bearing SKOV3 tumors treated with 5×10^6 control T-cells, mock or PD-1 KO LA HER2-ICOSZ CAR$^+$-T cells ($n = 10$, left panel) or with 3×10^6 control T-cells, mock or PD-1 KO HA HER2-ICOSZ CAR$^+$-T cells ($n = 7$ for control and $n = 8$ for mock and PD-1 KO, right panel). **c** Quantification of IFN-γ and IL-2 production by PD-1 KO or mock LA HER2-BBZ CAR-T cells, alone or in combination with anti PD-1 or anti PD-L1 antibodies, after 24 h of co-culture with SKOV3 tumor cells (E:T = 3:1) as measured by ELISA ($n = 3$ for all groups except for mock+anti PD-L1 with $n = 1$). **d** Tumor measurements of NSG mice bearing SKOV3 tumors treated with 3×10^6 control-T cells ($n = 8$), mock ($n = 8$) or PD-1 KO ($n = 10$) LA HER2-BBZ CAR$^+$-T cells. **e** Quantification of IFN-γ and IL-2 production by PD-1 KO or mock Meso−28Z CAR-T cells, alone or in combination with anti PD-1 or anti PD-L1 antibodies, after 24 h of co-culture with CAPAN2 tumor cells (E:T = 3:1) as measured by ELISA ($n = 3$). **f** Tumor measurements of NSG mice bearing CAPAN2 tumors and treated with 2×10^6 control T cells, mock or PD-1 KO Meso-28Z CAR$^+$-T cells ($n = 12$). Data in (**b**, **d**, **f**) are represented as mean tumor volume ± SEM and n indicates tumors per group. Data in (**c**, **e**) are represented as mean ± SEM of absolute levels (left panel) or fold change of indicated groups as compared to mock CAR-T cells (right panel). Data is pooled from independent experiments where each dot indicates a different donor for CAR-T generation (n). *p* values by two-way ANOVA with Sidak multiple testing correction (**b**), two-way ANOVA with Tukey's multiple testing correction (**f**), one-way ANOVA with Tukey post hoc test (**e**, absolute levels) or one-sample *T*-test (**e**, fold change) are indicated. Source data are provided as a Source Data file.

previously described[65]. Briefly, $CD4^+$ and $CD8^+$ T cells were negatively isolated using RosetteSep Kits (Stem Cell Technologies) and stimulated separately with CD3/CD28-activating Dynabeads (Invitrogen) at a 2:1 bead-to-cell ratio in the presence of human IL-7 and IL-15 (Miltenyi biotec) at a concentration of 10 ng/mL. Approximately 24 h after activation, T cells were transduced with CAR-encoding lentiviral vectors. Beads were removed from cultures at day 4 and T cells were counted and maintained at a concentration of 0.8×10^6 cells/mL in RPMI-1640 (Gibco) supplemented with 10% FBS (Sigma, Lot#F4531), Penicillin-Streptomycin (#15070063, ThermoFisher), 10 mM GlutaMax (#35050061, ThermoFisher), 10 mM HEPES (15630080) and 10 ng/mL of human IL-7 and IL-15 (Milenyi Biotec). For CRISPR, CAR-T cells were electroporated with buffer alone (Mock CAR-T cells) or Cas9 and a chemically synthesized sgRNA targeting *PDCD1* exon 1 (sequence: CGACUGGCCAGGGCGCCUGU) at day 4 post-activation. Ribonucleoprotein complex was mixed at sgRNA:Cas9 molar ratio of 3.3:1, incubated during 5–20 min and returned to the incubator. CAR-T cells were then expanded ex vivo until day 10–11, when $CD4^+$ and $CD8^+$ T cells were mixed at a 1:1 ratio and cryopreserved. To confirm editing events in the PDCD1 locus, DNA from PD-1 KO edited CAR-T cells was extracted using the DNeasy Blood&Tissue kit (Qiagen) according to the manufacturer's protocol. The region surrounding the site of interest was amplified using the primers (forward: TTTCCCTTCCGCTCACCTCC and reverse: CAAAGAGGGGACTTGGGCCA) and KO efficiency was assessed by Sanger sequencing and quantified by using ICE v3.0 software (Synthego) on day 10 of T-cell expansion.

In vitro co-culture experiments

Tumor cells (1×10^5) were seeded in 48-well plates. Primary healthy cells (1×10^4) were seeded in 96-well plates. After overnight incubation, T cells were added at an effector/target ratio of 3:1. At indicated experiments, anti PD-L1 (Durvalumab) and anti PD-1 (Nivolumab) antibodies were added to CAR-T cells at a final concentration of 10 µg/mL. For cytokine secretion, supernatants were collected 24 h after co-culture, and IFN-γ and IL-2 were analyzed using the DuoSet® ELISA Development Kit (R&D Systems, DY285B/DY202) as per the manufacturer's protocol. Absorbance data was collected using Gen5 2.07 (Biotek) or iControl 2.0 (LifeSciences) software. For T-cell proliferation assays, absolute numbers of live cells were calculated for each group using trypan blue exclusion before coculture and after 6 days of incubation with tumor cells. For the experiments with the SLBs, CAR-T cells (3×10^4) were resuspended in 100 µL of imaging buffer, seeded onto SLBs and incubated at 37 °C for 15 min. Following incubation, 450 µL of RPMI 1640 medium supplemented with 25 mM HEPES, 10% FBS, 100 µ/mL of penicillin/streptomycin, 2 mM L-glutamine and 50 µM of 2-mercaptoethanol was added, and the cells were further incubated for 24 or 72 h, as indicated. The supernatant was collected and stored in 100 µL aliquots at −80 °C until further use. The secretion of IFN-γ was measured by performing ELISA using a commercially available kit (ELISA MAX™ Deluxe Set, BioLegend). For intracellular staining assays, tumor cells (5×10^5) were seeded in 12-well plates. After overnight incubation, T cells were added (effector/target ratio of 1:3). 24 h later, GolgiPlugTM (ref. 555029, BD Bioscience) was added to each well. Cell stimulation cocktail (ref. 00–4970, eBioscience) was added to the corresponding positive control wells. 4 h later, flow cytometry staining was performed as described below. For CD107a degranulation assays, target cells (1×10^5) were seeded in 48-well plates. After overnight incubation, T cells were added (effector/target ratio of 1:1) and incubated for 2 h at 37 °C. To enable the detection of the CD107a marker, a protein transport inhibitor containing brefeldin A, GolgiPlugTM (ref. 555029, BD Bioscience) was added to each well along with anti-CD107a antibody. The co-culture was extended for an additional 4 h. Then, T cell staining was analyzed by flow cytometry analysis as described below.

Mouse xenograft study

NOD/SCID/IL2-receptor γ chain knockout (NSG) mice were purchased from Jackson Laboratory. Mice were bred and maintained within the Animal Facility at the University of Barcelona, with a 12 h light/dark cycle, a temperature range of 20–24 °C and a humidity range of 45–65%. Mice health status was regularly monitored by qualified personnel. 6–8 week old female (SKOV3 and HCC1954) or male (CAPAN2) NSG mice were implanted subcutaneously with $4–5 \times 10^6$ tumor cells in a 50% solution of Matrigel (Corning) in PBS and treated intravenously with $2–5 \times 10^6$ control T cells, CAR-T cells or PD-1 KO CAR^+-T cells in 100 µL of PBS when tumors reached 150–250 mm^3, following previously published protocols[66]. PD-L1–blocking antibody (Durvalumab) was administered intraperitoneally at a dose of 10 mg/kg every 5 days during the specified experiment. Tumor dimensions were measured weekly with a digital calliper and volumes were calculated using the formula V = 6 x (L x W2) / π, where L is length and W is width of the tumor. Mice were sacrificed when tumors reached 1500 mm3. In some cases, this limit has been exceeded, but we ensured that that no mice remained with tumor volumes above this threshold for longer than 5 days and animals exhibiting signs of pain, discomfort, or distress were euthanized immediately.

Immunohistochemistry staining

Tumors were harvested at the experimental endpoint and embedded in paraffin. Immunohistochemistry stainings were performed by the Biobanc HCP-IDIBAPS Core according to standard protocols. Briefly, tumor sections were incubated with a 1:100 dilution of anti-PD-L1 antibody (#15165, Cell Signaling) followed by a rabbit specific IHC polymer detection kit HRP/DAB. Slides were counterstained with hematoxylin, dehydrated and mounted. Images were obtained using a Nikon Eclipse E600 inverted microscope and a Olympus DP72 camera.

IsoLight polyfunctionality assay

Co-cultures of CAR-T cells and SKOV3 tumor cells were established at a E:T ratio of 1:3. 20 h later, cells were collected and HER2+ tumor cells were depleted by using Anti-ErbB-2 MicroBeads (Miltenyi Biotec) following manufacturer's instructions. Enriched T cells were then stained with a cell membrane dye and an anti-CD8 AF647 antibody for differentiation of $CD4^+$ and $CD8^+$ T-cell populations. Subsequently, 30.000 viable cells were loaded onto the 32-plex human IsoCode Single-Cell Adaptive Immune chip (IsoPlexis) and chips were loaded into the IsoLight machine. Data was collected and analyzed by using IsoSpeak 2.9.0 software (IsoPlexis, Branford, CT).

Gene expression analysis

Gene expression analysis was performed using the CAR-T cell characterization panel from Nanostring Technologies (Seattle, WA). Briefly, CAR-T cells were co-cultured with SKOV3 tumor cells (effector/target ratio of 1:3) for 48 h. $CD45^+$ cells were then flow sorted and total RNA was extracted using the RNeasy Mini kit (Qiagen). Samples were prepared according to the manufacturer's protocols for the nCounter CAR-T Characterization Panel. Cartridges were run on the nCounter SPRINT Profiler. Gene expression levels were normalized against the housekeeping genes and data analysis was conducted using the Rosalind Platform (www.rosalind.bio/nanostring). Enrichr online software (https://maayanlab.cloud/Enrichr/) was used for the analysis of biological pathways and Gene Ontology (GO) terms associated with the differentially expressed genes by using the list of under- and over-expressed genes as input.

Flow cytometry (Surface and Intracellular stainings)

Cell viability was determined using L/D eFluor™ 450 (eBioscience, 65-0863-14) followed by surface antibody staining in FACS buffer. Cells were incubated with surface antibodies for 30 min in the dark. To detect CAR expression, cells were stained using goat anti-mouse IgG-

biotin (Jackson ImmunoResearch) followed by streptavidin-PE or streptavidin- eFluor450 (ThermoFisher, 12-4317-87 and 48-4317-82). Intracellular staining was performed with the Foxp3/Transcription Factor Staining Buffer set (ThermoFisher, 00-5523-00) according to the manufacturer's instructions. All experiments were performed on a FacsCanto 3 L, Fortessa 4 L HT and Fortessa 5 L (BD Biosciences) and the data was analyzed with FlowJo software (V.10, TreeStar). Antibodies listed on Supplementary Table 2 were used.

Statistical analysis

All statistical analyses were performed using GraphPad Prism v9.4.1 (GraphPad Software Inc.). For comparisons of two groups, two-tailed *t* tests or one-sample *t* test were used. One-way analysis of variance (ANOVA) with Tukey post hoc test was used for the comparison of three or more groups in a single condition and two-way ANOVA test with Sidak or Tukey's multiple testing correction. Exact *p* values are indicated in the figures.

Reporting summary

Further information on research design is available in the Nature Portfolio Reporting Summary linked to this article.

Data availability

Transcriptomics data have been deposited in the Gene Expression Omnibus database under accession number GSE252036. The remaining data are available within the Article, Supplementary Information or Source Data file. Source data are provided with this paper.

References

1. June, C. H. & Sadelain, M. Chimeric antigen receptor therapy. *N. Engl. J. Med.* **379**, 64–73 (2018).
2. Del Bufalo, F. et al. GD2-CART01 for relapsed or refractory high-risk neuroblastoma. *N. Engl. J. Med.* **388**, 1284–1295 (2023).
3. Majzner, R. G. et al. GD2-CAR T cell therapy for H3K27M-mutated diffuse midline gliomas. *Nature* **603**, 934–941 (2022).
4. Qi, C. et al. Claudin18.2-specific CAR T cells in gastrointestinal cancers: phase 1 trial interim results. *Nat. Med.* **28**, 1189–1198 (2022).
5. Rodriguez-Garcia, A. et al. CAR-T cells hit the tumor microenvironment: strategies to overcome tumor escape. *Front. Immunol.* **11**, 1109 (2020).
6. Patsoukis, N., Wang, Q., Strauss, L. & Boussiotis, V. A. Revisiting the PD-1 pathway. *Sci. Adv.* **6**, eabd2712 (2020).
7. Sharpe, A. H. & Pauken, K. E. The diverse functions of the PD1 inhibitory pathway. *Nat. Rev. Immunol.* **18**, 153–167 (2018).
8. Cherkassky, L. et al. Human CAR T cells with cell-intrinsic PD-1 checkpoint blockade resist tumor-mediated inhibition. *J. Clin. Investig.* **126**, 3130–3144 (2016).
9. Choi, B. D. et al. CRISPR-Cas9 disruption of PD-1 enhances activity of universal EGFRvIII CAR T cells in a preclinical model of human glioblastoma. *J. Immunother. Cancer* **7**, 304 (2019).
10. Dotsch, S. et al. Long-term persistence and functionality of adoptively transferred antigen-specific T cells with genetically ablated PD-1 expression. *Proc. Natl Acad. Sci. USA* **120**, e2200626120 (2023).
11. Guo, X. et al. Disruption of PD-1 enhanced the anti-tumor activity of chimeric antigen receptor T cells against hepatocellular carcinoma. *Front. Pharm.* **9**, 1118 (2018).
12. Hu, W. et al. CRISPR/Cas9-mediated PD-1 disruption enhances human mesothelin-targeted CAR T cell effector functions. *Cancer Immunol. Immunother.* **68**, 365–377 (2019).
13. Liu, X. et al. CRISPR-Cas9-mediated multiplex gene editing in CAR-T cells. *Cell Res.* **27**, 154–157 (2017).
14. Rafiq, S. et al. Targeted delivery of a PD-1-blocking scFv by CAR-T cells enhances anti-tumor efficacy in vivo. *Nat. Biotechnol.* **36**, 847–856 (2018).
15. Ren, J. et al. Multiplex genome editing to generate universal CAR T cells resistant to PD1 inhibition. *Clin. Cancer Res.* **23**, 2255–2266 (2017).
16. Rupp, L. J. et al. CRISPR/Cas9-mediated PD-1 disruption enhances anti-tumor efficacy of human chimeric antigen receptor T cells. *Sci. Rep.* **7**, 737 (2017).
17. Wang, Z. et al. Phase I study of CAR-T cells with PD-1 and TCR disruption in mesothelin-positive solid tumors. *Cell Mol. Immunol.* **18**, 2188–2198 (2021).
18. Kalinin, R. S. et al. Engineered removal of PD-1 from the surface of CD19 CAR-T cells results in increased activation and diminished survival. *Front. Mol. Biosci.* **8**, 745286 (2021).
19. Wei, J. et al. PD-1 silencing impairs the anti-tumor function of chimeric antigen receptor modified T cells by inhibiting proliferation activity. *J. Immunother. Cancer* **7**, 209 (2019).
20. Liu, X. et al. Affinity-Tuned ErbB2 or EGFR chimeric antigen receptor T cells exhibit an increased therapeutic index against tumors in mice. *Cancer Res.* **75**, 3596–3607 (2015).
21. Lynn, R. C. et al. High-affinity FRbeta-specific CAR T cells eradicate AML and normal myeloid lineage without HSC toxicity. *Leukemia* **30**, 1355–1364 (2016).
22. Gudipati, V. et al. Inefficient CAR-proximal signaling blunts antigen sensitivity. *Nat. Immunol.* **21**, 848–856 (2020).
23. Axmann, M., Schütz, G.J., Huppa, J.B. Single Molecule Fluorescence Microscopy on Planar Supported Bilayers. J. Vis. Exp. **104**, e53158 (2015)
24. Wherry, E. J. et al. Molecular signature of CD8+ T cell exhaustion during chronic viral infection. *Immunity* **27**, 670–684 (2007).
25. Beider, K. et al. Molecular and functional signatures associated with CAR T cell exhaustion and impaired clinical response in patients with B cell malignancies. *Cells* **11**, 1140 (2022).
26. Giordano, M. et al. Molecular profiling of CD8 T cells in autochthonous melanoma identifies Maf as driver of exhaustion. *EMBO J.* **34**, 2042–2058 (2015).
27. Jung, I. Y. et al. Type I interferon signaling via the EGR2 transcriptional regulator potentiates CAR T cell-intrinsic dysfunction. *Cancer Discov.* **13**, 1636–1655 (2023).
28. Chen, G. M. et al. Integrative bulk and single-cell profiling of premanufacture T-cell populations reveals factors mediating long-term persistence of CAR T-cell therapy. *Cancer Discov.* **11**, 2186–2199 (2021).
29. Sumida, T. S. et al. Type I interferon transcriptional network regulates expression of coinhibitory receptors in human T cells. *Nat. Immunol.* **23**, 632–642 (2022).
30. Chen, E. Y. et al. Enrichr: interactive and collaborative HTML5 gene list enrichment analysis tool. *BMC Bioinforma.* **14**, 128 (2013).
31. Kuleshov, M. V. et al. Enrichr: a comprehensive gene set enrichment analysis web server 2016 update. *Nucleic Acids Res.* **44**, W90–W97 (2016).
32. Willinger, T. et al. Human naive CD8 T cells down-regulate expression of the WNT pathway transcription factors lymphoid enhancer binding factor 1 and transcription factor 7 (T cell factor-1) following antigen encounter in vitro and in vivo. *J. Immunol.* **176**, 1439–1446 (2006).
33. Good, C. R. et al. An NK-like CAR T cell transition in CAR T cell dysfunction. *Cell* **184**, 6081–6100.e26 (2021).
34. Rossi, J. et al. Preinfusion polyfunctional anti-CD19 chimeric antigen receptor T cells are associated with clinical outcomes in NHL. *Blood* **132**, 804–814 (2018).
35. Guedan, S. et al. ICOS-based chimeric antigen receptors program bipolar TH17/TH1 cells. *Blood* **124**, 1070–1080 (2014).
36. Zolov, S. N., Rietberg, S. P. & Bonifant, C. L. Programmed cell death protein 1 activation preferentially inhibits CD28.CAR-T cells. *Cytotherapy* **20**, 1259–1266 (2018).

37. Beatty, G., Engels, B., et al. Human mesothelin chimeric antigen receptors and uses thereof (International application, Patent No WO2015090230A1). Novartis AG, The Trustees of the University of Pennsylvania (2015).
38. Guedan, S. et al. Time 2EVOLVE: predicting efficacy of engineered T-cells—how far is the bench from the bedside? *J. Immunother. Cancer* **10**, e003487 (2022).
39. Rodriguez-Marquez, P. et al. CAR density influences antitumoral efficacy of BCMA CAR T cells and correlates with clinical outcome. *Sci. Adv.* **8**, eabo0514 (2022).
40. Albelda, S. M. CAR T cell therapy for patients with solid tumours: key lessons to learn and unlearn. *Nat. Rev. Clin. Oncol.* **21**, 47–66 (2024).
41. Espie, D. & Donnadieu, E. New insights into CAR T cell-mediated killing of tumor cells. *Front. Immunol.* **13**, 1016208 (2022).
42. Kantari-Mimoun, C. et al. CAR T-cell entry into tumor islets is a two-step process dependent on IFNγ and ICAM-1. *Cancer Immunol. Res.* **9**, 1425–1438 (2021).
43. Larson, R. C. et al. CAR T cell killing requires the IFNgammaR pathway in solid but not liquid tumours. *Nature* **604**, 563–570 (2022).
44. Dong, E. et al. IFN-gamma surmounts PD-L1/PD1 inhibition to CAR-T cell therapy by upregulating ICAM-1 on tumor cells. *Signal Transduct. Target Ther.* **6**, 20 (2021).
45. Zou, F. et al. Engineered triple inhibitory receptor resistance improves anti-tumor CAR-T cell performance via CD56. *Nat. Commun.* **10**, 4109 (2019).
46. Odorizzi, P. M. et al. Genetic absence of PD-1 promotes accumulation of terminally differentiated exhausted CD8+ T cells. *J. Exp. Med.* **212**, 1125–1137 (2015).
47. Zhao, Z. et al. Structural design of engineered costimulation determines tumor rejection kinetics and persistence of CAR T Cells. *Cancer Cell* **28**, 415–428 (2015).
48. Teijaro, J. R. et al. Persistent LCMV infection is controlled by blockade of type I interferon signaling. *Science* **340**, 207–211 (2013).
49. Wilson, E. B. et al. Blockade of chronic type I interferon signaling to control persistent LCMV infection. *Science* **340**, 202–207 (2013).
50. Evgin, L. et al. Oncolytic virus-derived type I interferon restricts CAR T cell therapy. *Nat. Commun.* **11**, 3187 (2020).
51. Hui, E. et al. T cell costimulatory receptor CD28 is a primary target for PD-1-mediated inhibition. *Science* **355**, 1428–1433 (2017).
52. Kamphorst, A. O. et al. Rescue of exhausted CD8 T cells by PD-1-targeted therapies is CD28-dependent. *Science* **355**, 1423–1427 (2017).
53. Kim, S. et al. Reprogramming of IL-12 secretion in the PDCD1 locus improves the anti-tumor activity of NY-ESO-1 TCR-T cells. *Front. Immunol.* **14**, 1062365 (2023).
54. Sachdeva, M. et al. Repurposing endogenous immune pathways to tailor and control chimeric antigen receptor T cell functionality. *Nat. Commun.* **10**, 5100 (2019).
55. Caraballo Galva, L. D. et al. Novel low-avidity glypican-3 specific CARTs resist exhaustion and mediate durable antitumor effects against HCC. *Hepatology* **76**, 330–344 (2022).
56. Ghorashian, S. et al. Enhanced CAR T cell expansion and prolonged persistence in pediatric patients with ALL treated with a low-affinity CD19 CAR. *Nat. Med.* **25**, 1408–1414 (2019).
57. Morgan, R. A. et al. Case report of a serious adverse event following the administration of T cells transduced with a chimeric antigen receptor recognizing ERBB2. *Mol. Ther.* **18**, 843–851 (2010).
58. Mao, R., Kong, W. & He, Y. The affinity of antigen-binding domain on the antitumor efficacy of CAR T cells: Moderate is better. *Front. Immunol.* **13**, 1032403 (2022).
59. Stadtmauer, E. A. et al. CRISPR-engineered T cells in patients with refractory cancer. *Science* **367**, eaba7365 (2020).
60. Bonini, C. et al. Genome Editing in Engineered T Cells for Cancer Immunotherapy. *Hum. Gene Ther.* **34**, 853–869 (2023).
61. Adusumilli, P. S. et al. A phase I trial of regional mesothelin-targeted CAR T-cell therapy in patients with malignant pleural disease, in combination with the Anti–PD-1 agent pembrolizumab. *Cancer Discov.* **11**, 2748–2763 (2021).
62. Carter, P. et al. Humanization of an anti-p185HER2 antibody for human cancer therapy. *Proc. Natl Acad. Sci. USA* **89**, 4285–4289 (1992).
63. Castella, M. et al. Development of a Novel Anti-CD19 chimeric antigen receptor: a paradigm for an affordable CAR T cell production at academic institutions. *Mol. Ther. Methods Clin. Dev.* **12**, 134–144 (2019).
64. Dull, T. et al. A third-generation lentivirus vector with a conditional packaging system. *J. Virol.* **72**, 8463–8471 (1998).
65. Andreu-Saumell, I., Rodriguez-Garcia, A. & Guedan, S. Genome Editing in CAR-T Cells Using CRISPR/Cas9 Technology. *Methods Mol. Biol.* **2748**, 151–165 (2024).
66. Rodriguez-Garcia, A., Watanabe, K. & Guedan, S. Analysis of anti-tumor effects of CAR-T cells in mice with solid tumors, in *Chimeric Antigen Receptor T Cells: Development and Production* (eds K. Swiech, K.C.R. Malmegrim, and V. Picanço-Castro) (Springer US: New York, NY, 2020).

Acknowledgements

This work received funding from the Spanish Ministry of Science and Innovation under a Ramon y Cajal grant (RYC2018-024442-I to S.G.) and Retos Investigación (PID2019-109546RA-I00-PI), the Innovative Medicines Initiative 2 Joint Undertaking under grant agreement No 116026 (this Joint Undertaking receives support from the European Union's Horizon 2020 research and innovation program and EFPIA),"la Caixa" Foundation under the grant agreement LCF/PR/SP23/52950004, the Spanish Association Against Cancer (LABAE20022GUED to S.G., INVES222988RODR to A.R-G. and INVES21943BRAS to F.B-M.) and a nCounter Immunology grant from Diagnóstica Longwood S.L, Nanostring. L.A. is recipient of a Rio Hortega 2020 Contract (Ministry of Health, Spain). A.P. received funding from Fundación CRIS contra el cáncer PR_EX_2021-14, Agència de Gestó d'Ajuts Universitaris i de Recerca 2021 SGR 01156, Fundación Fero BECA ONCOXXI21, Instituto de Salud Carlos III PI22/01017, Asociación Cáncer de Mama Metastásico IV Premios M. Chiara Giorgetti, Breast Cancer Research Foundation BCRF-23-198, and RESCUER, funded by European Union's Horizon 2020 Research and Innovation Programme under Grant Agreement No. 847912. We are indebted to the Biobank core facility, to the Flow Cytometry and Cell Sorting core facility of Institut d'Investigacions Biomèdiques August Pi i Sunyer (IDIBAPS) for their technical help and to the animal facility of the Universitat de Barcelona. We thank S. Bragado from IsoPlexis and D. Benítez from the Immunology department for advice and assistance with the single-cell secretome assay and P. Galván, O. Castillo and P. Blasco from the Translational genomics and targeted therapies in solid tumors group for assistance with the gene expression assay. We thank A. Gros, R. Alemany and M. Juan for helpful scientific discussions. Panels in Fig. 3a and Fig. 7h were created with BioRender.com, released under a Creative Commons Attribution-NonCommercial-NoDerivs 4.0 International license, or with Adobe Illustrator, respectively, as indicated in figure legends.

Author contributions

I.A.-S. and A.R-G. designed and performed the experiments, analyzed and interpreted the data and wrote the manuscript. M.G.-A., V.M., S.C., L.A. and M.N. performed experiments. J.C. performed in vivo experiments. F.B-M assisted with transcriptomic data analysis. H.C. developed some of the CAR constructs used in the study and assisted with in vivo experiments. B.M. developed some of the CAR constructs and tumor cell lines used in the study. M.S-C helped with lentiviral production. P.B.

assisted with in vivo experiments. J.B.H. designed experiments, provided conceptual guidance and revised the manuscript. A.P. and A.U-I provided conceptual guidance and revised the manuscript. S.G supervised the project, including design of experiments, data analysis and interpretation and manuscript writing.

Competing interests

S.G. is an inventor on patents related to CAR-T cell therapy, filed by the University of Pennsylvania and licensed to Novartis and Tmunity, and has received commercial research funding from Gilead. A.R-G. is an inventor on patents related to CAR-T cell therapy, filed by the University of Pennsylvania. The remaining authors declare no competing interests.

Additional information

Supplementary information The online version contains supplementary material available at https://doi.org/10.1038/s41467-024-47799-z.

Correspondence and requests for materials should be addressed to Alba Rodriguez-Garcia or Sonia Guedan.

Peer review information *Nature Communications* thanks Ondrej Stepanek and the other, anonymous, reviewer(s) for their contribution to the peer review of this work. A peer review file is available.

Appendix 8.2 - Book chapter

Chapter 12

Genome Editing in CAR-T Cells Using CRISPR/Cas9 Technology

Irene Andreu-Saumell, Alba Rodriguez-Garcia, and Sonia Guedan

Abstract

CAR-T cell therapy is revolutionizing the treatment of hematologic malignancies. However, there are still many challenges ahead before CAR-T cells can be used effectively to treat solid tumors and certain hematologic cancers, such as T-cell malignancies. Next-generation CAR-T cells containing further genetic modifications are being developed to overcome some of the current limitations of this therapy. In this regard, genome editing is being explored to knock out or knock in genes with the goal of enhancing CAR-T cell efficacy or increasing access. In this chapter, we describe in detail a protocol to knock out genes on CAR-T cells using CRISPR–Cas9 technology. Among various gene editing protocols, due to its simplicity, versatility, and reduced toxicity, we focused on the electroporation of ribonucleoprotein complexes containing the Cas9 protein together with sgRNA. All together, these protocols allow for the design of the knockout strategy, CAR-T cell expansion and genome editing, and analysis of knockout efficiency.

Key words Genome editing, CAR-T cells, CRISPR/Cas9, T-cell engineering

1 Introduction

Adoptive transfer of CAR-T cells has shown tremendous promise for the treatment of cancer [1]. Treatment with autologous CAR-T cells targeting CD19 or BCMA can achieve high rates of long-term complete responses in patients with relapsed/refractory leukemia and lymphoma or multiple myeloma, respectively [2]. While the power of CAR-T cells in B-cell malignancies is truly unprecedented, the majority of patients with solid tumors or certain hematologic malignancies do not benefit yet from these therapies. Translation of CAR-T therapy to more difficult-to-treat tumors will require further genetic modifications of CAR-T cells, including elimination of genes that could diminish CAR-T cell efficacy or overexpression of genes that can drive more potent antitumor responses [3].

Irreversible silencing of protein expression can be easily achieved using genome editing tools that allow efficient knockout

Velia Siciliano and Francesca Ceroni (eds.), *Cancer Immunotherapy: Methods and Protocols*,
Methods in Molecular Biology, vol. 2748, https://doi.org/10.1007/978-1-0716-3593-3_12,

of genes of interest [4, 5]. Genome editing technology consists on the combination of engineered nucleases with sequence-specific DNA-binding domains that directs the nuclease to the target DNA cut site [6]. In the field of CAR-T cells, genome editing approaches have been used in three main applications [3]. First, the KO of components of the TCR and the HLA allow for the generation of allogeneic universal "off-the-shelf" CAR-T cells [4]. Significant efforts are under way to translate the use of universal CAR-T cells into the clinics, with the first clinical trials already reporting feasibility, safety, and efficacy [7, 8]. Second, genome editing approaches have been used to generate CAR-T cell products resistant to fratricide for the treatment of T-cell malignancies [9]. In this regard, CAR-T cells targeting CD7 with disrupted CD7 and TRAC genes are already being tested in the clinic [10]. Finally, strategies to silence inhibitory receptors or any other protein that can impair CAR-T cell efficacy are also being widely explored [11–13].

Long-term expression of novel or native proteins is typically achieved using retroviral and lentiviral vectors or transposon systems that can randomly integrate the gene of interest in the T-cell genome [3]. A more elegant strategy would be to knock in the gene of interest into selected endogenous loci, allowing the expression of the transgene under the natural promoter of the targeted gene. Considerable progress in the field over the past years make it now possible to knock in genes in specific loci using these same genome editing tools in combination with a donor DNA that encodes the transgene of interest [14, 15]. The first approach in the field in this regard was focused on knocking in the CAR into the endogenous TCR locus [14]. As the field expands, other transgenes (such as IL-12) are being knocked in in different loci (such as PDCD1 or CD25) [16]. While the field is poised for rapid advancement, as of now, the protocols for knock-in approaches in T cells require further optimization to increase efficiency and will not be discussed in this chapter.

Different genome editing tools have been efficiently used to install the desired genetic modifications, including zinc-finger nucleases (ZFNs), transcription activator-like effector nucleases (TALENs), and the clustered regularly interspaced short palindromic repeats (CRISPR)–Cas9 platform [6]. Due to its simplicity, flexibility, and effectiveness, in this chapter we will focus on the use of the CRISPR–Cas9 platform. The protocols described here allow for the obtention of genome-edited CAR-T cells with high knockout efficiencies. Methods and tools to test the efficacy and toxicity of these genome-edited CAR-T cells have been reviewed elsewhere [17, 18].

2 Materials

2.1 T-Cell Isolation

1. Fresh blood or buffy coat.
2. Lymphoprep (StemCell Technologies Catalog # 7811).
3. Phosphate-buffered solution without calcium and magnesium (PBS −/−, Invitrogen, catalog # 20012–068).
4. Fetal bovine serum (FBS) (Merck, catalog # F4135).
5. RosetteSep Human CD8+ T-cell enrichment kit/human CD4+ T-cell enrichment kit (StemCell Technologies, catalog # 15062 and 15,063).
6. R10 medium: RPMI 1640 (Merck, Catalog # R6504-10X1L) supplemented with 10% (v/v) heat-inactivated FBS, 1X GlutaMax (Thermo Fisher, catalog # 35050–061), 100 μg/mL penicillin, 100 U/mL streptomycin (Thermo Fisher, catalog # 15140122), 10 mM HEPES (Sigma, catalog # H0887-100ML), 10 ng/mL human recombinant IL-7, and 10 ng/mL human recombinant IL-15 (Miltenyi, catalog # 130–095-362 and 130–095-764).
7. Anti-CD3/CD28 magnetic beads (Invitrogen, catalog # 11132D).
8. DynaMag-2 and Dynal 15-mL magnet (Invitrogen, catalog # 12321D and 12301D).
9. Hemocytometer ([BRAND™]_VWR, catalog # BE718605).
10. Trypan blue solution (Sigma, catalog # T8154).

2.2 Generation of CRISPR/Cas9-Edited CAR-T Cells

11. CAR-expressing lentivirus vector stock.
12. Multiparameter flow cytometer (e.g., BD FACSCanto II).
13. FlowJo software.
14. Chemically modified sgRNA (CRISPRevolution sgRNA EZ Kit, Synthego).
15. Neon™ Transfection System 100 μL Kit (Thermo Fisher, catalog # MPK10096).
16. Neon™ Transfection System Pipette (Thermo Fisher, catalog # MPP100).
17. Neon™ Transfection System Pipette Station (Thermo Fisher, catalog # MPS100).
18. Neon™ Transfection System (Thermo Fisher, catalog # MPK5000).
19. TrueCut™ Cas9 Protein v2 (Thermo Fisher, catalog # A36499).
20. Deionized water (Thermo Fisher, catalog # 15230089).

Table 1
List of antibodies to analyze T-cell purity, CD4/CD8 T-cell ratio, CAR, and PD-1 expression during primary expansion by flow cytometry

Target	Fluorochrome	Catalog #	Company
CD3	PE	12–0037-42	Thermo fisher
CD4	FITC	557,695	BD bioscience
CD8	APC	17–0086-42	Thermo fisher
CAR (murine scFv)	Biotin goat anti-mouse IgG	115–065-072	Jackson ImmunoResearch
CAR (human or humanized scFv)	Biotin goat anti-human IgG	109–066-006	Jackson ImmunoResearch
Streptavidin	PE	12–4317-87	Thermo fisher
PD-1	PeCy7	561,272	BD bioscience

2.3 Analysis of Knockout Efficiency

21. DNA extraction kit (e.g., DNeasy Blood & Tissue Kit, Qiagen, catalog # 69504).
22. High-fidelity DNA polymerase, buffer, and dNTPs (e.g., Phusion ® High-Fidelity DNA Polymerase, NEB, catalog # M0530S).
23. 10 μM forward and reverse primers (IDT).
24. PCR cleanup kit (e.g. PCR PureLink™, Thermo Fisher, catalog # K310001).
25. Nuclease-free water (Thermo Fisher, catalog # AM9906).
26. Standard 1% agarose gel.
27. Tris–acetate EDTA (TAE) buffer (Bio Rad, catalog # 1610743).
28. DNA ladder 1 kb (WERFEN ESPAÑA S.A.U, catalog # 174N3232S).
29. DNA loading dye (Thermo Fisher, catalog # R0611).
30. Gel electrophoresis equipment.
31. Thermocycler.
32. Tris-Buffered Saline (TBS) (Bio Rad, catalog # 1706435).
33. Tween-20 (PanReac-AppliChem, catalog # A4974,0250).
34. GraphPad software (Table 1).

3 Methods

In this protocol, CRISPR/Cas9 technology will be used to genetically edit CAR-T cells. This methodology relies on two components: a single-guide RNA (sgRNA) which will bind to the targeted

DNA sequence and the endonuclease Cas9 which will induce DNA double-strand breaks (DSBs) at that specific point. Then, error-prone endogenous DNA repair mechanisms will introduce insertions or deletions (indels), potentially leading to loss-of-function mutations of the targeted gene.

Since primary T cells are hard-to-transfect cells, alternative methods are needed to deliver the required components to the cells. Methods based on the delivery of Cas9 and/or sgRNA by using either non-integrating (adenoviral) or integrating (lentiviral) viral vectors have been reported [19, 20]. However, limited transduction rates result into relatively low editing efficiencies, and multiplex editing is limited by the packaging capacity of the vector [21]. In addition, in the case of integrating vectors, the long-term expression of Cas9 and sgRNA can lead to undesirable off-target effects. Alternatives to this could be to incorporate multiple sgRNAs in the CAR lentiviral vector and deliver the Cas9 by the electroporation of protein or mRNA [22], or to deliver in vitro-transcribed sgRNA and Cas9 RNA by electroporation [5]. DNA nucleofection is another CRISPR/Cas9 delivery method by which T-cell editing has been achieved, although it is associated to high toxicity to T cells [23, 24].

In this protocol, we will genetically modify T cells by electroporation of a ribonucleoprotein (RNP), consisting of a Cas9 protein complexed with sgRNA. This method is simple and fast and has shown good efficiency on T cells as well as reduced off-target effects and toxicity as compared to the above-described methods [25]. In addition, it is a flexible platform that allows for multiplex editing [12] and it has been reported to enhance efficiencies of challenging knock-in approaches [25].

3.1 Generation of CAR-T Cells

The starting amount of T cells will depend on the intended application for the expanded cells. Taking into account that electroporation can result into 50% of T-cell death, a 10- to 30-fold increase in T-cell numbers is expected from day 0 to day 10. An example of the numbers used to start a CAR-T cell expansion when electroporating RNPs is shown in Table 2.

3.1.1 T-Cell Isolation

1. Isolate $CD4^+$ and $CD8^+$ T cells from blood or buffy coats using RosetteSep T-cell-negative selection kit following manufacturer's instructions (*see* **Note 1**).
2. Assess T-cell purity and CD4/CD8 T-cell ratio by staining the purified sample with anti-CD3, anti-CD4, and anti-CD8 antibodies for flow cytometry analysis. The T-cell purity ($CD3^+$) should be above 95%.

Table 2
Example of T-cell numbers used to start an expansion depending on the application

	Million T cells			Observations
	Day 0	Day 4 (electroporation)	Day 10	Electroporation of T cells can be performed on day 2. It is important to take into account that T cells do not double till day 3–4. Electroporating less than two million cells can result in increased T-cell death
In vitro studies	2	4	20–60	
In vivo studies	5	10	100–300	

3.1.2 T-Cell Stimulation and Transduction

1. Prepare T cells in R10 complete medium to a concentration of 1×10^6 cells/mL and aliquot the required number of cells into appropriate multi-well flat-bottom plates or flasks. Use as many wells as experimental groups. Include a control group of untransduced T cells (UTD) (*see* **Note 2**).
2. Based on a ratio of two beads to one T cell, calculate the amount of anti-CD3/CD28 magnetic beads needed (*see* **Note 3**).
3. Thoroughly resuspend the magnetic beads and transfer the calculated volume to a 1.5-mL tube placed on the DynaMag-2 magnet.
4. After 1 min, discard the beads' buffer. Remove the tube from the magnetic field and wash the beads with 1 mL of pre-warmed R10 medium. Repeat the washing step twice.
5. After the last wash, resuspend the beads in a small volume of R10 medium (i.e., 50 μL of media per million beads).
6. Transfer the beads to the corresponding wells containing the T cells and mix.
7. Twenty-four hours later, transduce the activated T cells with the CAR-encoding lentivirus at a multiplicity of infection (MOI) of 5 (*see* **Note 4**). Simply add the volume of virus needed to achieve the corresponding MOI and mix gently.
8. Feed the cells with one volume of R10 complete medium on the third day after stimulation.

3.2 Gene Editing by CRISPR/Cas9 Technology

For most targets, gene editing can be done indistinctly two to four days after stimulation, when T cells have received sufficient activation from the CD3/CD28 beads and are actively proliferating. However, for certain targets, genome editing might be required at earlier timepoints. This can apply, for instance, to CAR-T cells targeting antigens that are expressed on T cells, in order to avoid co-expression of the CAR and the targeted antigen and to prevent fratricide (i.e., CD7). In this scenario, the knockout should be

Table 3
Suggested experimental CRISPR/Cas9 controls

Control	Description	Purpose
Positive control	CAR-T cells are electroporated with Cas9 complexed with sgRNAs that have demonstrated high editing efficiency (i.e., sgRNA for TRAC)	Ensures that all reagents, protocol, and equipment are functioning at optimal conditions This control might be used when optimizing a protocol or when trying a sgRNA for the first time
Negative control: Non-electroporated T cells	T cells are not electroporated and cultured in the absence of Cas9 and sgRNA	This control determines cell growth at basal conditions
Mock control: Electroporated T cells	CAR-T cells are electroporated with Cas9 complexed with a nontargeting sgRNA, a sgRNA targeting a genomic safe harbour (i.e., AAVS1 or Rosa26) or an intron, or with no sgRNA.	It controls for toxicity from RNP (or Cas9), cell death from electroporation, or possible viability issues associated with editing the specific gene of interest. Ensures that the observed phenotype is due to the specific editing and not to the transfection process No indels are expected to occur at any genome location
	CAR-T cells are electroporated with no Cas9 or sgRNA	It might be used to avoid costs associated with the electroporation of RNP or Cas9. It is similar to the above control except it does not control for RNP and/or Cas9 toxicity It is highly recommended to have a mock control in all studies

achieved before the CAR is expressed in the T-cell membrane (*see* **Note 5** for protocol variations). A list of suggested experimental CRISPR/Cas9 controls to include as part of the expansion protocol is shown in Table 3.

3.2.1 Debeading

Prior to electroporation, beads must be removed from the cell culture and electroporation of RNPs is performed on the same day.

1. Count T cells using trypan blue exclusion or an automated cell counter (*see* **Note 6**).
2. Calculate the volume of R10 medium needed to adjust the cell concentration to 1×10^6 cells/mL.
3. Place two uncapped 15-mL tubes per sample on the 15-mL Dynal magnet.

4. Mix the cells thoroughly in their own medium to free the cells off the beads.
5. Transfer the sample into the first falcon tube. After 1 min, the beads should accumulate on the magnet-side walls.
6. Without disturbing the beads, carefully transfer the sample to the second tube for another minute and then transfer the sample into the corresponding well/flask (refer to **step 2** from Subheading 3.2.4 to determine the container). This step is required to assure that all beads have been eliminated from the T-cell culture.
7. Following the sequential order of transfer, use the previously calculated volume of medium in **step 2** to wash the beads after each transfer and feed the cells with the washing medium. This step is necessary to collect T cells that remain bound to the beads.
8. Leave the cells resting in a humidified 37 °C, 5% CO2 incubator for 2–4 h before the electroporation step.

3.2.2 Single-Guide RNA (sgRNA) Design

For this protocol, the CRISPR Design Tool from Synthego (https://www.synthego.com/products/bioinformatics/crispr-design-tool) was used to design the sgRNA (*see* **Note 7**). This tool uses a sequential algorithm to rank candidate guide RNA sequences that have a high chance of knocking out the gene of interest while minimizing off-target effects. To be suggested as candidates, guides need to accomplish the following features: (I) target a common exon in the primary transcript, (II) target an early region of the gene, (III) have an on-target score of >0.5 based on the Azimuth 2.0 model, and (IV) have no off-target sites within the same genome that have 0, 1, or 2 mismatches compared to the guide RNA sequence. Chemically modified sgRNAs which have shown to provide superior editing in most cell types (including T cells) were used [26]. Of note, it would be recommendable to test various sgRNA for the same target gene in order to screen for the best candidate. Screening of sgRNAs can be alternatively performed in Jurkat cells in order to reduce costs associated to T-cell activation, transduction, and expansion, as well as to save time.

3.2.3 T-Cell Preparation

1. Centrifuge T cells at 300 × *g* for 7 min and remove the supernatant. **Important!** Keep the conditioned media (supernatant) to resuspend T cells after electroporation, as it contains cytokines and factors secreted by T cells that are required for proper T-cell expansion.
2. Add 10–20 mL of PBS (no calcium, no magnesium) and centrifuge T cells at 300 × *g* for 7 min.
3. Resuspend the T cells in Resuspension Buffer R at the desired concentration in order to have 2–3 × 10^6 cells per reaction in a

volume of 50 μL and place the cells on ice for no longer than 20 min, as this will reduce cell viability and transfection efficacy (*see* **Note 8**). **Important!** The number of cells per reaction could be increased up to 8–10 × 10^6 cells, although this might reduce KO efficiency (around 50% depending on the target locus). This lower efficiency may be desired in specific cases (e.g., to evaluate if the elimination of the gene of interest generates an enrichment of the knockout T-cell population). However, if higher editing efficiencies are desired (>80%), T cells should be electroporated in rounds of 2–5 × 10^6 cells.

3.2.4 Preparation of RNP Complexes

1. During the T-cell centrifugation step, prepare RNP complexes. Mix 10 μg of Cas9 protein (2 μL of TrueCut™ Cas9 Protein v2) and 2.5 μg of sgRNA (~2 μL of 100 μM – 100 pmol/μL sgRNA) in a final volume of 50 μL of Resuspension Buffer R per reaction. The molar ratio Cas9/gRNA is 1:3.3. Mix well gently (*see* **Note 9**).
2. Incubate the Cas9/gRNA complex at room temperature (RT, 15 to 25 °C) for 5–20 min.
3. Add the Cas9/gRNA complex (from **step 5**) to the T cells (from **step 6**) and mix well.

3.2.5 Electroporation of RNP Complexes

1. Pipette 100 μL of the T cells mixed with Cas9/gRNA complexes into the Neon™ 100-μL tip. **Important!** Avoid creating air bubbles while loading the electroporation tip, as this will result in lowered or failed transfection. If air bubbles are noticed in the tip, the sample must be returned to its tube and carefully pitetted again.
2. Use program #24 (1600 V/10 ms/3 pulses) for electroporation.
3. Immediately transfer the electroporated cells into the appropriate vessel containing the needed volume of conditioned medium to adjust CAR-T cell concentration to 1.5 × 10^6 cells/ml and transfer the plate to a humidified 37 °C, 5% CO2 incubator (*see* **Note 10**). After 48 h, proceed with post-editing CAR-T cell expansion.

3.2.6 Postediting CAR-T Cell Expansion

During the logarithmic phase of T-cell expansion (days 6–9), T cells must be counted and fed daily with fresh medium in order to prevent the T cell concentration get above 2 × 10^6 cells/mL. Maintain T cells in culture until they rest down (as determined by both decreased growth kinetics and cell size). Following this protocol, this will typically happens around day 10–12 after activation, when T cells can be cryopreserved or used for functional assays.

1. Count the cells using trypan blue exclusion or an automated cell counter.

Table 4
Recommended plates and flask sizes for the T-cell expansion

N	Well plate/flask type
2 to 5	24-well plate
5 to 8	12-well plate
8 to 20	6-well plate
20 to 40	T25 flask–horizontal
40 to 112.5	T75 flask–horizontal
>112.5	T150 flask–horizontal

The "N" column specifies the range of values for the parameter N. The "Well plate/flask type" column provides the corresponding type of container for each size range. The term "horizontal" indicates the orientation of the flask

2. Transfer the cells to the appropriated well or flask based on the formula and Table 4 below:

$$N = \frac{Total\ cell\ number}{3.5\ x\ 10^5}$$

3. Add fresh R10 medium to adjust the cell concentration to 0.8×10^6 cells/mL. To minimize cell loss during well/flask transfers, use the feeding medium to wash the well/flask.
4. Use 1×10^5 to 2×10^5 cells to assess CAR expression on $CD4^+$ and $CD8^+$ T cells at the end of primary expansion (day 8–10). CARs can be stained by using either conjugated target recombinant proteins or anti–mouse/human IgG (depending on the CAR's ScFv origin). Anti-CD4 and anti-CD8 antibodies may also be included, and if the protein being knocked out is expressed on the cell surface, specific antibodies might be also included to assess KO efficiency as described below (*see* Subheading 3.3.2). Analyze by flow cytometry.
5. **(Optional)** If genome editing is on a surface molecule (i.e., CD3, T-cell receptor components, or components of the MHC-I complex such as β2m), edited CAR-T cells could be enriched by negative selection (e.g., by using magnetic microbeads) before cryopreservation or functional experiments.
6. Keep at least 1×10^6 cells per group to quantify editing efficiency (*see* Subheading 3.3.1).
7. Cryopreserve T cells by day 10 or use them fresh by day 10 to 12. $CD4^+$ and $CD8^+$ T cells can be cryopreserved and/or tested separately or can also be mixed at a 1:1 ratio for cryopreservation and/or further characterization.

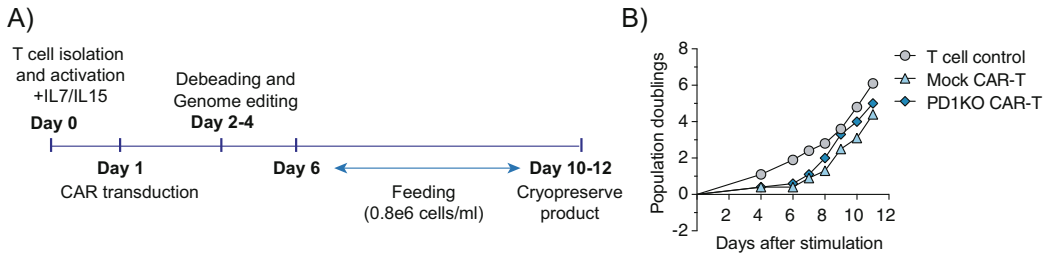

Fig. 1 Ex vivo expansion of gene-edited CAR-T cells. (**a**) Schematic representation of T-cell expansion and CRISPR/Cas9 editing protocol in primary human CAR-T cells. (**b**) Population doublings in genome-edited CAR-T cells during primary T-cell expansion

8. Calculate population doubling: Use the total cell numbers obtained from day 0 to the end of T-cell primary expansion (day N) to calculate the population doubling relative to the number of cells stimulated on day 0, using the following formula:

$$\text{Pop.Doub.} = \left(\log_2 \text{Total Cells}_{\text{DayN}}\right) - \left(\log_2 \text{Total Cells}_{\text{Day0}}\right)$$

T cells should double approximately 4–5 times from day 0 to day 10. Population doublings below 4 at day 10 are unusual and may indicate a problem during T-cell expansion. Representative T-cell expansion data after gene editing is shown on Fig. 1b.

3.3 Analysis of Knockout Efficiency

Assessment of editing efficiency is a critical step and can be done at different timepoints during T-cell expansion (i.e., at day 6, 8, and 10) to assess if the knockout provides a proliferative advantage to the cells, resulting in an enrichment of the gene-edited population (or the opposite). Editing efficiency can be determined at DNA or protein level.

For assessing editing efficiency at the DNA level, genomic DNA must be extracted and the target gene amplified by PCR. Then, different methodologies can be used to assess KO efficiency. Mismatch repair assays such as T7E1 or Surveyor Mismatch Cleavage rely on the activity of T7 nucleases that cleave DNA when there are mismatches, when editing has occurred. These methods are time-consuming and not very accurate and often underrepresent editing efficiency [27]. More accurate methods are those based on sequencing. Ideally, next-generation sequencing (NGS) of amplicons could be used, but elevated cost prevents its routine use. More cost-effective methods such as inference of CRISPR edits (ICE, Synthego) or tracking of indels by decomposition (TIDE) rely on Sanger sequencing to resolve indel size frequencies from edited cell populations by comparing and decomposing Sanger traces made from PCR products of targeted regions from unedited/mock and edited templates. For this protocol, we have used ICE to assess editing efficiency.

For assessing editing efficiency at the protein level, flow cytometry (surface or intracellular staining), ELISA, or western blot could be used depending on the cellular localization of the targeted protein.

3.3.1 DNA Level

1. Extract genomic DNA from at least 1×10^6 cells (from both edited and unedited/mock pool of cells) by using a commercial DNA extraction kit according to the manufacturer's specifications (e.g., DNeasy Blood & Tissue Kits, QIAGEN).
2. Use 150 ng of genomic DNA to amplify the targeted region by standard polymerase chain reaction (PCR) (i.e., Phusion ® High-Fidelity DNA Polymerase from NEB). For this protocol, the benchling software (https://benchling.com/) was used to design specific primers flanking the region including the potential cleavage site (*see* **Note 11**).
3. Purify PCR product by using a PCR purification kit (e.g., PCR PureLink™, Thermo Fisher). Use a sample of the purified product to confirm amplification by running a 1% agarose electrophoresis gel.
4. Perform Sanger sequencing of the purified amplicons from the mock and edited samples. Primers used for the amplification step might be used as long as they are at a distance enough to ensure good sequencing quality at the region containing the indels.
5. Quantify the total indel percentage (frequency of sequences that contain an insertion or deletion) and the knockout score (frameshift-inducing indels or deletions of >21 bp) by using ICE (https://ice.synthego.com/). A higher knockout score will indicate a higher likelihood of indels resulting in a functional KO of the targeted gene. R2 values indicate how well the indel distribution fits the Sanger sequence data of the edited sample. All the obtained parameters can be then graphically displayed (*see* Fig. 2).

3.3.2 Protein Level

1. For target proteins expressed at the cell surface, stain 2×10^5 T cells with fluorochrome-labeled antibodies for flow cytometry analysis and compare expression levels in mock/unedited samples versus edited cells (e.g., PD-1 and CD3, Fig. 3a and b).
2. For target proteins that are secreted (e.g., cytokines), supernatants can be analyzed by enzyme-linked immunosorbent assay (ELISA) for protein detection.
3. For target proteins expressed intracellularly, intracellular staining (ICS) protocols can be performed for flow cytometry analysis as well as protein detection by standard western blot protocols.

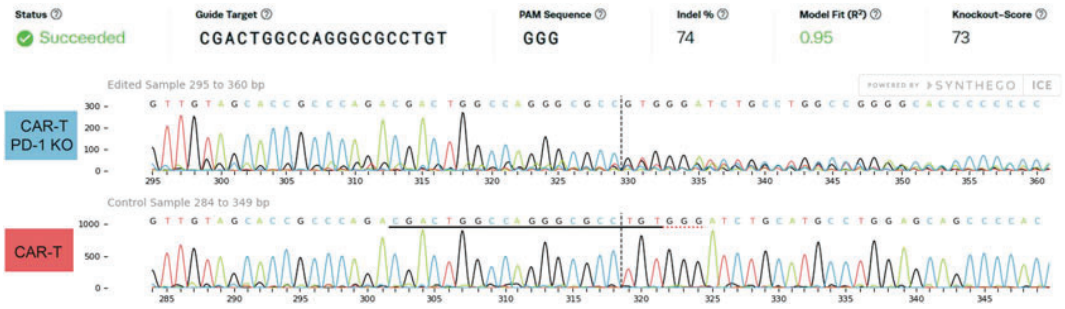

Fig. 2 Example of a Trace tab of PD-1 KO obtained using the ICE analysis tool. The traces tab edited (CAR-T PD-1 KO) and control (CAR-T, bottom) Sanger traces in the region around the guide RNA binding site (horizontal black line) and the PAM site underlined with a red dotted line. The cut site is indicated with a vertical dotted line on both traces

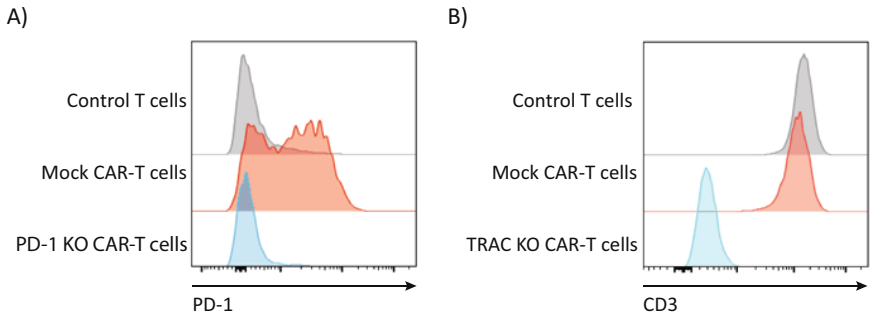

Fig. 3 (**a**) PD-1 expression was assessed by flow cytometry in CAR-T cells at day 8 of T-cell expansion. (**b**) CD3 surface expression on CAR-T cells after CRISPR/Cas9 KO of TRAC as assessed following antigen stimulation

4 Notes

1. Other technologies may be used (e.g., microbeads from Miltenyi Biotec).
2. Media supplementation with IL-7 and IL-15 until day 9 of expansion limits T-cell differentiation during T-cell culture and is reported to improve antitumor efficacy of CAR-T cells [28–30].
3. The manufacturer recommends a bead/cell ratio of 1:1. However, a ratio of 2:1 may be used to obtain a better stimulation of the cells.
4. Lentivirus should have been previously tittered in sub-T1, Jurkat cells, 293 T cells, or T cells.
5. An alternative genome editing protocol is to perform CRISPR/Cas9 on day 2 post-stimulation and to transduce T cells with the CAR lentivirus on day 3 (instead of day 1). From day 5 to 10, proceed with typical CAR-T cell expansion.

Alternatively, naïve (non-stimulated) T cells could be genome edited on day 1 after isolation. Electroporation conditions as well as IL-7/15 concentrations must be modified in this case (i.e., 2200 V 20 ms 1 pulse, 25 ng/mL IL-7/15) [31]. Then, T cells are activated on day 2, transduced with the lentiviral CAR on day 3, and expanded up to day 12.

6. Other automated cell counter with cell diameter gating options and with cell volume or diameter average display can be used (e.g., Countess, from Life Technologies).
7. Other informatic tools might be used for sgRNA design (e.g., Benchling, GeneArt CRISPR Search, and Design tool from Invitrogen, CRISPR–Cas9 guide RNA design checker from IDT, E-CRISPR, CHOP-CHOP, etc.).
8. It is recommended to prepare an extra amount of cells to avoid pipetting errors.
9. It is recommended to prepare an extra amount of RNP complexes to avoid pipetting errors.
10. Electroporation causes significant cell death (roughly 50% of the total population). Taking this into account, it is recommended to leave the T cells at a high concentration, of at least 1.5×10^6 cells/mL.
11. For best results: (I) use primers with Tm > 55 °C, (II) design primers that are 18–22 bp in length and have 45–60% GC content, (III) primers should yield amplicon lengths between 400 and 500 bp, and (IV) the potential cleavage site should not be in the center of the amplicon so the detection reaction will yield two distinct product bands that could be easily distinguished. Amplification of difficult targets might require troubleshooting and PCR optimization. For instance, a temperature gradient can be used to optimize the annealing temperature for each primer pair. Amplification of GC-rich sequences or sequences with secondary structure may be improved by the presence of additives such as DMSO or by the use of specific buffers.

References

1. Guedan S, Ruella M, June CH (2019) Emerging cellular therapies for cancer. Annu Rev Immunol 37:145–171
2. Majzner RG, Mackall CL (2019) Clinical lessons learned from the first leg of the CAR T cell journey. Nat Med 25:1341–1355
3. Irving M, Lanitis E, Migliorini D, Ivics Z, Guedan S (2021) Choosing the right tool for genetic engineering: clinical lessons from chimeric antigen receptor-T cells. Hum Gene Ther 32:1044–1058
4. Poirot L et al (2015) Multiplex genome-edited T-cell manufacturing platform for "off-the-shelf" adoptive T-cell immunotherapies. Cancer Res 75:3853–3864
5. Ren J et al (2017) Multiplex genome editing to generate universal CAR T cells resistant to PD1 inhibition. Clin Cancer Res 23:2255–2266
6. Gaj T, Gersbach CA, Barbas CF (2013) ZFN, TALEN, and CRISPR/Cas-based methods for genome engineering. Trends Biotechnol 31: 397–405

7. Qasim W et al (2017) Molecular remission of infant B-ALL after infusion of universal TALEN gene-edited CAR T cells. Sci Transl Med 9
8. Benjamin R et al (2018) Preliminary data on safety, cellular kinetics and anti-leukemic activity of UCART19, an allogeneic anti-CD19 CAR T-cell product, in a Pool of adult and pediatric patients with high-risk CD19+ relapsed/refractory B-cell acute lymphoblastic leukemia. Blood 132:896–896
9. Gomes-Silva D et al (2017) CD7-edited T cells expressing a CD7-specific CAR for the therapy of T-cell malignancies. Blood 130:285–296
10. Wang X et al (2020) Abstract CT052: clinical safety and efficacy study of TruUCAR™ GC027: the first-in-human, universal CAR-T therapy for adult relapsed/refractory T-cell acute lymphoblastic leukemia (r/r T-ALL). Cancer Res 80:CT052
11. Wang Z et al (2021) Phase I study of CAR-T cells with PD-1 and TCR disruption in mesothelin-positive solid tumors. Cell Mol Immunol
12. Stadtmauer EA et al (2020) CRISPR-engineered T cells in patients with refractory cancer. Science 367
13. Zhang Y et al (2017) CRISPR-Cas9 mediated LAG-3 disruption in CAR-T cells. Front Med 11:554–562
14. Eyquem J et al (2017) Targeting a CAR to the TRAC locus with CRISPR/Cas9 enhances tumour rejection. Nature 543:113–117
15. Roth TL et al (2018) Reprogramming human T cell function and specificity with non-viral genome targeting. Nature
16. Sachdeva M et al (2019) Repurposing endogenous immune pathways to tailor and control chimeric antigen receptor T cell functionality. Nat Commun 10:5100
17. Guedan S et al (2022) Time 2EVOLVE: predicting efficacy of engineered T-cells - how far is the bench from the bedside? J Immunother Cancer 10
18. Donnadieu E et al (2022) Time to evolve: predicting engineered T cell-associated toxicity with next-generation models. J Immunother Cancer 10
19. Li C et al (2015) Inhibition of HIV-1 infection of primary CD4+ T-cells by gene editing of CCR5 using adenovirus-delivered CRISPR/Cas9. J Gen Virol 96:2381–2393
20. Wang W et al (2014) CCR5 gene disruption via lentiviral vectors expressing Cas9 and single guided RNA renders cells resistant to HIV-1 infection. PLoS One 9:e115987
21. Kabadi AM, Ousterout DG, Hilton IB, Gersbach CA (2014) Multiplex CRISPR/Cas9-based genome engineering from a single lentiviral vector. Nucleic Acids Res 42:e147–e147
22. Ren J et al (2017) A versatile system for rapid multiplex genome-edited CAR T cell generation. Oncotarget 8:17002–17011
23. Su S et al (2016) CRISPR-Cas9 mediated efficient PD-1 disruption on human primary T cells from cancer patients. Sci Rep 6:20070
24. Pankaj K. Mandal et al., Efficient ablation of genes in human hematopoietic stem and effector cells using CRISPR/Cas9. Cell Stem Cell 15, 643–652 (2014)
25. Schumann K et al (2015) Generation of knock-in primary human T cells using Cas9 ribonucleoproteins. Proc Natl Acad Sci U S A 112:10437–10442
26. Hendel A et al (2015) Chemically modified guide RNAs enhance CRISPR-Cas genome editing in human primary cells. Nat Biotechnol 33:985–989
27. Sentmanat MF, Peters ST, Florian CP, Connelly JP, Pruett-Miller SM (2018) A survey of validation strategies for CRISPR-Cas9 editing. Sci Rep 8:888
28. Cieri N et al (2013) IL-7 and IL-15 instruct the generation of human memory stem T cells from naive precursors. Blood 121:573–584
29. Schluns KS, Kieper WC, Jameson SC, Lefrançois L (2000) Interleukin-7 mediates the homeostasis of naïve and memory CD8 T cells in vivo. Nat Immunol 1:426–432
30. Zhou J et al (2019) Chimeric antigen receptor T (CAR-T) cells expanded with IL-7/IL-15 mediate superior antitumor effects. Protein Cell 10:764–769
31. Leoni C, Bianchi N, Vincenzetti L, Monticelli S (2021) An optimized workflow for CRISPR-Cas9 deletion of surface and intracellular factors in primary human T lymphocytes. PLoS One 16:e0247232